A-1028

ENGINEERING EXPERIMENT STATION
GEORGIA INSTITUTE of TECHNOLOGY

hysical Sciences Division
225 North Avenue N.W.
Atlanta, Georgia 30332
(404) 873-4211 Ext. 220

17 July 1967

National Aeronautics and Space Administration
George C. Marshall Space Flight Center
Huntsville, Alabama 35812

Attention: Mr. William J. McKinney

Subject: Monthly Progress Letter 1, Project A-1028
"Study of Feasibility of Optically Exciting a Magnetic Memory"
Contract No. NAS8-20813
Covering the Period from 6 June to 5 July 1967

Gentlemen:

This report covers work performed under Contract NAS8-20813 from contract initiation, June 6, through July 6, 1967. The purpose of the work to be carried out under Phase I of this contract is to determine the feasibility of changing the compensation point of a ferrimagnetic garnet by optical pumping. If such a technique is feasible, it will provide an approach to achieving a high density magnetic storage medium without the necessity of employing thermal writing processes.

Both theoretical and experimental efforts are being carried out to provide the desired information. Two new men have been added to the group to strengthen the technical capability in specific areas. Mr. W. M. Winn, a doctoral candidate in physics at Georgia Tech, will be working approximately one-third time with his efforts directed to theoretical predictions of the interaction cross-sections. In addition, Dr. David Hinson has joined the group for 3 months to initiate the optical absorption and emission measurement experiments. Dr. Hinson's experience is in the area of studying material characteristics through their optical properties.

The following paragraphs briefly describe the progress to date in the individual areas.

Theoretical

The theoretical effort was initiated so as to obtain more insight into the underlying physical processes involved in the optical pumping of

the rare earth garnets. This is particularly important if it becomes necessary to synthesize materials which are magnetically sensitive to optical excitation and do not relax through strong lattice coupling.

A detailed survey of the literature is being conducted in order to provide a basis for the required calculations. It is not yet clear exactly what type of interactions are involved in excitation of the rare earth atoms. From spectroscopic information, it is clear that the transitions of interest are of an intra band nature within the 4f shell. However, the changes in quantum numbers violate the simple first order selection rules. Thus, calculations apparently must include spin-orbit coupling, wave function mixing, etc., in order to yield finite probabilities for the transitions involved. At present this work is continuing at a literature study level in order to acquire a more detailed understanding of the processes involved.

Experimental

In order to measure the cross-sections and attainable pumping levels in the materials to be studied, an experimental facility is being assembled to measure optical absorption, reflection and excited emission. This apparatus includes a 1,000 watt, high pressure mercury vapor light source, prism-type spectrometer covering 8,000 Å to 2,500 Å, and an enclosed sample chamber with appropriate substrate mounts, shuttering capabilities, and detectors. This apparatus should be operational during the latter part of July.

The problem of measuring changes in magnetization from optical pumping is being attacked through two separate efforts. The first is through the design and construction of a very sensitive, fast-response torque magnetometer. Such an instrument is needed in order to make ballistic type torque measurements to determine magnetization changes. A ballistic measurement is desired since continuous radiation at the power densities required are not readily available. In addition, it is desirable to make measurements typical of the pulsed mode which will occur in memory operation. The design of this instrument is unique in the area of torque magnetometers and should provide a valuable addition to the field of magnetic instrumentation. The torque sensitivity is to be in the

(10^{-4} - 10^{-5}) dyne-cm range with a first order time constant of 1μ sec.

The second method of measuring magnetization being investigated is by a Mössbauer experiment. Using the Mössbauer effect, it is possible to measure the change in hyperfine splitting resulting from the magnetic field associated with the electron spin system of an atom. In this approach, a measurement of the rare earth sublattice magnetization is obtained rather than the net garnet magnetization as with the torque method. Equipment to perform this experiment is already in existence at Georgia Tech; however, we are currently studying the achievable sensitivity to determine whether useful information can be obtained with relatively low photon radiation available. Hopefully, a more detailed report on the feasibility of applying this technique to the optically pumped garnets can be made in the next monthly report.

Another phase of instrumentation being added to the program is the growing of single crystal garnets. Initially, it had been planned to purchase the desired materials. However, the flexibility of modifying material properties as required appears desirable enough to warrant an in-house facility. As a result of this decision, information has been gathered and equipment is being ordered to provide this capability. It is anticipated that the first crystals will be available by late September.

During this period, the Faraday apparatus furnished by M.S.F.C. for use in this research was transported via Georgia Tech truck to this laboratory. The apparatus has not yet been assembled; however, arrangements are being made for an additional room where the experiment can be set up with no interference from other activities.

Future Work

During the following month, efforts will continue toward developing a theoretical understanding of the physical processes involved in the optical pumping operation.

Also, optical absorption data will be taken on a gadolinium sample presently on loan.

Work on the development of the fast response torque magnetometer and crystal growing facility will be continued.

Financial

The expenditures on this project as of July 1, 1967 are:

Personal Services		$ 1,010.51
Overhead		575.99
		$ 1,586.50
Contract Funding		$29,993.00
	Balance	$28,406.50

Respectfully submitted,

F. L. Grismore
Project Director

FLG/srt

Approved:

E. J. Scheibner, Chief
Physical Sciences Division

A-1028

ENGINEERING EXPERIMENT STATION
GEORGIA INSTITUTE of TECHNOLOGY

ysical Sciences Division

225 North Avenue N.W.
Atlanta, Georgia 30332
(404) 873-4211 Ext. 220

15 August 1967

National Aeronautics and Space Administration
George C. Marshall Space Flight Center
Huntsville, Alabama 35812

Attention: Mr. William J. McKinney

Subject: Monthly Progress Letter 2, Project A-1028
"Study of Feasibility of Optically Exciting a Magnetic Memory"
Contract No. NAS8-20813
Covering the Period from 6 July to 5 August 1967

Gentlemen:

This report covers work performed under Contract NAS8-20813 during the period July 6 through August 6, 1967. Phase I of the program is directed toward obtaining data on material properties and a theoretical basis of the processes involved in optically pumping a ferrimagnetic garnet. With this information the feasibility of an optically excited memory can be obtained. Optical pumping, to effect a magnetic moment change, provides an optical memory accessing technique not limited by lattice structure thermal properties of the material.

In general, Phase I involves both experimental and theoretical efforts. Theoretically we are developing the techniques to determine transition probabilities involved in optical pumping. This work permits evaluation of the significant material parameters affecting the transitions of interest. The experimental program is essentially subdivided into the areas of fundamental and functional measurements. The first area involves study of the transmission, reflection and emission properties of the material. Functional tests are directed toward measurements of coercive force and magnetization as a function of optical pumping.

Theory

An effort to calculate transition probabilities for induced absorption in the rare earths has been undertaken with the hope of gaining some understanding of the processes involved in optical writing, and with the

intent of having a basic reference with which to compare experimental measurements. To illustrate what is involved in these calculations, we present a brief description of the important features of the absorbing system, and discuss which features are important to the present application.

We consider a rare earth ion situated in a crystal lattice and subjected to an external radiation field. The Hamiltonian for such a system, in the central field approximation, consists of five principle parts.

$$\mathcal{H} = \mathcal{H}_{cf} + \mathcal{H}_{es} + \mathcal{H}_{so} + \mathcal{H}_{L} + \mathcal{H}_{R} \quad .$$

The first two terms are due to the central field and the electrostatic repulsion between atomic electrons, respectively. These two terms represent, for the Lanthanide series, the basic zero order Hamiltonian, and the principle correction to the atomic energy levels. In a calculation involving only these two terms, the total orbital angular momentum L^2 and the total spin angular momentum S^2 are diagonal, and the appropriate coupling between atomic electron is Russell-Saunders.

The third term in the Hamiltonian is the spin-orbit coupling and it does not commute with either L^2 or S^2. Consequently, with its inclusion, the appropriate electronic coupling is no longer Russell-Saunders, but intermediate. In the rare earths, energy splitting produced by this term is small compared to the electrostatic repulsion term, and the departure from Russell-Saunders coupling is not large.

The fourth term in the Hamiltonian is the lattice, or crystalline potential. Its form depends on the symmetry character of the crystal lattice, and its effect on the atomic system is to introduce configuration mixing; in which case the parity of the atomic states is no longer pure, and previously forbidden transitions become allowed. The energies of splitting associated with this term are generally much smaller than those of either the electrostatic or spin-orbit splittings.

The fifth term represents the external radiation field responsible for induced absorption.

Experimental evidence indicates that the principle contribution to the line spectra of the rare earths in crystals comes from electric dipole

transitions within the 4f shell of the atom. Such transitions are strictly parity forbidden unless one includes the lattice contribution in the Hamiltonian. In our particular application, we are interested specifically in "spin-flip" transitions in which the S quantum number changes by at least one unit. Such transitions are observed in the rare earths, and to account for them theoretically, it is necessary to include the spin-orbit term in the Hamiltonian.

Present State-of-the-Art

Calculations have appeared in the literature in which the energy levels for the Hamiltonian:

$$\mathcal{H}_{ef} + \mathcal{H}_{es} + \mathcal{H}_{so} \tag{1}$$

have been computed for the Lanthanide rare earths. These calculations can not be directly applied to our problem since the transitions of interest depend on the inclusion of the crystalline term $\mathcal{H}_L$. There are calculations in the literature which treat the lattice term in the approximation:

$$\mathcal{H} = \mathcal{H}_{cf} + \mathcal{H}_L \tag{2}$$

These approximations, however, do not include the spin-orbit coupling term responsible for the spin-flip transitions. Consequently, the calculations involved in our problem may proceed in either of two ways. First, we may use the states defined by (1) to compute matrix elements of $\mathcal{H}_L$. The states defined by diagonalization of this matrix will then be used to compute the transition matrix elements of $\mathcal{H}_R$. Second, we can use the states defined by (2) and compute matrix elements of $\mathcal{H}_{so}$. Diagonalization then yields the appropriate states for the transition matrix calculation.

Either of the procedures mentioned will probably require extensive application of Group techniques, and the diagonalization will require the use of a computer. Once the calculational procedure has been established, it can probably be applied to all useful members of the Lanthanide series without excessive alteration.

Experimental

The basic optical facility for measurement of reflectivity, transmission and emission became operational over this period and some initial reflectivity data obtained on GdIG. The sample presently being evaluated was obtained from Bell Telephone Laboratories, and little is known of its fabrication history. A larger sample is being prepared from a 1 cm diameter single crystal obtained from the IBM Thomas J. Watson Research Lab. This crystal was grown by an improved PbF_2 flux technique. Our own crystal growing facility is not yet in operation; however, it is anticipated that significant strides toward that goal will be made during August.

A diagram of the optical measurement test facility is shown in Figure 1. For reflection data the arrangement of apparatus is as shown in the figure. For transmission measurement the sample holder is rotated so the sample is perpendicular to the light beam from the monochrometer. Additionally, the light pipe is rotated clockwise to intercept the transmitted beam. Finally, for emission measurements a second monochrometer is mounted at the auxiliary port with the PM tube attached to its output aperature. The sample is rotated so that maximum emitted light is intercepted at the auxiliary port. In this mode of operation optical pumping is affected by monochromatic light emanating from the Gaertner monochrometer and the emitted photon spectrum is analyzed via the monochrometer and photo multiplier tube at the auxiliary port.

A plot of the reflection spectra for the GdIG sample presently being tested is shown in Figure 2. This data covers a range not previously published, i.e., above 1.5 ev.[1] However, it does not cover the range of major interest to us, namely, 3.5 ev to 5 ev. It is within this region that the electronic transitions of gadolinium take place. The data is limited to 3.5 ev because of optical absorption due to a Glann-Thompson polarizer at the output of the monochrometer. This is being removed and unpolarized data will be taken over the entire range from 2.0 ev to 5.0 ev during the following period. No attempt to correlate the structure observed in this data with optical transitions has yet been made. The data is, however, reproducible and it is believed to indicate Fe electronic transitions.

---

1 Wood and Remeika, "Effect of Impurities on the Optical Properties of Yttrium Iron Garnet," J. Appl. Phys. 38, 1044 (1967).

The MSFC Faraday apparatus has been set up and is operating. In order to adapt the equipment to perform measurements of $\mathcal{H}_c$ it has been found necessary to redesign the Helmholtz drive coils and this is presently in progress. Additional optics will also be required to insert the pumping beam but no other additions should be necessary to perform the required measurements of this research program.

A preliminary Mössbauer experiment has been designed to test the sensitivity limitations of this method for detecting the small moment changes of optically pumped gadolinium iron garnet. In this experiment, spectra of FeS and Fe_2Cl_6 will be measured separately and in mixtures of different ratios. Since iron exists as Fe^{++} in FeS and Fe^{+++} in Fe_2Cl_6 the effects of a spin change in the 3d magnetic shell can be studied. Thus, in FeS the spin moment of the iron atoms will be four Bohr magnetons and in the Fe_2Cl_6 it will be five Bohr magnetons. By measuring the Mössbauer spectra of mixtures of these compounds it will be possible to determine if the two spin moments can be separately identified. By varying the ratios of the two compounds it will be possible to estimate the minimum population redistribution observable when optically pumping a sample of GdIG.

These experiments are easy to perform and permit us to estimate the sensitivity of the Mössbauer measurement before setting up the relatively complicated experiment with GdIG.

Future Work

During the following period reflectivity measurements up to 5 ev will be carried out in order to determine if the gadolinium electronic transitions do in fact occur. The crystal fabrication facility will be assembled. Work on the Faraday apparatus will continue with the goal of having an M-H facility operable by the next report.

Respectfully submitted,

F. L. Grismore
Project Director

FLG/srt

Approved:

E. J. Scheibner, Chief
Physical Sciences Division

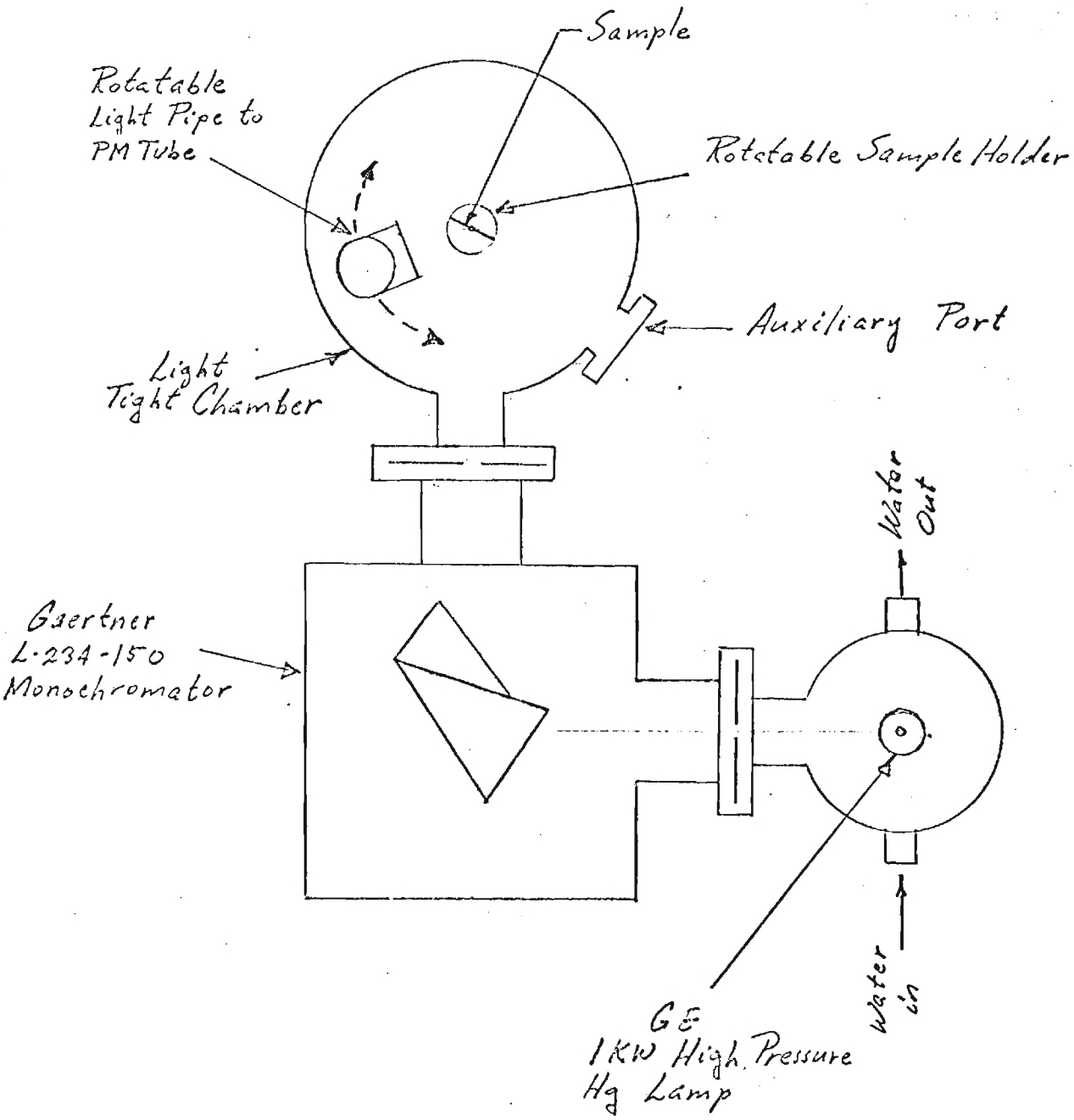

Figure 1 Sketch of Optical Measurements Facility

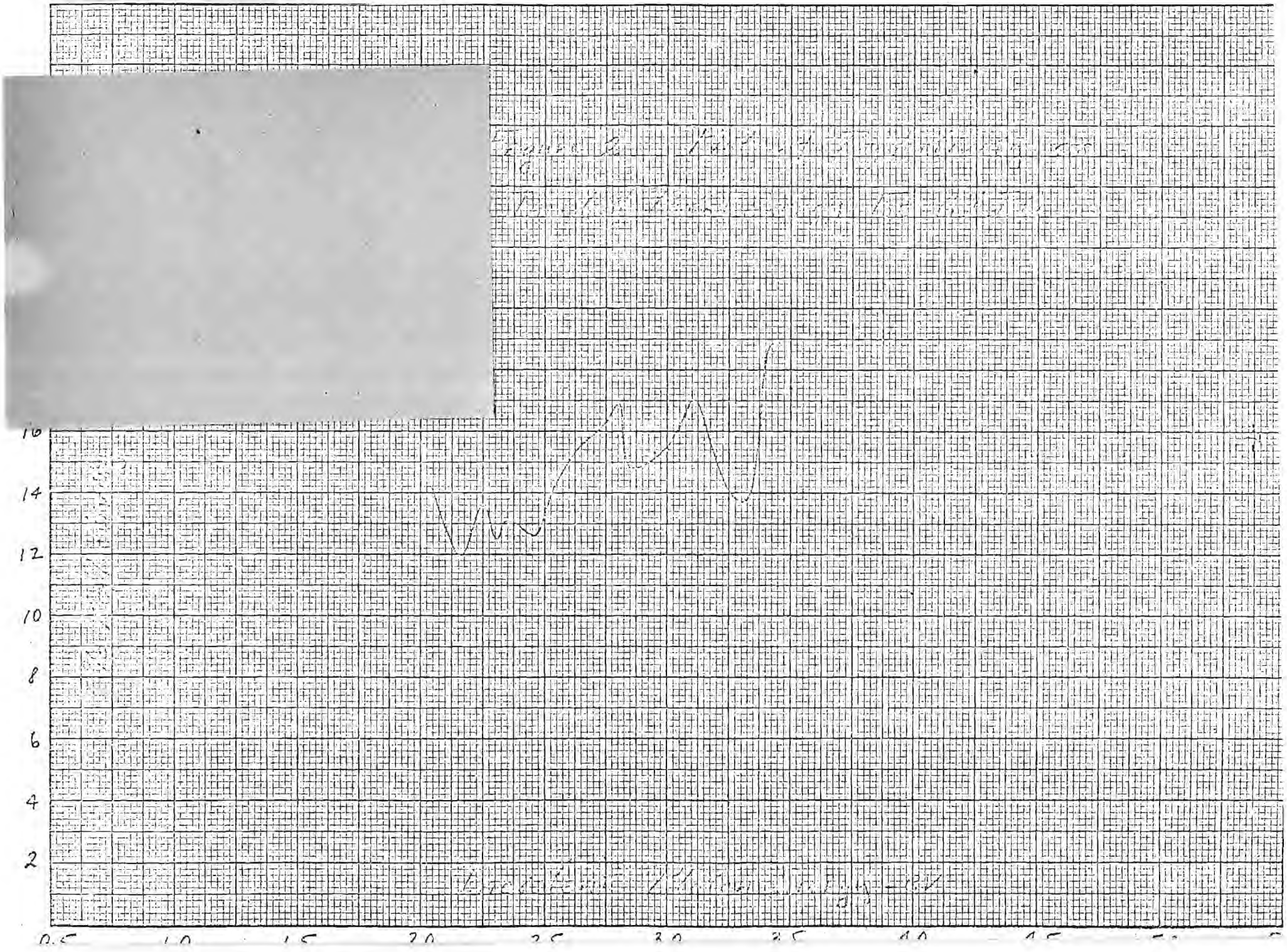
16
14
12
10
8
6
4
2

A-1028

ENGINEERING EXPERIMENT STATION
GEORGIA INSTITUTE of TECHNOLOGY

Physical Sciences Division
225 North Avenue N.W.
Atlanta, Georgia 30332
(404) 873-4211 Ext. 220

September 19, 1967

National Aeronautics and Space Administration
George C. Marshall Space Flight Center
Huntsville, Alabama 35812

Attention: Mr. William J. McKinney

Subject: Monthly Progress Letter 3, Project A-1028
"Study of Feasibility of Optically Exciting a Magnetic Memory"
Contract No. NAS8-20813
Covering the Period from 6 August to 12 September 1967

Gentlemen:

This report describes the work performed under Contract NAS8-20813 from August 6 to September 12, 1967. The purpose of this research is to study the feasibility of optically pumping a ferrimagnetic garnet to cause a change in magnetic moment.

The initial measurements phase is progressing nicely and initial reflection data is now complete. This is, to our knowledge, original data and will be submitted for publication in the future. Design of the furnace for crystal fabrication is now complete and parts are being ordered. Details of these phases of the program as well as others are included in the following paragraphs.

Optical Measurements

Reflection measurements have been completed over the photon energy range of 1.5 to 5.5 electron volts. The purpose of this data is to determine if the gadolinium electronic transition at 36×10^3 cm^{-1} can be detected. This is the absorption transition which populates the $^6P_{7/2}$ spin flip state of the gadolinium atoms. As previously discussed, transmission measurements are not possible in this energy range, on bulk samples, because of the high absorptions due to the band gap at about 2.5 electron volts.

The measurements were performed in the spectrometer shown in the last monthly report. The data for unpolarized incident light is shown in Figure 1. The term unpolarized here means only that there was no polarizing prism in the light path and hence we do not know the state of incident light polarization. The significant feature of this data is the very strong structure between 4.0 and 5.0 electron volts. Here we see a sharp peak at about 4.3 ev followed by a significant dip. Since four to five electron volts corresponds to 32×10^3 to 36×10^3 cm^{-1} it is highly likely that this structure is a result of the desired transition.

It is also found, by examining the classical model associated with an optical transition that the structure is qualitatively of the correct shape. For example, the material can be described in terms of a complex polarizability

$$\alpha = \alpha' - j\alpha'' \tag{1}$$

where α' is the conventional real polarizability and α'' can be shown to be σ/ω and corresponds to an absorption process. The conventional complex index of refraction N is then describable in terms α' and α''. The real and complex parts of N are given as

$$N = n - jk \tag{2}$$

and since it can be shown that

$$N^2 = \left[(1 + 4\pi\alpha') - j\,(2\sigma/V) \right] \tag{3}$$

where V is the frequency of the radiation, then

$$n^2 - k^2 = 1 + 4\pi\alpha'$$

and (4)

$$nk = 2\pi\alpha'' \ .$$

Similar relationships exist between n and k and the complex dielectric constant components ϵ' and ϵ''. Finally, since α'' corresponds to a loss phenomena it can be related directly to the conventional absorption coefficient η where η is defined according to the relationship

$$\bar{w} = \bar{w}_o e^{-\eta x} .$$

Here $\bar{w}$ corresponds to the radiation energy density at any point x within the material and $\bar{w}_o$ is that value at the surface. The equation relating η and α'' is simply

$$\eta = \frac{8\pi^2}{\lambda} \cdot \alpha'' \qquad (5)$$

where λ is the radiation wavelength in free space.

The reflection from the air-garnet interface can be expressed in terms of n and k and this relationship is given by the Fresnel equations. A detailed description of this classical derivation can be found in P. Drude, "The Theory of Optics." Since the reflection coefficient $R = f(n, k, \theta)$, then given two values of R at different known values of θ it is possible to solve for n and k. Knowing n and k, equations (4) are used to find the real and imaginary components of the polarizability. Equation (5) yields the absorption coefficient once α'' is known. This computation can be repeated for different incident energies yielding the desired data of absorption coefficient versus wavelength.

We expect the gadolinium to cause a peak in absorption at the critical energy of approximately 4.5 electron volts. As this energy is approached from the low side the real component of α associated with this transition increases to a positive maximum then falls rapidly through zero to a negative maximum then decreases towards zero. Over this same energy range the imaginary component α'' starts at zero and reaches a positive peak at the same energy where α' passes through zero. For increasing energy it then

decreases monotonically to zero. Using this qualitative structure in conjunction with the Fresnel reflectivity expression one then predicts a peak in reflectivity at the energy where maximum α' occurs followed by a dip as α'' becomes larger than $1/4\pi$. This is only a qualitative characterization based on the Fresnel equation at $\theta = 0$, i.e.,

$$R = \frac{(n-1)^2 + k^2}{(n+1)^2 + k^2}$$

and in general the reflectivity varies significantly with angle and polarization. It is however interesting to note that this is the characteristic strongly present in the 70° reflection measurement using unpolarized light.

The same characteristic is observable in the 4 - 4.5 electron volt interval in Figures 2 and 3. These data correspond to light polarized parallel to the plane of incidence. Figure 4 however exhibits a significantly different characteristic in this energy range. This is possibly due to the fact that 70° is very nearly equal to the Brewster angle for this material.

Little additional information is available from this raw data at present. A computer program has been written to convert the data to values of n and k as a function of energy. From these the absorption coefficient can be determined. The program is about 90% debugged at the present time. Detailed information obtained from this analysis will be given next month but it appears now that the desired transition is observable and that the included data is the first to indicate this.

The optical facility is currently being set up to perform an emission experiment on the garnet. In this test, the garnet is optically pumped with monochromatic light and the emitted light from the sample is scanned with an analyzing monochrometer. Initial data has already been obtained but no reportable conclusions can be made until it has been studied in detail.

The Faraday apparatus from MSFC has been equipped with a new set of drive field coils so that steady state M-H loops can be made at 60 Hz. It

is now possible to take H_c and relative M_r data versus temperature for garnet samples. The signal to noise ratio is very good and data obtained is reproducible.

Crystal Growing

Several furnace designs have been considered for producing the highly controlled 1300°C temperature necessary to grow single crystal samples. We have tentatively fixed the design using a glow bar approach and component parts are now being ordered. The platinum crucible required is also ordered. A target date of November 15 for crystal growing capability has been set.

Theoretical

No details of the theoretical analysis of transition probability calculations can be made at this time. The required calculations are being formulated and crystal field parameters and spin orbit coupling parameters have been obtained from the literature. This work will also require a computer program to be written.

Future Work

Major effort during the next reporting period will be devoted to analyzing the reflection data incorporated in this report and to obtain and analyze the emission experiment data.

Respectfully submitted,

F. L. Grismore
Project Director

FLG/brj

Approved:

E. J. Schaibner, Chief
Physical Sciences Division

A-1028

ENGINEERING EXPERIMENT STATION
GEORGIA INSTITUTE of TECHNOLOGY

ıysical Sciences Division
225 North Avenue N.W.
Atlanta, Georgia 30332
(404) 873-4211 Ext. 220

6 November 1967

National Aeronautics and Space Administration
George C. Marshall Space Flight Center
Huntsville, Alabama 35812

Attention: Mr. William J. McKinney

Subject: Monthly Progress Letter 4, Project A-1028
"Study of Feasibility of Optically Exciting a Magnetic Memory"
Contract No. NAS8-20813
Covering the Period from 12 September to 12 October, 1967

Gentlemen:

This report covers the work performed under Contract NAS8-20813 from September 12 to October 12, 1967. Efforts during this period have been directed toward experimental observation of the optical pumping phenomena yielding a change in the magnetic moment of GdIG. The experiments performed have been purely optical in nature because of the significant amount of information attainable with relatively simple hardware.

Reflectivity and fluorescence measurements have been carried out on a sample of gadolinium iron garnet. As a result of these measurements we have determined the complex index of refraction for this material in the 3 ev to 5 ev range. We have also identified a characteristic electronic absorption at approximately 4.2 ev which might be associated with the desired gadolinium transition. This appears to be data not yet reported in the literature. The fluorescence measurements, designed to detect radiative emission from excited rare earth atoms has not, however, confirmed the existence of the excited state.

Mössbauer spectra have been obtained for Fe^{++} and Fe^{+++} in the compounds Fe_3O_4 and Fe_2O_3. Although detailed analysis is not yet complete it appears that detection of the small volume fraction of optically pumped gadolinium would be extremely difficult.

Design of the oven and temperature controller for crystal fabrication is now complete. Parts have been ordered and some initial fabrication begun. The oven will be used to grow samples of dysprosium and terbium iron

garnets. These rare earths exhibit a transition energy of the 4-f electrons lower than gadolinium. In addition, they appear, from spectroscopic data, to have significantly larger absorption cross-sections.

Optical Measurements

The computer program for calculating complex index of refraction from reflection data has been debugged and is completely operable. We have used this program to calculate n and k, the real and imaginary components of the refractive index for a GdIG sample. In addition, the program calculates the absorption coefficient from the values of n and k.

Figures 1 through 3 show the reflection data obtained from the sample under test. Reflectivity was measured at three angles of incidence, i.e., 70°, 45°, and 20°. The calculated absorption coefficient is shown in Figure 4. Note the broad peak observed around 4.2-4.3 ev. This is the approximate energy of the prominent 4-f transitions of gadolinium. The separate peak occurring at 3.8 ev, however, is at too low an energy to be associated with the rare earth.

We observe an absorption coefficient of 6.5×10^5 cm^{-1} to 7×10^5 cm^{-1} in the energy range of 3.7 ev to 4.7 ev. It is interesting to compare this with data reported recently by MacDonald, Vogeli, and Mee, J. Appl. Phys., Sept. 1967, page 4101. They plot optical density, i.e., $\log_{10} I_0/I$ versus photon energy and show a relatively flat plateau between 32×10^3 cm^{-1} and 40×10^3 cm^{-1} (4 ev to 5 ev). At lower energies the absorption decreases rapidly and at higher energy it increases rapidly. Our data agrees essentially with this structure although ours falls off for energy lower than 3.7 ev and rises at energies above 4.7 ev. Their plateau, therefore, is shifted about 0.3 ev toward higher energy. Employing their reported sample thickness of 0.1 micron, one can calculate the absorption coefficient for the published data. The result is $\alpha \approx 3 \times 10^5$ cm^{-1}. This is lower than our value of 6.5×10^5 cm^{-1} by a factor of two. The agreement is in general quite reasonable considering the fact that their measurements were made by transmission through a polycrystalline garnet film and ours were made by reflection on a bulk single crystal specimen.

The data reported by MacDonald et al is on such a scale that detailed structure in the 4 ev to 5 ev range is not determinable. However,

they do give data of circular birefringence vs. energy which shows a large peak at 33×10^3 cm^{-1} (4.1 ev). This is very close to the transition we observe at 4.3 ev shown in Figure 4. They attribute the large Faraday rotation at 33×10^3 cm^{-1} to Fe^{+++} ions; however, no justification for this assignment is given.

We can conclude there is reasonable evidence that the data reported here is correct and that the absorption peak at 4.3 ev does exist. Whether it is due to Gd^{+++} or Fe^{+++} is, however, not yet clear. Figure 5 shows plots of n and k as a function of photon energy. Note the shape of the curves are consistent with a broad transition frequency around 4.2 ev or 4.3 ev. In general, the magnitude of n is approximately 2 and that of k approximately 0.9.

There are two factors associated with the absorption peak under discussion which leads us to believe it may not be caused by the gadolinium. The first is that the width of the absorption peak is much larger than would be expected for the 4-f transitions of rare earth ions. From Gandy and Ginther (Appl. Phys. Lett., Vol. 1, No. 1, 1962) a half width of 0.1 ev might be anticipated for gadolinium. We observe a width of approximately 0.4 ev. Secondly, the absorption cross-section as estimated from the absorption data is much larger than Gandy and Ginther (op. cit) report for gadolinium doped glass. From Figure 4 it seems reasonable to approximate the "excess" absorption associated with the peak at 4.2 ev as no less than 0.5×10^5 cm^{-1}. The absorption cross-section is defined as:

$$dN = \sigma_a N \rho dx$$

where

N = incident photon density in photons/cm^2

ρ = volume density of absorbing atoms

σ_a = absorption cross-section per atom.

Thus the quantity $\sigma_a \rho$ is equivalent to the absorption coefficient and

$$\sigma_a = \frac{\alpha}{\rho} \text{ cm}^2/\text{atom} \quad .$$

The volume density of gadolinium atoms in GdIG is approximately 9×10^{21} atoms/cm^2. The resulting cross-section then becomes

$$\sigma_a = \frac{0.5 \times 10^5}{9 \times 10^{21}} = 5 \times 10^{-18} \text{ cm}^2 .$$

This is at least 3 orders of magnitude greater than the values measured for gadolinium by Gandy and Ginther.

If the gadolinium absorption is as large as 5×10^{-18} cm^2 then it should be detectable by a fluorescence measurement. Such an experiment was carried out with negative results. In this experiment the sample was pumped with light from the 1 kw mercury arc lamp described in previous reports. The light was monochromated by transmission through two cascaded quartz prism monochrometers in order to eliminate spurious photon energies. A third analyzing monochrometer viewed the sample surface at an angle approximately 10° removed from the angle of incidence. Pumping photon energy was varied in discrete overlapping steps and at each step the analyzing monochrometer was scanned from the pump energy to about 1 ev. We were unable to observe any fluorescent emission in any of these runs.

Evaluation of the sensitivity of this experiment indicates that conversion cross-sections of 5×10^{-18} cm^2 would produce photon flux at least an order of magnitude above the noise level. However, for cross-sections as small as those reported by Gandy and Ginther the emission would not be detectable. The main source of low sensitivity is the result of a rapid decrease in light output from the mercury lamp at wavelengths below 280 milli microns. It is believed that this is the result of absorption by the cooling water. To overcome this problem an air colled lamp assembly is being constructed. From measurements made on the original source it is estimated that this will increase the light output by a least 2 orders of magnitude.

The problems of employing GdIG for optically pumping are associated with the fact that there are very large competing absorption processes which "rob" incident photons. These are apparently phonon producing processes and hence raise the garnet temperature. This is the very process we want to avoid. In order to find a more suitable material we are now

directing efforts toward the preparation and evaluation of Dy and Tb iron garnets. Primary efforts for the following two months will be directed toward completing the crystal growing facility.

Respectfully submitted,

F. L. Grismore
Project Director

FLG:srt

Approved:

E. J. Scheibner, Chief
Physical Sciences Division

Report of Budget as of October 1

Personal Services	Budget	$17,537.00
	Expended	6,610.00
Materials and Supplies	Budget	1,950.00
	Expended	741.64
Travel	Budget	300.00
	Expended	82.41
Overhead	Budget	9,996.00
	Expended	3,768.15
Total	Budget	29,993.00
	Expended	11,203.05
	Free Balance	$18,789.95

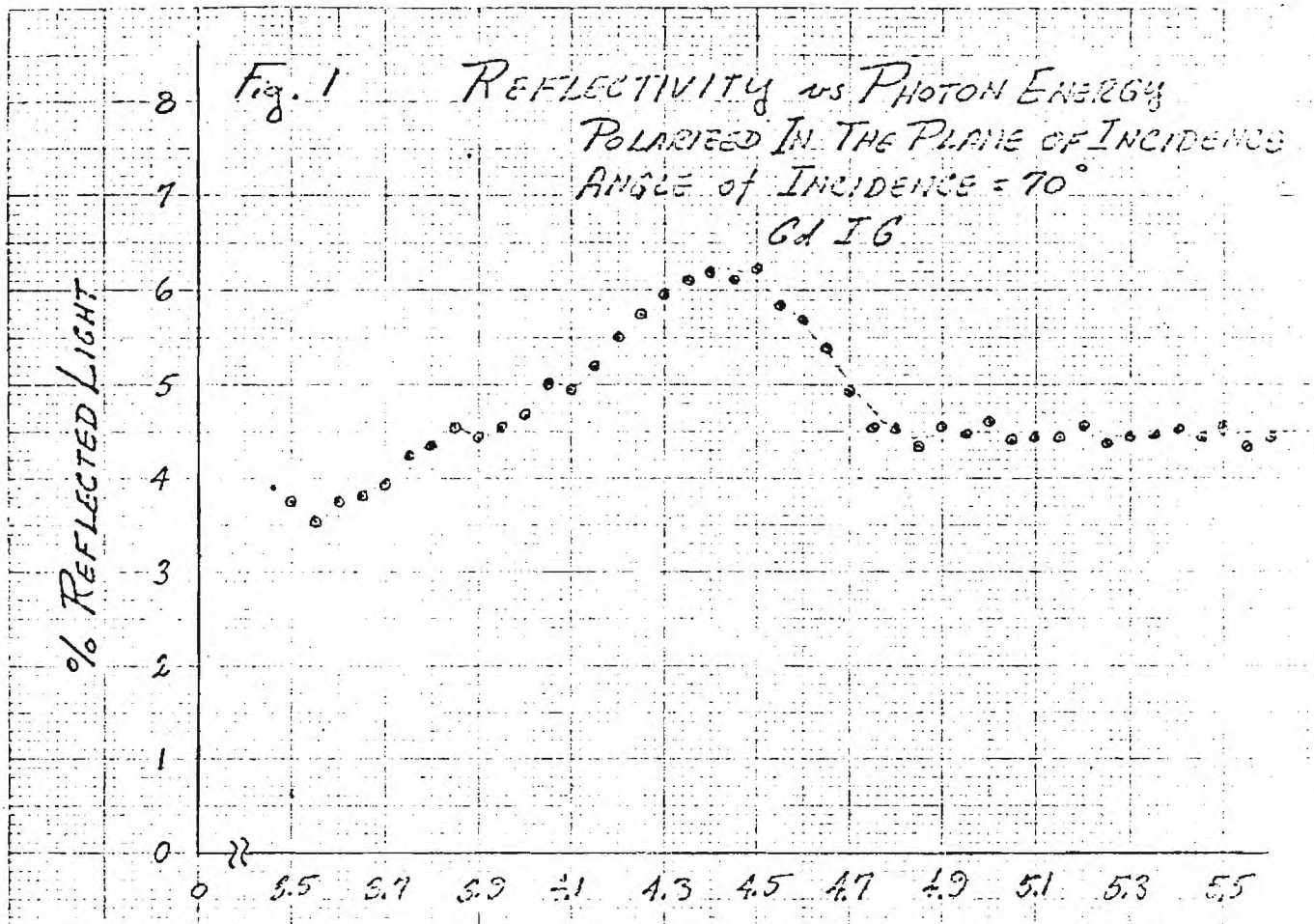

Fig. 1 Reflectivity vs Photon Energy
Polarized In The Plane of Incidence
Angle of Incidence = 70°
Cd I G

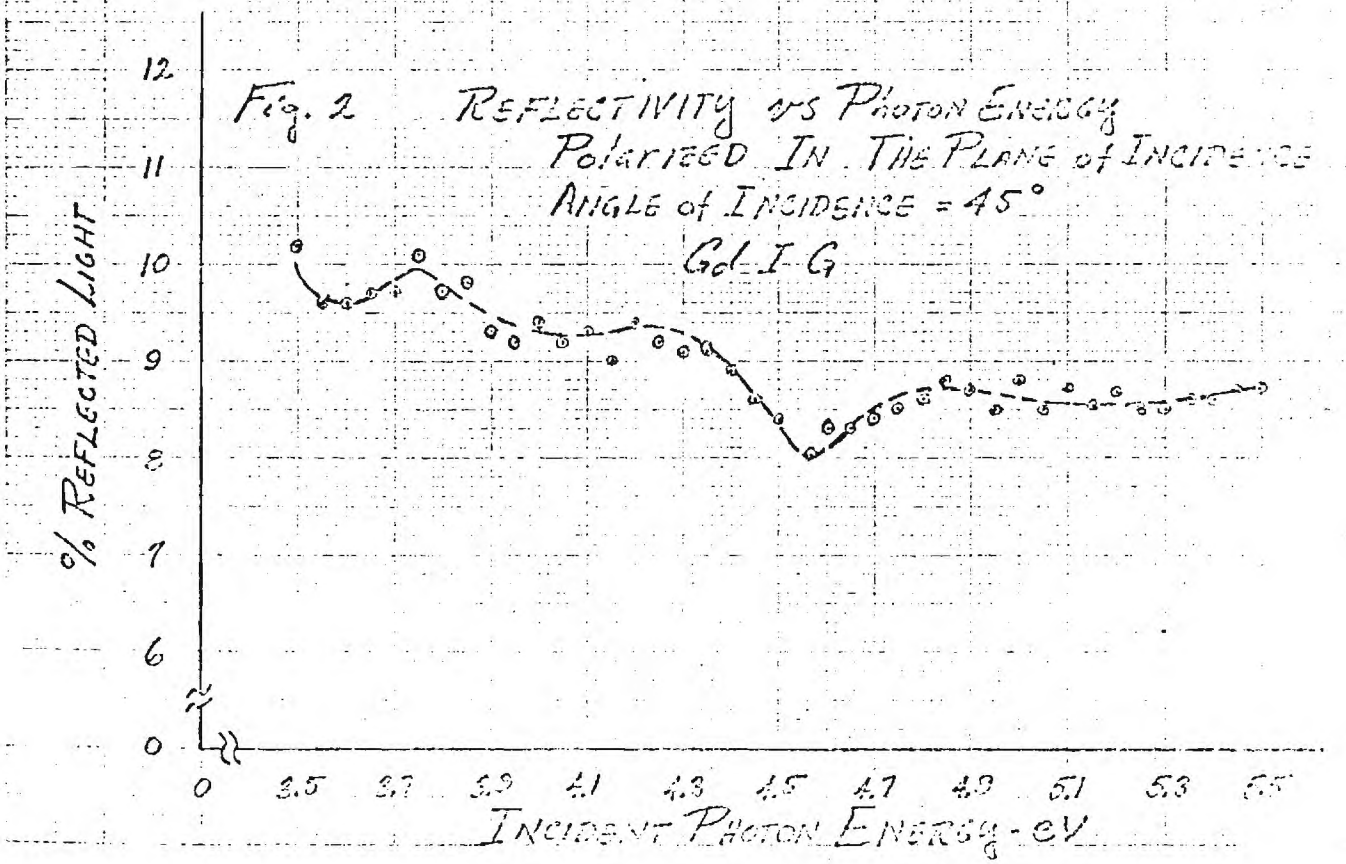

Fig. 2 Reflectivity vs Photon Energy
Polarized In The Plane of Incidence
Angle of Incidence = 45°
Cd I G

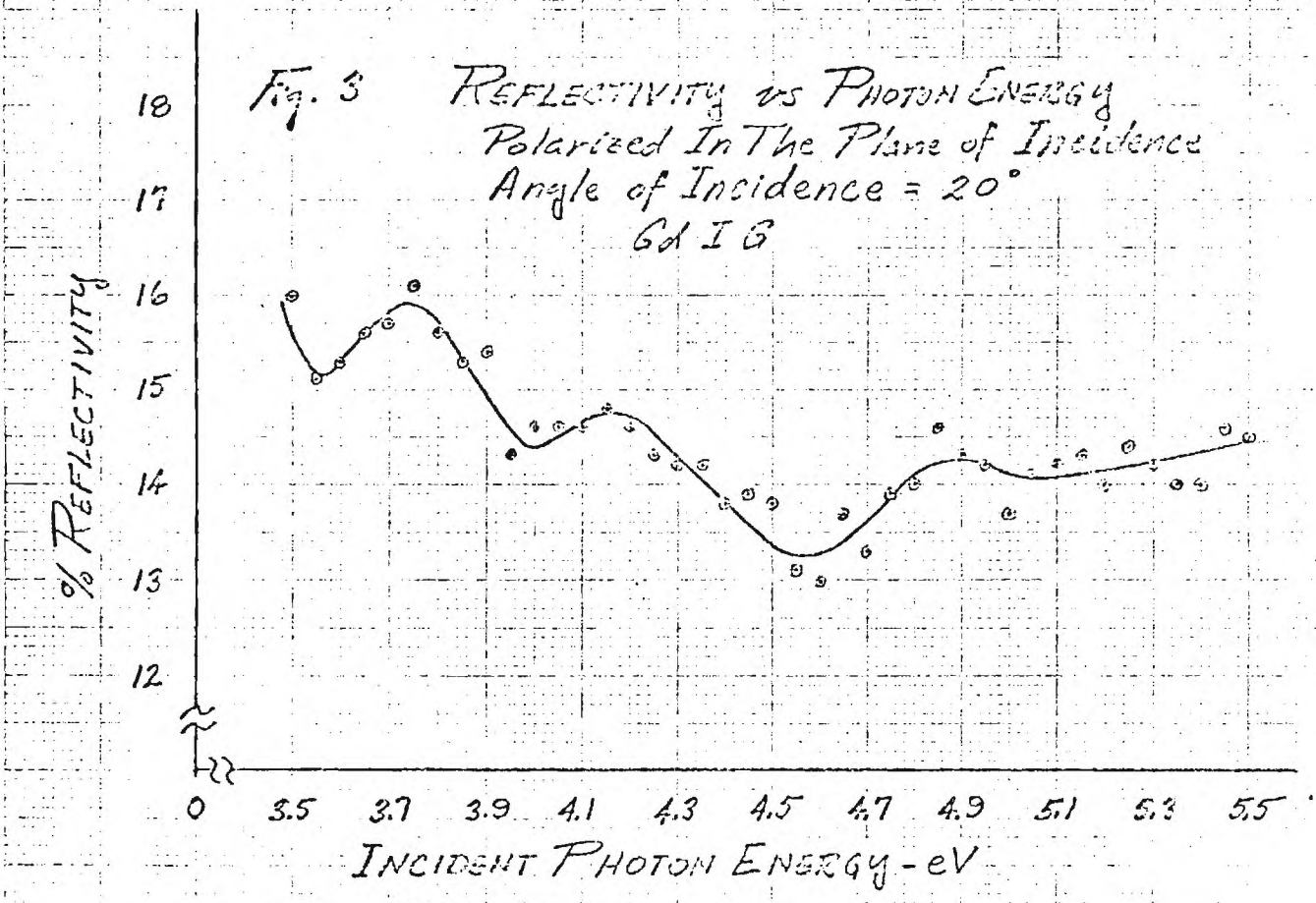

Fig. 3 Reflectivity vs Photon Energy
Polarized In The Plane of Incidence
Angle of Incidence = 20°
GdIG

Fig. 4 Absorption Coeff. vs Photon Energy

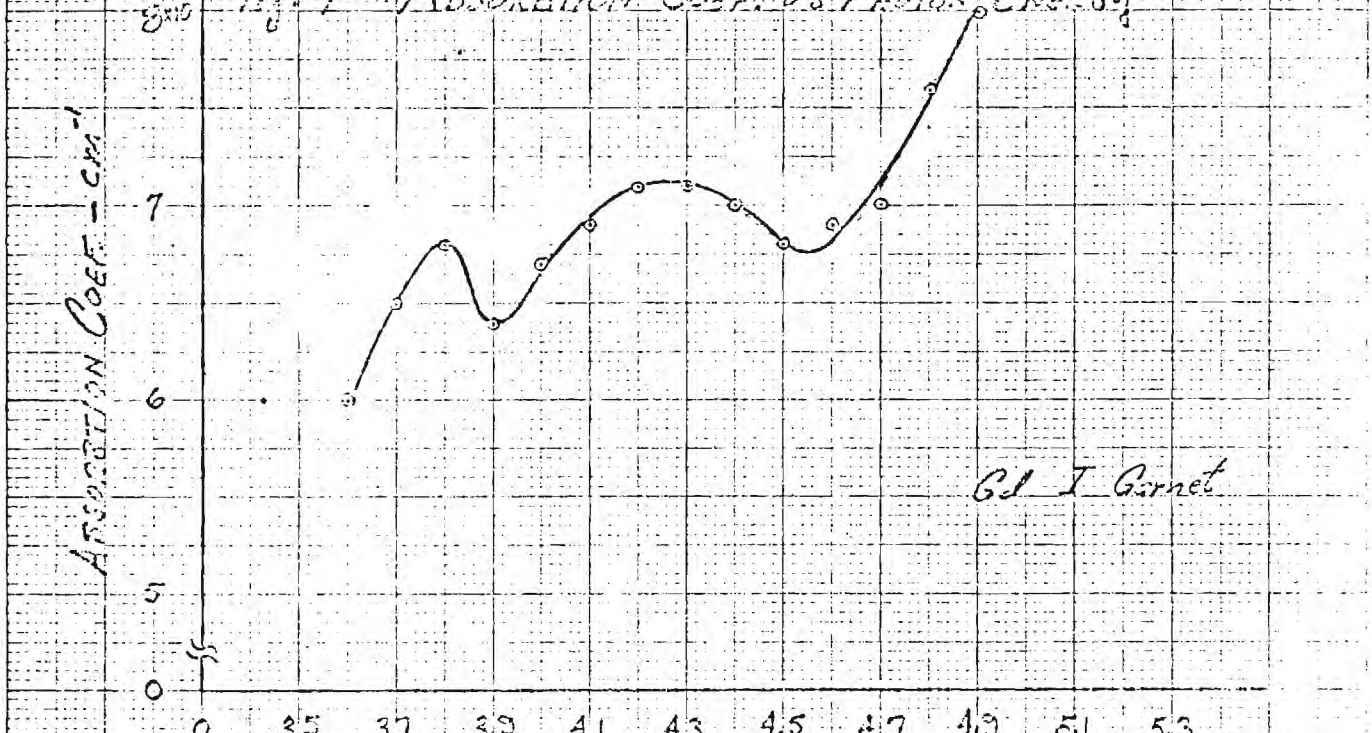

Fig. 5 Complex Index of Refraction vs Photon Energy

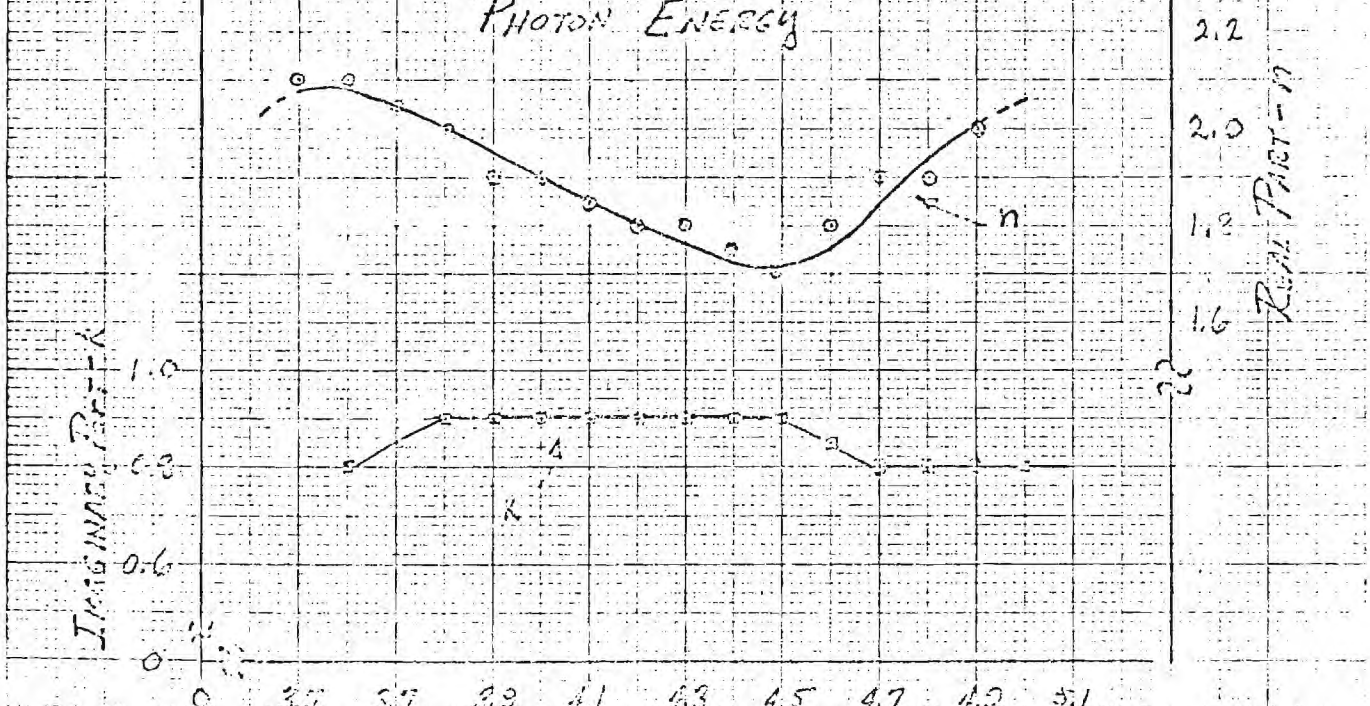

A-1028

ENGINEERING EXPERIMENT STATION
GEORGIA INSTITUTE of TECHNOLOGY

Physical Sciences Division

825 North Avenue N.W.
Atlanta, Georgia 30332
(404) 873-4211 Ext. 220

30 November 1967

National Aeronautics and Space Administration
George C. Marshall Space Flight Center
Huntsville, Alabama 35812

Attention: Mr. William J. McKinney

Subject: Monthly Progress Letter 5, Project A-1028
"Study of Feasibility of Optically Exciting a Magnetic Memory"
Contract No. NAS8-20813
Covering the Period from 12 October to 12 November 1967

Gentlemen:

This report covers the work performed during the period of October 12 to November 12. The work is continuing in Phase I of the above listed contract. This is a 9 month phase for determining the feasibility of optically pumping a ferrimagnetic material to effect a change in the magnetic moment. Such a change, occurring with the ferrimagnet temperature biased to its compensation point, causes a change in coercive force which can be exploited for memory applications.

As mentioned in previous letters, the initial work on GdIG has provided a great deal of insight into the required material properties for such an effect to occur. First, one of the magnetic sublattices must be formed from an element which fluoresces under optical pumping. In addition, the lifetime of the meta-stable state from which the fluorescing transitions occur must be short enough for practical memory applications but long enough to keep required pumping power acceptable. Values of $10^{-6} \leq \tau \leq 10^{-4}$ seconds are reasonable for initial work.

The rare earths gadolinium, terbium, and dysprosium satisfy these requirements. However, it has been shown that the energy level of the fluorescing meta-stable state of gadolinium is significantly higher than the band gap of gadolinium iron garnet. Thus, nearly all incoming photons are absorbed in the process of creating hole-electron pairs and these recombine through phonon generating processes. Little, if any, optical pumping of the gadolinium occurs and the desired effect is not observed.

There are, however, other materials which offer promise of overcoming these limitations and work is now being directed toward fabricating facilities to obtain samples of them. We are concentrating initially on dysprosium iron garnet since dysprosium has a spin flip meta-stable level near the band gap edge. The furnace for fabricating these crystals has been completed during this period and initial manual controlled runs have shown it will easily attain a temperature of 1300°C, quite adequate for the conventional lead flux technique of growing these crystals. The attached photograph shows the oven and power supply. The oven chamber is a vertical tube 2-3/4" inside diameter and 8 inches long. The element is a commercially available coiled strap heater manufactured by Kenthal Corporation. The element is shielded by a ceramic outer liner and the whole assembly is then mounted in the steel shell housing. The element is rated at 1.5 KW at a maximum voltage of 28 volts RMS. In the photograph the platinum crucible is shown positioned on the alumina hearth which can be raised vertically into the tube. In the growing process the appropriate oxides are sealed in the crucible and brought to a molten state at approximately 1250° C. The temperature is then lowered very slowly in a controlled manner at approximately 1°C per hour. At 900°C the hearth is lowered and the melt allowed to cool rapidly to ambient temperature.

A digital controller has been designed in our laboratory to automatically regulate and sequentially decrease the temperature of the oven. A block diagram of the controller system is shown in Figure 1.

This unit will regulate to ± 0.5°C and uniformally decrease the temperature over any selectable 400°C range. The particular 400°C range is selected by adjusting the regulated bias voltage in series with the thermocouple voltage. The net voltage of this series group is amplified by a chopper stabilized amplifier. This temperature dependent voltage is then converted to a pulse width by the ramp generator and coincidence detector.

Operation of this conversion is similar to that employed in many digital voltmeters. When the control logic activates the ramp "gate" line a controlled voltage-time ramp is started. The coincidence detector output jumps to logical 1 as the range passes through zero volts and remains up until the ramp passes through the temperature dependent amplified

voltage level. Thus, higher temperatures result in larger pulse widths.

The pulse width from the coincidence detector activates a gate which transmits pulses from a crystal controlled oscillator. Each pulse increments the A register count by one unit. At the end of this counting period the control logic activates the gate line to the detector circuit and the accumulated count in the A register is compared with the reference count stored in the B register. If A < B a signal is sent to the triac control rectifier which subsequently allows one full cycle of 60 cps line voltage to be applied to the heater supply transformer.

The system is in essence an on-off feedback controller where the reference level is a binary number stored in the B register. This register is initially set at maximum count and if unchanged the temperature would regulate to a constant value associated with that count, (determined by the level of the regulated bias) for example 1250°C. This reference level is, however, incremented down one count every 32 minutes by the 1 revolution per minute synchronous motor activating a micro switch. The 32:1 binary scaler produces an output transition once every 32 minutes. The gain of the system is adjusted to correspond to 0.5°C per binary increment and hence the rate of controlled temperature decrease is approximately 1°C per hour.

The sequence of sampling and gating takes place once every cycle of the line supply current and so a decision is made every 1/60th of a second as to activate or not activate the heater current during the next complete cycle. Power is supplied to the heater in single, complete cycle, increments. Since this is a short time period compared with the thermal time constant of the oven, control is essentially continuous.

The controller is being fabricated from RTL integrated logic modules on one printed circuit board is complete and populated. It is anticipated the complete system will become operational during the next reporting period.

In an effort to obtain a greater amount of information concerning excitation processes of the gadolinium atom in GdIG, an electron beam pumping experiment was initiated during this month. Of the wide variety of possible pumping techniques, photon and electron beam processes are the two most likely to have practical applications in memory systems. Recently

RCA reported achievement of ultra violet lasing action using zinc oxide pumped by electron beam bombardment. Lasing action occurred at an accelerating voltage of 15,000 to 20,000 volts and a current density of 3 amp/in^2. Fluorescence, however, occurred at much lower pumping density. They estimated that each incident electron excited 10^3 atoms in the zinc oxide.

Our experiment was designed around the Acton MS-64 electron microprobe apparatus. This instrument provides a scanning electron beam of controllable incident energy and current density. The viewing optics integral to this machine are of the reflecting type except for the eyepieces and vacuum port. The vacuum port was replaced by a quartz, optically flat window. The normal binocular eyepiece assembly was removed and fixturing designed so that the Gaertner monochrometer could be mounted at the viewing port. Thus any fluorescence resulting from electron beam pumping is analyzed by the monochrometer and detected by a photomultiplier tube at the exit slit.

In initial experiments on the sample of GdIG used for our previous measurements accelerating voltage was adjusted between 9,000 and 25,000 volts. It was found that even at the low potential, damage to the garnet occurred. Optical microscopy revealed the path of the electron beam as small surface "bubbles" apparently resulting from actual melting of the material.

Strong fluorescence was observed at 3140Å which is probably due to the spin flip meta-stable $^6P_{7/2}$ state. However, this fluorescence could only be obtained at locations on the garnet surface where significant damage had previously occurred due to electron beam heating. It seems possible that in these regions agglomerations of gadolinium metal may have occurred and it was this, rather than the garnet, which produced the radiation.

The reason for the lack of detectable fluorescence in the bulk garnet is not clearly understood. Although the energy of incident electrons was too large for a 1:1 resonance transfer it was anticipated that multiple excitations would occur to absorb the energy as reported in the RCA work. However, it is possible that excitation occurred at such a depth of penetration that the resulting radiation was reabsorbed before reaching the surface. An approximate expression for the maximum depth of penetration

of an electron into a material is given as $R = \frac{E_o^n}{b}$ where

E_o = incident electron kinetic energy
b = constant proportional to density of the material
n = constant between 1.5 and 1.7

This is known as Schonland's formula. From the tables presented in Schonland's original paper (Proc. Roy. Soc., London, A104, 235-47 (1923)) the depth of penetration of the electrons at 18,500 volts accelerating potential would be expected to be 1.3×10^{-4} cm. This is approximately an order of magnitude greater than the optical skin depth we previously measured at 3140Å. Thus, if excitation occurs predominately at the depth of penetration for the electrons we could not observe the resulting fluorescence.

This experiment is being modified to permit pumping with lower energy electrons. In this new apparatus electrons from 1 ev to 1 Kev can be applied. Such energies will surely not damage the garnet. In this apparatus incident energies equal to the resonance of the gadolinium absorption level or multiples there of can easily be produced. This should provide a great deal of added information on the excitation processes.

Future Efforts

During the next reporting period efforts will be directed toward completing the crystal fabrication facility. In addition, the low energy electron pumping apparatus should be completed. Samples from the garnet material under test have been submitted to the analytical group for crystallographic and compositional analysis. This data should be available next month.

Respectfully submitted,

F. L. Grismore
Project Director

FLG:srt
Approved:

E. J. Scheibner, Chief
Physical Sciences Division

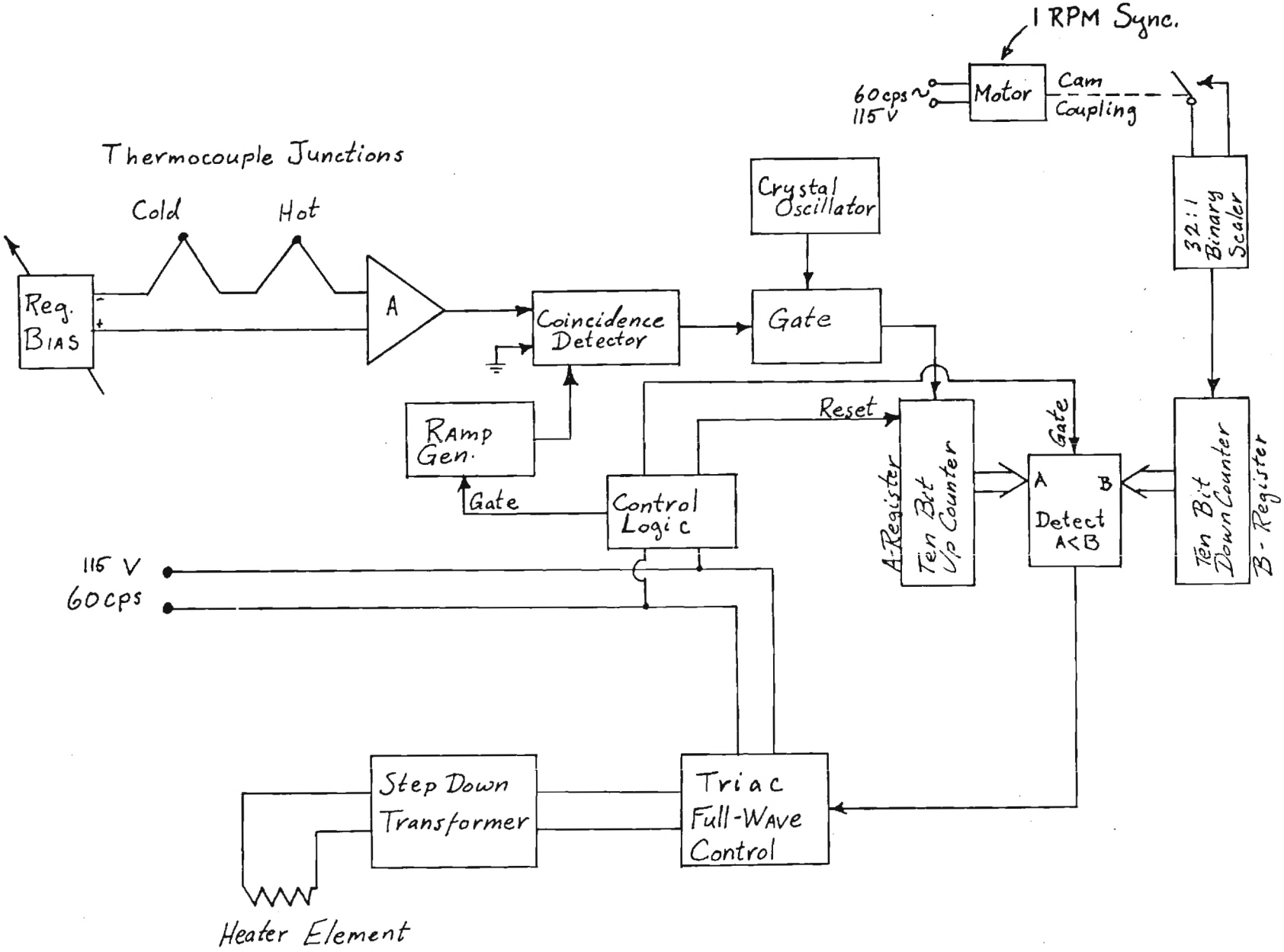

FIGURE 1 - CONTROLLER BLOCK DIAGRAM

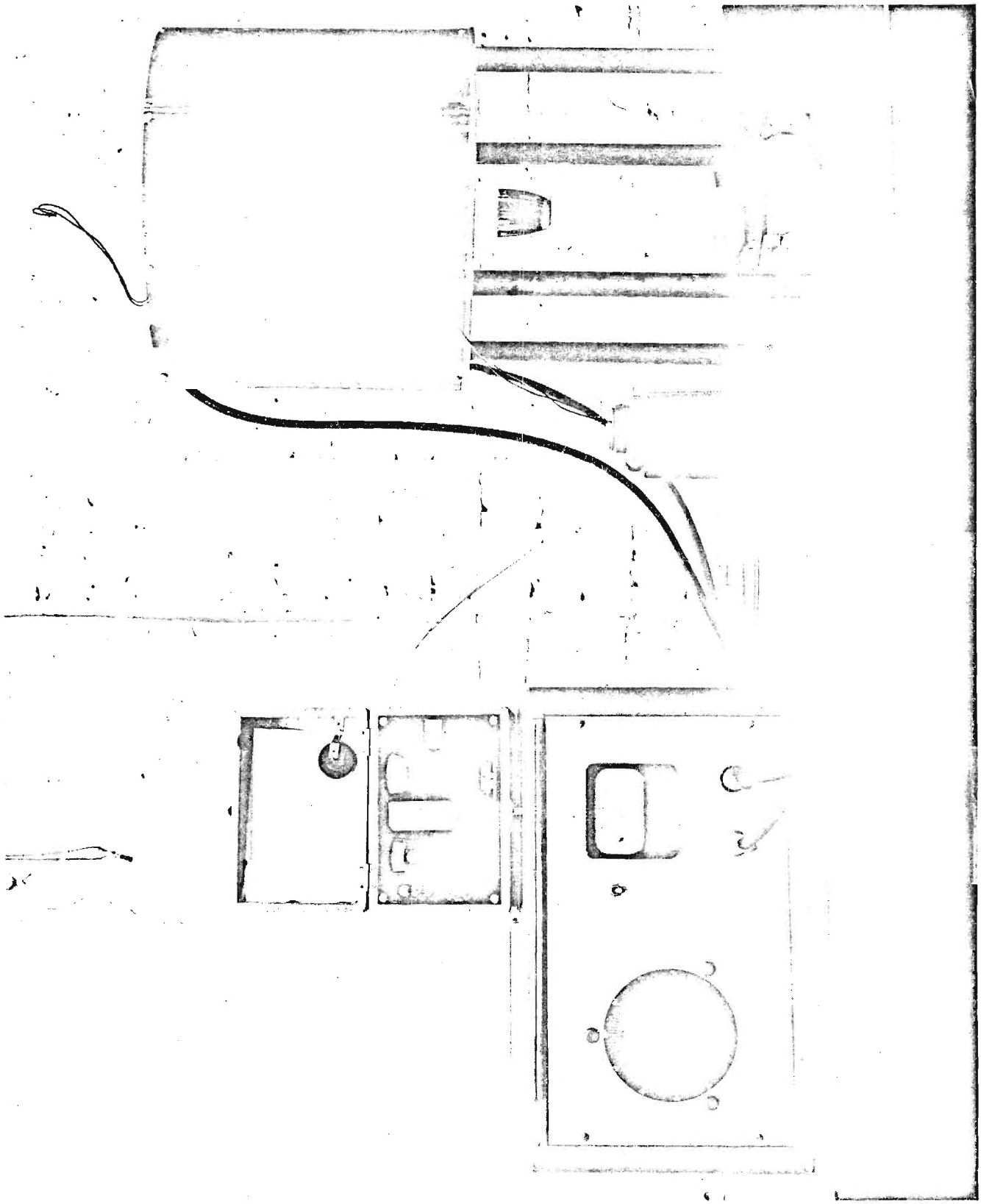

A-1028

ENGINEERING EXPERIMENT STATION
GEORGIA INSTITUTE of TECHNOLOGY

ıysical Sciences Division
225 North Avenue N.W.
Atlanta, Georgia 30332
(404) 873-4211 Ext. 220

5 January 1968

National Aeronautics and Space Administration
George C. Marshall Space Flight Center
Huntsville, Alabama 35812

Attention: Mr. William J. McKinney

Subject: Monthly Progress Letter 6, Project A-1028
"Study of Feasibility of Optically Exciting a Magnetic Memory"
Contract No. NAS8-20813
Covering the Period from 12 November 1967 to 12 December 1967

Gentlemen:

This report covers work performed under Contract NAS8-20813 which is directed toward development of an optically excited magnetic memory. Efforts are continuing to complete the crystal fabrication facility. This is a bottleneck at present to continuation of the measurements phase of the program. A systems evaluation study has been begun to attempt a realistic evaluation of the present and future potential of an optical memory system. As a result of this effort a basic memory system design will be submitted which will be implementable at the current state of the art. Correlation of predicted and actual performance can be evaluated directly as a result of this effort.

As a result of the total program work to date, it is believed that the basic concept of optically pumping is indeed valid but that a concentrated materials effort will be required to develop a satisfactory ferrimagnet. To this end it has been decided to expand the theoretical effort to provide better direction toward obtaining the optimum magnetic material.

Crystal Fabrication

The crystal growing furnace per se is complete and has been evaluated in manual run-ups. The maximum temperature is somewhat above 1300° C using a supply of 24 volts at 60 amps. A complete temperature profile along the tube length has been run. A special die press fixture has been constructed to permit pressing the constituent oxides into a pellet before melting. Discussions with Dr. J. P. Hanton at Montana State University have revealed that

significantly larger crystals can be grown if the starting materials are first highly compacted. This die is machined to dimensions identical to the platinum crucible used to grow the crystals. Compacting forces of up to several tons may be applied. The die is split so that after compaction, the crucible shaped pellet can be removed by die disassembly.

Some redesign on the temperature controller and slow delivery of some integrated circuits has delayed completion of this instrumentation. Most of the design has, however, been checked on the Georgia Tech digital synthesizer. and modified as necessary to provide the required performance. We believe this controller to be a significant improvement over any commercially available today.

Test Facilities

The vacuum system for low energy cathodeluminescence studies has been completed and pumped down. With no cold trapping the system reaches about 8×10^{-5} Torr. The pump employed is a 1-$\frac{1}{2}$" CVC Model MB10-01 oil diffusion pump, with a heater power of 150 watts. Since the electron gun planned for the system has an oxide coated cathode it seems desirable to add some form of cryogenic trapping and pumping capability. This will be added in the form of a liquid nitrogen reservoir located in the input throat to the chamber.

The gun to be installed in the system is one being developed at Georgia Tech primarily for LEED work. It is a self focusing design using a cylindrical lens system. The beam stays in focus over an accelerating voltage range of from approximately 1 to 1000 volts.

System Analysis

The initial system effort has involved literature reviews and searches to collect necessary background data on previous optical memory systems. Of major initial concern are problems of determining basic system organization in view of the density and resolution requirements. While most approaches presently being considered involve single bit addressing because of simplicity it is apparent that this is a very inefficient process. Initial work, however, indicates that there is no obvious alternative. This general problem is receiving additional attention. The optical deflection operation is still and will probably continue to be a major limitation in beam steered memories.

Theoretical Work

Our initial theoretical work was directed toward investigating techniques which would provide valid transition probability calculations. We have

come to realize that this, while solvable in principle, is not practical for the needs of this program. That is, the amount of time and expense involved is too large in relation to the significance of the result. Information of this type can be better obtained experimentally. It seems, however, that we do need the capability of estimating, with reasonable accuracy, the atomic energy level structure of the various ions in an insulating lattice. This would permit a preliminary evaluation of various materials without having to actually grow, then experimentally evaluate, each one individually. The general problem is one of being able to predict the relative energy transitions of spin flip processes in contrast to charge transfer processes. We know for example that there are some transition metal oxides, NiO for example, where the charge transfer levels are greater than 3.5 ev. In GdIG such transfer processes occur at approximately 2.5 ev. In fact a complete solution of the GdIG energy level system is still not available. The results of this effort should permit us to perform a rather rapid evaluation and relative merits of the various materials potentially capable of being optically pumped.

Future Work

Efforts will continue toward completion of the oven controller. At this point in time no hard estimate of an operational date can be made. Work will continue in compiling and organizing data associated with performing the system design. Finally we are starting to gather information providing a background in permitting calculation of energy levels of ions in an insulating lattice.

Respectfully submitted,

F. L. Grismore
Project Director

FLG/srt

Approved:

E. V. Scheibner, Chief
Physical Sciences Division

Budget Structure as of November 1, 1967

Personal Services	
Budget	$17,537.00
Expended	8,742.16
Materials & Supplies	
Budget	$ 1,950.00
Expended & Encumbered	1.121.15
Travel	
Budget	$ 300.00
Expended & Encumbered	142.41
Overhead	
Budget	$ 9,996.00
Expended	4,983.00
Free Balance	$15,004.26

A-1028

ENGINEERING EXPERIMENT STATION
GEORGIA INSTITUTE of TECHNOLOGY

hysical Sciences Division

225 North Avenue N.W.
Atlanta, Georgia 30332
(404) 873-4211 Ext. 220

12 February 1968

National Aeronautics and Space Administration
George C. Marshall Space Flight Center
Huntsville, Alabama 35812

Attention: Mr. William J. McKinney

Subject: Monthly Progress Letter 7-8, Project A-1028
"Study of Feasibility of Optically Exciting a Magnetic Memory"
Contract No. NAS8-20813
Covering the Period from 13 December 1967 to 12 February 1968

Gentlemen:

This report covers work performed under Contract NAS8-20813 during the two month period of December 13, 1967 to February 12, 1968. The purpose of the contract is to determine the feasibility of optically pumping a magnetic oxide in order to alter its magnetic moment. Demonstration of this phenomena would open the way for development of high density bulk memory for space born computers.

Efforts over this period have been devoted to system analysis, material studies and continual development of the crystal growing furnace temperature programmer. A systematic approach to the systems analysis problem has been established involving a card file system. In this way a variety of independent areas may be analyzed separately while relating directly to the overall problem solution. A new concept has been conceived relating to the type of material desired for optical pumping. This involves the use of an anti-ferromagnetic material rather than a ferrite temperature biased to its compensation point. Finally we have completed fabrication of approximately 75% of the temperature controller. Most of this has been checked and is currently operating. The analog-to-digital conversion card required the greatest effort but recently completed temperature evaluation experiments show it operates at the specified accuracy over an ambient temperature range of greater than 30°F. This is a much larger swing than is encountered in the laboratory environment and hence desired accuracy should be adequately maintained over the extended periods of growing the materials.

Details of the work in these areas are included in the following paragraphs.

Theoretical Considerations

One of the most exciting results of our current work is the evolution of a new concept in the type of material required to perform in the optical pumping experiment. This concept is based on use of an anti-ferromagnet rather than a ferrimagnetic operating at its compensation point. We have previously discussed the problems of applying GdIG to the optical pumping experiment. These revolve around the fact that competing photon capture processes are so large that non-radiative transitions predominate. Thus even if optical pumping was existent, one would be limited primarily by thermal time constants since the garnet must be stabilized at its compensation temperature.

Consider now, however, an anti-ferromagnet operating well below its Neîl temperature. This material will be magnetically compensated over a wide range of temperatures and thus non-radiative transitions within its atomic system will not alter the magnetic state through phonon interaction. However, it should be possible to pump magnetic electrons into spin flip states in a manner similar to that proposed for the rare earth garnets. In general, the anti-ferromagnets are single element oxides, e.g., Mn_2O_3, Ni_2O_3, etc. In a material of this type the two magnetic sublattices are composed of identical atoms, distinguished by the fact that they have different lattice symmetry, e.g., octahedral vs. tetrahedral. The difference in energy level splittings does not however appear to offer a satisfactory means of selectively exciting only one sublattice. In a material of this nature optical pumping of electrons into spin flip states would occur in both sublattices simultaneously and the material would remain magnetically compensated. There are, however, several families of antiferromagnets which are composed of two element systems. An example of this is $Co_{3-x}M_{nx}O_4$ which is anti-ferromagnetic at $X \approx 0.8$. This same effect occurs in several oxides containing Mn and is the result of a tetragonal distortion created by the size of the Mn^{+++} atom.

It is an established fact that manganese exhibits a spin flip transition at an incident photon energy of about 2.2 ev. Johnson and Williams[1] for example using resonance techniques measured the change in moment of Mn atoms under optical excitation. They found that the moment of the excited atoms was

1 Williams, F. E., "Solid State Luminescence," Advances in Electronics, 5, 148 (1953).

approximately one Bohr magneton less than those in the ground state. Using an anti-ferromagnet of this type it should thus be possible to uncompensate the spin system locally by optically pumping the Mn atoms.

It appears that these materials offer several advantages over the ReIG and in fact over temperature compensated ferrites in general. For example, the spin flip excitation energy is lower for Mn than any of the rare earths. This means that there is less chance of having to compete with charge transfer or inter band conduction producing transitions. Additionally, since moderate temperature variations will not affect the general magnetic system, the occurrance of radiationless transitions will not cause problems associated with thermal time constants. This also means of course that it is unnecessary to maintain a tight temperature control on the magnetic material as with a temperature compensated garnet. This is especially appealing when considering memories for space applications. These are significant advantages and we are directing our study toward a more thorough examination of these types of anti-ferromagnetic oxides.

Temperature Controller

Included in this report is a description of the boards and circuits of the controller which have been checked out to date. In addition to these, one other board is completely fabricated but has not yet been operated. Results of its performance will be discussed in the next report.

Timing Circuit: Figure 1 shows a diagram of the timing circuit and the generated waveforms. The entire logic system is synchronized to the 60 cps line as discussed in a previous report. Essentially a temperature sample is taken during the positive half cycle and the sample compared with the reference during the negative half cycle. Levels A and B are used throughout the system to gate on these respective operations. Pulses T_1 and T_2 precede these levels to perform initiating functions.

The resistor-zener diode network on the transformer secondary simply clips the voltages to below 4 volts. Diodes D_1 and D_2 provide a 0.7 volt offset allowing a dead space around the zero crossings. This dead space is used to generate the T_1 and T_2 pulses. Flip flops FF1 and FF2 are used to provide sharp transitions at the edges of the desired levels and normalize amplitudes to the remainder of the logic. A little study reveals that the flip flops produce (A and $\bar{A}$) and (B and $\bar{B}$) as drawn on the timing diagram. The triangular

elements are simple invertors and the half circles represent conventional positive true NOR logic gates. When these elements are used as negative true NAND gates they are diagrammed with a dot, e.g., G_1 and G_2. Flip flop FF3 is used to separate pulse T_1 from T_2. Both of these pulses are logically defined by $\bar{A} \cdot \bar{B}$. The separation is effected by gating them according to the previously existing level. Thus when level B is high FF3 is in a state such that G_2 is gates on and G_1 is gated off. FF3 remains in this state during the succeeding dead space interval where $\bar{A} \cdot \bar{B} = 1$, yielding an output at T_1 and nothing at T_2. Just the opposite occurs when A level goes positive. The output of this circuit controls the remainder of the system. T_1 and T_2 are approximately 500_u sec duration.

SCR Power Switch: This circuit is designed to provide power in full cycle intervals. This is necessary since the oven heating element is supplied through a transformer and it is desirable to prevent high transient currents by starting and stopping currents at zero voltage. Operation is quite simple. Assume the trigger SCR, SCR3 is biased non conducting. Then as the ac supply starts to increase during the positive half cycle SCR2 is triggered on by current through R_1. This occurs within only the first few volts of the cycle. SCR2 conducts the load current through diode D2 during the entire positive half cycle. A small but non negligible current is established through L1 during this interval due to the finite voltage drop across D1. As the negative half cycle begins SCR2 reverse biases and cuts off. The current flowing through L1 must thus flow into the gate terminal of SCR1 turning it on and allowing a conduction path during the negative interval. Note that once this cycle starts, i.e., once SCR2 fires, it will continue for the complete period regardless of the state of SCR3. If SCR3 is still off as the next positive half cycle begins the cycle will repeat. If, however, SCR3 is gates on sometime during the period of conduction the next cycle will be open circuited. This happens because with SCR3 conducting SCR2 is prevented from triggering during the positive half cycle.

In the controller being built, the state of SCR3 is determined during the negative half period of each supply cycle, i.e., during the timing period B. Thus power is delivered to the heater element in one cycle increments.

Analog to Digital Converter: This circuit, one of the most fundamental to the system operation caused the greatest debugging problems. Basic operation is straightforward. A temperature dependent voltage appears at the out-

put of A1 as a result of adding the sum of a thermocouple emf and an offset voltage from the zener-regulated bias circuit. This temperature dependent voltage acts as a reference level at the comparator OA3. It is always a negative value ranging from zero to approximately -6 volts. The other comparator OA2 has a ground reference.

Normally logic level $\bar{A}$ is at +3 volts holding transistor T1 conducting. This connects the 180 K input resistor of the integrator OA1 to -15 volts, rapidly driving the output of OA1 to +10 volts. The output is limited to +10 by zeners Z_3 and Z_4. Limiting is necessary because of the fact that most operational amplifiers hang-up when allowed to saturate to supply voltages. In the steady state then, the summing nodes to both comparators are positive. Since OA2 is connected as a non inverting (NI) amplifier its output is high, i.e., +15 volts. OA3 however, connected in an inverting mode, has a low output, i.e., -15 volts.

When the A timing interval begins $\bar{A}$ = 0 volts and T1 becomes non conducting. D2 becomes reverse biased and the integrator sees the zener voltage V(Z1) through 550 K. The output of OA1 is thus a negative going ramp. When the ramp voltage equals the temperature sensitive voltage from A1, comparator OA3 snaps to +15 volts. This causes FF1 to change states gating G1 on and allowing the passage of oscillator clock pulses to the output terminals. The system remains in this state until the ramp from OA1 passes through zero volts. This causes OA2 to snap negative resetting FF1 to its original state and inhibiting G1. The number of output pulses are thus directly proportional to the temperature voltage.

Features of this design are its relative simplicity as compared for example to a two-step up-down integration scheme. Since the comparators are identical, a shift in offset voltage with temperature should be similar in each tending to eliminate any error. Also, since the zener voltage is used both as a thermocouple bias and the integrating source self-compensating effects occur for slight temperature caused variations in this potential.

The stability of the zener voltage and the output of A1 are extremely important. The diode chosen is a high stability Motorola unit and the amplifier A1 is chopper stabilized providing an offset drift of less than 1_{μ} volt per degree C and exceptional long term stability.

A series of evaluation tests have been made on this circuit using a

Berkley EPUT meter to measure pulse width variations and output count over a range of temperatures in excess of those encountered in the lab. The output count is constant to within ± 1 part in 10^3 which is the accuracy desired for this application.

The comparator board is completed and ready for evaluation. One additional board containing the storage registers must yet be fabricated. Progress toward completion of the entire facility will be reported again next month.

System Analysis Effort

Our collection of reprints, references and notes on many and varied aspects connected with our work on system considerations of a magneto-optical memory was growing unmanageably. This collection includes items on basic material properties, optical systems that might be associated with the memory, and switching circuits. Several man-days were spent to take the measure of these items and to search for a systematic arrangement in which they might be placed.

A tentative outline was set down that was to serve as a basic table of contents for a file of 5 x 8 inch cards. An attempt was made to fill in a small part of the outline by summarizing certain formulae and notes onto cards keyed to the general outline and to the references from which they were drawn.

On the basis of this experience, the proposed framework is presently being reviewed with the purpose of modifying the present outline to best serve our purposes, or possibly, to decide to attempt organization along some other line.

Future Work

Work will continue toward completing the temperature controller. It is anticipated this will be continued during the following month. Specific details for formal energy level calculations will be formulated and this work begun. We hope also to re-establish the reflection measurement apparatus in a new laboratory and this construction will be started.

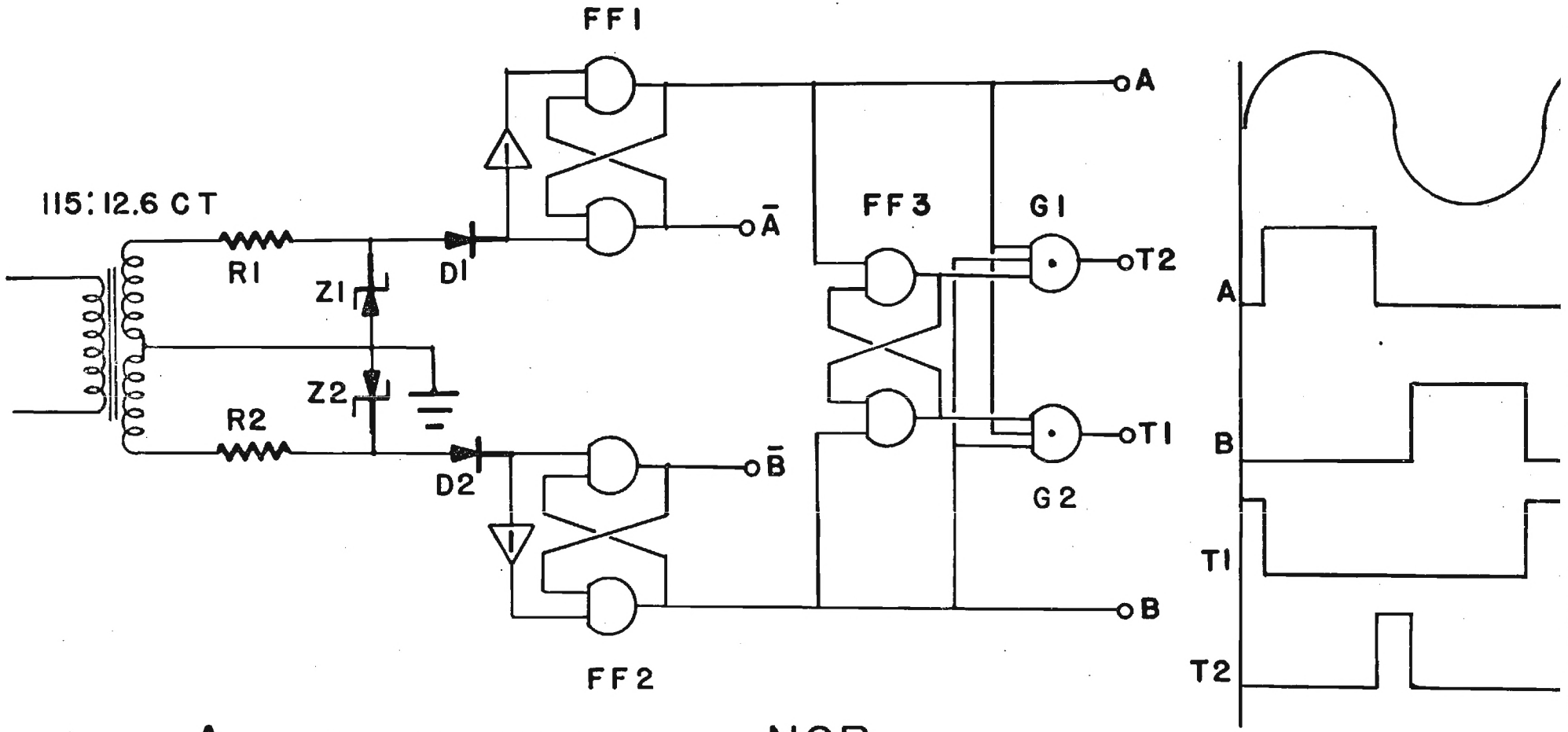

ALL LOGIC ARE POSITIVE TRUE NOR

MRTL 7900 SERIES.

FIGURE 1. TIMING GENERATOR LOGIC

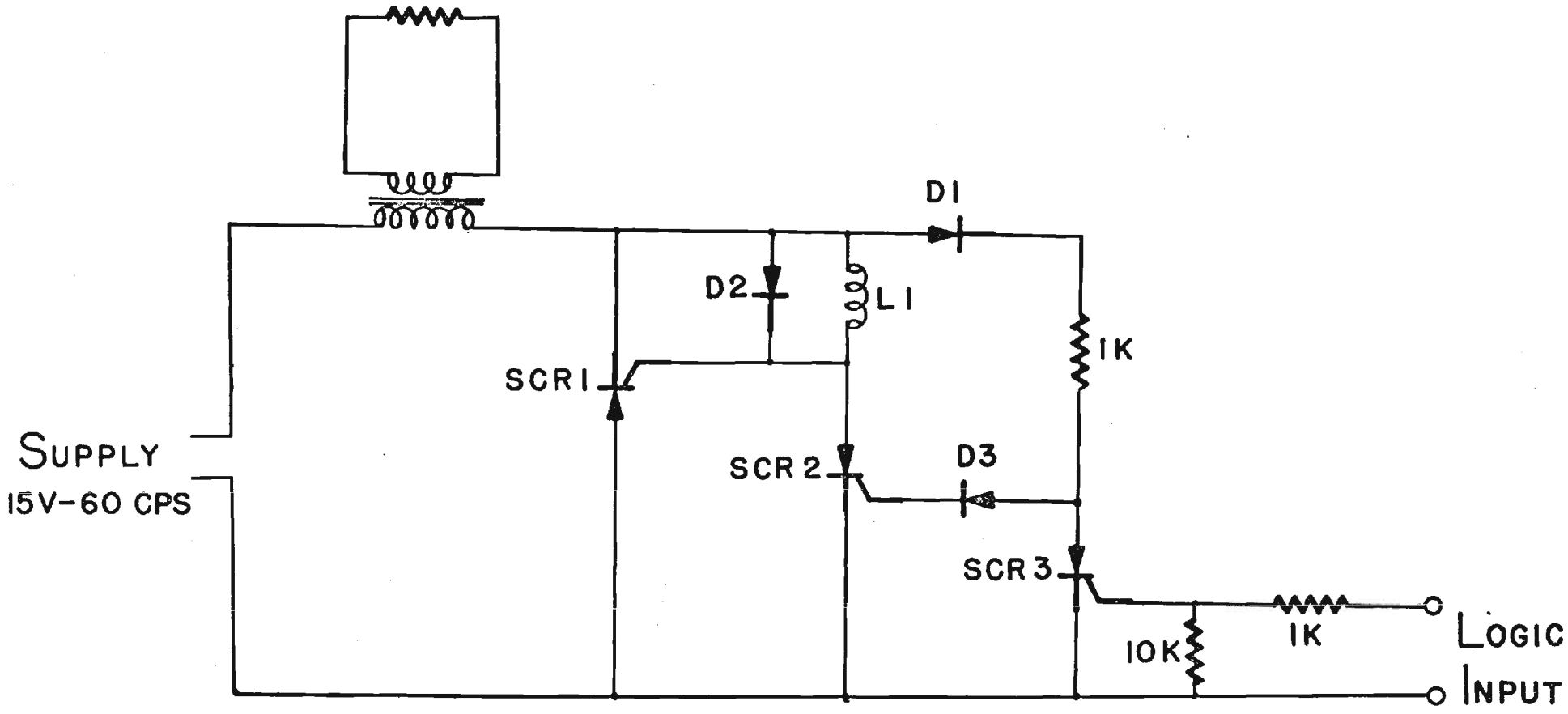

FIGURE 2. SILICON CONTROLLED RECTIFIER POWER SWITCH.

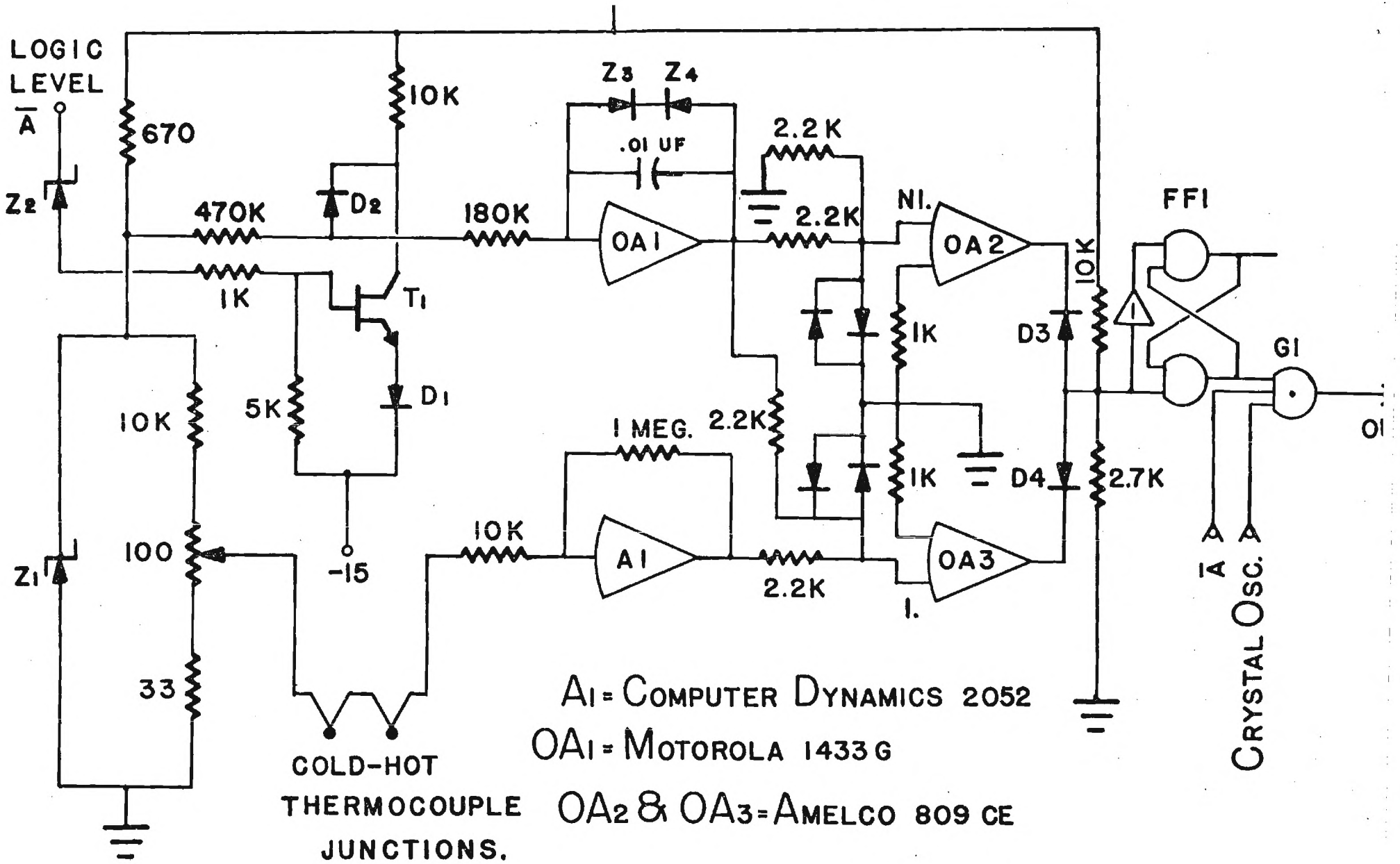

Figure 3. Analog To Digital Convertor.

Budget Structure as of 1 February 1968

Personal Services	
Budget	$17,537.00
Expended	14,717.71
Materials & Supplies	
Budget	$ 1,950.00
Expended & Encumbered	1,562.08
Travel	
Budget	$ 300.00
Expended & Encumbered	192.45
Overhead	
Budget	$ 9,996.00
Expended	8,389.08
Free Balance	$ 5,131.68

Respectfully submitted,

F. L. Grismore
Project Director

FLG/srt

Approved:

E. J. Scheibner, Chief
Physical Sciences Division

Budget Structure as of 1 February 1968

Personal Services	
Budget	$17,537.00
Expended	14,717.71
Materials & Supplies	
Budget	$ 1,950.00
Expended & Encumbered	1,562.08
Travel	
Budget	$ 300.00
Expended & Encumbered	192.45
Overhead	
Budget	$ 9,996.00
Expended	8,389.08
Free Balance	$ 5,131.68

Respectfully submitted,

F. L. Grismore
Project Director

FLG/srt

Approved:

E. J. Scheibner, Chief
Physical Sciences Division

A-1028

ENGINEERING EXPERIMENT STATION
GEORGIA INSTITUTE of TECHNOLOGY

Physical Sciences Division

225 North Avenue N.W.
Atlanta, Georgia 30332
(404) 873-4211 Ext. 220

2 May 1968

National Aeronautics and Space Administration
George C. Marshall Space Flight Center
Huntsville, Alabama 35812

Attention: Mr. William J. McKinney

Subject: Monthly Progress Letter 9, Project A-1028
"Study of Feasibility of Optically Exciting a Magnetic Memory"
Contract No. NAS8-20813
Covering the Period from 6 March to 5 April 1968

Gentlemen:

Work during this period has concentrated on bringing the furnace and controller into an operational condition. In order to complete this task an analog reference has been incorporated to replace the digital register originally designed into the controller. This has greatly facilitated completion of the controller, which is now complete and running. We have performed operational checks on the accuracy of temperature regulation and find it agrees with the design estimates of ± 0.2°C around the nominal. Temperature cooling rate is adjustable but present operation is at 0.9°C/hr. A sketch of the system is shown in Figure 1.

The temperature reference in this controller is derived simply from a motor driven potentiometer connected across the high stability zener diode. This same zener provides a regulated offset voltage to back out the thermocouple signal at maximum temperature. Thus as the reference pot is driven to deliver greater positive voltage, oven temperature must decrease to maintain the thermal controlled voltage equal to the reference. The comparator is logically synchronized with the 60 ~ line supply so that only full cycle intervals of heater current are delivered. This reduces electrically generated system noise by eliminating high di/dt intervals. The thermocouple amplifier has turned out to be the most critical element in the controller. It was found very difficult to achieve a high degree of stability and noise rejection while maintaining a gain of nearly one thousand. Noise pick-up on the thermocouple leads was a particularly frustrat-

ing problem, however combinations of proper shielding and appropriately placed low pass filtering has resulted in a quite acceptable design. Long term drift of the amplifier is much less than the programmed temperature change and the room ambient is maintained to within ± 3°C to minimize temperature induced variations.

The first crystal growing run was begun on April 3, and will be completed on about April 18. Crystal cutting and polishing facilities are available within the Solid State Branch. The first run, now under way is constituted to grow dysprosium iron garnet. As discussed in the interim report only DyIG and TbIG are considered as being potentially useful for the desired pumping process. During the month we received the previously ordered Tb_2O_3 and a run to grow terbium iron garnet will be started as soon as the DyIG run is complete.

The measurement apparatus is being re-configured to allow more precise reflection and fluorescence data. This includes an air-cooled 1 kw mercury arc lamp with much higher output in the U.V. spectral region than was available when the GdIG data was taken. This is especially important for the fluorescence measurements where high incident flux is necessary to overcome dark current noise in the photomultiplier detector.

The interim report has been nearly completed and should be released during the following reporting period.

Respectfully submitted,

F. L. Grismore
Project Director

FLG/srt

Approved:

E. J. Scheibner, Chief
Physical Sciences Division

FIGURE 1. FEEDBACK TEMPERATURE CONTROLLER

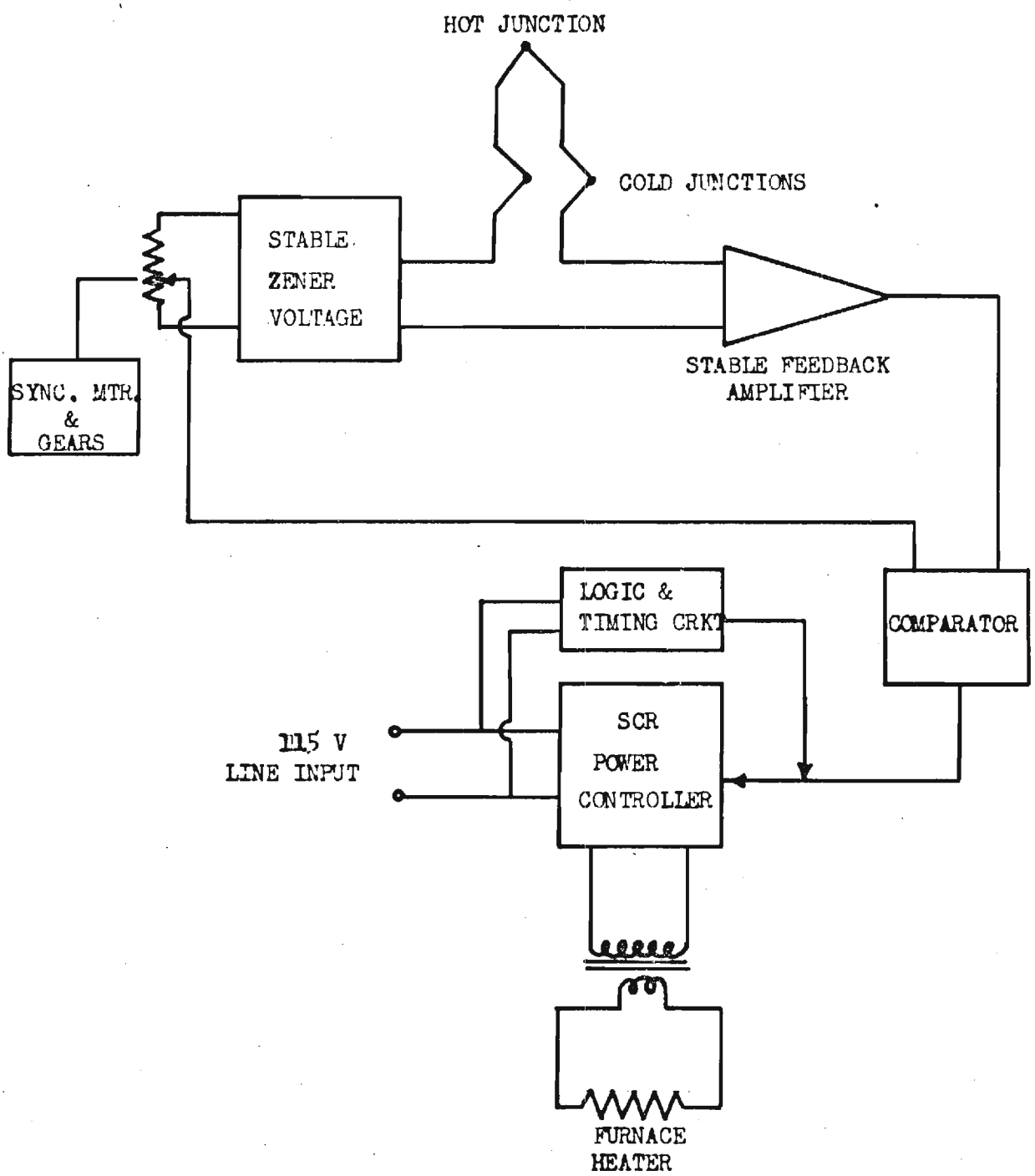

A-1028

ENGINEERING EXPERIMENT STATION
GEORGIA INSTITUTE of TECHNOLOGY

Physical Sciences Division

225 North Avenue N.W.
Atlanta, Georgia 30332
(404) 873-4211 Ext. 220

4 June 1968

National Aeronautics and Space Administration
George C. Marshall Space Flight Center
Huntsville, Alabama 35812

Attention: Mr. William J. McKinney

Subject: Monthly Progress Letter 10, Project A-1028
"Study of Feasibility of Optically Exciting a Magnetic Memory"
Contract No. NAS8-20813
Covering the Period from 6 April to 5 May 1968

Gentlemen:

During the last period the crystal growing furnace and controller became operational and the first run was started. The results of the run, which was completed during this period, were quite satisfactory. The melt yielded one crystal with a long axis of nearly 2 cm plus a number of crystals measuring approximately 0.5 to 1 cm. Several slices have been removed from the big crystal using a 10 mil diameter wire saw. The surface of one slice has been prepared for reflectivity measurements by successive lappings on wet paper followed by polishing on a wheel polisher.

Samples have been provided to the analysis laboratory for spectroscopic analysis and crystallographic orientation information We are also providing several samples for an x-ray topography study to determine the feasibility of observing domain structure by this technique. In this approach domain walls are often visible using low angle Bragg reflections because of the magnetostrictively induced change in d-spacing. This effect is caused by the large field gradients occurring near a domain wall. If walls are indeed visible it may be possible to obtain data on wall mobility and switching thresholds in bulk single crystal samples Since all previous data on wall characteristics has been obtained by Faraday measurements on mechanically polished samples this will provide added insight into the intrinsic magnetic characteristics of the magnetic garnets.

This first completed batch of crystals is DyIG. Dysprosium was chosen because it exhibits the lowest energy spin flip optical transition

of all the rare earths. While we expect terbium to exhibit a longer excited state lifetime, dysprosium has a somewhat better chance of being excited by photon energies below the band gap energy of the basic iron containing garnet.

A run to grow terbium iron garnet was started, but was curtailed within 24 hours as a result of the furnace heating element burning through. This was apparently caused by the corrosive action of the lead fumes escaping from the crucible during the first run. In order to overcome this problem we intend to add a ceramic liner to the furnace to protect the heating element. In the interim we have been able to adapt the controller to another furnace in our lab. Thus the run has been started again and will be completed during the following reporting period. This furnace is not as ideal for growing crystals as the one we designed because it is an annealing oven with a large capacity chamber and requires a large power input. As a result, direct SCR control of the primary power was not possible and it has been necessary to actuate a contactor with the controller output. This contactor in turn delivers power to the furnace heater elements. Because of the mechanical limitations of the contactor it is impossible to regulate the temperature as closely as with the other oven. We have chosen to regulate to ± 0.5 degree; this being a compromise between contactor cycle period and crystal growing considerations. A second limitation with furnace is that proper temperature gradient i.e., the top of the crucible 10° C to 15° C hotter than the bottom, is difficult to achieve. Nevertheless, we anticipate some useable crystals to be grown and since time is of the utmost importance we cannot afford the delay of rebuilding the burned out furnace.

As reported last month the optical measuring apparatus is being redesigned to provide more accurate and meaningful data. This design is now complete and has been submitted to the shop for fabrication. A number of improvements have been incorporated into the apparatus, resulting in more accurate alignment of the sample and greater reproducibility of angular settings and measurements. We have used a concave reflector for imaging the light source on the monochrometer rather than a quartz lens. This overcomes the difficulties associated with the variation of focal length

with wavelength in a lens system. The sample holder and photomultiplier mount have been constructed as an integral assembly with accurate pin registration of incident and reflecting angles. A complete description of the equipment will be included in the final report. The apparatus should be operational next month and we hope to complete the basic optical reflection measurements on DyIG and TbIG during that period.

Respectfully submitted,

F. L. Grismore
Project Director

FLG:srt

Approved:

for E. J. Scheibner, Chief
Physical Sciences Division

A-1028

ENGINEERING EXPERIMENT STATION
GEORGIA INSTITUTE of TECHNOLOGY

Physical Sciences Division
825 North Avenue N.W.
Atlanta, Georgia 30332
(404) 873-4211 Ext. 220

9 August 1968

National Aeronautics and Space Administration
George C. Marshall Space Flight Center
Huntsville, Alabama 35812

Attention: Mr. William J. McKinney

Subject: Monthly Progress Letter 11, Project A-1028
"Study of Feasibility of Optically Exciting a Magnetic Memory"
Contract No. NAS8-20813
Covering the Period from 6 May to 5 June 1968

Gentlemen:

This contract is directed towards investigation of optically pumping a magnetic material to effect a change in the net magnetic moment. Successful demonstration of this phenomena will provide the basis for development of a magneto-optic memory which is not speed-limited by thermal time constants.

This phase of the contract was initially planned as an overall systems evaluation of a memory employing optical pumping. However, after reviewing the progress of work with Mr. G. A. Bailey it was decided that the program should continue to address itself to a study of the basic phenomena. Delays in crystal fabrication during the first part of the contract had limited our experimental investigations to only GdIG. Since TbIG is the most promising of the rare earth iron garnets, it was decided that more experimental work was necessary.

We are therefore directing the effort of this third phase to two main experimental efforts.

1. Detailed optical absorption measurements of TbIG and DyIG in the energy range surrounding the rare earth transitions.

2. Pumping experiments employing the MSFC Faraday apparatus modified by the addition of a second light source.

Several additional crystal growing runs are planned to study the relationship of the rare earth spin flip transition energy to the observed "band edge."

During this month progress was somewhat limited due to vacation periods by investigators. The shop completed work on the new reflection measuring apparatus and we have begun assembling this experiment. In reviewing our original data it was concluded that the observed breadth of absorption lines could be due to poor angular resolution of the experimental apparatus. This new set-up has been designed to provide us with much more refined data and as a result we hope to gain detailed knowledge of the important rare earth transitions. In addition to the improved angular precision of this apparatus we employed the air-cooled 1 kw mercury arc lamp developed during Phase II. This lamp provides us with at least two orders of magnitude more light in the high energy range thus permitting much greater detail than was previously possible.

The crystal growing oven temperature controller was rebuilt this month, consolidating the several boards and sub-chassis into a single assembly. This controller has been duplicated by other groups at Georgia Tech and has proven to be a very capable instrument.

Because the "band gap" absorption is of such critical importance to the proposed phenomena we are again looking at the effect from a theoretical point of view. Recent work in molecular orbital theory has led us to believe that fairly accurate qualitative results can be obtained by considering the octahedral and tetrahedral iron sites as molecular entities. Applying molecular orbital theory as outlined by Ballhausen and Gray (Molecular Orbital Theory, Benjamin, 1965) it appears possible to adequately describe the transition involving all iron and oxygen atoms. Work is now being started to develop the computer programs necessary to carry out these calculations. An important asset along these lines is the recent work of Synick sponsored under W.A.D.C. research grants. His calculations for the iron ion in various excited states are the most accurate of any to date. Without this accuracy our calculations could only be qualitative in nature.

Future Plans

During the following month we hope to have the optical reflection apparatus operational. Data will be available as soon as this equipment is properly aligned. Work will continue on the development of a satisfactory molecular orbital calculation.

Finance (Thru June 1968)

	Budgeted	Expended
Personal Services	$32,885.00	$20,187.87
Material & Supplies	2,400.22	2,240.22
Overhead	18,744.00	10,931.00
Miscellaneous (Computer, Travel, etc.)	940.00	745.06

Respectfully submitted,

F. L. Grismore
Project Director

Approved:

E. J. Scheibner, Chief
Physical Sciences Division

A-1028

ENGINEERING EXPERIMENT STATION
GEORGIA INSTITUTE of TECHNOLOGY

hysical Sciences Division

825 North Avenue N.W.
Atlanta, Georgia 30332
(404) 873-4211 Ext. 220

December 3, 1968

National Aeronautics and Space Administration
George C. Marshall Space Flight Center
Huntsville, Alabama 35812

Attention: Mr. William J. McKinney

Subject: Monthly Progress Letter 12, Project A-1028
"Study of Feasibility of Optically Exciting a Magnetic Memory"
Contract No. NAS8-20813
Covering the Period from 6 June to 5 July 1968

Gentlemen:

This report covers work performed on project NAS8-20813 directed towards the goal of achieving memory read-write operation by optically pumping an optically-active antiferromagnet. The period herein reported is from June 6 to July 12, 1968.

Experimental

We had anticipated that operational status of the reflectivity apparatus would be achieved during this period. Equipment failures however have prevented this from taking place. During the initial run, the power supply choke for the mercury arc lamp became hot and it was found to be underated for the lamp being used. Several alternate arrangements were tried in order to achieve a satisfactory power supply but to date none have been successful. In the process of this work, the lamp itself failed and the spare lamp was broken during the process of replacing the one burned out.

New lamps have been ordered and should arrive during the following report period. In the meantime we have made arrangements with the Physics Department to borrow their power supply and a spare lamp.

Several features have been added to the equipment to facilitate alignment and control of light intensity. It was found that instabilities in photo-multiplier current readings were the result of high light intensity under some measurement conditions. To control incident light,

we have added two additional polarizers. Adjusting the relative angle between these two polarizers allows control of extinction over several orders of magnitude intensity. Except for the lamp the system is now operational and we anticipate data on GdIG to be available during the next reporting period.

Theory

In Progress Report 11 it was related that molecular field theory was being applied to attempt a detailed understanding of the absorption band edge at about 2.5 ev in the rare earth iron garnets. In this letter a brief outline of the general approach being taken is presented.

A. Crystal Field Theory

The first and crudest approach used to study the effects of placing an ion in a solid is that of crystal field theory. In this approach the ion is viewed as if it were in space as a free ion except that it is in an electrostatic field resulting from the surrounding charged ions on adjacent lattice sites. This electric field is assumed to be small with respect to the internal ionic forces and thus may be considered as a perturbation potential on the free ion. The result is that the free ion energy levels are split and a redistribution of electrons take place at the new energy levels of the perturbed ion.

It is generally found that a rigorous calculation of the perturbing field due to adjacent atoms, is not possible. A major reason for this is the distributed nature of the charge at the atomic sites. If however the perturbing atoms could be considered as point charges the potential could be calculated with any desired degree of accuracy. For example if the ion in question is surrounded by six perturbing ions located at the corners of a cube then the potential in the vicinity of the first ion would be given by:

$$V = \frac{2e_i}{R}\left[3 + \frac{35}{8R^4}\left(x^4 + y^4 + z^4 - \frac{3}{5}r^4 + \ldots\right)\right],$$

where R = distance from ion to the perturbing point charges

e_i = magnitude of charge at perturbing sites.

x, y, z, r = coordinates of electron

While the exact potential cannot be accurately calculated, its symmetry is that of the point charge distribution and in actual calculations the spatial expression in curved brackets is employed with an adjustable coefficient D to control the magnitude.

To find the state functions (eigenfunctions, or wave functions) of the perturbed system it is first assumed they can be expressed as a linear combination of the original unperturbed wave functions. This is valid since a characteristic of a complete orthogonal set of functions is that they may be used in linear combinations to form any other well behaved function in the same space. Using a truncated approximation, for example four terms, it is then possible to write the perturbed state functions as:

$$\begin{bmatrix} \Psi_1 \\ \Psi_2 \\ \Psi_3 \\ \Psi_4 \end{bmatrix} = \begin{bmatrix} K_{A1} & K_{B1} & K_{C1} & K_{D1} \\ K_{A2} & K_{B2} & K_{C2} & K_{D2} \\ K_{A3} & K_{B3} & K_{C3} & K_{D3} \\ K_{A4} & K_{B4} & K_{C4} & K_{D4} \end{bmatrix} \begin{bmatrix} \Psi_A \\ \Psi_B \\ \Psi_C \\ \Psi_D \end{bmatrix} \qquad (1)$$

where Ψ_1, Ψ_2 --- are the perturbed state functions
Ψ_A, Ψ_{B1} --- are the original unperturbed functions

and the K's are coefficients which must be determined. These latter are found by the variational method. Applying the variational principle to these assumed solutions it is easy to show[1] that the optimum values of the K's, i.e. the ones which lead to an energy minimum are given by the following system of equations:

$$\begin{bmatrix} 0 \\ 0 \\ 0 \\ 0 \end{bmatrix} = \begin{bmatrix} (H_{AA}-E) & H_{AB} & H_{AC} & H_{A4} \\ H_{BA} & (H_{BB}-E) & H_{BC} & H_{BD} \\ H_{CA} & H_{CB} & (H_{CC}-E) & H_{CD} \\ H_{DA} & H_{DB} & H_{DC} & (H_{DD}-E) \end{bmatrix} \begin{bmatrix} K_{A1} \\ K_{B1} \\ K_{C1} \\ K_{D1} \end{bmatrix} \qquad (2)$$

[1] Slater, "Quantum Theory of Atomic Structure," Vol. I, McGraw-Hill, 1960.

where the H's represent "matrix elements" given as

$$H_{AA} = \int_{\text{all volume}} \Psi_A^* (V_{\text{crystal field}}) \Psi_A d\tau$$

$$H_{BA} = \int_{\text{all volume}} \Psi_B^* (V_{\text{crystal field}}) \Psi_A d\tau \text{ etc.}$$

In the above, $d\tau$ is the infinitesimal volume element.

Since the unperturbed wave functions are known the matrix elements can in principle be evaluated, resulting in a number. This is assuming we could actually express the crystal potential completely. Now for the above matrix equation to hold for non-zero values of the K's it is necessary that the determinant of the H matrix must be zero. This leads then to what is called a secular equation:

$$\begin{vmatrix} (H_{AA}-E) & H_{AB} & H_{AC} & H_{AD} \\ H_{BA} & (H_{BB}-E) & H_{BC} & H_{BD} \\ H_{CA} & H_{CB} & (H_{CC}-E) & H_{CD} \\ H_{DA} & H_{DB} & H_{DC} & (H_{DD}-E) \end{vmatrix} = 0 \qquad (3)$$

Solving this resulting set of equations, assuming the matrix elements are previously determined, results in four values of E. Each value of E, substituted back into (2) permits the determination of a set of K coefficients. In this example there are 4 values of E and four sets of coefficients. It is seen that each E gives a different set of K's when substituted back into (2). Each set of K's then defines a different wave function of the perturbed ion.

The above sketch covers the basic philosophy of the crystal field theory approach. It provides very useful results when applied to electrons in an inner unfilled shell provided the crystal field potential can be accurately described. Because of the problems previously discussed this is not possible from first principles and the potential must be

described in terms of adjustable crystal field parameters which can be manipulated to attempt a fit between experimental data and the calculations. While such parameters have been calculated for many specific materials, each new system must be experimentally determined.

The major disadvantage for our work however is that crystal field theory cannot account for electron transitions between anion and cation. This is because the new wave functions calculated contain terms of only one atom. Thus by its very formulation it can only be used to determine transitions within the shells of the ion considered. This limitation can be removed if we extend the concept to a molecular orbital calculation where the perturbed wave functions are combinations of orbitals from both the cation and anion.

B. Molecular Orbital Calculation

It is assumed in this model that the solid can be considered as an ordered arrangement of molecular ions. This concept fits well with previous work in the garnets which picture the crystal as being composed of a, c, and d molecular sites. In this picture the a site is an octahedrally coordinated Fe ion surrounded by six oxygen anions, the c site is a dodecahedral configuration consisting of the rare earth ion surrounded by eight oxygen ions and the d site is a tetrahedrally coordinated iron ion.

Using a molecular model, it is postulated that the wave functions of the molecular group can be described by a combination of atomic orbitals from the constituent ions. It is easy to show that wave functions of this type will indeed provide for a transition between ions. For example consider two molecular orbitals written as

$$\Psi_{M1} = a\Psi_d + b\Psi_L$$

$$\Psi_{M2} = C\Psi_{d'} + d\Psi_{L'}$$

where Ψ_{M1}, Ψ_{M2} = molecular orbitals

$\Psi_d, \Psi_{d'}$ = d atomic orbital of central metal ion

$\Psi_L, \Psi_{L'}$ = ligand ion atomic orbitals.

Here the molecular orbitals are made up of a linear combination of atomic orbitals from anion and cation as proposed. Now the interaction matrix element between these two molecular orbitals is simply

$$M = \int_{\substack{\text{all}\\\text{space}}} \Psi_{M1}^{*} H \Psi_{M2} \, d\tau$$

where H is the perturbation Hamiltonian operator inducing the transition. This becomes simply

$$M = \int (c\Psi_d{}'^{*} + d\Psi_L{}'^{*}) H(a\Psi_d + b\Psi_L) d\tau$$

$$= ca \int (\Psi_d{}'^{*} H \Psi_d) d\tau + db \int (\Psi_L{}'^{*} H \Psi_L) d\tau$$

$$+ cb \int (\Psi_d{}'^{*} H \Psi_L) d\tau + da \int (\Psi_L{}'^{*} H \Psi_d) d\tau \, .$$

Here it is apparent that inter ion transitions are inherent in a molecular orbital excitation as shown by the last two terms. These terms are transition matrix elements between anion and cation orbitals. The significance of this to our research is the potential capability it provides for explaining the rare earth iron garnet absorption spectra and how this spectra is related to the atomic states of the constituent ions. This information is of vital importance if we are to correlate magnetic moment changes and absorption data.

Conceptually there are many similarities between molecular orbital theory and crystal field theory. The problems of performing a rigorous solution to the resulting wave equations is beyond present capability. Generally we are left with only the alternative of introducing variable "fudge factors" to attempt a theory-experiment match. Recently however, Ballhausen and Gray[2] have outlined a self-consistent type formulation which permits an approximate evaluation of the "uncalculable" matrix elements by use of valence state ionization energies. Calculations of this

[2] Ballhausen and Gray, Molecular Orbital Theory, W. A. Benjamin, Inc., 1965.

type provide first order results which then can possibly be improved upon by experimental results.

The general idea of a molecular orbital calculation can be understood by examining a simple 2 ion molecule.

Assume we have two ions located on sites A and B as shown below.

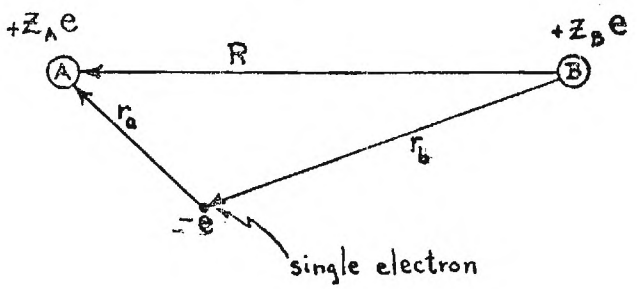

Here $Z_A e$ and $Z_B e$ represent two different ions including the nuclei and all electrons but the one under consideration. The problem is to determine the wave function associated with this electron. It is reasonable to expect that when in the vicinity of A the electron can be described accurately in terms of a wave function made up of one electron atomic orbitals of ion A. When near B the wave functions would surely be describable in terms of atomic functions associated with B. We assume then that in general we can describe the "molecular" wave function of the electron as:

$$\Psi = a\Psi_A + b\Psi_b$$

this form being known as an LCAO approximation. Normalization of a wave function of this type produces a term not encountered in crystal field theory, namely the overlap integral. Normalization requires

$$N^2 \int \Psi^* \Psi d\tau = 1$$

and assuming we choose real wave functions (Slator orbitals) this becomes simply

$$N^2 \int (a\Psi_A + b\Psi_B)\ (a\Psi_A + b\Psi_B) d\tau = 1$$

or

$$a^2 \int \Psi_A{}^2 d\tau + b^2 \int \Psi_B{}^2 d\tau + 2ab \int \Psi_A \Psi_B\, d\tau = \frac{1}{N^2} .$$

If the atomic wave functions are normalized to start with the first two integrals are identically 1 giving

$$a^2 + b^2 + 2ab \int \Psi_A \Psi_B d\tau = \frac{1}{N^2} .$$

The remaining integral is called the overlap integral and often designated as S so that normalization has resulted in the constraint.

$$a^2 + b^2 + 2abS = \frac{1}{N^2}$$

where $S = \int \Psi_A \Psi_B d\tau$ = overlap integral.

The molecular wave function thus becomes:

$$\Psi = \frac{1}{[a^2+b^2+2abS]^{\frac{1}{2}}} (a\Psi_A + b\Psi_B) .$$

The energy of the state defined by this wave function is simply

$$\langle E \rangle = N^2 \int \Psi H \Psi d\tau .$$

where H is the Hamiltonian operator of the system.

The Hamiltonian contains the kinetic operator term for the electron, the Coulomb interaction between the electron and the nucleii and ionic electrons, etc. We do not here detail these terms explicitly because the proposed calculation permits a self-consistent type solution to be performed

without actually evaluating this Hamiltonian. As previously indicated in the crystal field problem, the idea is to find values of the coefficients a and b which will minimize the expected energy of electron described by Ψ. This is again a variational type problem and in the simple two term approximation postulated here as an example, the result is a set of simultaneous equations in a and b given as

$$\begin{matrix} 0 \\ 0 \end{matrix} = \begin{matrix} (H_{AA}-E) & (H_{AB}-ES) \\ (H_{BA}-ES) & (H_{BB}-E) \end{matrix} \begin{matrix} a \\ b \end{matrix}$$

In this expression

$$H_{AA} = \int \Psi_A H \Psi_A d\tau$$

$$H_{AB} = H_{BA} = \int \Psi_A H \Psi_B d\tau$$

and

$$S = \int \Psi_A \Psi_B d\tau = \text{overlap integral} .$$

It is observed that the overlap of the wave functions on different sites shows up explicitly in this equation. For a and b to be non-zero we are led finally to a secular equation of the form

$$\begin{vmatrix} (H_{AA}-E) & (H_{AB}-ES) \\ (H_{BA}-ES) & (H_{BB}-E) \end{vmatrix} = 0$$

Since Ψ_A and Ψ_B are assumed known at the outset, then if H, the Hamiltonian operator were known explicitly the secular equation could be solved for E and this in turn would allow determination of a and b from the matrix equation thus completely defining Ψ.

It is obvious from the secular equation form that it is, in this example, quadratic in E resulting in two solutions. Diagramatically the relationship between the energies of the original atomic orbitals and that of the new molecular orbital is shown below.

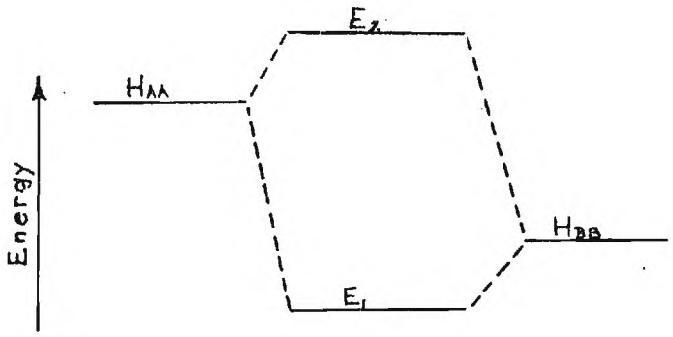

The lower energy E_1 is called a bonding energy level and the higher energy is called non-bonding. The diagram shows that the electron possesses a lower energy in the molecular orbital than it could in either atomic orbital and this is in actuality a bonding effect.

The significance of this approach is now apparent in that we are able to describe the electron states in terms of the cation and anion orbitals. Thus excitations which previously had to be qualitatively described as a charge transfer process from anion to cation can now be quantitatively evaluated as a transition from a molecular orbital of predominantly anion nature to another of predominantly cation nature. The predominate nature of a molecular orbital is determined by the relative magnitude of the coefficients, e.g. a and b, in the LCAO molecular wave function.

The above idea can be extended to molecular orbitals of transition metal ion complexes where the metal ion is symmetrically surrounded by anions such as oxygen. Examples of such an arrangement are the iron octahedral and tetrahedral sites in the R.E. Garnets.

In this case the molecular orbital is written as

$$\Psi = N(\Psi_M + \lambda\Phi_{lig})$$

where Ψ_M is a metal atomic orbital

$$\Phi_{lig} = \sum_i a_i \Psi_{i\,cation}$$ = linear combination of cation atomic orbital

λ = mixing coefficient

N = normalizing coefficient .

Since $\int \Psi\Psi^* d\tau = 1$ we have

$$N^2(1 + \lambda^2 + 2\lambda G) = 1$$

where $G = \int \Psi_M \cdot \Phi_{lig} d\tau$ = total overlap integral .

The appropriate combinations of cation wave functions used in conjunction with a given metal orbital to make up a molecular orbital is determined by symmetry considerations. Once these combinations are determined the concept of the solution of the problem is identical to that for the two ion example discussed previously. In a practical situation however we are left with finding some way to evaluate the matrix elements without complete knowledge of the appropriate Hamiltonian. One way around this is to employ the method of valence state ionization potentials as described by Ballhausen and Gray.[3] It is known that the self-energy of an electron in a given orbital is closely related to the ionization energy of that electron. Thus

$$\text{Ionization Energy} \approx \int \Psi_i H \Psi_i d\tau = H_{ii} .$$

The ionization energies are a function of the charge distribution on an atom and have been calculated for all charge distributions of significant interest for atoms thru krypton. These calculations performed by Vista

[3] Ballhausen, C. J. and Gray, H. B., "The Electronic Structure of the Vanadyl Ion," Inorg. Chem., 1, 111-122 (1962).

and Basch at Columbia include ions of 1+ and 2+ and some cases 3+ ionization states.

The off-diagronal matrix elements are estimated from the overlap integral and stability of the constituent orbitals, i.e., we know the mutual energy should be directly proportional to the overlap and in some way increase with the self-energy of the orbits. Ballhausen and Gray suggest an expression of:

$$\int \Psi_i H \Psi_j d\tau = H_{ij} = -2G_{ij}(H_{ii} \cdot H_{jj})^{\frac{1}{2}} .$$

Using these approximations the problem is solved self-consistently in the following manner. The electrons outside of the closed shell, i.e. 3d- and 4s-electrons of the iron atom and the 2s and 2p from oxygen are given some initial assumed orbital distribution on the ions. Fractional assignments are valid and in general most of the charge is distributed around the anions. Tabulated values of ionization energy for this assumed distribution are now used to estimate the matrix elements as previously discussed. Once these are known the secular equation can be solved, and using the solutions for the energy E the coefficients of the wave function are calculated. Thus the complete system is specified. The resulting electron distribution is now determined from the wave functions. If this is different from the one initially assumed it forms the basis of a second cycle in the self-consistent calculation. The procedure is repeated until the final charge distribution is identical to the starting assumed distribution.

This technique has proven capable of giving reasonable first order fit to experimental data. In this way, by comparing the results with our experimental reflectivity data it should be possible to make initial assignments of the observed transitions. Once this is done, the calculations can be performed permitting the matrix elements to be adjustable parameters. By varying them systematically around the previously calculated values a best fit criteria should produce fairly reliable analytical results.

Our program is structured around this approach, i.e., making accurate reflectivity measurements to obtain good data on transition energies

and intensities along with the molecular orbital calculations to provide data showing what atomic process is involved in each transition. In this way it is possible to separate out charge transfer processes from intra-band excitations. The latter are the excitations we are interested in pumping to effect a magnetic moment change.

Respectfully submitted,

F. L. Grismore, Jr.
Project Director

FLG/srt

Approved:

E. J. Scheibner, Chief
Physical Sciences Division

A-1028

ENGINEERING EXPERIMENT STATION

GEORGIA INSTITUTE of TECHNOLOGY

hysical Sciences Division

225 North Avenue N.W.
Atlanta, Georgia 30332
(404) 873-4211 Ext. 220

17 September 1968

National Aeronautics and Space Administration
George C. Marshall Space Flight Center
Huntsville, Alabama 35812

Attention: Mr. William J. McKinney

Subject: Monthly Progress Letter 13, Project A-1028
"Study of Feasibility of Optically Exciting a Magnetic Memory"
Contract No. NAS8-20813
Covering the Period from 12 July to 12 August 1968

Gentlemen:

Introduction

This report covers July 12 to August 12, 1968. Our work, related to the concept of optically pumping an antiferromagnet to cause a magnetization change, is progressing along two directions. Experimentally we are making optical reflectivity measurements to determine the existence and resonant wavelength of the spin flip excitation state of the rare earth sublattice in the rare earth iron garnets. Operational status of the reflectivity apparatus has finally been achieved and new data on gadolinium iron garnet is included in this report. Theoretically, molecular orbital theory is being applied to the garnet structure in order to identify the source and exact nature of the "band gap" absorption observed experimentally. We are encouraged by the progress of this work even though it is a quite complicated calculation.

Experimental Measurements

The reflectivity measurement apparatus became operational during this period. The new lamps have been received and the instrument alignment completed. A sample mount has been fabricated which permits accurate positioning of the sample laterally in two dimensions and rotationally around three axes. Accurate reflectivity data can only be obtained if the illuminated portion of the crystal does not change during measurements at different angles. It is of course also important that incident light be completely intercepted by the sample surface in order to eliminate widely scat-

tered light. At angles of incidence around 70 degrees this requires very accurate sample positioning when using small crystals.

The first sample evaluated was a single crystal of gadolinium iron garnet. Reflectivity data obtained from these measurements is shown in Figure 1. The upper two curves show the reflectivity at 20 and 45 degrees angle of incidence while the lower curve shows data at 70 degrees incidence. The 70 degree incidence curve is plotted on an expanded scale. These curves show definite structure at 3.35 ev, 4.1 ev, 4.35 ev and 5.3 ev. There also appears to be minor variations at 3.1 ev and 3.7 ev.

Using the program developed previously in this contract the absorption coefficient was calculated from the data of Figure 1. The program performs this calculation in the following manner. Using initially assumed values of the real and imaginary components, n, and k, of the refractive index, the Fresnel reflection equation is solved for angles of incidence of 20, 45 and 70 degrees. These computed values are compared with the measured values and a mean square error is computed. This process is repeated eight times for values of n and k slightly larger and smaller than that initially assumed. The points chosen are shown below.

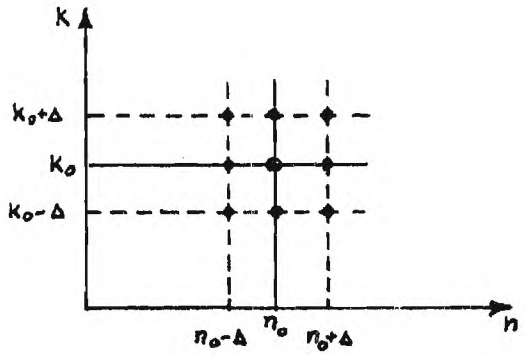

The errors computed at each point are compared and the one with the least error becomes the new center point. The process is repeated until the center point has the least error. The value of Δ used in the computations presented here was 0.01. When the optimum value of n and k have been found in this manner, the absorption coefficient is calculated as

$$\alpha = \frac{4\pi nk}{\lambda} \times 10^7$$

where

α = absorption coefficient in cm^{-1}

λ = light wavelength in mili-micron.

The resulting absorption coefficient is plotted in Figure 2. Here it is seen that three prominent absorption lines are evident at 3.4 ev, 4.35 ev and 5.35 ev. Two smaller absorptions are discernible one at 3.7 ev and another at 4.1 ev. It is almost certain that the peaks at 4.1 ev and 4.35 ev are the spin flip gadolinium transitions sought. Figure 4 shows the free ion absorption and emission spectra for the rare earths. It is observed that the ^6P multiplet is centered around 33,000 cm^{-1} and the ^6I multiplet is centered around 36,000 cm^{-1}, i.e., 4.09 ev and 4.46 ev respectively. The correspondence with observed absorption peaks is thus very convincing.

The detail in the absorption data is very rewarding after such an extended period in getting the equipment operational. The results are much improved over that taken previously and provide us with quite accurate determination of the desired absorptions. It is interesting to note that the crystal field perturbation on the rare earth absorption spectrum is apparently quite small as would be predicted because of the inner shell nature of the electrons being excited.

Figure 3 shows the plots of n and k computed by the program. The shape of these curves is consistent with that expected at resonant frequencies.

Theory. Work is continuing on the molecular field calculations to investigate the absorption edge beginning at 2.5 ev. Previous workers have attributed this high absorption to a change transfer process between oxygen and iron ions. If the high absorption is a result of iron-oxygen transitions it is more nearly correct to describe the process as transitions between molecular orbitals of the iron-oxygen complex. To this end we are developing the techniques to calculate the orbitals for the tetrahedral and octahedral iron-oxygen combinations. The solution has been organized and outlined in detail so that each calculation required has been determined. We have completed writing the program required to calculate overlap integrals and are in the process of debugging. The atomic orbitals forming the irreducible set for

the complex have been determined for the octahedral group and the wave function components for the molecular orbital have been found. During the coming month we hope to complete the overlap integral calculations and begin the program for the self consistent solution of the eigenstates of the octahedral complex.

Respectfully submitted,

F. L. Grismore
Project Director

Approved:

E. J. Scheibner, Chief
Physical Sciences Division

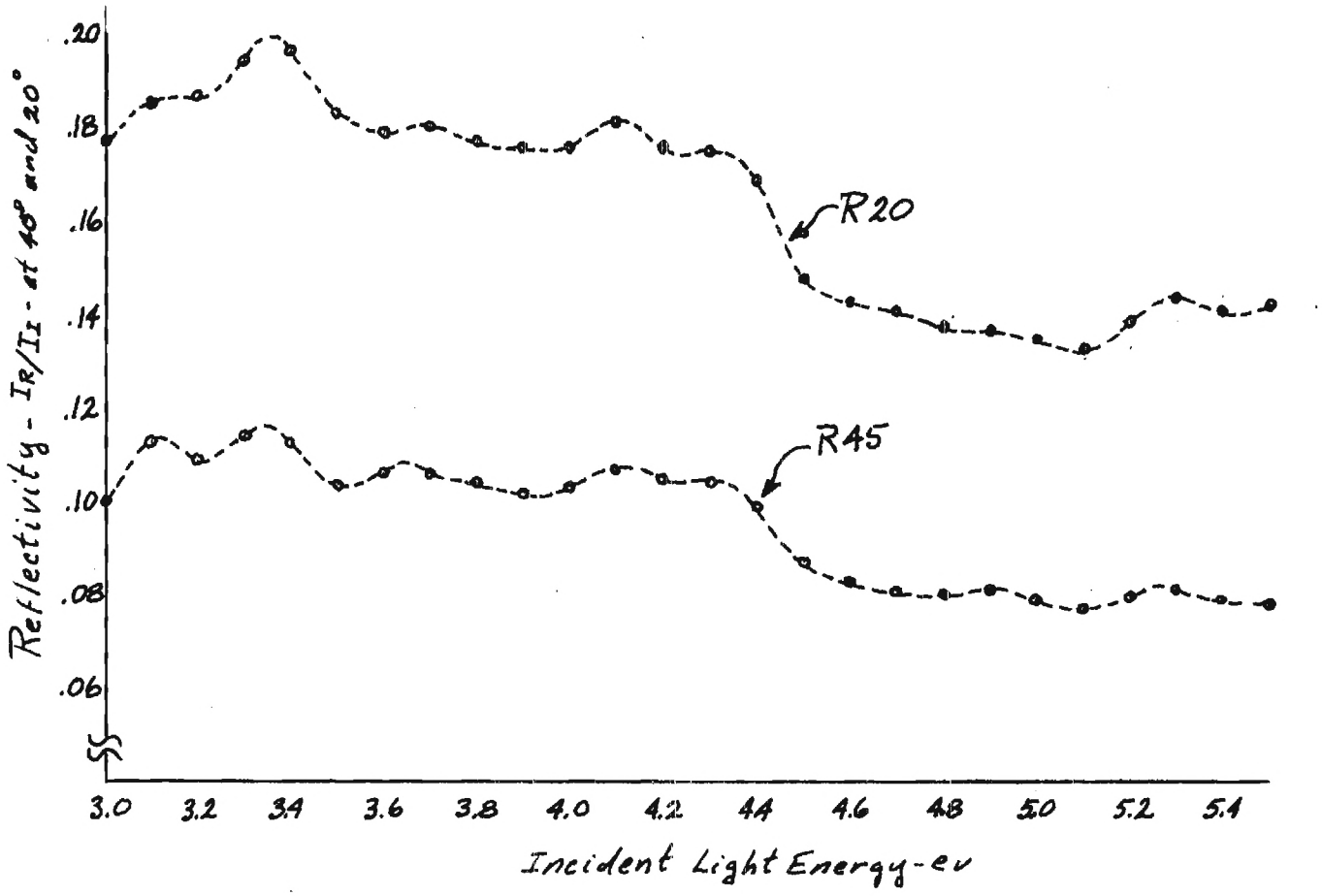

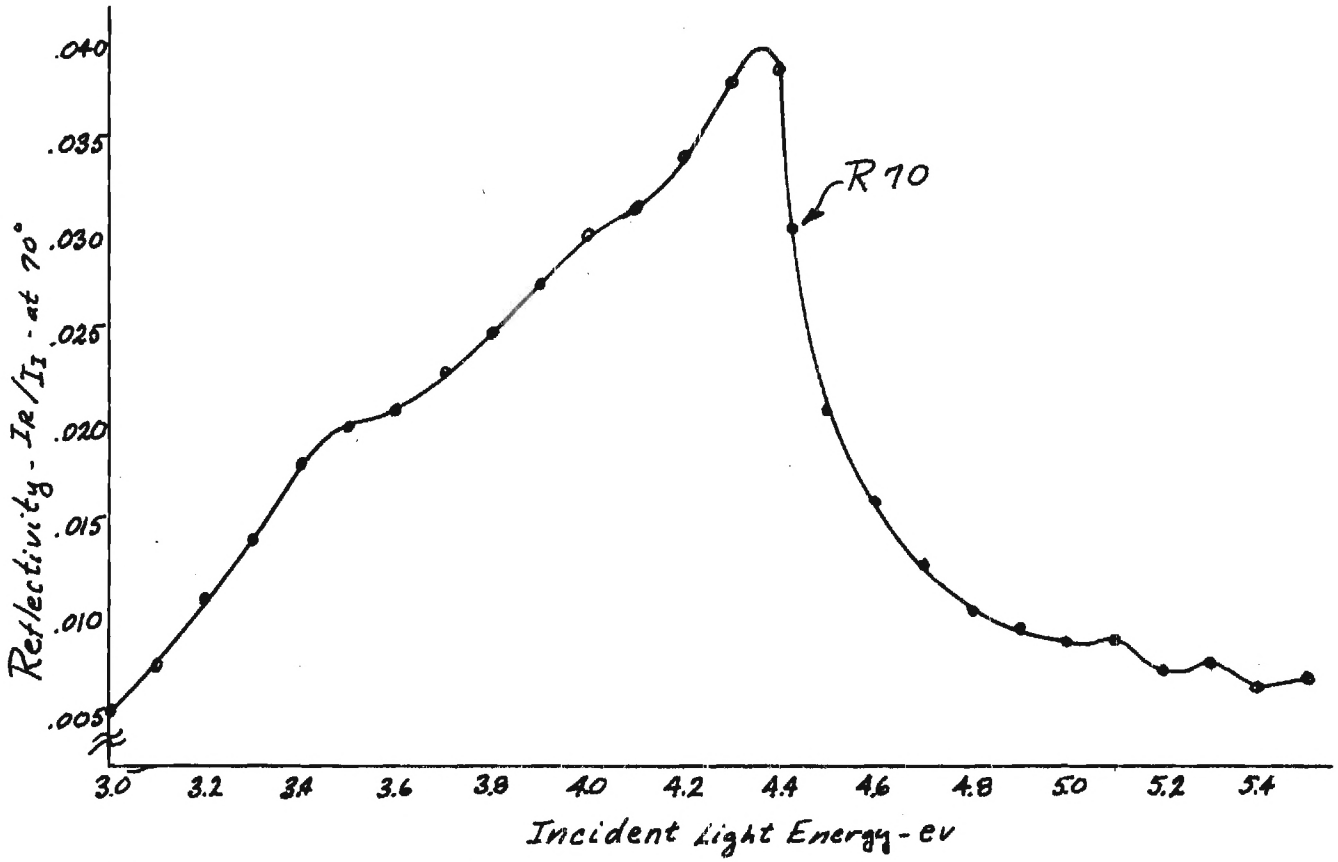

Figure 1. Measured Reflictivities for GdIG

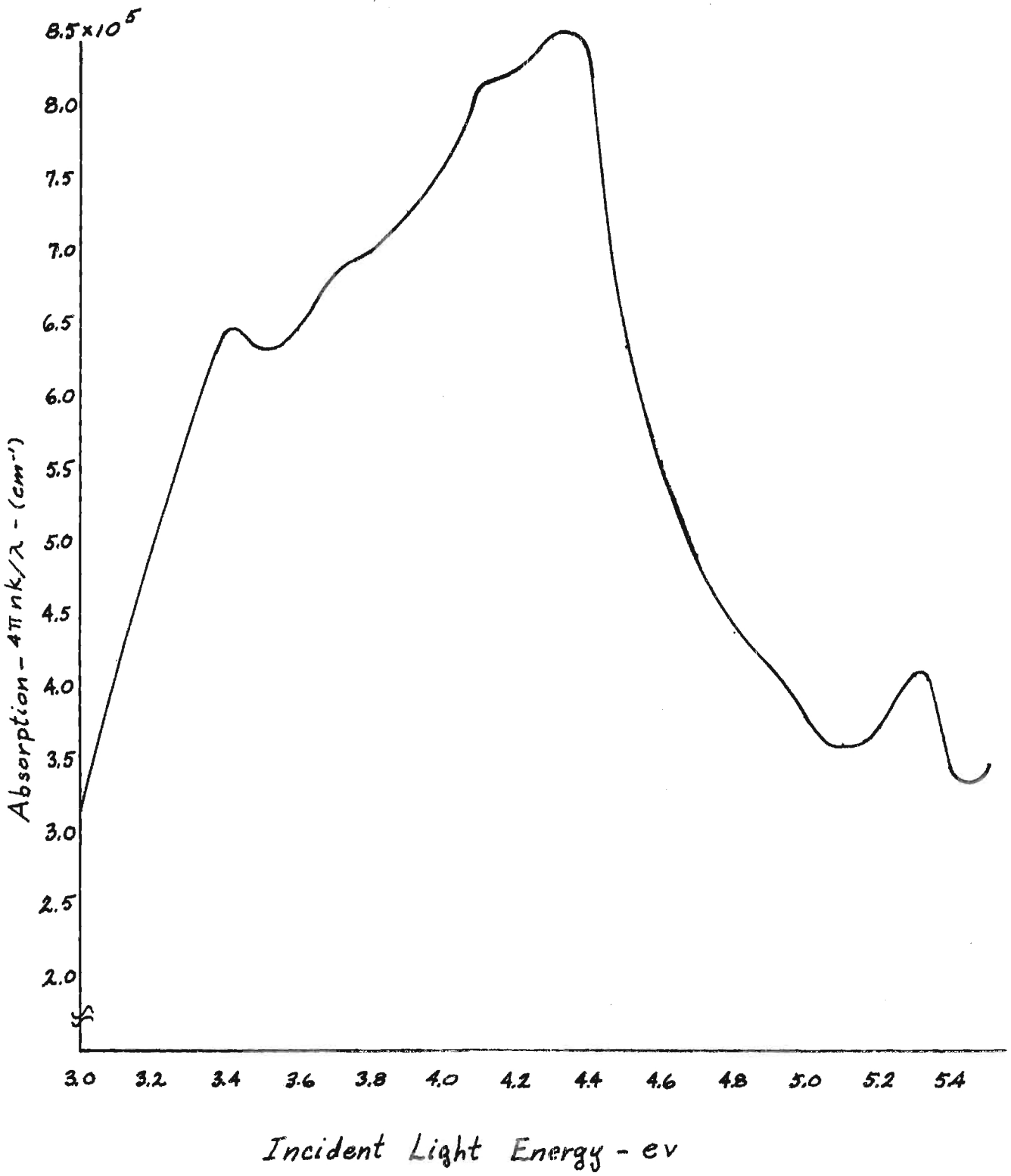

Figure 1. Loss Function ($4\pi nk/\lambda$) Calculated From Optical Data

Figure 3

Complex Index of Refraction

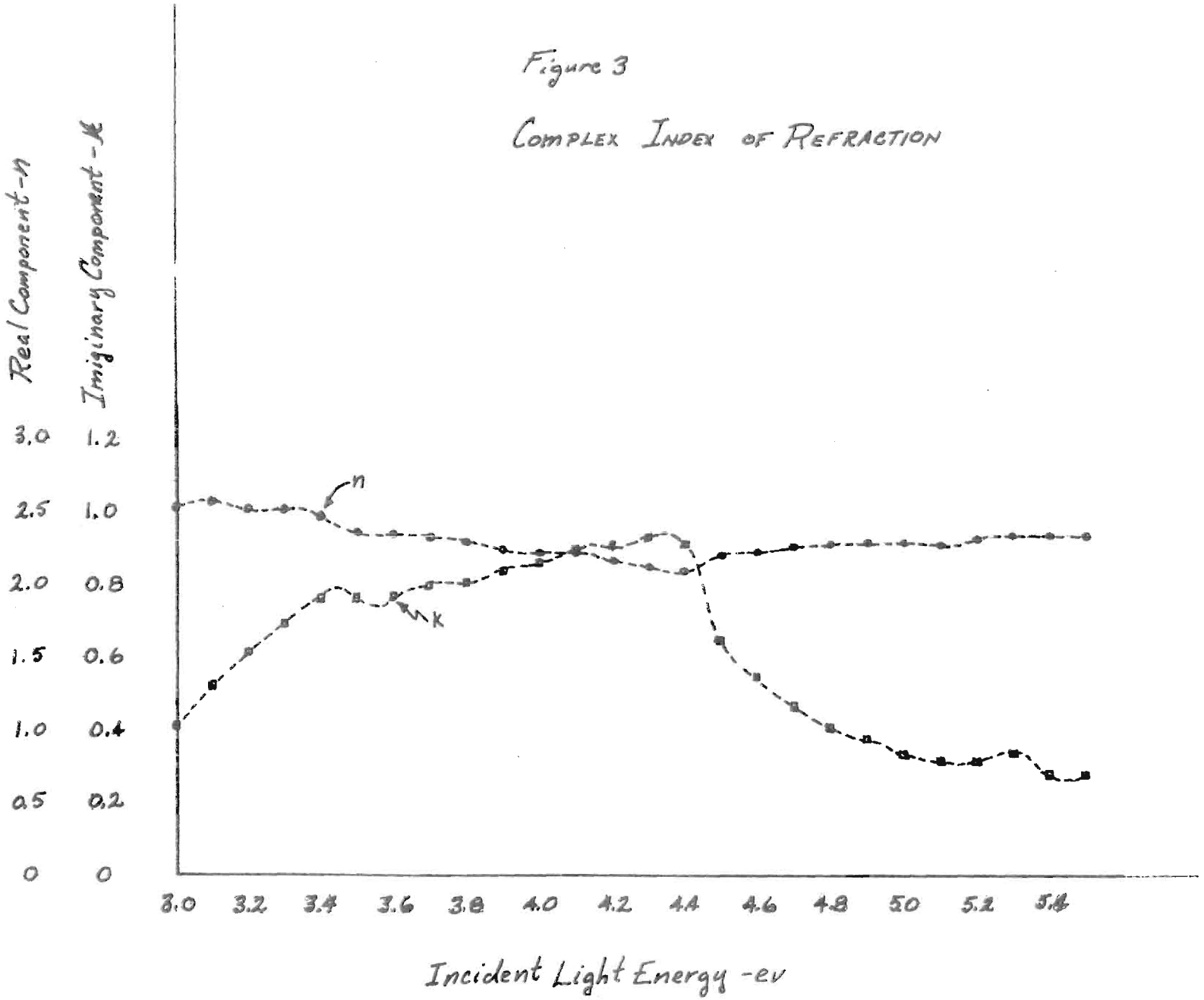

Fig. 4 FREE ION SPECTRA FOR Gd, Tb, & Dy

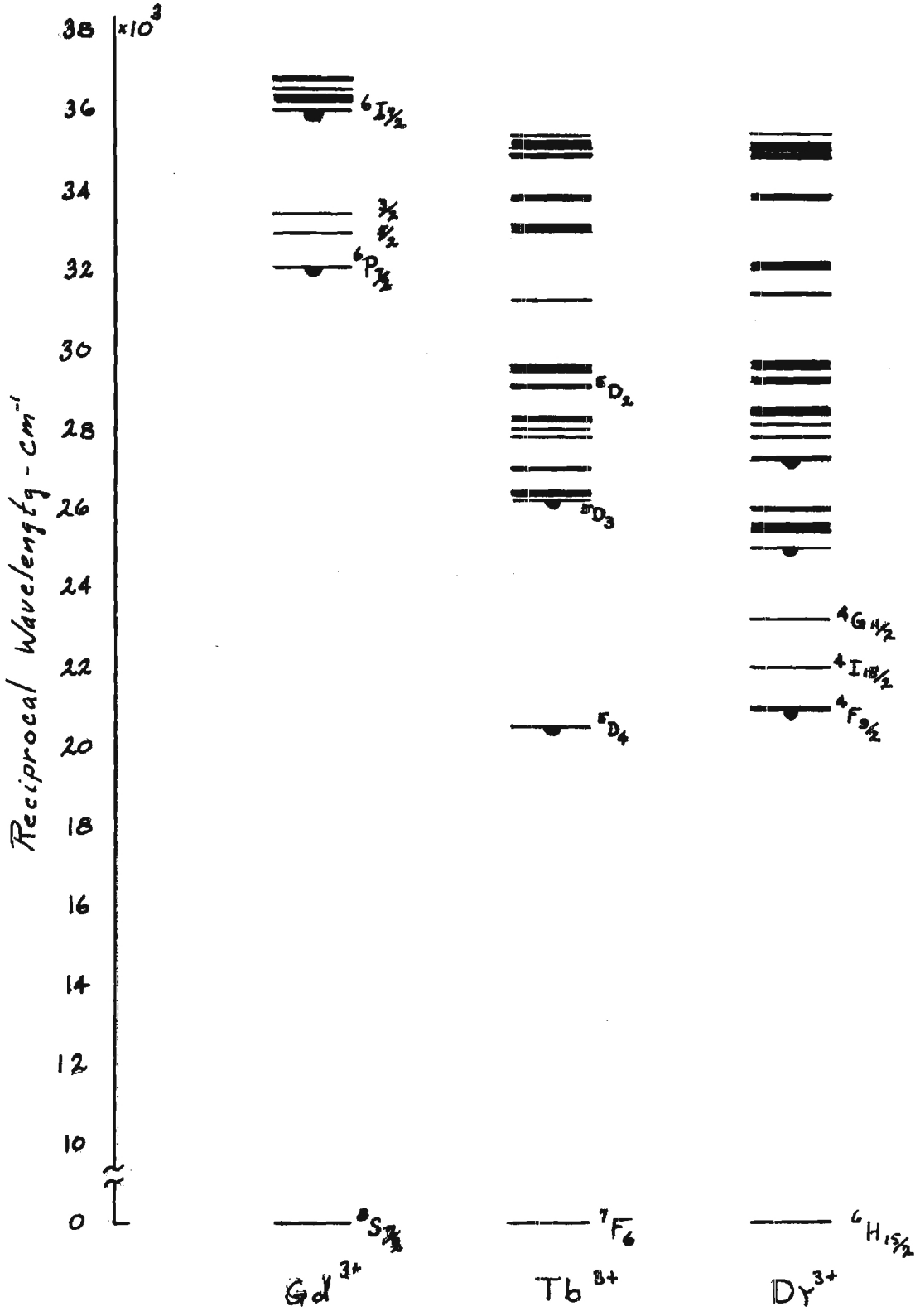

A-1028

ENGINEERING EXPERIMENT STATION
GEORGIA INSTITUTE of TECHNOLOGY

ysical Sciences Division

325 North Avenue N.W.
Atlanta, Georgia 30332
(404) 873-4211 Ext. 220

September 30, 1968

National Aeronautics and Space Administration
George C. Marshall Space Flight Center
Huntsville, Alabama 35812

Attention: Mr. William J. McKinney

Subject: Monthly Progress Letter 14, Project A-1028
"Study of Feasibility of Optically Exciting a Magnetic Memory"
Contract No. NAS8-20813
Covering the Period from 12 August to 12 September 1968

Gentlemen:

During this month we have obtained experimental data on terbium iron garnet which is very encouraging. The results shown in Figure 1, indicate an absorption peak just below 2.5 ev which corresponds quite favorably with the free ion spin flip absorption at 20,000 cm^{-1}, i.e., 2.48 ev. The free ion spectrum of Gd, Tb, and Dy were included in last month's report. Terbium also shows a number of rather broad absorption lines from 26,000 cm^{-1} to 35,000 cm^{-1}. Our absorption data shows a broad absorption peak between 3.1 ev and 3.7 ev, i.e., 25,000 cm^{-1} to 30,000 cm^{-1}, and a sharper peak at 3.9 ev, i.e., 32,000 cm^{-1}. These features agree well with the free ion structure. The absorption structure in our data at 2.8 to 3.0 ev does not correlate with free ion terbium and we are not able at present to predict its source. It is anticipated that the molecular orbital calculations of the iron-oxygen complexes will shed some light on these features.

The computer program used to derive the optical constants from the reflection data was modified some during this period. We have found it desirable to calculate the error at each trial value of n and k as the sum of a percentage squared. The previous calculations minimized an error of the form

$$E = \sum_{\theta} \left[R_{(\theta)_{measured}} - R_{(\theta)_{calculated}} \right]^2$$

where θ took discrete values of 20°, 45°, and 70°.
This form of error does not satisfactorily weigh the effects of the reflection at 70° because the magnitude of R at this angle is nearly an order of magnitude smaller than that at 20° and 45°. For this reason we now use an error of the form

$$E = \sum_{\theta} \left[\frac{R_{(\text{measured})}(\theta) - R_{\text{calculated}}(\theta)}{R_{\text{measured}}(\theta)} \right]^2$$

This appears to give more uniform results and is considered to be an improvement over the original technique originally proposed by Hunter.[1]

Overlap integral calculation of the molecular orbital problem have still not been determined because of complications arising in the development of the computer program. It now appears that the numerical method first employed will not be satisfactory because of the long computer time necessary for the required accuracy. A different technique is now being developed which involves the calculation and summation of less than 20 simple terms. This should permit accurate and very rapid calculation of these quantities. The approach will be discussed in detail later if found to be satisfactory. Once this program is operational the orbital calculations can proceed rapidly and we hope to have initial results in approximately two months.

Future Work

During the following month we will continue our reflectivity measurements on TbIG, on different crystal faces and with different polarizations of light. Specifically we plan to investigate the effect of circular polarization on the momentum transfer process associated with the spin flip transitions.

Work on the molecular orbital calculations will continue. It is anticipated that the overlap integral calculations will be completed during this period.

---

1 W. R. Hunter, "Errors in Using the Reflectance vs. Angle of Incidence Method for Measuring Optical Constants," J. Optical Soc. Amer., 55, No. 10, Part 1, October, 1965.

Financial

	Budget	Free Balance
Personal Services	$32,885.00	$ 9,108.12
Materials & Supplies	2,400.00	- 70.36
Travel	450.00	108.45
Computer	490.00	234.44
Overhead	18,744.00	5,191.18
Total	$54,969.00	$14,571.83

Respectfully submitted,

F. L. Grismore
Project Director

Approved:

E. J. Scheibner, Chief
Physical Sciences Division

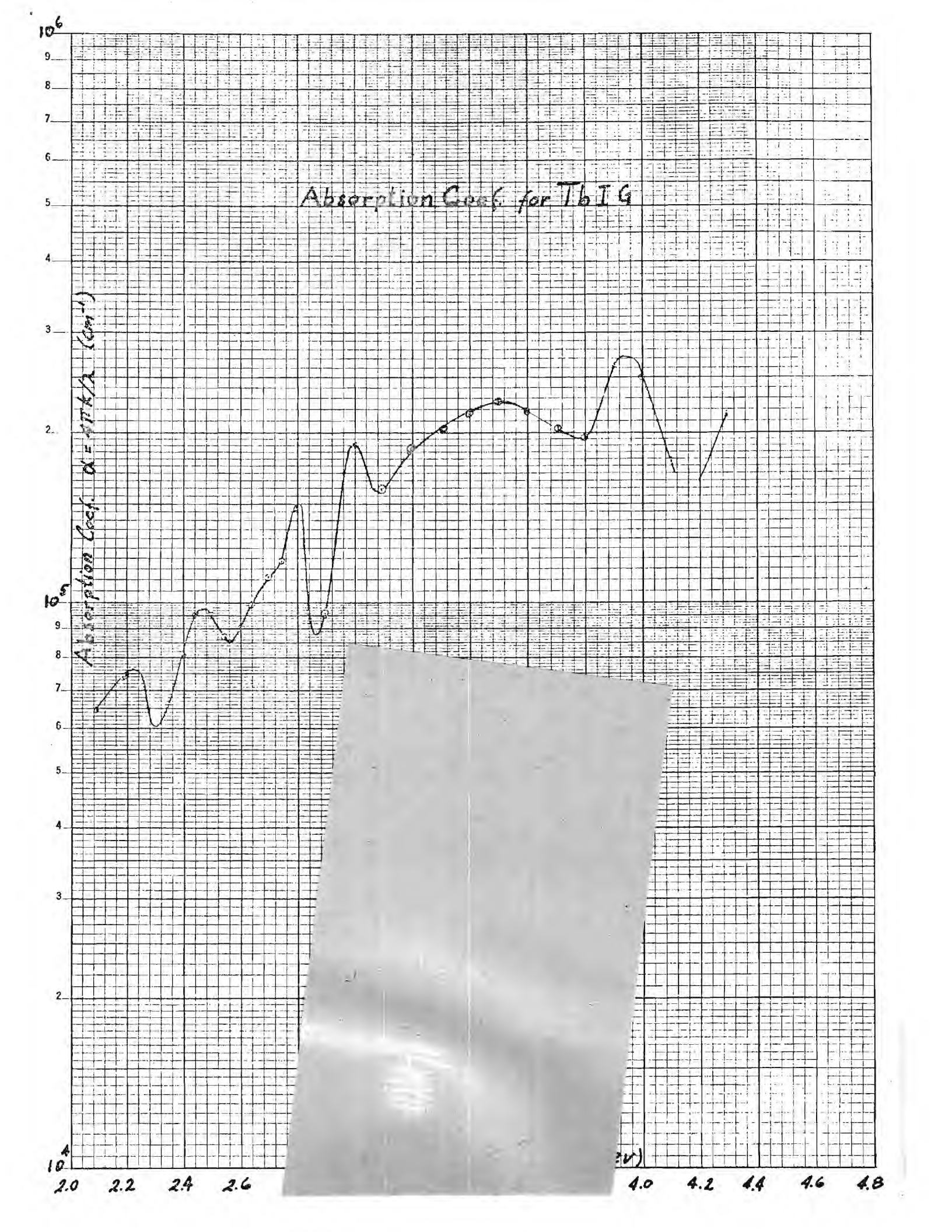
Absorption Coef. for TbIG
Absorption Coef. α = 4πk/λ (cm⁻¹)
10⁶
9
8
7
6
5
4
3
2
10⁵
9
8
7
6
5
4
3
2
10⁴
2.0
2.2
2.4
2.6
4.0
4.2
4.4
4.6
4.8

A-1024

ENGINEERING EXPERIMENT STATION

GEORGIA INSTITUTE of TECHNOLOGY

ıysical Sciences Division

225 North Avenue N.W.
Atlanta, Georgia 30332
(404) 873-4211 Ext. 220

6 February 1969

National Aeronautics and Space Administration
George C. Marshall Space Flight Center
Huntsville, Alabama 35812

Attention: Mr. William J. McKinney

Subject: Monthly Progress Letter 15, Project A-1028
"Study of Feasibility of Optically Exciting a Magnetic Memory"
Contract No. NAS8-20813
Covering the Period 12 September to 12 October 1968

Gentlemen:

We have continued to take and analyze data on several samples of the TbIG single crystals grown during this project. Using the reflectivity techniques developed we can obtain data from single crystal surfaces as grown. This eliminates the possibility of modification of observed spectra by surface damage from polishing. Thus we are able to obtain information on bulk material with the precision attainable only on thin films using transmission spectroscopy.

Of particular interest is recent data using circularly polarized light. In this experiment, a quartz quarter wave plate was incorporated into the optical path and reflectivity data taken in the manner described in previous reports. It was anticipated that excited states involving a change in magnetic moment from the ground state would show an energy shift under excitation of resonant circularly polarized light. This is a result of the selection rules associated with Zeeman splitting of the atomic states.

The rare earth atoms at room temperature essentially form a paramagnetic assembly in a large superexchange molecular field. Based on the known magnetization of the sublattice at room temperature of approximately 1700 Gauss, it is possible to estimate the effective field from the Brillouin function expression:[1]

1 A. H. Morrish, The Physical Principles of Magnetism, John Wiley & Sons, Inc., New York, 1965, Section 13.

$$M = NgJ\mu_B B_J(y)$$

where

$$y = \frac{Jg\mu_B H_{eff}}{kT} .$$

The result is $H_{eff} \approx 0.5 \times 10^7$ Oersted. Such a field would cause splitting of the degenerate atomic states in intervals of

$$\Delta E = 2\mu_B H \approx 1 \times 10^{-13} \text{erg} = 0.062 \text{ ev} .$$

The selection rules for transitions between various levels of states split by a magnetic field are

$$\Delta J = \pm 1$$

when observing the spectrum along the axis of the magnetic field. Linearly polarized light will create both allowed transitions while circularly polarization will create $\Delta J = +1$ or $\Delta J = -1$ depending on the direction of circular polarization. Using the free ion notation for the ground and first excited states of terbium, i.e., $^7F_6$ and $^5D_4$ respectively one can calculate that a shift of approximately 0.12 ev should be observed for such a transition in going from linear to circularly polarized light.

In this experiment we did in fact observe a shift of approximately 0.1 ev in the line at 2.4 ev under excitation with circularly polarized light. Referring to Progress Letter 14 it is this line we tentatively assigned as being the terbium spin flip first excited state. This new information adds support to this assignment. The remainder of the structure remained essentially unchanged under circularly polarized radiation. We therefore feel that the absorption peak at approximately 2.4 ev is the line in TbIG which must be pumped to cause the desired change in sublattice magnetization.

Mike Wynn who has been working on the computer programs for the overlap integrals has left the project as a result of teaching responsibilities in the Physics Department. During this period he has written a report of the work relating to the theoretical calculations and this will be included in the Final Report. Due to the small budget it appears that the theoretical work will not be able to be completed.

Future Work

During the next reporting period we anticipate obtaining data on the DyIG samples which have been fabricated.

Financial

	Budget	Free Balance
Personal Services	$32,885.00	$ 7,203.59
Materials and Supplies	$ 2,400.00	$ - 77.38
Travel	$ 450.00	108.45
Computer	$ 490.00	$ - 227.58
Overhead	$18,744.00	$ 4,105.60
Total	$54,969.00	$11,112.68

Respectfully submitted,

F. L. Grismore, Jr.
Project Director

Approved:

E. J. Scheibner, Chief
Physical Sciences Division

A-1028

ENGINEERING EXPERIMENT STATION

GEORGIA INSTITUTE of TECHNOLOGY

ıysical Sciences Division

225 North Avenue N.W.
Atlanta, Georgia 30332
(404) 873-4211 Ext. 220

6 February 1969

National Aeronautics and Space Administration
George C. Marshall Space Flight Center
Huntsville, Alabama 35812

Attention: Mr. William J. McKinney

Subject: Monthly Progress Letter 16, Project A-1028
"Study of Feasibility of Optically Exciting a Magnetic Memory"
Contract No. NAS8-20813
Covering the Period 12 October to 12 November 1968

Gentlemen:

During this month we have completed taking the first set of data from the DyIG samples. The experimental apparatus has been modified to permit data to be accumulated without the time consuming tedium of point by point measurement. There are however some problems with the new apparatus and it will probably be necessary to take more data in order to feel confident of the results.

The technique involves sweeping the monochrometer while synchronously tracking a recorder at the output of the photomultiplier. By taking only three runs (20° incidence, 70° incidence and direct radiation) the reflectivities can subsequently be extracted from the records. We have made several runs to check the stability of the lamp and find the data quite repeatable. The main problem however lies in the fact that because of the sharp intensity spectrum of the mercury arc lamp, the data we obtain is often on the sharp edge of a peak in incident light intensity. This creates a degree of uncertainty in extracting small variations in reflectivity due to the sample.

In order to reduce the recorded data, the computer program to calculate complex refractive index has been rewritten. The details of the new program will be included in the final report. In brief, the data of photomultiplier detector output current as a function of linear distance on the output record is punched onto paper tape, serving as input to the program.

A fifth order polynomial correlates recorder distance to monochrometer wavelength. Such a high order polynomial was found necessary to match the dispersion characteristic of the monochrometer. By inserting appropriate gain and conversion coefficients the current amplitudes are reduced to normalized intensity values from which the complex index and absorption coefficients are calculated. Due to computer system problems as well as some programming problems a complete set of calculations have not been performed to date.

From the data that has been analyzed of the DyIG run we do observe a wide absorption region starting at about 20,000 cm^{-1} with much fine structure to about 34,000 cm^{-1}. Referring to the Dy^{3+} spectra given in Report 13 it is observed that this is consistent with what would be expected. We observe prominent peaks at about 28,000 cm^{-1}, 30,000 cm^{-1}, and 32,000 cm^{-1} which correlate approximately with the free ion data. However, the line at 20,000 cm^{-1} is yet in doubt. This is the line we were hoping to see and while we do have some structure in the data at this energy it is very weak. We hope to resolve this question with subsequent data.

Future Work

The computer program debugging effort will continue and possibly more data will be taken on the DyIG sample. During the next period we anticipate a reduction in effort will be required because of pressing demands of program personnel on other projects.

Financial

	Budget	Free Balance
Personal Services	$32,885.00	$ 5,837.83
Materials and Supplies	$ 2,400.00	$ - 98.21
Travel	$ 450.00	$ 108.45
Computer	$ 490.00	$ - 241.11
Overhead	$18,744.00	$ 3,327.12
Total	$54,969.00	$ 8,934.08

Respectfully submitted

F. L. Grismore, Jr.
Project Director

Approved:

E. O. Scheibner, Chief
Physical Sciences Division

A-1028

ENGINEERING EXPERIMENT STATION

GEORGIA INSTITUTE of TECHNOLOGY

ysical Sciences Division

225 North Avenue N.W.
Atlanta, Georgia 30332
(404) 873-4211 Ext. 220

13 February 1969

National Aeronautics and Space Administration
George C. Marshall Space Flight Center
Huntsville, Alabama 35812

Attention: Mr. William J. McKinney

Subject: Monthly Progress Letter 17, Project A-1028
"Study of Feasibility of Optically Exciting a Magnetic Memory"
Contract No. NAS8-20813
Covering the Period 6 November-5 December, 1968

Gentlemen:

As reported in the previous letter, some cut-back in effort was necessary because of personnel committment to other programs. There have however been several new findings which are of significant importance to this research.

During the week of November 18, F. L. Grismore attended the Conference on Magnetism and Magnetic Materials in New York City. There were two papers which add both credence and impetus to our work of attempting the optical pumping of the rare earth iron garnets for memory selection.

The first of these was the work of Andreadakis and Williams of the University of Delaware, who have observed significant optical pumping of Mn ions in ZnMnS. In their work, they measured the change in magnetic susceptibility under the influence of radiation for varying concentrations of Mn ions. It is very noteworthy that the pumping effect became increasingly large as they increased the Mn concentration to 30% (the maximum value attempted in their experiments). This is rather unexpected, but in a good way for us, since the 3d electrons responsible for the Mn magnetic moment are greatly influenced by the crystal field of the lattice. It has generally been assumed, from fluorescence data, that at concentrations exceeding a few per cent the lifetime of the excited states became so short that significant pumping would be impossible. Andreadakis and Williams have

shown that this is not the case and show that the effect is large even as antiferromagnetic exchange sets in at the higher concentrations. We feel more confident than ever that a similar but larger effect will occur in the rare earth garnets because of the shielded environment of the $4f$ magnetic electrons of the rare earth ions.

In a second important paper, Kahn and Pershan from Harvard, reported on ultra-violet Kerr measurements on several ferric oxides in an attempt to measure the charge transfer spectra of the octahedral and tetrahedral iron sites in these materials. They conclude from the experimental results that there is a charge transfer transition at 4 ev associated with octahedral sites and at 5 ev, associated with tetrahedral sites. These data should be of significant value to us in helping make assignments to our experimental measurements on the rare earth iron garnets which also contain iron ions in these symmetry locations.

In conferring with Dr. Kahn during the conference I related to him our work with the garnets. He indicated much interest, especially in the theoretical work we are attempting in calculating these transitions via a molecular orbital approach. He pointed out as I have done in previous letter reports, that at present there simply has been no detailed work which will permit a satisfactory description of the optical transitions in these materials.

Some additional work has been carried out to debug the new reflectivity program written last month. We still however have some problems. Some results have been obtained, however it has only been over a limited energy range. We hope to obtain complete compilation of the DyIG data in the near future.

Future Work

Because of the uniqueness of the data taken on GdIG and TbIG we hope to submit a paper to the Intermag Conference this year. During the next reporting period, an effort will be made to organize much of the presently acquired data and present a paper abstract to the Intermag Technical Committee.

Financial

	Budget	Free Balance
Personal Services	$32,885.00	$5,659.67
Materials and Supplies	2,400.00	-130.64
Travel	450.00	108.45
Computer	490.00	-244.70
Overhead	18,744.00	3,225.57
Total	$54,969.00	$8,618.35

Respectfully submitted,

F. L. Grismore, Jr.
Project Director

FLG/srt

Approved:

to Edwin J. Scheibner, Chief
Physical Sciences Division

A-1028

ENGINEERING EXPERIMENT STATION

GEORGIA INSTITUTE of TECHNOLOGY

ıysical Sciences Division

225 North Avenue N.W.
Atlanta, Georgia 30332
(404) 873-4211 Ext. 220

13 February 1969

National Aeronautics and Space Administration
George C. Marshall Space Flight Center
Huntsville, Alabama 35812

Attention: Mr. William J. McKinney

Subject: Monthly Progress Letter 18, Project A-1028
"Study of Feasibility of Optically Exciting a Magnetic Memory"
Contract No. NAS8-20813
Covering the Period 6 December 1968-5 January 1969

Gentlemen:

Work during this month has been centered around detailed evaluation of the GdIG and TbIG data presently available in order to extract the information significant to the achievement of the goal of optically exciting a magnetic memory.

We have calculated the transition oscillator strength and lifetime of the lines we believe to be magnetic spin flip excitations. The oscillator strength is a common non-dimensional "quality factor" in optical spectroscopy and is directly proportional to the transition probability. The optical pumping power required to achieve a given excited population of the atomic system is proportional to the (absorption cross-section)·(lifetime) product. Therefore values of the product $f\tau$ are also a measure of required pump power since f, the oscillator strength is directly proportional to the absorption cross-section.

The oscillator strength is related to the absorption coefficient as

$$f = \frac{mc^2}{\pi e^2 N} \int \frac{K(\lambda)\,d\lambda}{\lambda^2}$$

where $K(\lambda)$ is the wavelength dependent absorption coefficient

N is the number of absorbing atoms per cm^3 in the material

and the integration is performed over the wavelength range of the absorption line. From the data taken during this contract we have extracted, in an approximate fashion, the single line absorption due to the single transition of interest and calculated the oscillator strength. The lifetime can then be calculated from the oscillator strength.[1] The results for GdIG and TbIG are similar yielding an oscillator strength of $f \approx 10^{-3}$ and a lifetime of $\tau \approx 1 \times 10^{-7}$. The resulting $f\tau$ product is nearly identical to the free ion value measured by Gandy and Ginther.[2] They reported $f \approx 10^{-7}$ and $\tau = 10^{-3}$. Thus the crystal field effects which increase the transition probability for absorption reduce the lifetime by an equivalent amount to keep the $f\tau$ product constant. This is of course a result of the fact that the ratio of A/B, i.e., the Einstein coefficients for spontaneous and stimulated transitions, is a fundamental constant.

We have written a program to decompose the measured absorption spectra into discrete spectra using a linear combination of lines of the form

$$K = \frac{K_o}{(\omega_o - \omega)^2 + \left(\frac{\Gamma}{2}\right)^2}$$

This is the classical line shape form where ω_o is the center frequency of the line and Γ is the half-width. The program treats K_o and Γ as adjustable parameters and seeks a best fit of the adjustable line intensities and bredths to the experimental data. From these results to oscillator strength and lifetime are computed.

An abstract has been written and submitted to Intermag for presentation at the Amsterdam conference in April. A copy is attached to this letter.

---

[1] S. Wang, Solid State Electronics, McGraw-Hill, 1966, p.728.

[2] H. W. Gandy and R. J. Ginther, "Stimulated Emission of U.V. Radiation From Gadolinium-Activated Glass," Appl. Phys. Lett. 1, No. 1 (September, 1962).

Future Work

The absorption data will continue to be analyzed through the use of the new computer programs. A thermal analysis of the proposed memory will be carried out based on the power requirement determined from the oscillator strength data.

Financial

	Budget	Free Balance
Personal Services	$32,885.00	$5,387.40
Materials and Supplies	2,400.00	-130.89
Travel	450.00	108.45
Computer	490.00	-264.04
Overhead	18,744.00	3,070.38
Total	$54,969.00	$8,171.30

Respectfully submitted,

F. L. Grismore, Jr.
Project Director

FLG/srt

Approved:

for
Edwin J. Scheibner, Chief
Physical Sciences Division

FINE STRUCTURE ABSORPTION MEASUREMENTS OF BULK R.E.IG SINGLE CRYSTALS BY REFLECTIVITY TECHNIQUES

F. L. Grismore, Jr. and J. Elmer Rhodes, Jr.
Georgia Institute of Technology, Atlanta, Georgia 30332

Because of the potential memory applicability of the rare earth iron garnets in optically accessed memories a detailed understanding of optically excited electronic transitions is of considerable importance. In this paper we report the results of measurements made on bulk samples using reflectivity techniques to obtain new fine structure absorption data through the visible and near ultraviolet where the crystals are opaque. Using an analysis technique originally proposed by Hunter[1] we have computed the complex index of refraction of GdIG, TbIG, and DyIG bulk single crystals over an energy range of 2 to 5.5 electron volts. These data contain the absorption coefficient K, the oscillator strength and an excited state lifetime for the prominent absorption lines. We attribute much of the fine structure in this absorption data to intraband transitions of $4f$ electrons in the rare earth ions.

The crystals used were grown by the molten flux method at a cooling rate of $\frac{1}{2}$° C/hour. Measurements have been made on natural crystallographic faces and surfaces cut and mechanically polished parallel to the natural face. Reflectivity measurements were made using a 1 kw air-cooled mercury vapor lamp, type BH-6, in conjunction with a Gaertner L-234-150 prism monochromator and type EMI9601B photomultiplier tube. The radiation incident on the sample was linearly polarized in the plane of incidence. Reflectance was measured at 20° and 70° angle of incidence over the desired wavelength range. Typical data for GdIG is shown in Figure 1. For any specified wavelength λ, the Fresnel equations may then be solved in a self-consistent manner to obtain complex index of refraction. Figure 2 shows the result for the GdIG reflectivity data of Figure 1. The absorption coefficient $K = \frac{4\pi k}{\lambda}$ is contained in the complex index; the calculated K for the same sample is shown in Figure 3. By subtracting out the background absorption and fitting the remaining fine structure with normal shaped absorption lines we can estimate the absorption coefficient and line width for each line of the fine structure. In this manner it is possible to estimate the oscillator strength and excited state lifetime associated with the various absorption lines.

Of particular interest are the lines visible in Figure 3 at approximately 4.1 and 4.35 ev. We believe these to be intraband transitions of gadolinium corresponding to free ion excited states of $^6P_{7/2}$ and $^6I_{7/2}$. The free ion energies for such transitions are known to be at 3.97 ev and 4.45 ev respectively. Oscillator strengths for these lines are of the order of $f \approx 10^{-3}$ and lifetimes are calculated of $\tau \approx 10^{-7}$ sec. Similar data is available for TbIG and DyIG. These transitions involve a change in spin, thus each excited gadolinium ion contributes to a reduction in gadolinium sublattice magnetization. The coercive force is very sensitive to sublattice magnetization when the material is temperature biased at the compensation point. The question

1. A7, Magneto-optics.
2. F. L. Grismore, Jr., Georgia Institute of Technology, Physical Sciences Division, E.E.S., Atlanta, Georgia, 30332.

arises as to the plausibility of optically pumping these rare earth excited states in order to effect a significant change in H_c as originally proposed by Forlani and Minnaja[2] for memory selection.

These data and optical and thermal considerations of such a memory selection technique are described.

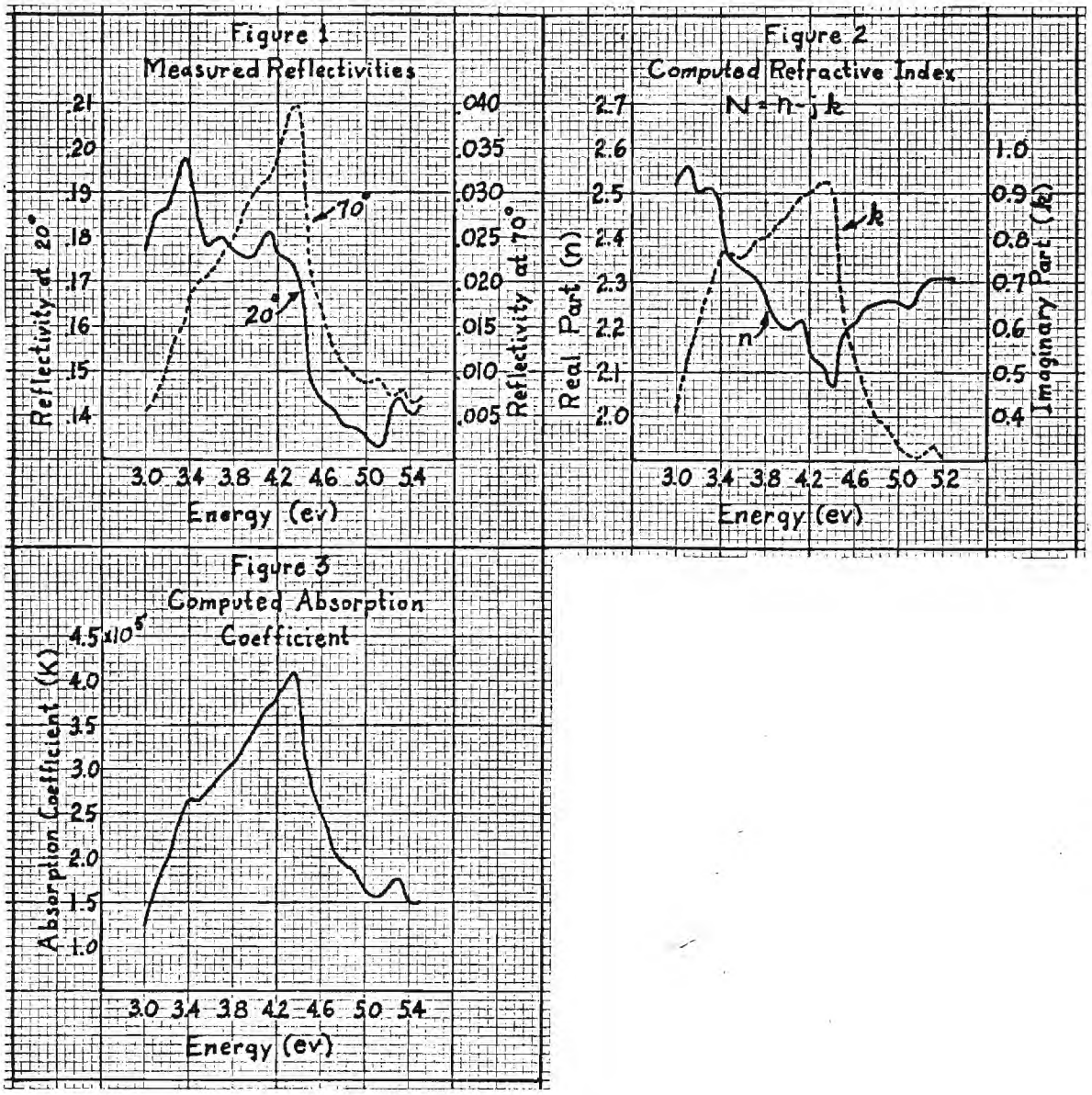

References

1. W. R. Hunter, J. Opt. Soc. Amer. 55, 1197-1204 (October 1965).
2. F. Forlani and N. Minnaja, Proc. IEEE 711-712 (April 1966).

A-1028

ENGINEERING EXPERIMENT STATION
GEORGIA INSTITUTE of TECHNOLOGY

hysical Sciences Division
225 North Avenue N.W.
Atlanta, Georgia 30332
(404) 873-4211 Ext. 220

24 April 1969

National Aeronautics and Space Administration
George C. Marshall Space Flight Center
Huntsville, Alabama 35812

Attention: Mr. William J. McKinney

Subject: Monthly Progress Letter 19, Project A-1028
"Study of Feasibility of Optically Exciting a Magnetic Memory"
Contract No. NAS8-20813
Covering the Period 6 January-5 February 1969

Gentlemen:

During this period our efforts have been directed towards the evaluation of several system aspects of an optically pumped memory system. This is now possible as a result of the data available from the reflectivity measurements and their subsequent reduction.

Using the program described in the previous report we have approximated the absorption spectra of GdIG and TbIG with a series of Lorentzian-shaped lines. The results of this analysis are shown in Figures 1 and 2. The line shape is given as

$$K = \frac{K_i}{(E - E_i)^2 + \left(\frac{T_i}{2}\right)^2}$$

where K = absorption due to the $i^{\underline{th}}$ line,
E_i = resonant energy of $i^{\underline{th}}$ line,
T_i = half-width of the $i^{\underline{th}}$ line,
K_i = amplitude coefficient of the $i^{\underline{th}}$ line.

The coefficients of the series approximations are given in Tables I and II. From these lines the oscillator strength and absorption line half-width are readily determined. This is the data necessary to evaluate the

feasibility, in terms of required pumping power, of an optically accessed memory using the pumping concept.

We believe the line at 3.9 ev in the GdIG spectrum and the one at 2.45 in the TbIG spectrum are associ ted with the inter $4f$ band rare earth transition and hence cause a significant change in sublattice magnetization.

We have developed the equation for the transition probability of a monochromatic radiation source pumping a distributed density of excited states. The details will be included in the final report; however the results is simply:

$$b = \frac{4\pi^2}{3c\hbar^2} n(\omega)\, I\, |M_{km}|^2 \qquad (1)$$

where
- b = transition probability in electrons/sec,
- $n(\omega)$ = density of states of the excited state,
- M_{km} = electric dipole moment matrix element,
- I = light source intensity in ergs/(cm^2 · sec).

The spontaneous transition rate, depopulating the excited state is given as

$$W = \frac{4\omega_{km}^3 N_T}{3\hbar c^3} |M_{km}|^2 \qquad (2)$$

where
- N_T = total number of rare earth ions per cm^3
- ω_{km} = resonant frequency of the absorption.

Assuming the excited density of states can be approximated by $n(\omega) = N_T/\Delta\omega$ where $\Delta\omega$ = absorption line radian half-width, the ratio of the spontaneous emission rate to the transition rate becomes

$$w/b = \frac{8\pi c \Delta E}{\lambda^3 I} \qquad (3)$$

where ΔE = absorption line energy half-width,
λ = resonant absorption wavelength.

As was shown in the interim report of this contract, the w/b ratio is the significant term in determining the population of excited state ions. The relationship is given as

$$\frac{n_2}{N_T} = \frac{1}{2 + w/b} \tag{4}$$

where n_2 = steady state population of excited ions.

Substituting (3) into (4) and solving for I gives

$$I = \left(\frac{8\pi c \Delta E}{\lambda^3}\right) \left(\frac{n_2}{N_T}\right) . \tag{5}$$

It can be shown that the population of excited ions must be approximately $n_2/N_T \approx 0.02$ in order to reduce the coercive force by a factor of two. From the TbIG data, Table II, it is seen that the line at 2.45 ev has a half-width of $\Delta E = 0.2$ ev. Substituting this in (5) gives a required pumping intensity of

$$I \approx 4 \times 10^3 \text{ watts/cm}^2$$

which is equivalent to 3 mw of laser output focused on a 10 μ diameter spot. The wavelength corresponding to 2.45 ev, i.e., $\lambda = 5040$Å is very close to the 5017Å Green line of an argon laser. We would therefore expect that this type of laser would be compatible with the desired pumping scheme.

An analysis of the thermal heating effect of pumping intensities shows that a temperature rise of up to 10° C may result at the bit being excited. Experimental results of other workers seems to indicate the

excursion is not this great at such low intensity levels. It is certain from the analysis that temperature excursions at adjacent bits would be negligible.

Details of these calculations will be published in the final report, however it is to be noted that the results to date offer much encouragement as to the feasibility of the optical pumping approach to access a magnetic memory. Achievement of this goal would be a significant advancement to the computer system state-of-the-art.

Respectfully submitted,

F. L. Grismore, Jr.
Project Director

FLG/srt

Approved:

/s/ Edwin J. Scheibner, Chief
Physical Sciences Division

TABLE I

Absorption Line Data for GdIG

Line Energy (ev)	3.40	3.72	3.9	4.1	4.35	4.9	5.3
$K_i \times 10^3$ ($cm^{-1}ev^2$)	2.7	6.0	1.5	7.0	5.4	1.0	0.6
T_i (ev)	0.40	0.53	0.48	0.46	0.34	0.46	0.24

TABLE II

Absorption Line Data for TbIG

Line Energy (ev)	2.20	2.45	2.73	2.80	3.02	3.25	3.54	3.95	4.34
$K_i \times 10^3$ ($cm^{-1}ev^2$)	1.00	3.00	2.20	0.60	1.30	5.00	144	25	25
T_i (ev)	0.20	0.20	0.18	0.07	0.08	0.20	0.60	0.25	0.27

Figure 1.

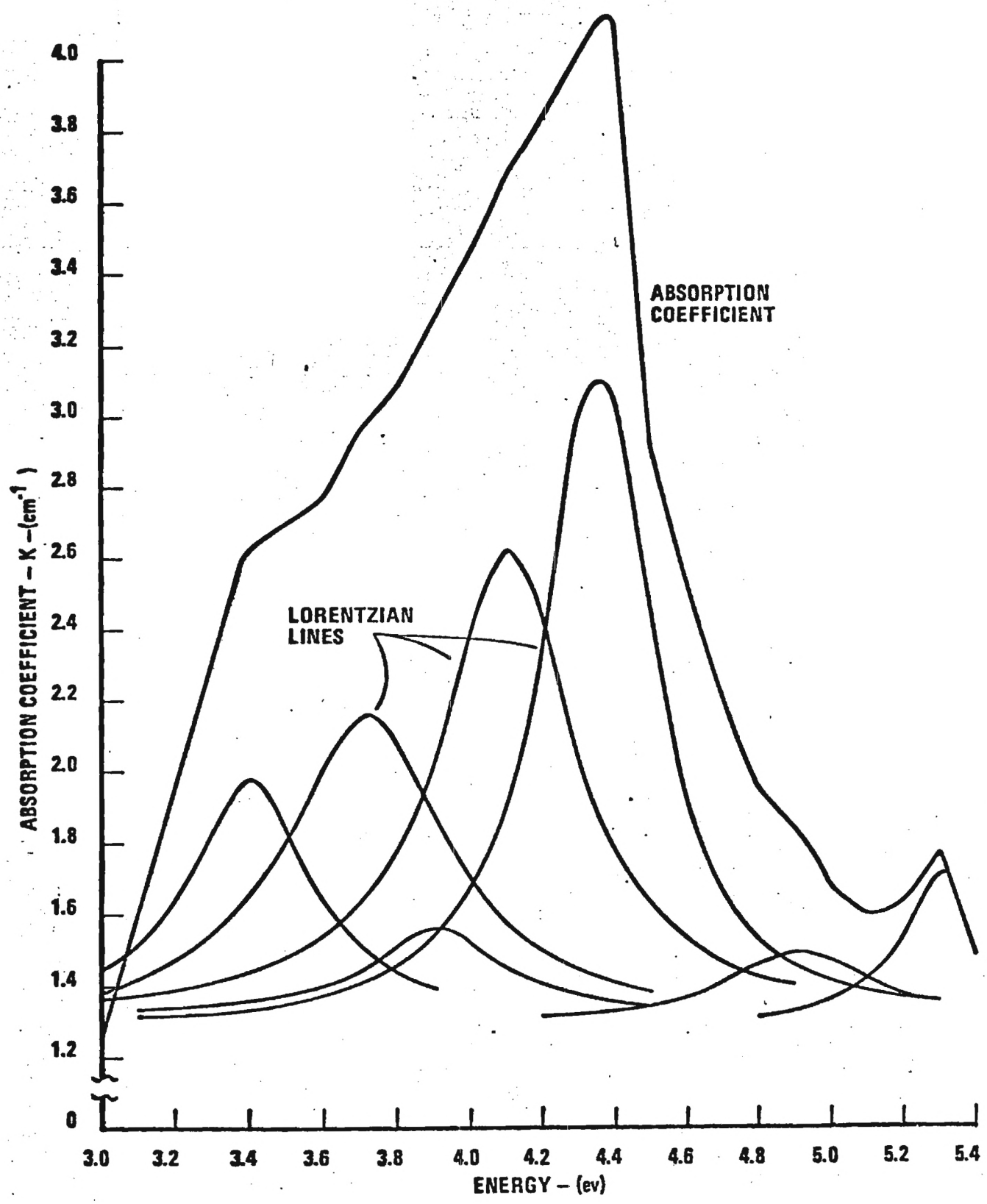
ABSORPTION COEFFICIENT
LORENTZIAN LINES
ABSORPTION COEFFICIENT – K –(cm⁻¹)
ENERGY – (ev)
4.0
3.8
3.6
3.4
3.2
3.0
2.8
2.6
2.4
2.2
2.0
1.8
1.6
1.4
1.2
0
3.0
3.2
3.4
3.6
3.8
4.0
4.2
4.4
4.6
4.8
5.0
5.2
5.4

Figure 2.

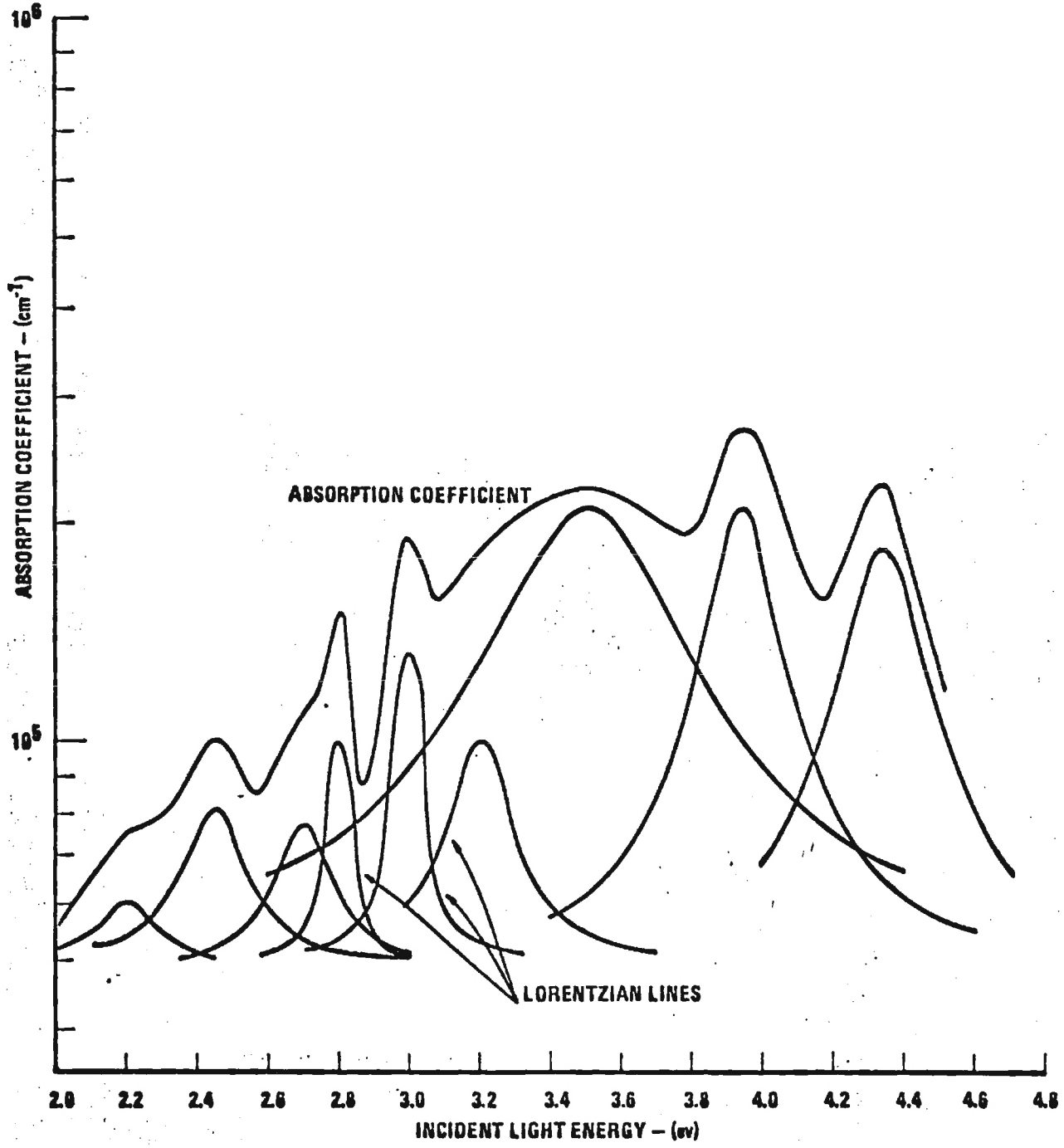
10^6
10^5
ABSORPTION COEFFICIENT – (cm^{-1})
ABSORPTION COEFFICIENT
LORENTZIAN LINES
2.0
2.2
2.4
2.6
2.8
3.0
3.2
3.4
3.6
3.8
4.0
4.2
4.4
4.6
4.8
INCIDENT LIGHT ENERGY – (ev)

GEORGIA INSTITUTE OF TECHNOLOGY
Engineering Experiment Station
Atlanta, Georgia

INTERIM REPORT

PROJECT A-1028

STUDY OF FEASIBILITY OF OPTICALLY EXCITING A MAGNETIC MEMORY

By

F. L. GRISMORE AND J. E. RHODES

Contract No. NAS8-20813

June 1967-March 1968

Prepared For
NATIONAL AERONAUTICS AND SPACE ADMINISTRATION
GEORGE C. MARSHALL SPACE FLIGHT CENTER
HUNTSVILLE, ALABAMA

TABLE OF CONTENTS

LIST OF FIGURES

I. INTRODUCTION

The purpose of this project is to investigate the feasibility of modifying the magnetic moment of a magnetically ordered material by optical pumping and apply the phenomena towards space borne digital memories. The program is divided into two phases, Phase I a feasibility study effort of 9 months duration and Phase II a 3 month fabrication effort. This interim report describes the results of Phase I work and provides recommendations for directions to be pursued during the remainder of the contract.

The potential of optically addressed (often referred to as beam addressable) digital memories has been discussed by a number of authors,[35,36,41] and is currently an area of much research. The goal to which these efforts are directed is the achievement of high density bulk memory with storage capacity of approximately 10^8 bits. This density can be achieved in reasonable size, for example a planar area of 10 cm x 10 cm, with bit resolution of 10 μ. Such a bit size is about an order of magnitude larger than diffraction limited resolution of visible light. Thus, optical approaches appear attractive. In addition, the interaction of polarized light with magnetic materials yielding the magneto-Kerr effect and Faraday effect provides a means for detecting the magnetization state of a local region via reflection or transmission providing communication with the "store" without interconnecting wires.

The limiting operation, however, in all presently proposed memory schemes is the write process. This has universally been accomplished by applying heat to the lattice in order to effect a change in coercivity of a local spot. The heat source may be a laser or electron beam, both have been proposed and experimentally studied. The use of temperature changes to modify the magnetic state of a memory media introduces speed performance limitations.

The thermal time constant for temperature changes in a rectangular bar is given approximately as

$$\tau \approx \frac{c\rho}{k} \frac{\ell^2}{\pi^2}$$

where c = specific heat in cal/gm-deg
k = thermal conductivity in cal/sec-cm-deg
ρ = density in gm/cm^3
ℓ = length of thermal path

Considering relative sizes of the parameters involved it can be shown that the value for garnet type materials is of the order of magnitude, $\tau \sim 10^{-4}$ sec for practical sizes. This places a limit on ultimate cycle time for memories employing thermal excitation. Thin metal films exhibit considerably shorter thermal time constants; however, read-out from such materials must make use of the Kerr effect. Problems associated with low sensitivity and awkward geometrical configuring seriously hamper practical utilization of metal films. The Faraday effect read-out of garnet film systems results in a significantly higher signal-to-noise ratio thus simplifying the sense electronics and increasing system reliability.

In addition to the relatively long time constants, an additional problem associated with thermal excitation is that of thermal creep. In order to prevent adjacent bit disturb effects it appears necessary to provide thermal barriers between storage element locations. This results in a reduction of achievable storage density and increases the fabrication process complexity.

To overcome these limitations associated with thermal excitation, this program is involved in a study to determine the feasibility of optically pumping a magnetic material to effect the switching process. This technique provides the potential of achieving excitation and decay times in the sub micro-second range without the problem associated with thermal creep.

The experimental work to date has been directed toward the rare earth iron garnets. These materials show a rapid change in coercive force versus temperature at the antiferromagnetic compensation temperature. This effect is attributed to the fact that slight variations in temperature cause a net magnetic moment to exist. The resultant moment provides a couple of $M \times H_A$ with any applied external field H_A, switching occurring by rotation whenever

$$H_A \geq H_K = \frac{2K_u}{M} .$$

Since H_K is inversely proportional to M, $H_K \rightarrow \infty$ as $M \rightarrow 0$. Although this is an oversimplified model the essential characteristics appear to be correct.

Thus we look for a technique whereby the lattice temperature can be held constant but M changed by optical excitation. An important aspect of the process must be that the excitation be accomplished without generating lattice phonons for then local temperature variations will cause shifts from the compensation point and we would again be speed constrained by thermal time constants. The rare earth atoms are unique because of the fact that atomic transitions involve $4f$ electrons which are shielded from lattice interactions by filled 5s and 5p sub shells. As a result these atoms show very sharp line fluorescence from excited states in a variety of lattices including YGaG:RE. We therefore anticipated that relaxation from excited states could occur via spontaneous photon emission thus re-radiating the incident energy. In this way the phonon density of states would remain essentially unchanged.

The concept of optically pumping the rare earth garnet to cause a change in magnetic moment can be understood by considering gadolinium iron garnet. Gadolinium iron garnet is a ferrimagnetic material exhibiting a compensation point of approximately 282°K. At this temperature the iron and gadolinium sublattice magnetizations are equal and anti-parallel resulting in zero net moment. The material is therefore essentially uncoupled with respect to an external field and the coercive force is very high. If the magnetization of either sublattice can be changed to uncompensate the material a significant reduction in coercive force results. It is proposed that optically induced transitions of gadolinium atoms can cause such a change. Thus this program is directed towards the study of the variation of coercive force and gadolinium magnetic moment as a function of photon excitation.

The concept of optically induced magnetic moment variations is based on previous observations[11] of a strong emission line from gadolinium in the optical region. The emission wavelength agrees closely to the free ion transition from the excited state $^6P_{7/2}$ to the ground state $^8S_{7/2}$. From this information it is easily shown that this transition corresponds to a significant change in magnetic moment of the gadolinium atom. From the spectroscopic notation the total atomic spin, orbital, and angular momenta are given as:

Ground State

Spin -(2S + 1) = 8 - S = 7/2

Orbit - The letter S represents a net orbital momentum of L = 0

Total Angular Momentum - - - - - - - - - - - - - - - - - - - J = 7/2

Excited State

Spin -(2S + 1) = 6 - S = 5/2

Orbit - The letter P represents a net orbital momentum of L = 1

Total Angular Momentum - - - - - - - - - - - - - - - - - - - J = 7/2

The magnetic moment of an atom exhibiting LS coupling (characteristic of the rare earth elements) is simply

$$m = (gJ)u_B$$

where g is the Lande splitting factor given as

$$g = 1 + \frac{J(J + 1) + S(S + 1) - L(L + 1)}{2J(J + 1)}$$

and u_B is the Bohr magneton.

Thus it is found that the moment of the gadolinium atom in its ground state is

$$m \text{ (ground)} = 7.9 \text{ Bohr magnetons}$$

and in the excited state

$$m \text{ (excited)} = 5.5 \text{ Bohr magnetons} .$$

This shows that it should be possible to achieve a change in magnetic moment of $\Delta m = 2.4$ Bohr magnetons per excited gadolinium atom. Excitation can be produced by optical pumping with light of wavelength $\lambda = 2770\text{Å}$ which corresponds to a high absorption energy associated with the previously discussed excited state.

The write process employing this excitation phenomena will then take place as follows. The GdIG storage plane is temperature biased to its compensation point resulting in a net magnetization of zero and hence a high

coercivity. Application of an external field H, where H < Hc, does not affect the state of any region of the material. Photon energy incident on a local region of the material excites the gadolinium atom as previously discussed resulting in a decrease of the gadolinium magnetic moment. The garnet is thus uncompensated, exhibiting a net moment in the direction of the Fe. This increases the coupling with the external field and the excited region switches so that the net moment is parallel with the external field. Removal of the light and H field leave the switched region in a stable state with the iron moment along the applied field direction. Read-out of stored states would take place using Faraday rotation induced by the iron sublattice.

Detailed results of the work to date will be discussed in subsequent sections of this report. In general however it may be stated with some assurance that gadolinium iron garnet will not permit operation in the proposed mode. We believe, however, that several other materials do provide potential for achieving magnetic pumping. Our measurements on single crystal gadolinium iron garnet have been restricted to reflection and optical emission experiments. It has been found that the absorption of photons by non-radiative process dominates the optical characteristics in the desired spectrum range. As a result, even though the desired absorption does exist, heat is added to the lattice at a rate which completely masks the magnetic pumping effects. In an energy band picture of the material the discrete absorption and emission levels can be pictured as embedded in a "conduction" band having a lower band edge energy of approximately 2.5-2.75 ev. Thus it is not possible to pump the gadolinium atoms without simultaneously creating conduction electrons. In addition the probability of a non-radiative transition to ground state is radically increased. Thus the energy absorbed to pump the magnetic atoms is given up mostly to the lattice rather than being re-radiated as photons. The net result is that it is impossible to hold the temperature of a sample constant at the compensation point.

A possible alternate to gadolinium iron garnet is terbium iron garnet. The terbium atom can be excited by absorption of 2.5 ev photons. This is right at the conduction band edge and along with a similar characteristic of dysprosium offers the only remaining possibility, in our opinion, of achieving optical pumping of a temperature compensated ferrimagnet. The furnace to fabricate these materials is finally near operational and samples should be available within a month.

A more promising alternative however is the possibility of optically

pumping an antiferrimagnetic material. The advantage of this type material is that heat introduced into the lattice as a result of pumping will not cause deleterious effects. A literature review and technical discussion with several solid state researchers here at Georgia Tech has produced an optimistic attitude toward the feasibility of this approach. Potential materials to be investigated will be discussed in Section IV.

In general then, the project status at the end of Phase I can be itemized as follows. An optical investigation of gadolinium iron garnet has shown the material to be unsuitable for optical magnetic pumping. The reasons for this have been studied and as a result other materials circumventing these problems are proposed. Facilities for evaluating optical pumping processes have been assembled and a furnace to grow new specimens constructed. The ability to grow samples is an important part of any such program, and future results should occur much more rapidly as a result of this facility. We are not in a position at this time to enter Phase II as a final fabrication phase. Alternatively we propose Phase II as a phase of fabrication and evaluation effort directed toward evaluating the material concepts developed during Phase I. We especially believe TbIG and DyIG should be studied. Future work should concentrate on several promising antiferromagnets.

II. THEORY AND REVIEW OF LITERATURE ON OPTICAL PUMPING

A. Basic Theory of Optical Pumping

The concept of magnetic moment alignment via an optical excitation process apparently originated with Kastler.[54] Following his initial lead a number of authors have extended and diversified the experiments. The basic idea is as follows. Assume the sample is a paramagnetic gas consisting of atoms such as sodium. The ground state of the sodium atoms is $3^2S_{\frac{1}{2}}$ since there is one electron in the 3s sub shell. The n = 1 and n = 2 shells are completely filled. Therefore the ground state is degenerate by a factor of two due to the direction of spin. In an applied laboratory field the degeneracy is removed. The relative population of the two spin up and spin down levels will be determined by the Boltzman factor

$$\frac{N_{up}}{N_{down}} = e^{\frac{1}{2}\mu_B gH/kT} / e^{-\frac{1}{2}\mu_B gH/kT} \qquad (1)$$

where μ_B = Bohr magneton
H = applied field .

For small fields the ratio is approximately unity and the two levels are nearly equally populated. The resultant paramagnetic moment is very low. The first excited state for sodium is $3\,^2P_{\frac{1}{2}}$, i.e., it corresponds to the electron existing in the $\ell = 1$ orbital. This excited state is also split by the applied field the splitting being somewhat less than the ground state since $g < 2$ as a result of the orbital moment. Figure 1 shows the energy level diagram of such a system.

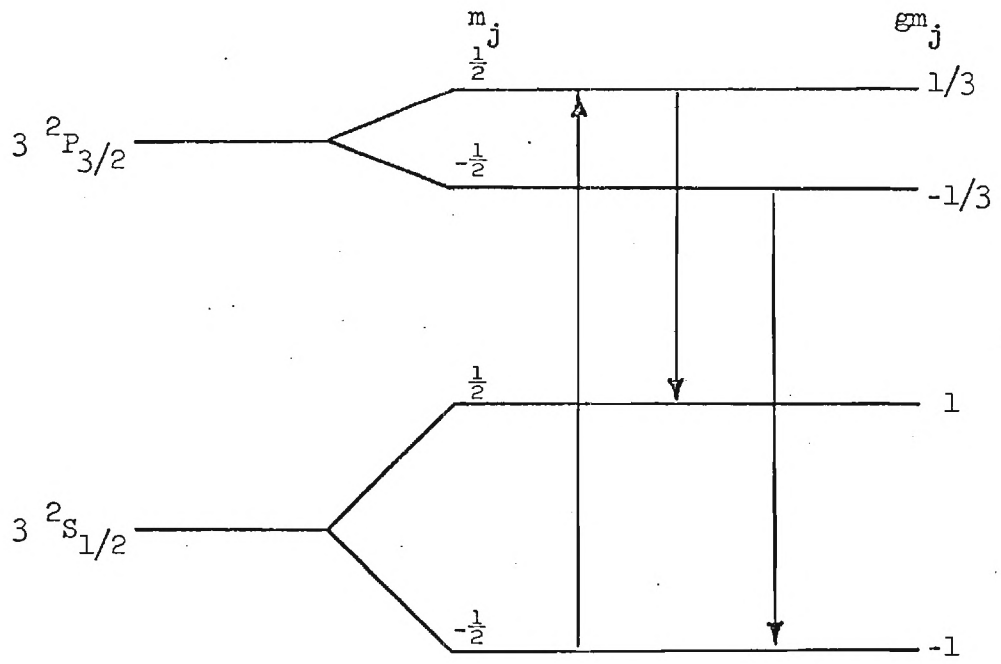

Fig. 1 Energy Level Diagram for Sodium.

The transitions involved in magnetic alignment by optical pumping are included in this figure. The pumping process here makes use of the selective excitation of right hand circularly polarized light propagating

along the direction of the field. In this case conservation of angular momentum requires a selection rule of $\Delta J = +1$ and hence pumping can occur only between the $m_j = -\frac{1}{2}$ level of the ground state and $m_j = +\frac{1}{2}$ level of the excited state. Spontaneous emission of either right or left hand circularly polarized photons is permitted with nearly equal probability. Thus for every two electrons pumped to the $^2P_{\frac{1}{2}}$ excited level only one returns to the $m_j = -\frac{1}{2}$ ground state. In this way it is possible to populate the $m_j = +\frac{1}{2}$ ground state level and in so doing an increase in the net magnetic moment of the ensemble. The level to which pumping occurs is only of secondary importance in this process. What is important is the relative values of the coefficients of spontaneous emission between the sub-levels of the ground state and the transition probabilities connecting sub-levels $-\frac{1}{2}$ and $+\frac{1}{2}$ through the intermediate excited level.

The relative importance of these parameters is seen by considering the generalized rate equations governing the population change of each ground state. Define

b_{ij} = probability per unit time of an electron initially in ground sub-state i, after interaction with pumping field, being transferred to ground sub-state j,

w_{ij} = probability per unit time that an electron in ground sub-state i will relax to ground sub-state j by means other than interaction with pumping field (spin lattice relaxation) .

Thus in the simple two sublevel system diagramed in Figure 1 the change in sub-state populations is given by the two simultaneous equations

$$\frac{dn_1}{dt} = (b_{21} + w_{21})n_2 - (b_{12} + w_{12})n_1 \qquad (2)$$

$$\frac{dn_2}{dt} = -(b_{21} + w_{21})n_2 + (b_{12} + w_{12})n_1 \qquad (3)$$

with the additional normalizing constraint equation

$$n_1 + n_2 = N_T . \qquad (4)$$

It is clear that either of the rate equations in addition to the constraint completely define the system. In general if there are N ground sub-states the above system of equations becomes:

$$\frac{dn_R}{dt} = \sum_{i=1}^{N} (b_{iR} + w_{iR})n_i - \sum_{j=1}^{N}{}' (b_{Ri} + w_{Rj})n_R \tag{5}$$

where the prime denotes omission of the terms i = R and j = R, i.e., those transitions which begin and end at the same sub-state. Such transitions obviously do not affect the population rate, however they do affect the absorption coefficient for incident light. Thus the average probability per unit time that an atom will absorb incoming photons and undergo a transition is

$$\beta = (b_{11} + b_{12})n_1 + (b_{21} + b_{22})n_2 \tag{6}$$

or in general:

$$\beta = \sum_{i=1}^{N} \sum_{j=1}^{N} b_{ij}\, n_i \quad . \tag{7}$$

At thermal equilibrium if the population of the sub-levels is nearly equal then $n_i \approx 1/N$ and the probability of absorption can be related to the equilibrium absorption cross-section as:

$$\beta_o = \frac{1}{N} \sum_{i}^{N} \sum_{j}^{N} b_{ij} = \int_o^\infty \Phi_\nu \sigma_\nu d_\nu \tag{8}$$

where Φ_ν = spectral photon flux density in photons per cm^2 per sec per unit frequency

σ_ν = absorption cross-section in cm^2 at frequency ν .

The relaxation coefficients are in general all assumed equal. Thus if we define a spin lattice relaxation time for the complete ground state system of sub-states as T_{SL} then

$$w_{ij} = \frac{1}{NT_{SL}} \tag{9}$$

a ground state of N sub-states. For the simple system of the example, $j = 2$ and the general rate equation would then become:

$$\frac{dn_2}{dt} = N_T\left(b_{12} + \frac{1}{2T_{SL}}\right) - \left(b_{21} + b_{12} + \frac{1}{T_{SL}}\right) n_2 \tag{10}$$

where we have incorporated the constraint into the second rate equation. The time varying solution of this differential equation is simply:

$$n_2 = n_{2_F}\left(1 - e^{-\frac{t}{\tau}}\right) \tag{11}$$

where

$$n_{2_F} = \frac{N_T\left(b_{12} + \frac{1}{2T_{SL}}\right)}{\left(b_{12} + b_{21} + \frac{1}{T_{SL}}\right)} \tag{12}$$

and

$$\tau = \frac{T_{SL}}{\left[T_{SL}(b_{21} + b_{12}) + 1\right]} \tag{13}$$

In the case of the example we assign sub-state two as $m_i = + \frac{1}{2}$ and sub-state one as $m_j = - \frac{1}{2}$. Then according to the selection rules $b_{21} = 0$. If the relaxation time T_{SL} is large so that

$$\frac{1}{T_{SL}} \gg b_{12}$$

we see $n_{2_F} \rightarrow N_T$ i.e., complete orientation occurs. The steady state population under pumping is therefore dependent upon the relative size of the

transition probability and the relaxation probability as shown by equation (12).

The transition probabilities are related to those calculated quantum mechanically for transitions between different energy levels of an atomic system. These are derived by assuming the incident light interacts with the atomic system as a potential perturbation. Very briefly, if the unperturbed atom possesses stationary state functions described by the Schrödinger equation

$$H_m \Psi_i = E_i \Psi_i \tag{14}$$

then under the perturbing influence of incident light we have the general time dependent Schrödinger equation

$$(H_m + H_I) f = - \frac{\hbar}{i} \frac{\partial f}{\partial t} . \tag{15}$$

The perturbed state function f is written as an expansion of the original stationary Ψ's as

$$f = a_o \Psi_o e^{- j \frac{E_o t}{\hbar}} + \sum_{i=1} a_i \Psi_i e^{- j \frac{E_i t}{\hbar}} \tag{16}$$

where a_o is unity at $t = 0$ and the a_i's approach zero at $t = 0$. Thus the atom is initially in the unperturbed ground state. Without going through the details it turns out that the solution for the a_i's involves a resonance term of the form

$$\left[(E_o - E_j) \pm h\nu \right] .$$

In this term ν is the frequency of the perturbing radiation, E_o the energy of the ground state and E_j the energy of an excited state. If ν is such that

$$E_o - E_j \pm h\nu \neq 0 \tag{17}$$

then the perturbed state function is oscillating in time and the system remains in the ground state but is perturbed around the stationary level. However, if the resonance condition is satisfied so that

$$E_o - E_j \pm h\nu = 0 \tag{18}$$

it is found that a_j becomes real and the atom undergoes a change of state to the excited level. Under a resonance condition of this nature only a_j is real and $|a_j|^2$ may be interpreted as the probability that the atom will be in state j at time t. We can see therefore that $|a_j|^2$ must be related to the b_{ij} coefficients of the previous discussions. Carrying through the development describing $|a_j|^2$ in terms of quantum mechanical matrix coefficients it is found that

$$b_{oj} = \frac{8\pi^3}{3h^2} |\bar{M}_{oj}|^2 \tag{19}$$

where

$$M_{oj} = -\int \Psi_j^* \left(\sum e\bar{r}_i \right) \Psi_o \, d\tau \quad . \tag{20}$$

Here $\bar{M}_{oj}$ is the conventional electric dipole matrix element. Recall however that the b_{ij}'s of (5) relate to transitions from a sub-level i of the ground state, i.e., Ψ_o, to another sub-level j of the ground state. The transition occurs however through a real intermediate excited state and the probability of that transition is given directly by (20).

When the incident radiation does not satisfy the resonance condition the a_i's no longer determine transition probabilities since the atom does not experience an actual change of state. Rather the light is considered as being scattered as a result of its interaction with the polarizable atomic system. The system is in turn described by a time varying state function f as previously discussed. This basic approach is extendable to nonlinear effects such as Raman scattering by considering transitions between perturbed state functions f_o and f_i. These later types of material-light interactions lead to the currently active field of photon-magnon interactions as discussed by Blombergen[53] and the discovery of the so-called inverse Faraday effect described by Pershan, Van der Ziel, and Malmstrom.[51,52]

Optical pumping involving selective population of ground state levels has been observed in solids for paramagnetic ions of Cr^{3+} in ruby.[54] However, the effective population change was very small because unpolarized light was used and even at temperatures as low as 2.78°K nearly complete thermalization of the ground state sub-levels occurred. These same authors however observed that the long lifetime associated with the excited states provided an opportunity to perform paramagnetic resonance experiments between excited state sub-levels. To accomplish this it is necessary to create a population difference in the sub-levels of the excited state and others[54] subsequently were able to perform this experiment using circularly polarized resonance radiation for pumping. It appears that population redistribution of ground state levels is practically unattainable in a solid ferromagnetic material; however, the concept of making use of the long lived excited state seems worthy of detailed consideration. In paramagnetic Cr^{3+} for example, the excited state is described by a pair of sub-levels with $M_j = + \frac{1}{2}$ and $M_j = - \frac{1}{2}$. The ground state, however, is made up of sub-levels with $M_j = + 3/2, + \frac{1}{2}, - \frac{1}{2}, - 3/2$. Thus the saturation magnetic moment per atom is decreased by a factor of 2/3 when it is raised to the first excited level. The same effect can be seen to occur with ions of M_n^{2+}. The ground state of M_n^{2+} has the spectroscopic notation $^6S_{5/2}$ while the first excited state is given by $^4P_{5/2}$. Atomically, the excited state is one in which one of the five 3d electrons is reversed in spin. While such a transition is forbidden by electric dipole interactions the state may be reached by exciting the atom to a higher state via an allowed transition. Subsequent decay through radiationless processes result in the atom existing in the metastable ^4P state. This is a long lived state since the transition to ground can not be effected by interaction with incident photons. Employing R-S coupling the magnetic moment of the ion is given as

$$M = - g\bar{J}\mu_B \tag{21}$$

where

$$g = 1 + \frac{J(J + 1) + S(S + 1) - L(L + 1)}{2J(J + 1)} \tag{22}$$

as described in Section I.

In the ground state the saturation moment is given as

$$M = -(2)\left(\frac{5}{2}\right)\mu_B = -5\,\mu_B$$

while for the excited state, g = 1.6 and

$$M = -(1.6)\,(5/2)\,\mu_B = -4\,\mu_B \ .$$

Johnson and Williams have measured the moment of M_n^{2+} ions in ZnS and ZnF_2 using resonance techniques. They have in fact observed a decrease in the moment by 1 Bohr magneton of ions excited by optical pumping.

Thus there is significant evidence of a sizeable interaction between light and the magnetic moment of a paramagnetic assembly of ions. The point of interest for this research is whether these optical pumping phenomena also exist in ferro and anti-ferro magnetic solids. In solids the ions can no longer be considered as absolutely separate entities. Interactions between adjacent atomic sites of a crystalline solid result from both binding forces and magnetic exchange. The electrostatic potential of neighboring atoms causes significant variations in atomic energy levels and mixing of states so that a state function is no longer simply describable by the quantum numbers n, ℓ, m_ℓ, and S.

Of particular interest is the question of whether the concept of localized atomic levels can be carried over to solids with sufficient accuracy to predict optical pumping phenomena. The question of the validity of tight binding models in solids is not a new one. The success of band theory models and spin wave theory have caused many to propound these as the only rigorous approaches to quantitative solid state analysis. Yet there are those who have achieved remarkable results with localized atomic models. Recent calculations by E. E. Lafon in his Ph.D. thesis have demonstrated that even in metals accurate energy levels and band phenomena can be arrived at using improved tight binding techniques.

Of major interest to this program is the magnetic moment, or rather the expectation of moment, for an atom in any selected excited state. In addition it is desired to estimate values of the excitation cross-section i.e., transition probabilities, and the lifetime of the excited state. In general the present state of the art in calculation from first principles is not sufficiently advanced to permit such estimates with high accuracy. It is possible however using crystal field theory[55] to obtain estimates of

the appropriate wave functions and energy levels using perturbation theory. This technique, involving a localized model, is reasonable for the insulating ferri- and anti-ferromagnet materials under study. For a more complete description of the energy levels and state functions molecular field theory, often called ligand field theory must be applied. The advantage of ligand field theory is that charge transfer band gaps are included naturally.

The general limitations however with crystal field and ligand field theory are that the significant parameters cannot be derived from first principles. Thus the crystal field parameter Dq, the so-called Racah interaction parameters, B and C, the spin orbit coupling parameter, etc. are of necessity left to experimental determination. In addition there appears to be no adequate theory to theoretically determine the lifetime of a given state in real materials. As a part of this research we have conducted a rather detailed study of the available theoretical approaches which could be applied to the problem of optically pumping a magnetic material. An appendix of this report includes a bibliography of papers studied. It has been concluded that while the detailed ligand field theory will be eventually useful in describing the experimental results of this work it can provide only qualitative direction of the experimental work.

B. Literature File and System Study

A card file system has been developed during this program to classify and reduce the significant amount of literature reviewed in the course of the work. This has especially been useful in organizing data pertaining to the system aspects of a beam addressable memory to which our efforts are directed. While we have been primarily concerned with the optical material properties of the storage media, it is important that all work be consistent with the hardware goal of a 10^8 bit mass memory system. Thus we must consider the potential of a material on the basis of available photon flux and energy, light distribution and deflection systems etc. The systems file begun during this phase of the program has started the collection of pertinent data related to such aspects. This effort is the forerunner of work to be carried out in greater depth during Phase III.

C. Example of Pumping to Spin Flip State

Gadolinium iron garnet can be used as a material to describe the optical orientation studied under this contract. It is the material employed in our measurements to date and has provided significant insight

into the characteristics of this form of optical pumping. The concept to be developed depends on creating a significant population of a metastable excited state thereby changing the magnetic moment.

Gadolinium iron garnet (GdIG) is a ferrimagnet consisting basically of an iron sublattice and gadolinium sublattice coupled via an antiparallel superexchange field. The material exhibits a compensation point with temperature where the sublattices are equal in magnitude and the material becomes antiferromagnetic. It is well-known that at this point H_c, the coercive force, reaches a very high value. When the material is uncompensated, by a temperature change for example, the coercive force is drastically reduced. This provides a selection mechanism for magnetic memory storage. The idea to be studied in this work is if the same effect can be caused by optical pumping. Thus if the material can be uncompensated at constant temperature by optically inducing a change in moment of one of the sublattices the coercive force is expected to change. In this material it is important that the temperature remain constant and therefore relaxation of excited atomic sites to ground state should occur by fluorescence.

With these background restrictions the gadolinium ion seems to offer great potential. The significant characteristics of all rare earth atoms result from the fact that the electrons responsible for magnetic moment are strongly shielded by filled outer shells. These are electrons in the $4f$ subshell. Gadolinium has seven $4f$ electrons and thus possesses a half filled shell. The ground state for a free ion triply ionized is given in spectroscopic notation as $^8P_{7/2}$. The first excited state is known to be $^6P_{7/2}$ and occurs as a result of a reversed spin of one of the $4f$ electrons. Employing R-S coupling it was shown in Section I that when the ion exists in the excited state the atomic moment is reduced by two Bohr magnetons. With such a large change in moment per atom, it is only necessary to excite approximately 4% of the gadolinium ions to significantly uncompensate the material. The $^6P_{7/2}$ state is additionally a long-lived metastable state and has been observed experimentally to decay by fluorescence to ground when studied as a paramagnetic dispersion in glass and also in $GdCl_3$. Because the rare earth elements are so well protected from crystal field and bonding influences they generally exhibit properties in solid state materials quite similar to those of a free ion. As a result estimates based on free ion states should be realistic within an order of magnitude.

Estimates of pumping powers required to achieve a 4% population of

excited atoms are easily made using the previously derived rate equations. The values for transition probabilities and excited state lifetime available for gadolinium have been measured in different materials and must be considered as quite tentative. The results however form a basis from which the projected efforts are directed.

The analysis assumes a three energy level atomic structure for the gadolinium. Since the $^6S_{7/2}$ metastable state is forbidden to electric dipole transitions in the free ion, population occurs via pumping to a higher excited state, ^6I, which decays rapidly to the $^6S_{7/2}$ level. The system of rate equations is quite similar to that for optically pumping ground state sub-levels as described by equation (5). Here however the transition probabilities are associated with different atomic states rather than sub-states of the ground level. In this case the transition probabilities b_{ij} are given directly by equation (19) and are interpreted as the probability of finding the atom in state j at time t if it was in state i at t = 0. The three energy level rate equations then can be written simply as:

$$\begin{bmatrix} dn_1/dt \\ dn_2/dt \\ dn_3/dt \end{bmatrix} = \begin{bmatrix} -(b_{12} + b_{13} + w_{12} + w_{13})\ (w_{21})\ (w_{31}) \\ (b_{12} + w_{12}) - (b_{23} + w_{21} + w_{23})\ w_{32} \\ (b_{13} + w_{13})\ (_{23} + w_{21}) - (w_{31} + w_{32}) \end{bmatrix} \begin{bmatrix} n_1 \\ n_2 \\ n_3 \end{bmatrix}$$

For resonance radiation adjusted to pump from ground level to the upper excited state, state 3, only b_{13} is significant. Also experiment has indicated that in $GdCl_3$ the relaxation from state 3 to state 2 is predominant and since state 2 is metastable w_{21} is very small. The energy separation between states is much larger than kT so relaxations from lower to higher states are essentially zero. These approximations yield the auxiliary equations:

$$b_{12} = b_{23} = 0$$

$$w_{12} = w_{13} = w_{23} = 0$$

$$w_{32} \gg w_{31}$$

$$w_{32} \gg w_{21} \ .$$

Introducing these restrictions into the rate equations gives

$$\dot{n}_1 = - b_{13} n_1 + w_{21} n_2 + w_{31} n_3$$

$$\dot{n}_2 = - w_{21} n_2 + w_{32} n_3$$

$$\dot{n}_3 = b_{13} n_1 - w_{32} n_3$$

In the steady state condition $\dot{n}_1 = \dot{n}_2 = \dot{n}_3 = 0$ and the second equation, in conjunction with $N_T = n_1 + n_2 + n_3$, yields

$$n_{2_F} = \frac{w_{32}(N_T - n_{1_F})}{w_{32} + w_{21}} \approx N_T - n_{1_F} ,$$

i.e., n_{3_F} is essentially zero. This is consistent with the fact that we assume relaxation from state 3 to be essentially instantaneous. Under these conditions the basic system rate equation is approximately

$$\dot{n}_2 = + b_{13} n_1 - w_{21} n_2$$

which, by incorporating $N_T = n_1 + n_2$, becomes

$$n_2 + (w_{21} + b_{13}) n_2 - b_{13} N_T = 0 .$$

The steady state population of state 2 is simply

$$n_{2_F} = \frac{(b_{13}/w_{21}) N_T}{(1 + b_{13}/w_{21})}$$

and is reached in a time constant of

$$\tau = \frac{1}{(w_{21} + b_{13})} .$$

The transition probability b_{13} is related to the zero level absorption cross-section simply by

$$b_{13} = \Phi\sigma$$

where as in equation (8) Φ is the photon flux in photons/m^2/sec and σ is the absorption cross-section in m^2. This is simply a limiting case of (8) assuming line source excitation. The cross-section σ has been measured for gadolinium doped glass[12] and was found to be

$$\sigma = 4.1 \times 10^{-25} \text{ m}^2$$

at λ = 2,770Å. Measurements of the lifetime of state 2 has been reported in glass and gadolinium chloride. The values at room temperature are approximately

$$\tau = \frac{1}{W_{21}} \approx 4 \times 10^{-3} \text{ sec.}$$

Using these values we find the incident flux required to cause a 4% population of state 2 is

$$\Phi = \frac{.04}{.96\sigma\tau} = 2.5 \times 10^{25} \text{ photons/m}^2\text{/sec.}$$

Since the incident power density is simply

$$P = \Phi h\nu$$

this corresponds to a light source capable of producing

$$P = 1.8 \times 10^{7} \text{ watts/m}^2 \quad .$$

A power density of this magnitude can be achieved by focusing the coherent output of a 1.5 mw laser onto a 10μ diameter spot.

As will be shown in the next section our experimental results to date indicate that the absorption cross-section is much larger and the lifetime much shorter than the values in $GdCl_3$. This is indicative of a larger interaction between the lattice and gadolinium ion. The fact that this is the case is not surprising since inter-atomic coupling is necessary to

produce the magnetic ordering. A simultaneous increase in absorption cross-section and reduced lifetime may not be detrimental as it is the product $\sigma\tau$ which determines the required pumping power. Since the lifetime τ determines memory cycle time it is desirable for practical operation that it be much less than the free ion value of 4×10^{-3} sec. However, if this decrease in lifetime is the result of interactions creating non-radiative transitions then the resulting energy produces lattice phonons. This is undesirable for operation with a compensated ferrimagnet but may be acceptable if other materials, e.g., antiferromagnets are used.

In general, there is no way to adequately describe the crystalline effects which control the lifetime of an atomic state. Many workers in the field of luminescence have studied the problem but there is as yet no effective single model. One approach involves determining the energy of the various states as a function of the physical position of the ion in the lattice. It is found that in general the energy minimum of an excited ion occurs at a different position from the ground state location. This effect can theoretically cause a configurational coordinate band overlap which allows radiationless transitions via transfer of phonon energy to the lattice. This technique was first proposed by Seitz[56] and has been extended by Williams[24] and Dexter, Klick, and Russell.[25] It is found however that the quantitative results are almost always in considerable error. Van Uitert[22] has studied the lifetime of various rare earth ions in different materials (tungstates, fluorides, hydrates). He indicates that three separate effects can be discerned, listing them as coulombic effects, concentration effects, and thermal effects. He is not able to base these observations on any calculable model. In a later paper Van Uitert et al.[23] discuss the concentration quenching of Eu^{3+} in various materials including tungstates, garnets, and orthoferrites. They conclude the decrease in lifetime of the excited states is a result of orbital mixing between the $4f$ electrons of the rare earth ions via the intermediate oxygen cation. Here again no calculations are made but it is a quite reasonable model. Only a detailed ligand field theory calculation would verify the assertion and it is questionable whether the wave functions could be determined accurately enough to permit the calculation of transition probabilities. In general then, only experimental measurements are useful in studying this problem.

2. Conclusion

In this section the concepts of optical pumping have been reviewed. We have discussed some of the problems of trying to mathematically analyze the proposed phenomena. It appears that the best one can hope to do theoretically is to explain the results of a given experimental observation and even then only with considerable effort and order of magnitude accuracy. Theory is not sufficiently advanced to allow a priori predictions of the optical pumping characteristics of a proposed material. We must, therefore, direct our efforts on the basis of previous experimental results and estimates based on extrapolations of free ion data. This approach is not new to research activities and the information gained in studying GdIG to date has provided significant insight into potentially useful materials.

III. EXPERIMENTAL WORK

Of the several garnets suggested for adaptation to this magneto-optical memory, only two samples have so far been available to us. These samples are alledged to be gadolinium iron garnet obtained, one from Bell Telephone Laboratories and one from IBM Thomas J. Watson Research Laboratory.

Our experimental work has consisted of several studies, mainly on one sample, and on design and construction of equipment to prepare our own garnet samples.

The samples we had, appeared to be opaque to visible radiation, and our measurements of reflectivity confirmed this and indicated that they are also very opaque to ultra violet. There is structure to the reflectivity and in the absorptivity and index of refraction computed therefrom, as function of wavelength; part of this structure may be associated with the transitions in gadolinium that we hope to exploit.

Attempts to observe the transition in fluorescence failed, but the sensitivity of our experimental arrangement was too low if reported absorption cross-section for exciting the radiation in $GdCl_3$ is comparable to the cross-section in gadolinium-iron-garnet.

Observation of fluorescent radiation, when the crystal was bombarded with 20 kv electrons, resulted in damaging the crystal surface; pits appeared that could have resulted from local melting. Radiation that could have been the sought-for gadolinium transition was observed only when the electron beam was directed into a particular one of the pits created by previous bombardment.

A spectroscopic analysis of a portion of the crystal indicated the ratios of gadolinium and iron to be about proper, but no interpretation of an x-ray analysis for crystal structure has been received.

The following sections report the foregoing studies in detail.

4. Reflectivity

1. Apparatus and Observations

A Gertner monochrometer was joined to a light tight sample chamber and a water-cooled high pressure mercury arc source in the configuration schematically represented in Figure 2.

The sample was mounted on a rod so that it could be placed in the beam from the monochrometer and rotated to the desired angle, or lowered to remove it from the beam.

Radiation in the direct beam or the beam reflected from the sample fell onto the end of a glass "light pipe," a rod of glass about a centimeter in diameter. The end of the pipe was coated with sodium salicylate to produce light that would pass the glass when the beam was ultra violet. The pipe was bent into a hook-shape that passed out the top of the sample chamber at its center. Above this end of the "pipe" was the face of a photomultiplier tube. The lower end of the "hook," the end coated with salicylate, was a vertical surface that could be rotated about the center of the sample chamber to receive the direct beam from the monochrometer when the sample was lowered, or to receive the reflected beam from the sample at any angle that did not put it in the way of the port where the radiation entered the chamber. The cylindrical sides of the light pipe were coated with a reflective coat of aluminum. The lamp capillary was parallel to the monochrometer slit; no condensing lens was used between the lamp and the monochrometer; the full aperture of the monochrometer was, thus, not used. Radiation from the exit slit was approximately the width of the slit and diverging very slightly. A stop in the sample chamber limited the vertical height of the beam, and confined its angle with respect to the beam axis. Our vertical beam spread was perhaps 2° each side of the axis and the horizontal spread up to 1° when the slits were open widest. The resulting measurements are subject to these limitations; there will be more narrow limits in a similar instrument now being assembled for further reflectivity measurements on samples we are growing ourselves.

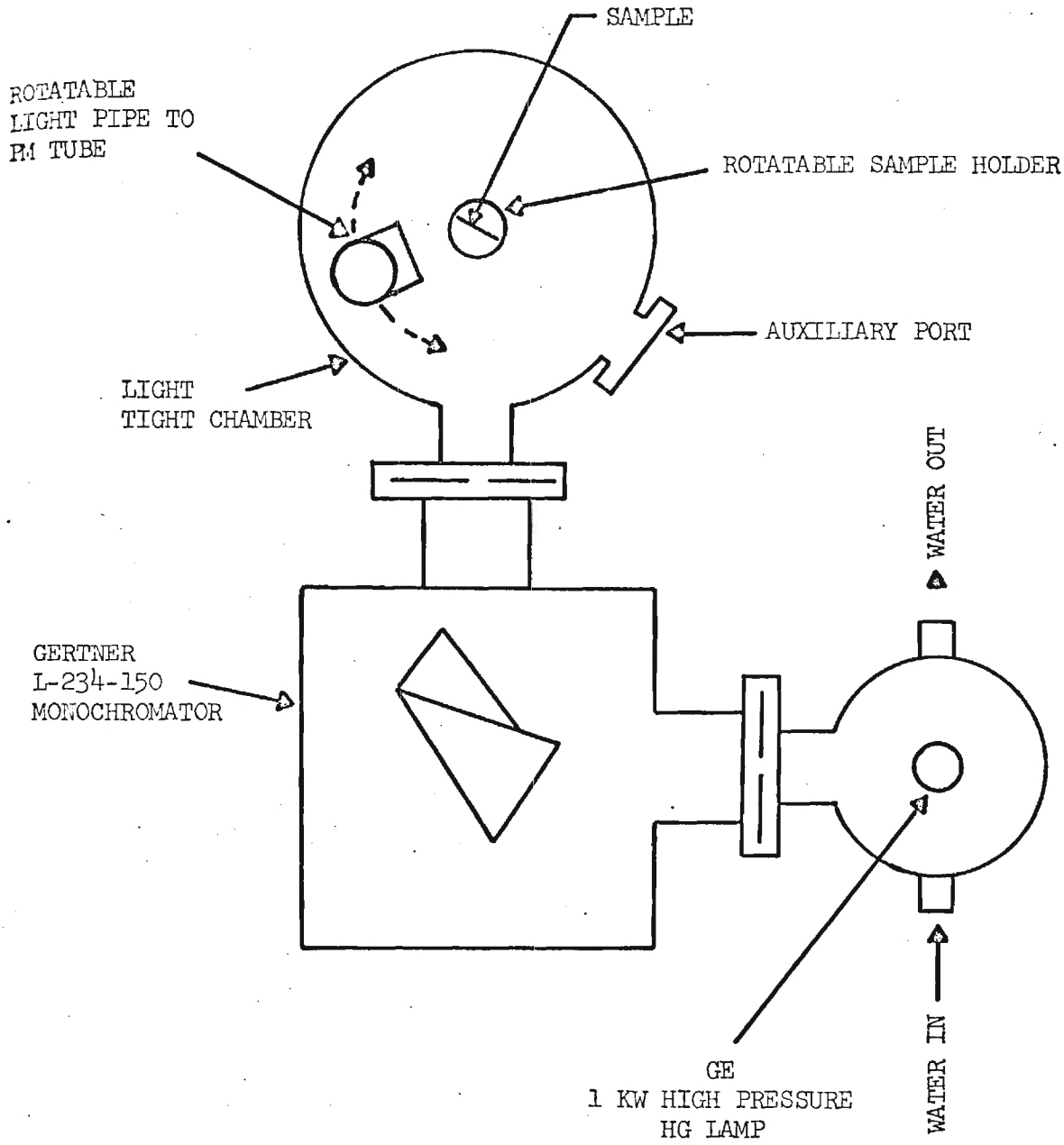

Fig. 2 Sketch of Optical Measurements Facility.

A Glan-Thompson prism was placed in the exit beam to define the polarization.

Reflectivity at any wavelength and angle was the ratio of the intensity of the reflected beam to the intensity of the beam directly intercepted by the end of the light pipe, with the sample lowered. Repeated measurements of reflectivity indicated that the source variation was not the limiting uncertainty in our measurements.

For the gadolinium iron garnet sample, polished plane, reflectivity data were taken at three different angles of incidence, 70°, 45°, and 20°, over the wavelength range corresponding to photon energies 3.5 to 5.5 eV. These are shown in Figures 3, 4, and 5. Some additional data taken without a polarizer at lower photon energies were not reduced.

2. Data Reduction

Fresnel's equations give the reflectivity of a plane surfaced, half infinite isotropic sample in terms of the angle of incidence and the complex index of refraction, N, which is a particular combination of the absorptivity, η, and the phase velocity of radiation relative to light in free space, 1/n.

$$N = n - j \frac{\lambda}{4\pi} \frac{\eta}{n}$$

For radiation polarized in the plane of incidence Fresnel's equation is

$$R = R_s \cdot \left[(a - \sin\Phi \tan\Phi)^2 + b^2\right] / \left[(a + \sin\Phi \tan\Phi)^2 + b^2\right]$$

where

$$R_s = \left[(a - \cos\Phi)^2 + b^2\right] / \left[(a + \cos\Phi)^2 + b^2\right]$$

$$a^2 = \tfrac{1}{2}\left\{\left[(n^2 - k^2 - \sin^2\Phi)^2 + 4n^2k^2\right]^{\frac{1}{2}} + (n^2 - k^2 - \sin^2\Phi)\right\}$$

$$b^2 = \tfrac{1}{2}\left\{\left[n^2 - k^2 - \sin^2\Phi)^2 + 4n^2k^2\right]^{\frac{1}{2}} - (n^2 - k^2 - \sin^2\Phi)\right\}$$

If reflectivity is available at two angles, then this equation yields n and η, the index of refraction and the absorptivity.

Fig. 3 Reflectivity vs. Photon Energy Polarized in the Plane of Incidence.

Angle of Incidence = 70°

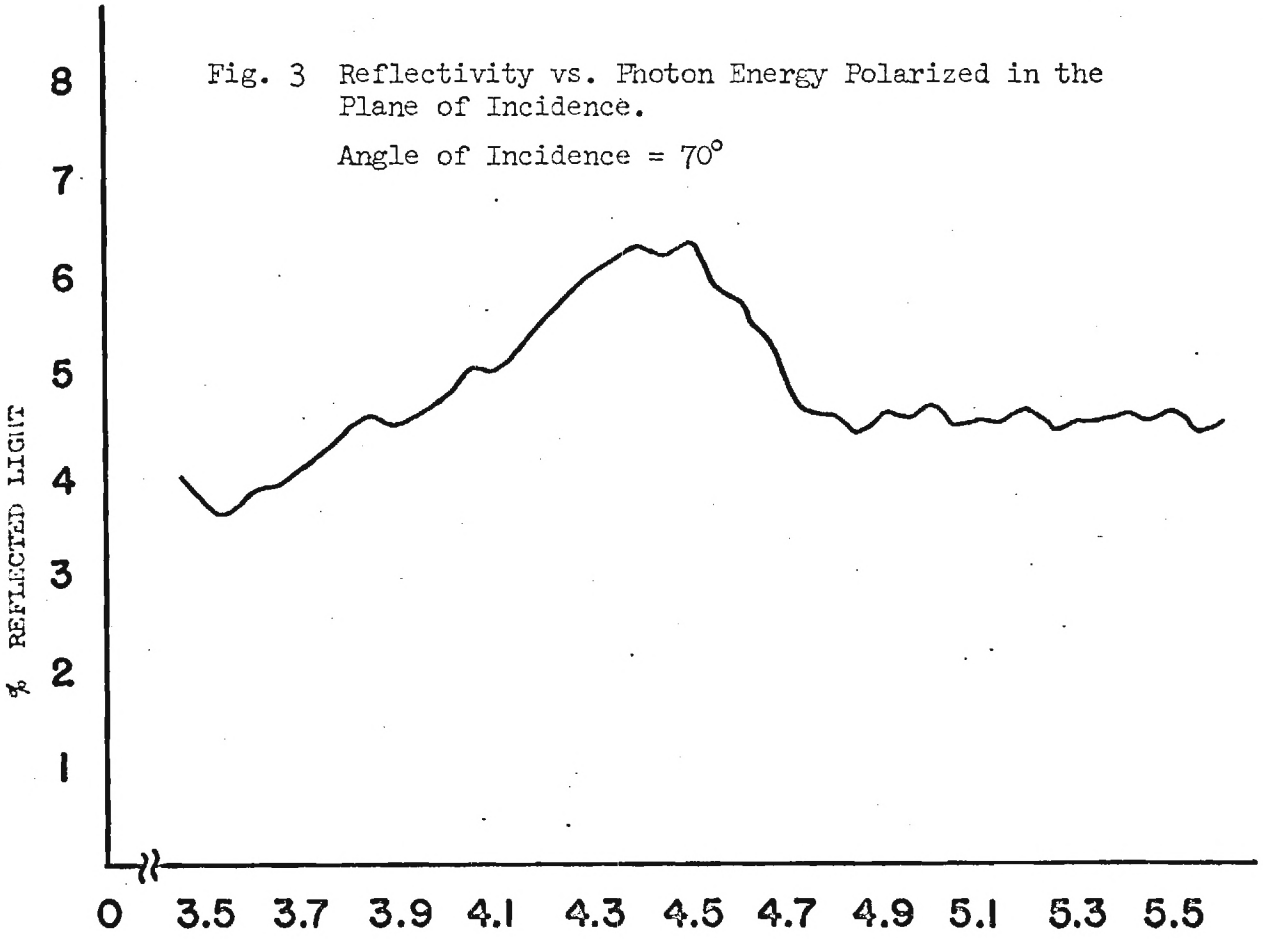

Fig. 4 Reflectivity vs. Photon Energy Polarized in the Plane of Incidence.

Angle of Incidence = 45°

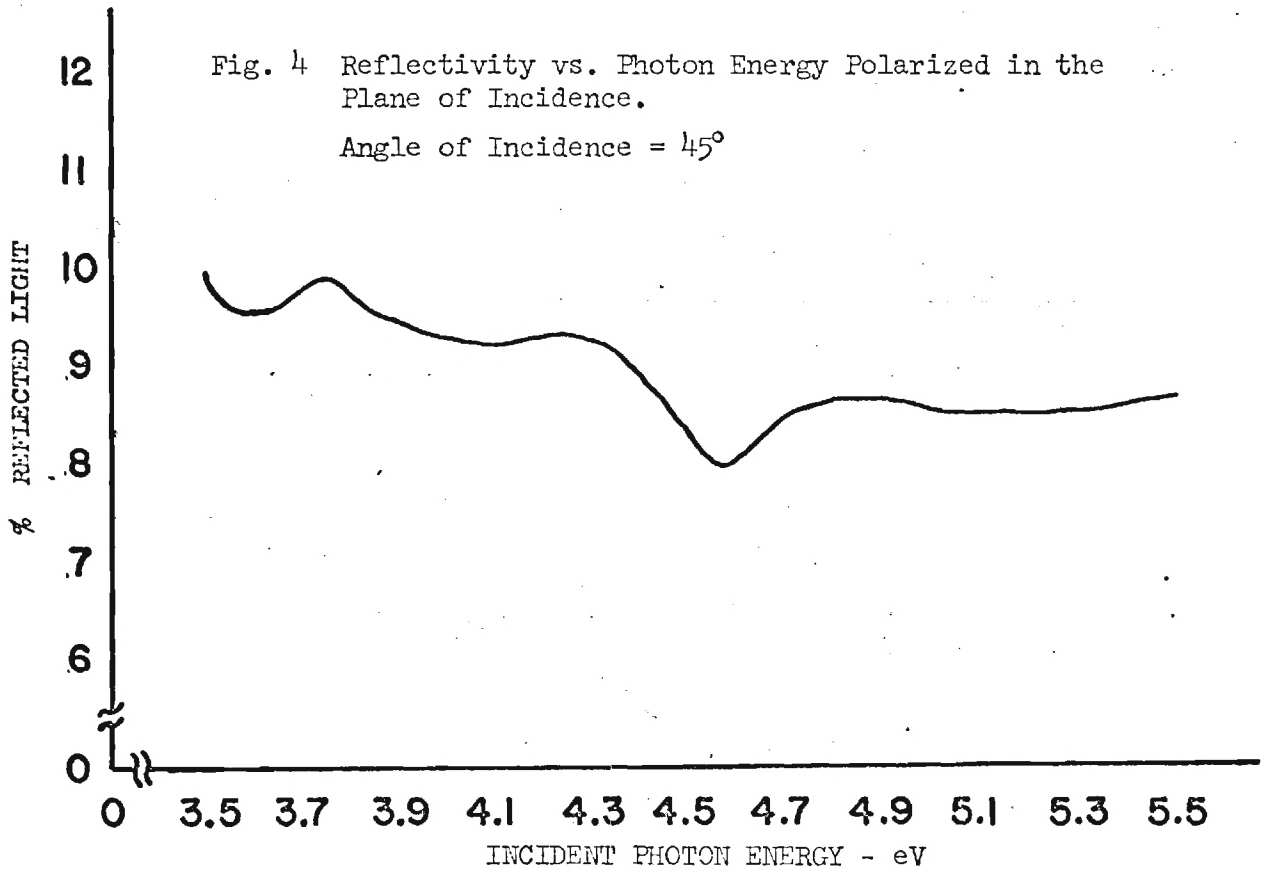

Fig. 5 Reflectivity vs. Photon Energy Polarized in the Plane of Incidence

Angle of Incidence = 20°

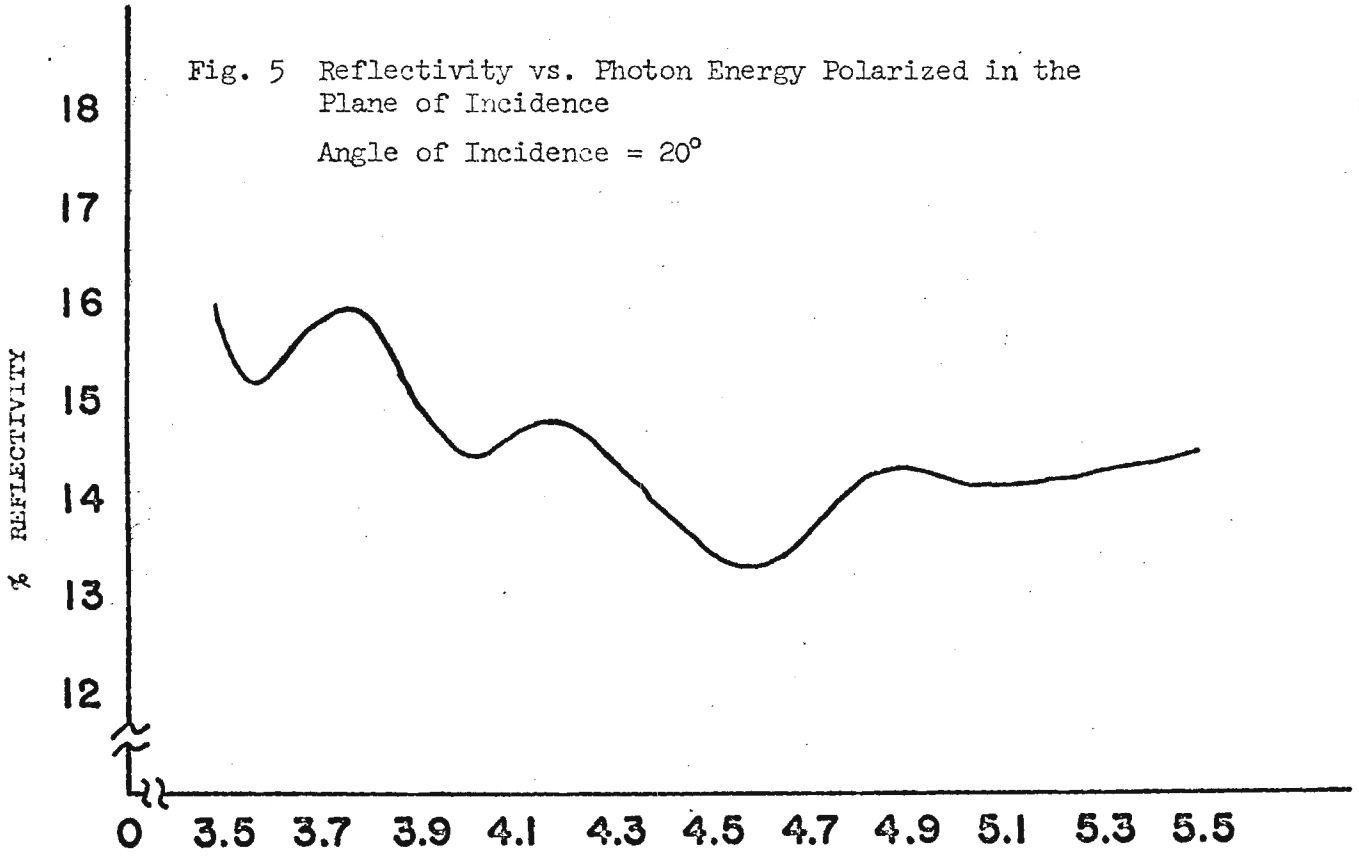

A computer program has been established to extract n and η from measured reflectivities. The structure of the program is the following:

Reflectivity is computed for inserted "trial" values of n and η and for specified increments in n and η to each side of the trial values. There are nine such combinations. This is done for each angle of incidence for which data is available. For each n and η the computed reflectivities are compared with the observed ones at the appropriate angles. One of the nine pairs of values of n and η are selected as giving the best fit (on a least square deviation basis). The selected value becomes a new trial value and the process is repeated until no improvement results from further iteration.

Experience has been gained with operating this program on the above data. Its reduction of the reflectivity data of the one sample studied is presented in Figures 6 and 7.

3. Interpretation

This data is of significance to our purposes in the following ways. Structure, as function of wavelength, in the optical properties of materials of interest can be revealed by measurements of this type, and experience is in hand for modifying the assembly of instruments to more efficiently give the data required, and to give data of better quality. This will be pursued when crystals of our own manufacture become available.

The gadolinium iron garnet was essentially opaque; in particular, it was too opaque to the radiation capable of "pumping" the transitions required for magnetic uncompensation for it to be of practical interest, except, possibly, in very thin (one micron thick) samples. Likewise, it is too opaque to the radiation that might have relaxed the uncompensation without heating the crystal.

It is comforting that our measurements yielded absorptivity only a factor of two different from other recently reported data.[14] No effort has been made to reconcile this difference, which might be due to different impurities in the two samples. Estimates of numerical reliability of reduced data will be made when samples of greater practical interest are in hand, and when the data is taken under improved conditions for which this work has pointed the way.

The broad peak in the absorptivity shown in Figure 6 around 4.3 ev could be associated with absorption by the transitions at 0.2741 μ and 0.2700 μ. This is the absorption we hoped would pump the magnetic transition. That the peak is broader than had been reported[12] is not surprising;

Fig. 6 Absorption Coefficient vs. Photon Energy.

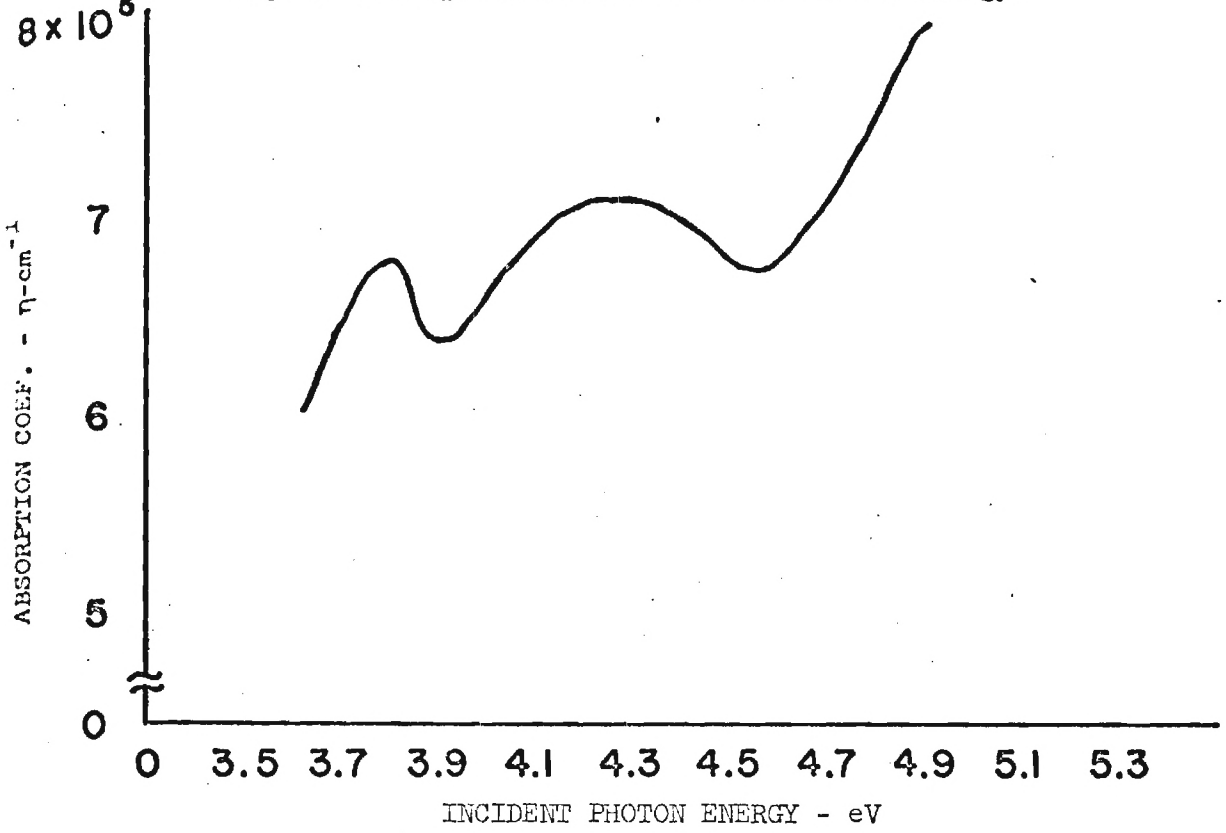

Fig. 7 Complex Index of Refraction vs. Photon Energy.

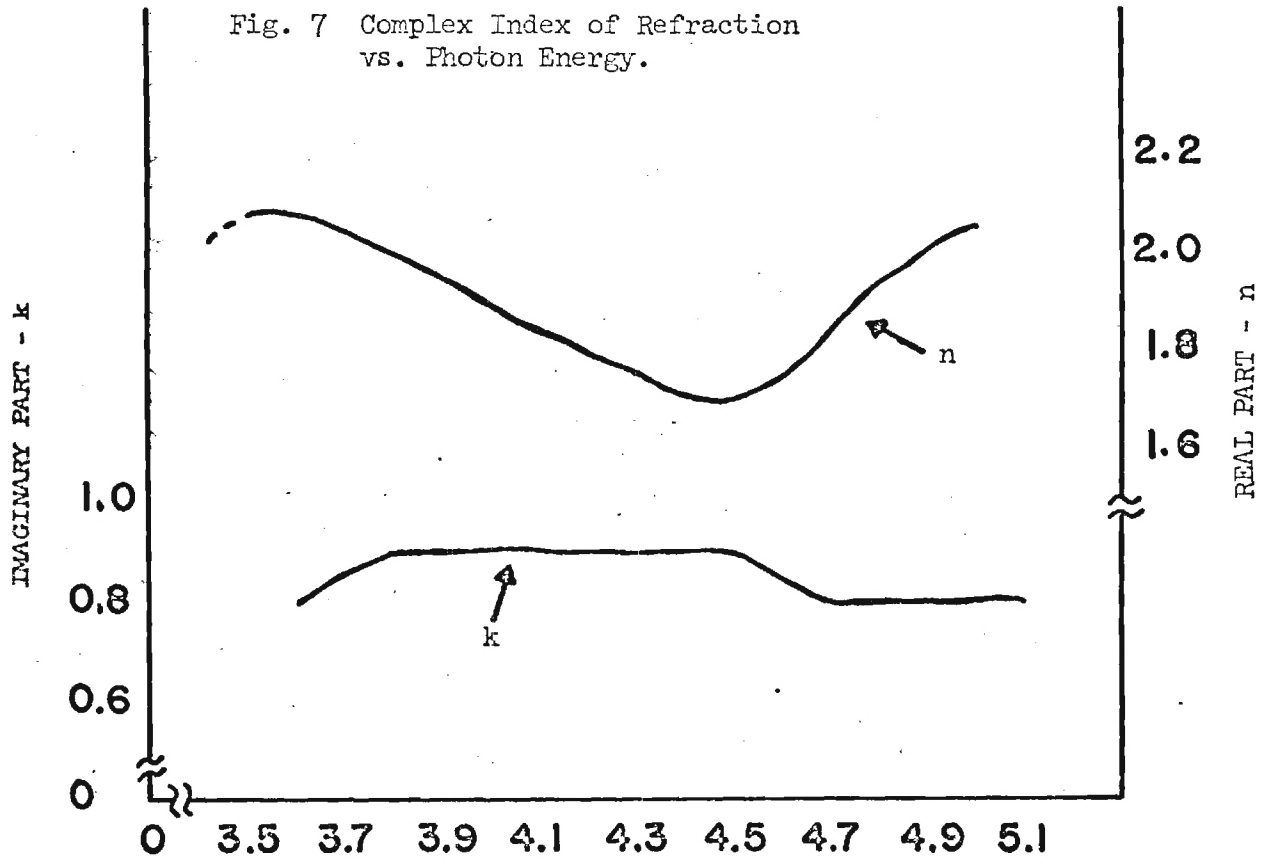

correlation of spins associated with the ferrimagnetism indicates some interaction between the $4f$ orbitals of different gadolinium atoms, interaction that was not present in the reported observations on gadolinium dissolved in glass where there was no exchange coupling.

Further removed from explanation than the broadness of the observed absorption is its strength. To be observed clearly above the general absorption of the crystal, absorption tentatively believed to be associated with an oxygen-iron charge transfer process, the absorptivity associated with the gadolinium must have been about 0.5×10^5 cm^{-1}. This would correspond to an absorption cross-section of about

$$\sigma = \frac{\alpha}{n} \geqq \frac{0.5 \times 10^5 \text{ cm}^{-1}}{.96 \times 10^{22} \text{ atoms/cm}^3} = .5 \times 10^{-17} \text{ cm}^2/\text{Gd atom},$$

compared with $\sigma \sim 10^{-20}$ cm^2 per gadolinium atom reported for the two transitions cited. Consequently we cannot be certain that the absorption peak is associated with the hoped for pumping transition. Such a question would be of greater practical significance with a less opaque crystal, such as we expect some of the other rare earth garnets to be; with them, however, there should be less uncertainty in all interpretation of experimental results.

B. Fluorescence

1. Apparatus and Observation

The reflectivity assembly was modified to study whether fluorescent radiation at 0.3 μ, or thereabouts (0.3125 for Gd in glass and close to this wavelength in $GdCl_3$) could be observed when the gadolinium iron garnet sample was irradiated with shorter wavelength ultraviolet. This fluorescent radiation corresponds to the forbidden transition $^6P_{7/2} \rightarrow {}^8S_{7/2}$, but has been observed in the cases cited.

The assembly indicated in Figure 2 was altered by replacing the lamp and its housing by an ultraviolet sensitized photomultiplier tube and its housing. The light pipe was removed from the sample chamber and radiation of limited band width was admitted through the auxiliary port from another monochrometer.

The exit slit of this monochrometer was focused onto the sample and this same area on the sample was focused onto the slit of the Gertner monochrometer, now employed as a spectrometer, or "analyzing monochrometer," by

a quartz condensing lens.

The same water-cooled mercury arc was the source of radiation. The monochrometer was an SI quartz prism instrument.

Preliminary alignment and focusing could be done with visible radiation. The analyzing monochrometer would be set to the same wavelength as the source and the sample turned to reflect radiation from the illuminated area into the analyzing instrument.

Finally, had fluorescent radiation been observed, the ratio of fluorescent emission to intensity of radiation was to be determined by the relative response of the photomultiplier to the fluorescence and to radiation of the fluorescent wavelength reflected off the sample, the reflectivity being known from the measurements described in Section III-1. The relative sensitivity of the photomultiplier at the two wavelengths would have been needed for reducing such data; tentatively we intended to assume that the quantum efficiency of the sodium salicylate is constant over the wavelength range; direct calibration would have been attempted if questions arose whose answers demanded it.

The source monochrometer passed a background at wavelengths for which it was not tuned with intensity about 10^{-4} of that for which it was tuned. This is about what is to be expected of the 1 cm prism aperture of the SI instrument. Some structure, associated with the mercury source spectrum could be observed.

Because our source lamp emitted much more strongly at wavelengths greater than 0.31 μ than at shorter wavelengths the effect of the background made observation of fluorescence impossible when the source monochrometer was tuned in the region of interest, 0.27 μ.

It was therefore necessary to use two SI instruments in tandem. Each was mounted on a Greenlee milling table to facilitate adjustment in transition and rotation. With the two, the background was reduced enough to warrant an attempt to observe the fluorescent radiation.

A sprocket was installed on the Gertner monochrometer wavelength shaft to drive a potentiometer. A voltage from the potentiometer actuated the x motion of an x-y plotter while the y motion measured the photomultiplier current. This arrangement made possible rapid surveys of limited wavelength ranges.

Even with two source monochrometers in tandem some mercury arc structure was visible when the analyzing monochrometer was tuned away from the

wavelength of the source and the sample was adjusted to directly reflect the source into the analyzing monochrometer. Rotating the sample a few degrees removed the direct reflection, but should not have appreciably altered fluorescent radiation emitted from the illuminated area that entered the analyzing spectrometer.

Indeed, rotation of the sample 10 degrees from the position for maximum reflection did reduce the signal through the analyzing monochrometer by a factor of 10^{-3} when tuned to the wavelength of the source monochrometer. Away from this wavelength the response was hidden in the photomultiplier noise.

No fluorescence was observed, but the noise level of our photomultiplier places an upper limit on the strength of the fluorescence. It will be shown that this upper limit corresponds to a larger cross-section than that reported for gadolinium in glass, so if the reported figures for absorption cross-sections apply to our sample, then the fluorescence would have been too weak to be observed with our apparatus. However, if the absorption peak above discussed, is associated with absorption by gadolinium, then it is possible, but not certain, that we could have observed fluorescence; the uncertainty lies in the unknown probabilities for the states excited by radiation around 0.27 microns terminating by transitions to the state responsible for fluorescence and by other means.

The procedure was as follows: After alignment of the system the three monochrometers would be tuned to the same wavelength, some wavelength in the ultraviolet shorter than the expected fluorescence at 0.31 microns. The monochrometer slits would be adjusted to match the bandwidths selected. For tuning of the three monochrometers, the sample would be oriented for reflection, or else it would be replaced by a front surfaced plane mirror.

After tuning, the sample would be oriented about 10 degrees from the position for reflection. The response of the photomultiplier would fall by a factor of 10^3, but there would be enough scattered radiation to be well above the noise level.

A typical response is sketched in Figure 8 taken from the x-y plotter record. The several items of interest are labeled and the numbers attached to the several branches are the photomultiplier current for full scale deflection for the associated sensitivity of the photomultiplier current.

This particular record had for the illumination wavelength band one

that included the wavelengths of the two transitions thought to populate the $^6P_{7/2}$ state through some process; these were reported at 0.274 μ and 0.277 μ. Our band was centered at 0.276 μ and the slits of the SI monochrometers were open 2 mm, which should correspond to a bandwidth of 0.02μ. The Gertner slits were opened 0.4 mm corresponding to a bandwidth of 0.05μ near 0.31 μ.

It is evident from the figure that the response is reduced to about 10^{-3} by rotating the crystal away from specular reflection. The response in the vicinity of 0.3125 μ, the expected wavelength of the fluorescence is down by another factor of 70; we would have observed a change amounting to half or one-third this average dark current level. Response at other wavelengths for the source were similar and none showed any fluorescence. There was a hint of fluorescence at 0.309 microns when the illumination was centered at 0.286 microns. Because of the limited sensitivity of the apparatus and the fact that the wavelength is shorter than anticipated we have not been able to identify this as the desired gadolinium fluorescence. The fluorescence cross-section, computed in the next section, for this fluorescence, would have amounted to

$$\sigma \sim 0.6 \times 10^{-18} \text{ cm}^2$$

When the illumination was centered at 0.297 microns the region of expected fluorescence was still well on the slope of the radiation scattered by the crystal surface.

2. Reduction of Observed Data

The ratio of response when adjusted for reflection and for fluorescences is thus greater than 7×10^4, and fluorescence, say 20×10^4 less than reflection could have been observed. The geometry of the configuration was such that the aperture of the analyzing monochrometer was filled. A cone from the sample with a solid angle of approximately

$$\omega = \frac{\pi}{4 \times 64} \text{ steradians}$$

(corresponding to $f/8$), was accepted and this was close to the spread of the cone from the source. Thus, the reflected response is a measure of the illumination of the sample, to the extent the above suppositions are correct.

The illuminating radiation inside the sample is rapidly reduced in intensity by all the absorbing processes. If the intensity just outside the surface is I, then inside the sample at distance Z, the intensity is $(1-R)\ Ie^{-\alpha Z}$, where R is the fraction reflected.

For fluorescence cross-section, σ, the emitted radiation intensity from a layer for unit time per unit area will be

$$I_f = (1 - R)\ \rho\sigma\left(\frac{\lambda}{\lambda_f}\right) Ie^{-\alpha z}dz$$

where ρ is the number of gadolinium atoms per unit volume and λ/λ_f accounts for the lower energy of the fluorescent quantum. The fluorescence will be emitted in all directions, throughout the solid angle 4π. The fraction of this that is emitted in solid angle ω' which will enter the analyzing monochrometer is $\omega'/4\pi$. The total fluorescent power entering the monochrometer from unit area on the sample is therefore

$$P_f = \left(1 - R\right)\int_0^\infty \frac{\omega'}{4\pi}\ \rho\sigma\left(\frac{\lambda}{\lambda_f}\right) Ie^{-\alpha z}e^{-\alpha_f z}dz$$

where α_f is the absorptivity for the fluorescent radiation. This development neglects the difference between the cosine of the angle the propagation direction makes with the normal and one, something less than the difference between 0.9 and 1.0.

The solid angle ω' is smaller than ω because the direction of propagation is closer to the normal in the solid than in the air outside. For incidence and exit close to the normal

$$\frac{\omega}{\omega'} \sim N^2$$

where N is the index of refraction, approximately 1.9 for the fluorescent radiation at about 4.0 ev (see Figure 7).

The ratio of power reflected into the monochrometer to power received from fluorescence is

$$\frac{IR}{P_f}$$

The ratio of the responses of the photomultiplier, assuming equal quantum efficiency for the salicylate coating at the two wavelengths is

$$\text{Ratio of Photo currents Reflection - Fluorescence} = \frac{\lambda}{\lambda_f}\,\frac{IR}{P_f}$$

$$= \frac{R}{1-R}\,\frac{4\pi N^2}{\omega n \sigma}\,\frac{1}{\int e^{-(\alpha+\alpha_f)z}\,dz}$$

$$= \frac{R}{1-R}\,\frac{4\pi N^2}{\omega n \sigma}\,(\alpha+\alpha_f)$$

R is the reflectivity for the incident radiation, N is the index for the fluorescent radiation. This is the response, without absorption, to the atoms in a layer 1/2 α thick if α and α_f are equal. Our observation gave the lower limit of this ratio, 20×10^4 for the example cited.

$$20 \times 10^4 \leqq \frac{R}{1-R}\,\frac{4 \times 4 \times 64\, N^2}{n\ \sigma}\,(\alpha+\alpha_f)$$

$$\sigma \leqq \frac{4 \times 4 \times 64}{20 \times 10^4}\,\frac{R}{1-R}\,\frac{N^2}{n}\,(\alpha+\alpha_f)$$

The reflectivity at 20°, 0.13, is a satisfactory value for R (Figure 5 at 4.5 ev). N at 4.0 ev, approximately the fluorescent quantum energy, is 1.9 (Figure 7). In gadolinium iron garnet n is 0.96×10^{22} cm^{-3}, and 6.8×10^5 cm^{-1} will do for α and α_f. Thus

$$\sigma \leqq \frac{4 \times 4 \times 64}{20 \times 10^4}\,\frac{0.13}{0.87}\,\frac{(1.9)^2}{.96 \times 10^{22}}\,(2 \times 6.8 \times 10^5)\ cm^2$$

$$= 0.4 \times 10^{-18}\ cm^2$$

3. Interpretation

Should the published value, 10^{-20} cm^2 be the cross-section for absorption in this wavelength region, the fluorescent cross-section would be even smaller and our instrument would not have detected fluorescence. Had the absorption peak we observed ($\sigma > 0.5 \times 10^{-17}$ cm^2) been truly associated with gadolinium, then we should have detected fluorescence if the fluorescence accounted for a sizeable fraction (more than 0.1 or 0.2) of the decay of the states excited by the absorption. If there were appreciable competition we still would not have detected fluorescence.

We will have more favorable conditions with future samples. The water-cooled mercury lamp will be replaced by an air-cooled one, which has been constructed and tested. From this lamp we expect higher ultraviolet output, which should allow observation of larger ratios of reflected response to fluorescent response. If necessary coherent detection will be introduced to reduce the dark current noise limit of the photomultiplier detector.

C. Electron Bombardment

An Acton MS-64 Electron Microprobe consists of an electron gun and beam focusing devices that will bombard with electrons a spot nominally 10 microns in diameter. The purpose for which the instrument was built is x-ray analysis of small selected areas on a sample. X-ray spectrometers analyze the x-rays emitted by the sample under bombardment by 9000 to 25000 volt electrons. The sample position is accurately controllable from outside the column, and the beam can be swept over the sample in a controlled manner. There is a low power microscope to facilitate location of the beam on a particular region of a sample. The objective of the microscope has only reflecting elements, so it should pass ultraviolet. Following the objective elements in the optical train is a glass window from the evacuated column to the outside. A tube carrying what amounts to a regular microscope eyepiece is mounted to look through that window; there is a beam splitter in the tube for illumination of the sample.

We modified the electron microprobe instrument as follows. The glass window was replaced by a quartz window so ultraviolet radiation emitted by the sample would pass out. The exterior part of the microscope, the tube, eyepiece, etc. were replaced by a tube with the entrance slit of a Gertner ultraviolet monochrometer located where the objective forms the image of

the sample. A salicylate coated photomultiplier collected radiation from the exit slit.

In summary, the electron beam column, the objective with reflecting optics, and the sample handling facilities of the Electron Microprobe were used in conjunction with an analyzing monochrometer and a photomultiplier detector to observe fluorescence excited by electron bombardment. The x-ray spectrometers were not used.

The same polished surface of gadolinium iron garnet used in the reflection and fluorescence observations of Sections III-A and III-B was bombarded. Serious damage to the surface occurred, even with only 9000 volts accelerating potential, the lowest available. Pits up to 40 microns deep (subsequently measured with a metallographic microscope with a micrometer scale on its objective adjustment) were formed, with glassy looking beads around their edges.

Fluorescence was observed at 0.314 microns when one of the deep pits was bombarded. Elsewhere on the sample there was no fluorescence. This is likely radiation associated with the $^6P_{7/2} \rightarrow {}^8S_{7/2}$ transition in the gadolinium ion. Its presence only from the damaged crater can be explained several ways, but we are not certain of what was taking place.

One attempt to explain the observation assumes that excitation by the high energy electrons in the beam occurs too deep in the crystal for the radiation to emerge. Excitation observed from the crater then arises either from bombardment by secondary electrons, which have lower energy, and therefore excite gadolinium ions near the surface, or else the damaged crystal has been converted, in part to a glass in which the radiation is not so strongly absorbed.

We have yet to test the first hypothesis with an apparatus that will produce an electron beam of lower energy. This low energy system has been fabricated and pumped down but time has not permitted evaluation of the low energy electron gun or study of any samples.

IV. MATERIALS CONSIDERATIONS

A. Crystal Growing Facility

As a result of our initial experiments a decision was made that significant additional work depended on the ability to fabricate a variety of material samples. We had initially intended to purchase the required

crystals, however, the expense and inflexibility of control turned out to be a severe limitation. Thus a furnace has been constructed which now permits crystal growing within our own laboratory. This furnace has a vertical tube resistance heated chamber approximately 2-3/4" in diameter and 8 inches long. The heating element is a standard commercial assembly manufactured by Kenthal. A photograph of the oven and power supply is shown in Figure 9.

Accurate control of oven temperature is essential using the molten flux crystal growth process. This technique for growing garnet materials has been developed to a large extent by Nielsen,[49] and requires a very slow cooling rate with minimum variation around the nominal value. A feedback controller has been designed, and is now in operation, which permits cooling rates of as low as 0.8° C/hr. and maintains the temperature within 0.2° C of the nominal value. This particular controller permits only a constant rate decrease during operation. A design has been completed however, which allows programmable rates over different intervals of the cooling cycle. We hope to complete fabrication of this unit during the remainder of this contract. Operation of a programmable controller permits more efficient use of the growing periods. It is possible to decrease temperature relatively rapidly from the high value at melting, then as the critical nucleation point is approached the rate can be reduced to a very low value to assure growth of large sound garnets. Subsequently it may be desirable to increase the rate again until a satisfactory pouring temperature is reached.

We have fabricated a special fixture to form slugs of the starting materials of identical shape to the crucible. This is anticipated in producing large crystals. Materials are on hand to grow terbium and dysprosium iron garnets and a variety of properties can be attained by selective doping. For example, using non-magnetic impurities with high absorption cross-sections at proper wavelengths it is possible to simultaneously adjust compensation temperature and absorption coefficient. Althoug considerable time has been expended in developing this fabrication facility it is believed to be the most practical approach towards achieving the long range goals of the program. It is important to note that its usefulness is not limited to fabricating garnets. It will also be used for preparing samples of antiferromagnetic materials to be studied in the future.

B. Evaluation of Rare Earth Iron Garnet Optical Properties

Section III contained the experimental results of the optical properties of gadolinium iron garnet in the 3.5 ev to 5 ev range. This data is

Fig. 9 Photograph of Crystal Fabrication Furnace.

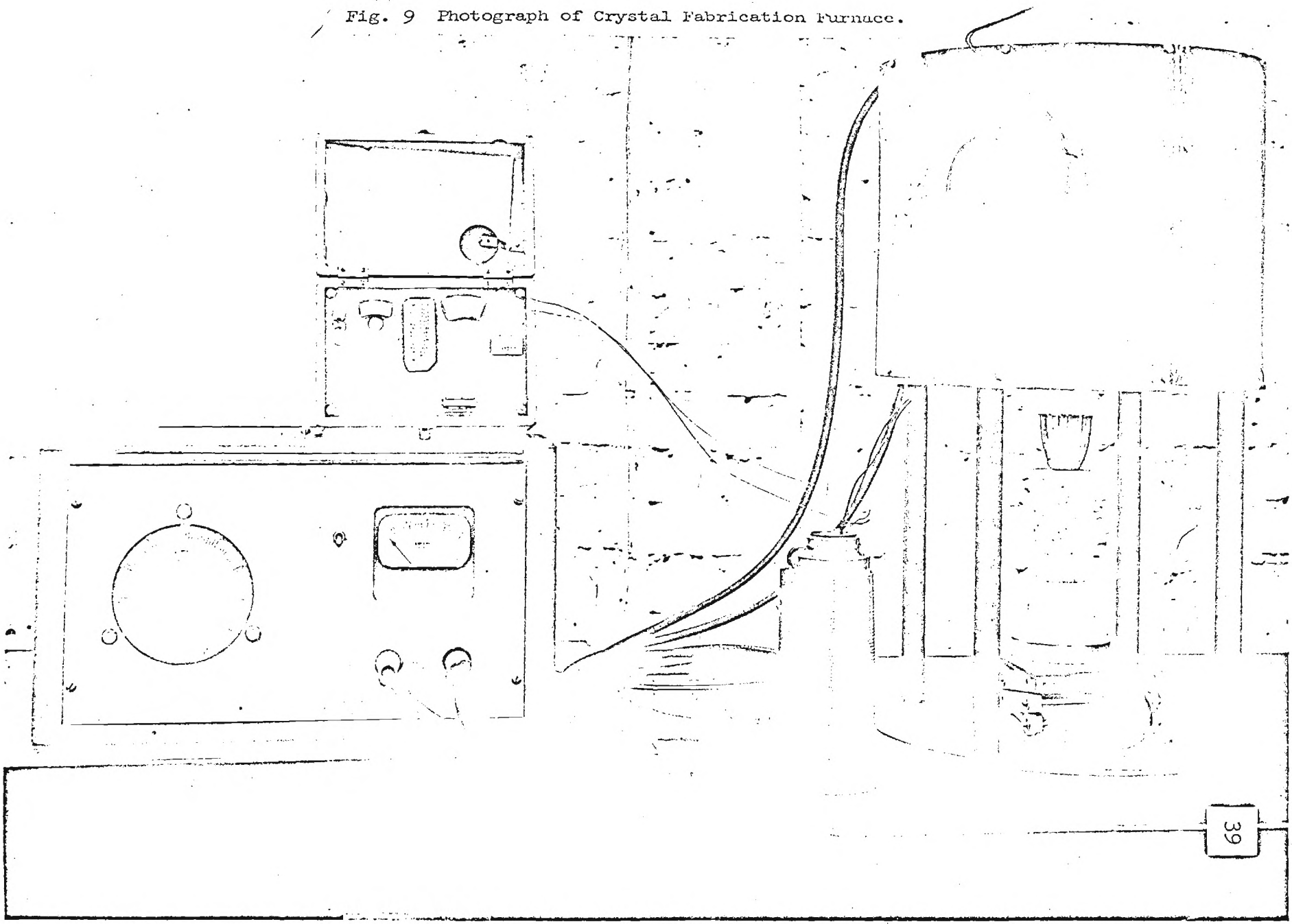

unique in the literature, emphasizing the characteristics in the vicinity of the gadolinium-free ion excitation energy. We have shown the existence of an absorption peak which seems likely to be associated with the gadolinium transition. While previous experimental limitations did not allow an unambiguous determination of the existence of fluorescence radiation there is reason to believe it may occur at very low intensity. However, as a result of the large absorption band width, it seems likely that competing non-radiative transitions were responsible for the greatest portion of decay from the excited state.

Such effects are quite reasonable when the entire absorption spectrum of GdIG is considered. We observe that the gadolinium transition frequency lies well within a very strong absorption band. This absorption appears to be a "conduction band" as evidenced by the magnitude of the absorption coefficient and recent data on photoconductivity of Grant and Rupple.[13] This conduction band is now generally attributed to a charge transfer from an oxygen anion to the unfilled 3d shell of the iron cations. It is therefore a characteristic of all the rare earth iron garnets and for that matter of all iron containing oxides. We cannot therefore expect free ion behavior for the gadolinium ions since in absorption charge transfer transitions compete with incoming photons and in emission the excited gadolinium atoms can easily give up their energy to the creation of hole-electron pairs.

It is interesting to note however that both terbium and dysprosium possess spin flip energy levels which are approximately at the conduction band edge. Thus there is the possibility that these materials could exhibit the desired optical pumping properties. There are several disadvantages to these ions in the rare earth iron garnet form.

First the measured lifetimes of the excited states has been shown to decrease as one gets further away from gadolinium in the periodic table. Terbium therefore has the next longest lifetime followed by dysprosium, holmium, etc. In dysprosium chloride, Dieke and Hall[11] have measured the lifetime as approximately 10 μ sec. For a given absorption transition probability the required pumping power increases inversely with the lifetime. No measurements are available however on the transition probability of these ions in the garnet lattice.

Secondly, the compensation temperature of the rare earth iron garnets decreases for terbium and dysprosium. This means it is somewhat more difficult to provide the required temperature bias around which memory operation

must take place. In both cases however, the required temperatures can be achieved by thermoelectric cooling units eliminating the need for liquid gas refrigeration.

If any of the rare earth iron garnets will work in the proposed scheme it will be TbIG or DyIG. This is because terbium and dysprosium are the only rare earth ions with spin flip transition at or below the charge transfer energy band gap of the iron containing garnets and in addition, exhibit fluorescent emission return to ground state. These materials are being fabricated now and will be evaluated for transition cross-section and fluorescence emission. In the event that these measurements yield positive results measurements of coercive force versus pumping will be attempted.

C. The Potential of Certain Antiferromagnets

One of the significant problems of optically pumping a temperature compensated ferrimagnet is the release of energy into the lattice. The ions are so tightly bound that energy transfer via non-radiative transitions is highly probable. In the garnets this creates an uncompensation because of thermal effects. As a result one is again limited by heat spreading and thermal time constant considerations. A possible way around this problem is to use materials whose compensation does not depend on temperature, i.e., antiferromagnets. These materials consist of two magnetic sublattices exchange coupled in an antiparallel fashion. In general the two sublattices contain identical atoms, e.g., MnO where the sublattices each contain only manganese ions; however, there are a number of antiferromagnets which are believed to be stable antiparallel arrangements of different ions.

An important example of this type is $CoMnO_3$ described by Bozorth and Walsh.[26] Magnetization measurements of this oxide indicate that is consists of antiparallel cobalt and manganese sublattices. The material is not completely compensated, an effect attributed to the different orbital contributions to the moments of the two ions. It is thus sometimes referred to as a weak ferromagnet, however the exchange interaction and basic magnetic structure is essentially antiferromagnetic. We would then expect a drastic change in coercivity if the magnetization of one sublattice could be changed, i.e., if the material were optically uncompensated. It seems that this should be possible since, as discussed earlier, manganese possesses a spin flip transition level and it generally occurs well down in the visible spectrum, e.g., 5,950 Å in $ZnF_2:Mn^{++}$. While the lifetime of the

excited state is known to be short, because of the 3d nature of the electrons, the absorption cross-section is probably high. Since heat resulting from relaxation via non-radiative processes would not affect the antiferromagnetic coupling appreciably such a material possesses significant advantage over the rare earth iron garnets. Other dissimilar ion antiferromagnetic materials are MC_rO_3 where M = certain rare earths, $DyFeO_3$, $HoCoO_3$, $HoMnO_3$, and Co_2MnO_4. Neutron diffraction data indicates that some of these may consist of two essentially independent antiferromagnetic sublattices each containing only one type of ion. There are instances where the data is inconclusive either way and these materials all merit further study.

Thus it appears that certain antiferromagnetic materials provide significant potential toward achieving memory operation by optical pumping. This is especially true of $CoMnO_3$ which could be operated at room temperature with no thermal control and would not depend on luminescent decay to achieve the desired operation.

V. CONCLUSIONS AND RECOMMENDATIONS

This report has cursorily described the status of our findings to date. While we have as yet no conclusive evidence to verify that the proposed pumping phenomena is a practical approach, we are in a position to select and fabricate materials with the greatest potential. It is apparent that the gadolinium iron garnet crystals grown by the present molten flux technique will not exhibit the desired characteristics. The conduction band causing the large competing absorption is probably a characteristic of the iron-oxygen combination rather than impurity induced interband gap levels. As such the rare earth garnets are all limited by this absorption edge. Only terbium and dysprosium offer a possibility of pumping at energies below the conduction band edge. Antiferromagnets overcome the problem of lattice phonons creating uncompensation but little is known of the optical properties of the potentially useful materials.

As of the originally proposed termination data for Phase I we are not in a position to proceed to a fabrication effort as conceived for Phase II. It is therefore proposed that the Phase II time be used to continue the required fabrication and optical evaluation of TbIG and DyIG. Time will not permit study of the antiferromagnets and it is strongly recommended that this work be funded during the following 12 month period. With the optical

apparatus and crystal growing facilities developed during this period the proposed future work can be carried out in greater detail and in a much shorter time than has been possible to date.

The concept of uncompensating an antiferromagnetically ordered system is of significant interest both theoretically and practically. The significance of achieving 10^8 bit high speed random access computer memories with passive element reliability should not be understated. Optical pumping is considered a powerful approach towards achieving that goal.

BIBLIOGRAPHY

Crystal Field Theory

1. G. Burns, "Crystal Fields at Rare-Earth Ions," J. Chem. Phys. 42 (1) 377-390 (1 January 1965).

2. A. M. Clogston, "Optical Faraday Rotation in Ferrimagnetic Garnets," Le Journal De Physique Et Le Radium 20, 151-154 (February 1959).

3. A. M. Clogston, "Structure of the Metastable State of Mn^{++} and Fe^{+++}," J. Phys. Chem. Solids 7, 201-206 (1958).

4. J. D. Dunitz and L. E. Orgel, "Electronic Properties of Transition-Metal Oxides-II," J. Phys. Chem. Solids 3, 318-323 (1957).

5. J. S. Griffith, "On the Stabilities of Transition Metal Complexes-I," J. Inorganic and Nuclear Chemistry 2, 1-10 (1956).

6. D. S. McClure, "The Distribution of Transition Metal Cations in Spinels," J. Phys. Chem. Solids 3, 311-317 (1957).

7. G. S. Ofelt, "Intensities of Crystal Spectra of Rare-Earth Ions," J. Chem. Phys. 37 (3) 511-520 (1 August 1962).

Magnetic and Physical Properties of Garnets

8. S. Geller, "Garnets: Magnetic Interactions and Distribution of Ions in the Garnets," J. Appl. Phys. 31 (Supplement) (5) 30S-37S (May 1960).

9. S. Geller, J. P. Remeika, R. C. Sherwood, H. J. Williams, and G. P. Espinosa, "Magnetic Study of the Heavier Rare-Earth Iron Garnets," Phys. Rev. 137 (3A) A1034-A1038 (1 February 1965).

10. C. D. Mee, "The Magnetization Mechanism in Single-Crystal Garnet Slabs Near the Compensation Temperature," IBM Journal 468-476 (July 1967).

Optical Characteristics of Rare Earth Ions and Garnets

11. G. H. Dieke and L. A. Hall, "Fluorescent Lifetimes of Rare Earth Salts and Ruby," J. Chem. Phys. 27 (2) 465-467 (August 1957).

12. H. W. Gandy and R. J. Ginther, "Stimulated Emission of Ultraviolet Radiation From Gadolinium-Activated Glass," Appl. Phys. Lett. 1 (1) 25-27 (1 September 1962).

13. P. M. Grant, "Reflectivity of YIG and YGG: Observation of Charge Transfer and Crystal Field Transitions," Appl. Phys. Lett. 11 (5) 166-168 (1 September 1967).

BIBLIOGRAPHY (Continued)

14. P. M. Grant and W. Ruppel, "Photoconductivity in Garnets," Solid State Communications 5, 543-546 (1967).

15. W. W. Holloway, Jr. and M. Kestigian, "Concentration Quenching of the Tb^{3+} Ion Fluorescence in $Y_3Al_5O_{12}$ Crystals," Phys. Lett. 21 (4) 364-366 (1 June 1966).

16. S. P. Keller and G. D. Pettit, "Visible Luminescence of Rare-Earth Yttrium Gallium Garnets," Phys. Rev. 121 (6) 1639-1648 (15 March 1961).

17. P. C. Bailey, "Absorption and Reflectivity Measurements on Some Rare Earth Iron Garnets and α-Fe_2O_3," J. Appl. Phys. 31 (Supplement) (5) 39S-40S (May 1960).

18. G. E. Peterson and P. M. Bridenbaugh, "Fluorescent Lifetime of Terbium in the Presence of Other Rare-Earth Ions," Letters to the Editor 53, 301-302 (January 1963).

19. R. C. Ropp, "Luminescence of Europium in the Ternary System: La_2O_3-Gd_2O_3-Y_2O_3," J. Electrochemical Soc. 112 (2) 181-184 (February 1965).

20. R. C. Ropp, "Spectral Properties of Rare Earth Oxide Phosphors," J. Electrochemical Soc. 111 (3) 311-316 (March 1964).

21. A. L. Schawlow, D. L. Wood, and A. M. Clogston, "Electronic Spectra of Exchange-Coupled Ion Pairs in Crystals," Phys. Rev. Lett. 3 (6) 271-273 (15 September 1959).

22. L. G. Van Uitert, "Factors Influencing the Luminescent Emission States of the Rare Earths," J. Electrochemical Soc. 107 (10) 803-806 (1960).

23. L. G. Van Uitert, R. C. Linares, R. R. Soden, and A. A. Ballman, "Role of f-Orbital Electron Wave Function Mixing in the Concentration Quenching of Eu^{3+}," J. Chem. Phys. 36 (3) 702-705 (1 February 1962).

24. F. E. Williams, "Theory of the Luminescence of Impurity-Activated Ionic Crystals," J. Phys. Chem. 57, 780-783 (November 1953).

25. D. L. Dexter, "Criterion for the Occurrence of Luminescence," Phys. Rev. 100 (2) 603-605 (15 October 1955).

Antiferromagnets

26. R. M. Bozorth and D. E. Walsh, "Ferromagnetic Moment of $CoMnO_3$," J. Phys. Chem. Solids 5, 299-301 (1958).

27. G. Busch, P. Schwob and O. Vogt, "Magnetic Properties of Some Rare-Earth Phosphides," Phys. Lett. 11 (2) 100-101 (15 July 1964).

28. W. C. Koehler, H. L. Yakel, E. O. Wollan and J. W. Cable, "A Note on the Magnetic Structures of Rare Earth Manganese Oxides," Phys. Lett. 9 (2) 93-95 (1 April 1964).

29. T. J. Swoboda, R. C. Toole and J. D. Vaughan, "New Magnetic Compounds of the Ilmenite-Type Structure," J. Phys. Chem. Solids 5, 293-298 (1958).

30. I. Tsuijikawa and E. Kanda, "Spectroscopic Studies of the Ordered State of the Manganous Halide Tetrahydrates," J. Phys. Soc. of Japan 18 (10) 1382-1390 (October 1963).

Mössbauer Papers

31. R. Bauminger, S. G. Cohen, A. Marinov, and S. Ofer, "Hyperfine Interactions in the Ground State and First Excited State of Dy^{161} in Dysprosium Iron Garnet," Phys. Rev. Lett. 6 (9) 467-470 (1 May 1961).

32. S. V. Karyagin, "Determination of the Local Field Parameters in Mossbauer Hyperfine Spectra," Soviet Physics--Solid State 8 (2) 391-396 (February 1966).

33. P. Kienle, "Recent Developments in Rare-Earth Mössbauer Studies. I," Rev. of Modern Phys. 372-393 (January 1964).

34. I. S. Lyubutin, "Effective Magnetic Fields at Sn^{119} Nuclei in Ferrite Garnets Having Compensation Points," Soviet Physics--Solid State 8 (3) 519-522 (September 1966).

Systems Oriented Papers

35. J. T. Chang, J. F. Dillon, Jr., and U. F. Gianola, "Magneto-Optical Variable Memory Based Upon the Properties of a Transparent Ferrimagnetic Garnet at Its Compensation Temperature," J. Appl. Phys. 36 (3) Part 2, 1110-1111 (March 1965).

36. F. Forlani and N. Minnaja, "A Proposal for a Magneto-Optical Variable Memory," Proc. IEEE 711-712 (April 1966).

37. S. Geschwind, P. Kisliuk, M. P. Klein, J. P. Remeika, and D. L. Wood, "Sharp-Line Fluorescence, Electron Paramagnetic Resonance, and Thermoluminescence of Mn^{4+} ub α-Al_2O_3," Phys. Rev. 126 (5) 1684-1686 (1 June 1962).

38. W. R. Hunter, "Errors in Using the Reflectance vs. Angle of Incidence Method for Measuring Optical Constants," J. Optical Soc. Am. 55 (10) Part 1, 1197 (October 1965).

39. W. F. Kosonocky, "Laser Digital Devices," IEEE Spectrum 183-186 (March 1965).

40. E. McLaughlin, "RCA Has Solid-State Laser to Produce Ultraviolet Light," Elec. News, August 22, 1966.

BIBLIOGRAPHY (Continued)

41. D. O. Smith, "Thin-Film Magneto-Optics in Information Processing," Optical and Electro-Optical Information Processing, Tippett, et al. MIT Press, 1965.

42. W. V. Smith, "Computer Applications of Lasers," Appl. Optics 5 (10) 1533-1538 (October 1966).

43. Tung-Po Lin, "Estimation of Temperature Rise in Electron Beam Heating of Thin Films," IBM Journal, 527-535 (September 1965).

Crystal Growing Papers

44. W. H. Grodkiewicz, E. F. Dearborn and L. G. Van Uitert, "Growth of Large Yttrium and Rare-Earth Aluminum and Iron Garnets," Proceedings of Intn'l. Conf. on Crystal Growth, Boston 20-24, June 1966.

45. M. Kestigian and W. W. Holloway, Jr., "Single-Crystal Growth and Optical Studies of Rare-Earth Aluminum Garnets," Crystal Growth, Proceedings of International Conference on Crystal Growth, Boston 20-24, June, 1966 Edited by H. S. Peiser, QD921.15, 1966.

46. D. A. Lepore, J. W. Nielsen, D. C. Leo, T. Lane, and F. Stallone, "Manufacturing Methods and Processes for Magnetic Garnets," Technical Report AFML-TR-65-376, November, 1965.

47. D. A. Lepore and D. C. Leo, "Manufacturing Methods for Growing Large Sound Yttrium Iron and Yttrium Gallium Iron Garnets," Progress Report, ASD Project No-9-542, 1 July 1966-30 November 1966.

48. D. A. Lepore and R. C. Puttbach, "Final Progress Report on the Preparation of Single-Crystal Ferrite Materials by the Floating Zone Technique," Report No. R11-441, January 27, 1964.

49. J. W. Nielsen, "Improved Method for the Growth of Yttrium-Iron and Yttrium-Gallium Garnets," J. Appl. Phys. 31 (Supplement) (5) 51S-52S (May 1960).

50. J. W. Nielsen and E. F. Dearborn, "The Growth of Single Crystals of Magnetic Garnets," J. Phys. Chem. Solids 5, 202-207 (1958).

Optical Pumping--Raman Effect--IFE

51. P. S. Pershan, J. P. Van der Ziel, and L. D. Malmstrom, "Theoretical Discussion of the Inverse Faraday Effect, Raman Scattering, and Related Phenomena," Phys. Rev. 143 (2) 574-583 (March 1966).

52. J. P. Van der Ziel, P. S. Pershan, and L. D. Malmstrom, "Optically-Induced Magnetization Resulting from the Inverse Faraday Effect," Phys. Rev. 15 (5) 190-193 (2 August 1965).

BIBLIOGRAPHY (Concluded)

53. Y. R. Shen and N. Bloembergen, Phys. Rev. 143, 372, 1963.

Books

54. R. Bernheim, Optical Pumping, W. A. Benjamin, Inc., 1965.

55. D. S. McClure, "Electronic Spectra of Molecules and Ions in Crystals," Part II of Solid State Physics, Vol. 9, Academic Press, 1959.

56. F. Seitz, The Modern Theory of Solids, McGraw-Hill, 1940.

57. A. Von Hippel, The Molecular Designing of Materials and Devices, M.I.T. Press, 1965.

58. D. Curie, Luminescence in Crystals, Wiley, 1963.

59. P. Goldberg, Luminescence of Inorganic Solids, Academic Press, 1966.

60. H. H. Theissing and P. J. Caplan, Spectroscopic Calculations for a Multielectron Ion, Interscience Publishers, 1966.

61. B. G. Wybourne, Spectroscopic Properties of Rare Earths, Interscience Publishers, 1965.

62. G. Bauer, Measurement of Optical Radiations, Focal Press, London, 1965.

63. D. E. G. Williams, The Magnetic Properties of Matter, American Elseivier Publishing Co., Inc., 1966.

64. S. Wang, Solid State Electronics, McGraw Hill, 1966.

65. J. H. Van Vleck, The Theory of Electric and Magnetic Susceptibilities, Oxford at the Clarendon Press, 1932.

66. J. Smit and H. P. J. Wijn, Ferrites, Wiley and Sons, 1959.

67. K. J. Standley, Oxide Magnetic Materials, Oxford at the Clarendon Press, 1962.

68. A. H. Morrish, The Physical Principles of Magnetism, Wiley and Sons, 1965.

GEORGIA INSTITUTE OF TECHNOLOGY
Engineering Experiment Station
Atlanta, Georgia

FINAL REPORT

PROJECT A-1028

STUDY OF FEASIBILITY OF OPTICALLY EXCITING A MAGNETIC THEORY

By

F. L. GRISMORE, J. ELMER RHODES, AND W. M. WYNN

CONTRACT NO. NAS8-20813

6 JUNE 1967 to 1 JULY 1969

Prepared for
NATIONAL AERONAUTICS AND SPACE ADMINISTRATION
GEORGE C. MARSHALL SPACE FLIGHT CENTER
HUNTSVILLE, ALABAMA

TABLE OF CONTENTS

LIST OF FIGURES

LIST OF FIGURES (Continued)

I. OPTICAL PUMPING

A. Introduction

An area of major concern in the development of digital computing hardware is the lack of a technology capable of providing high density random access memory. Thin magnetic films are currently used for memories of approximately 10^6 bits and cycle times of 500 nanoseconds. This technology however is limited by energy loss constraints as the input and output transmission lines become extremely small at higher bit densities. Cryogenic memories are potentially capable of overcoming this difficulty because of the negligible losses in superconducting paths. Work in this field has however not been successful after ten years of development.

An alternative to the cryogenic approach is one exploiting the magneto optical properties of certain materials. One proposal of this type[1] makes use of laser induced heating of a magnetic material to change the coercive force at one small spot in a ferrimagnet. In this approach storage density and switching times are limited by the thermal characteristics of the material.

A more promising approach is to exploit photon-electron interactions rather than photon-phonon interactions. Recently Forlani and Minnaja[2] observed that population of the first excited state by optically induced electronic transitions involving the $4f$ electrons in the rare earth ions should cause a significant change in their magnetic moment. This is referred to as optical pumping. They proposed that an excitation of this type should manifest itself as a reduction in magnetic coercivity in materials such as the rare earth garnets. The existence of this pheno-

mena would provide a memory technology with bit density being constrained primarily by the resolution limits of the incident light. Time constants for such an excitation would be governed by the lifetimes of the excited states, typically 10^{-6} to 10^{-7} seconds. A 10^{8} bit memory could be fabricated on a single plane of material 3 inches square.

This research program has been directed towards gathering the basic information required to predict the feasibility of an optically pumped approach. As a result of this work we have obtained a rather complete set of data which provides the first absorption spectra characteristic of bulk GdIG and TbIG over the 2 ev to 5 ev energy range. From these experimental results and the theoretical evaluation of the pumping and thermal processes it is concluded that there is a high probability of achieving the desired memory operation. The actual experimental phenomena was not demonstrated because of time limitations, and should be seriously considered as a program for continued funding as a result of the potential significance to future computer systems.

B. Optically Accessed Memory Concept

The memory concept to which the research applies is that the intrinsic saturation magnetization of an ordered spin system can be changed by optical pumping.

In certain materials, terbium iron garnet for example, the coercive force is very sensitive to changes in saturation magnetization of the terbium sublattice. TbIG is a ferrimagnet and the total magnetization is the vector sum of that due to the terbium sublattice and that of the iron sublattice. At low temperatures, e.g., 10°K, each sublattice is exchange ordered and the two are coupled in an antiparallel fashion via a superex-

change mechanism through the oxygen ions. At higher temperatures thermal energy overcomes the direct exchange of the terbium sublattice rendering the rare earth ions paramagnetic. There remains however a net terbium sublattice magnetization as a result of the superexchange molecular field. In this temperature range the terbium sublattice magnetization obeys a Curie type law so that

$$M_{Tb} = \frac{H_{eff}C}{T - T_c}$$

where H_{eff} is the superexchange effective field,

C is the Curie constant,

T_c is the Curie temperature.

The Curie temperature of the iron sublattice is much higher than that of the terbium sublattice but the saturation magnetization of the terbium sublattice is larger than that of iron. Thus as temperature is raised, the iron moment remains sensibly constant while the terbium moment varies inversely with temperature. At one temperature, approximately 246° K for TbIG the two sublattice magnetizations are equal and opposite. This temperature is called the compensation point. At this point there is no net magnetization of the material and hence no couple between the spin system and an external field since

$$\bar{M}_{net} \times \bar{H}_{ext} = 0.$$

As a result the coercive force becomes very high at this point approaching

infinity in a first order model. In actual practice a large but finite coercive force exists. Around this compensation point the coercive force is a very sensitive function of sublattice magnetization. For example, a change of 5% in the terbium magnetization can reduce the coercive by a factor of nearly 5.

A memory exploiting this effect would be accessed in the following manner. Assume a single crystal slab of terbium iron garnet is magnetically saturated to a single domain configuration with the iron sublattice moment pointing left and the terbium sublattice pointing right. The temperature of the sample is held constant at the compensation temperature. If a magnetic field directed from left to right is applied to the entire sample no switching will occur if the field strength is less than the coercive force. Assume the applied field has an amplitude of $H_c'/2$ where H_c' is the coercive force at the compensation point. Application of a focused laser beam to a predetermined spot would then through optical pumping reduce the terbium magnetization, uncompensating the net spin system, and hence reduce the coercive force at that spot. As a result there would be a local switching with the net moment pointing from left to right. Removal of the laser beam and magnetic field would then leave a stable reversed magnetic domain with the iron moment right directed and the terbium moment left directed. Such a configuration might be designated as binary "1" while the oppositely directed configuration would be called logical "0". The sense of a particular spot would be read out using the Faraday effect associated with the iron sublattice.

C. Theory of Optical Pumping

The magnetic moment of the rare earth ions is a result of the

orbital and spin angular momentum of a partially filled $4f$ shell. These electrons are shielded by completely filled 5s and 5p shells and thus the magnetic properties of these ions are not greatly affected by bonding and crystalline field perturbations. An additional result of the shielding of these electrons is that the free ion optical properties, especially those associated with the intraband $4f$ electronic transitions, are not significantly affected when the atoms are incorporated in a solid. It is therefore a good first order approximation to analyze the optical pumping effect based on free ion energy levels.

Terbium has eight $4f$ electrons and the ground state is described in spectroscopic notation as $^7F_6$. The spin degeneracy $2S + 1$ having a value 7 corresponds to a net spin moment of $\mu_s = 6\mu_B$ where μ_B is the Bohr magneton. The first excited state for terbium is given as $^5D_4$, corresponding to $\mu_s(\text{excited}) = 4\mu_B$. Hence when the terbium ion is raised to its first excited state the spin contribution to the total moment has decreased 33%. Experiments[3] show that the rare earth sublattice moment is due primarily to spin angular momentum, i.e., the orbital momentum is quenched. When studying the characteristics of optical pumping on net magnetic moment it is reasonable to consider only the change in spin.

The first excited state corresponds to a spin flip transition and as such is not normally allowed. Actually this selection rule generally does not hold rigorously in solids, especially in the rare earths where strong spin orbit coupling causes admixtures of different orbital parity which in turn produce finite transition matrix elements. However to keep the pumping expression completely general we consider a three level system. In this scheme an incoming photon excites an ion in the ground state, state 1, to a short-lived intermediate state, state 3, via an allowed transition.

The ion then is assumed to relax, via an electron phonon interaction, to the spin flip state 2.

The rate equations for this pumping scheme are then given simply as:

$$\dot{n}_1 = - b_{13}n_1 + w_{21}n_2 + w_{31}n_3$$

$$\dot{n}_2 = - w_{21}n_2 + w_{32}n_3$$

$$\dot{n}_3 = b_{13}n_1 - w_{32}n_3$$

where n_1, n_2, n_3 = number of ions per cm^3 in states 1, 2, 3, respectively,

b_{13} = transition rate for ions going from state 1 to state 3,

w's = relaxation rates.

These transitions are shown diagramatically in Figure I-1. There is in addition the constraint given by

$$n_1 + n_2 + n_3 = N_T$$

where N_T = total ions in the system. In the steady state, $n_1 = n_2 = n_3 = 0$ and the second rate equation in conjunction with the constraint yields

$$n_{2F} = \frac{w_{32}\,(N_T - n_{1F})}{w_{32} - w_{21}} \quad .$$

Making the assumption that state 3 is very short-lived with respect to state 2, we have $w_{32} \gg w_{21}$ with the result, $n_{2F} \approx N_T - n_{1F}$, i.e., state 3 is essentially unpopulated. If in addition $w_{32} \gg w_{31}$ the second and third rate equations, in conjunction with the approximation $n_2 = N_T - n_1$, results in a two-level approximation for n_2 of:

$$\dot{n}_2 = b_{13}n_1 - w_{21}n_2 \quad . \tag{1.1}$$

Since $N_T \approx n_1 + n_2$ in this approximation we find the steady state solution of the rate equation to be

$$n_{2F} = \frac{(b_{13}/w_{21})N_T}{(1 + b_{13}/w_{21})} = \frac{N_T}{(1 + \frac{w_{21}}{b_{13}})} \tag{1.2}$$

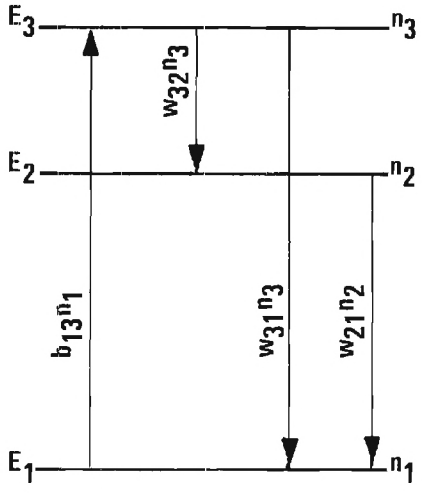

Figure I-1. Diagram of the transitions involved in the transition rate equations of the assumed optical pumping process.

and is reached in a time constant of

$$\tau = \frac{1}{(w_{21} + b_{13})} \quad . \tag{1.3}$$

These last two equations describe the steady state population of level 2 and the time constant required to reach it in terms of transition and relaxation probabilities.

At first sight it might be assumed that the coefficient w and b are simply the Einstein A and B coefficients so often discussed in laser theory. This is, however, not the case. The Einstein rate equations are based on the premise that the radiation inducing transitions between states can be described in terms of a radiation density $I(\nu)$, and that the spectral distribution is very broad with respect to the line width of the absorption. In the case to be considered in this research the absorption line will be excited with a monochromatic laser source. Hence the radiation line width is very narrow with respect to that of the absorption line.

Following the general line of development leading to the Einstein relationships, it has been possible to derive quantum mechanically the expression for the transition probability for absorption in the monochromatic case. It turns out that one must consider excitation not to a single higher state but a distribution of higher states described by a density of states $n(\omega)$ states/unit frequency/cm^3. The result as developed in Appendix I is

$$b = \frac{4\pi^2}{3c\hbar^2} n(\omega) I |M_{km}|^2 \tag{1.4}$$

where M_{km} = electric dipole moment matrix element associated with the ground state k and a state m in the upper density of states,

I = incident monochromatic radiation intensity.

It is possible to determine $|M_{km}|^2$ from optical absorption measurements. The absorption coefficient K can easily be shown to be related to the transition rate b as

$$K = \frac{bN\hbar\omega}{I} \tag{1.5}$$

where N = number of atoms/cm^3,

$\hbar\omega$ = energy between ground and excited levels.

From this it is seen that

$$|M_{km}|^2 = \frac{3c\hbar}{4\pi^2 N\omega n(\omega)} K . \tag{1.6}$$

To a first order approximation we can assume that the distribution of states is uniform. Since the integral

$$\int_{\text{line}} n(\omega)d\omega = N,$$

we can write approximately

$$n(\omega) \approx N/\Delta\omega \tag{1.7}$$

where $\Delta\omega$ = half width of the absorption line. Therefore, from (1.6) and (1.7) we can estimate the dipole moment matrix element from the amplitude and width of the measured absorption characteristic.

The spontaneous emission from an excited state $n(\omega_k)d\omega$ is:

$$dw_s = \frac{4\omega_{km}^3}{3\hbar c^3} |M_{km}|^2 \, n(\omega_k)d\omega$$

and integrating over the upper level, the total spontaneous transition rate to ground becomes

$$w_s = \frac{4\omega_{km}^3 N}{3\hbar c^3} |M_{km}|^2 .$$

We find therefore, neglecting stimulated down transitions, that the w/b ratio is given simply as:

$$\frac{w}{b} = \frac{8\pi c \Delta E}{\lambda^3 I} \tag{1.8}$$

where ΔE = the energy half width of the absorption line,

λ = wavelength of the absorption peak.

It is observed from equation (1.2) that the w/b ratio is the only factor determining the population of the excited state.

D. Potential Feasibility of Optical Pumping

There is experimental data available in the literature showing the relationship of coercive force versus temperature for the rare earth iron garnets near their compensation temperature.[4] In general it is found that a 2° C swing from the compensation temperature will cause a reduction in H_c by a factor of two. The iron sublattice remains nearly constant over such a small temperature differential at the compensation point. In addition the rare earth sublattice is essentially paramagnetic and hence its magnetization follows a Curie type variation as:

$$M(T) = \frac{M_o}{T}$$

since Curie temperature is much smaller than temperature range of interest. In the vicinity of the compensation temperature the percentage change of rare earth can then be approximated as

$$\Delta M = 1 - \frac{T_c}{(T_c + \Delta T)} \quad .$$

We can estimate the required number of excited rare earth atoms to achieve this change in M by using the high temperature approximation of the Brillouin function to describe the moment of the paramagnetic sublattice. Thus assuming the orbital angular momentum is completely quenched

$$M \approx H_{mol} Ng^2 [S(S+1)] u_B^2/3kT = K[N \cdot S(S+1)] \quad . \qquad (1.9)$$

where H_{mol} = Weiss Molecular field,

K is simply a constant of the system.

If there are N_T total rare earth ions, and n_{2F} are excited so as to have a different spin quantum number, the total sublattice magnetization is

$$M = K\left[n_{2F}\, S_e(S_3 + 1) + (N_T - n_{2F})S_g(S_g + 1)\right] \tag{1.10}$$

where S_g = spin quantum number in the ground state,

S_e = spin quantum number in the excited state.

The change in magnetization can then be written as

$$\Delta M = \frac{n_{2F}}{N_T}\left[1 - \frac{S_e(S_e+1)}{S_g(S_g+1)}\right] \tag{1.11}$$

Thus the population of optically excited atoms necessary to achieve a change in M equivalent to a ΔT excursion from compensation is

$$\frac{n_{2F}}{N_T} = \frac{\left[1 - \frac{T_c}{T_c + \Delta T}\right]}{\left[1 - \frac{S_e(S_e+1)}{S_g(S_g+1)}\right]}. \tag{1.12}$$

Since $S_e = 4$, $S_g = 6$ and $T_c = 246^\circ K$ for TbIG the population requirement of the equivalence of $\Delta T = 2^\circ K$ is

$$\frac{n_{2F}}{N_T} = 0.0135 \quad \text{or} \quad 1.35\% \ .$$

Knowing the desired excited state population, it is now possible to calculate the radiation intensity required. From equations (1.2) and (1.8) we obtain for the case $n_{2F} \ll N_T$

$$I = \left(\frac{8\pi c \Delta E}{\lambda^3}\right)\left(\frac{n_{2F}}{N_T}\right) \frac{\text{erg}}{\text{sec} \cdot \text{cm}^2} \ . \qquad (1.13)$$

In terbium iron garnet the absorption line of interest occurs at a wavelength of $\lambda = 5000\text{Å}$. Experimental measurements carried out during this research indicate the line width to be $\Delta E \approx 0.2$ ev. From this we can estimate the intensity required to produce an excited state population of $0.02\ N_T$ to be

$$I = 3.85 \times 10^{10} \frac{\text{erg}}{\text{sec} \cdot \text{cm}^2} = 3.85 \times 10^{7} \text{ watts/m}^2 \ .$$

Even though this is a high power density in terms of conventional radiation sources, it is easily achieved with a focused laser.

The output beam of a laser is nearly completely parallel, divergence being of the order of several miliradians. Thus high intensities can be achieved simply by focusing the beam to a small diameter spot.. For memory operation it would be desirable to have storage regions no larger than 10 microns in diameter. Actual size would be limited by the requirement of having a stable magnetic domain wall around the spot. Experimental

results[5] indicate 10μ is easily obtainable. To achieve a power density of approximately 4×10^7 watts/m^2 over a 10μ spot requires a total power of only

$$P = 3.14 \text{ milliwatts} ,$$

It therefore appears that the concept is indeed feasible. We can not be certain that the line observed in the absorption spectra is the desired terbium transition; however, the following sections present sufficient evidence that it is, to justify the carrying out of a complete pumping experiment. The following sections explain in some detail the optical measurements and data reduction and a thermal analysis of the proposed memory geometry. In addition we give an outline of the theoretical analysis which is ultimately necessary if a complete understanding of the magneto-optic effects is to be obtained. However, because of lack of time and funding during the present contract, it was impossible to carry out the actual pumping experiment. It is strongly recommended that a follow on program be initiated to carry out this crucial experiment.

II. EXPERIMENTAL RESULTS AND ANALYSIS

A. Introduction

During this contract experimental facilities were designed and assembled to grow single crystals by the molten flux method and perform optical reflectivity measurements. In addition two computer programs were written to perform reduction of the reflection data into optical absorption. This section will describe the experimental apparatus and the results obtained from the experimental phase.

B. Crystal Growing Facility

A vertical tube furnace was designed which is capable of ultimate temperatures of 1300°C. The heating element with its associated alumina and fittings can be purchased as a complete set from Kenthal Corporation. The unit used in this furnace is Kenthal Type No. REH-7-30 rated at 1350 watts. Figure II-1 shows a cross-sectional drawing of the unit and Figure II-2 is a photograph of the complete oven and power supply. During operation it was found that the gases evolved from the molten flux reacted with the Kenthal heating element causing failure after about 800 hours. To overcome this problem it is necessary to insert a protective alumina tube inside the heater. The oven requires 24 volts at approximately 60 amps. A silicon controlled rectifier power controller feeds power to the oven through a 115 volt to 24 volt transformer. The circuit diagram is shown in Figure II-3. The SCR network is a zero cross-over firing network providing one complete cycle of power each time a logic signal is received.

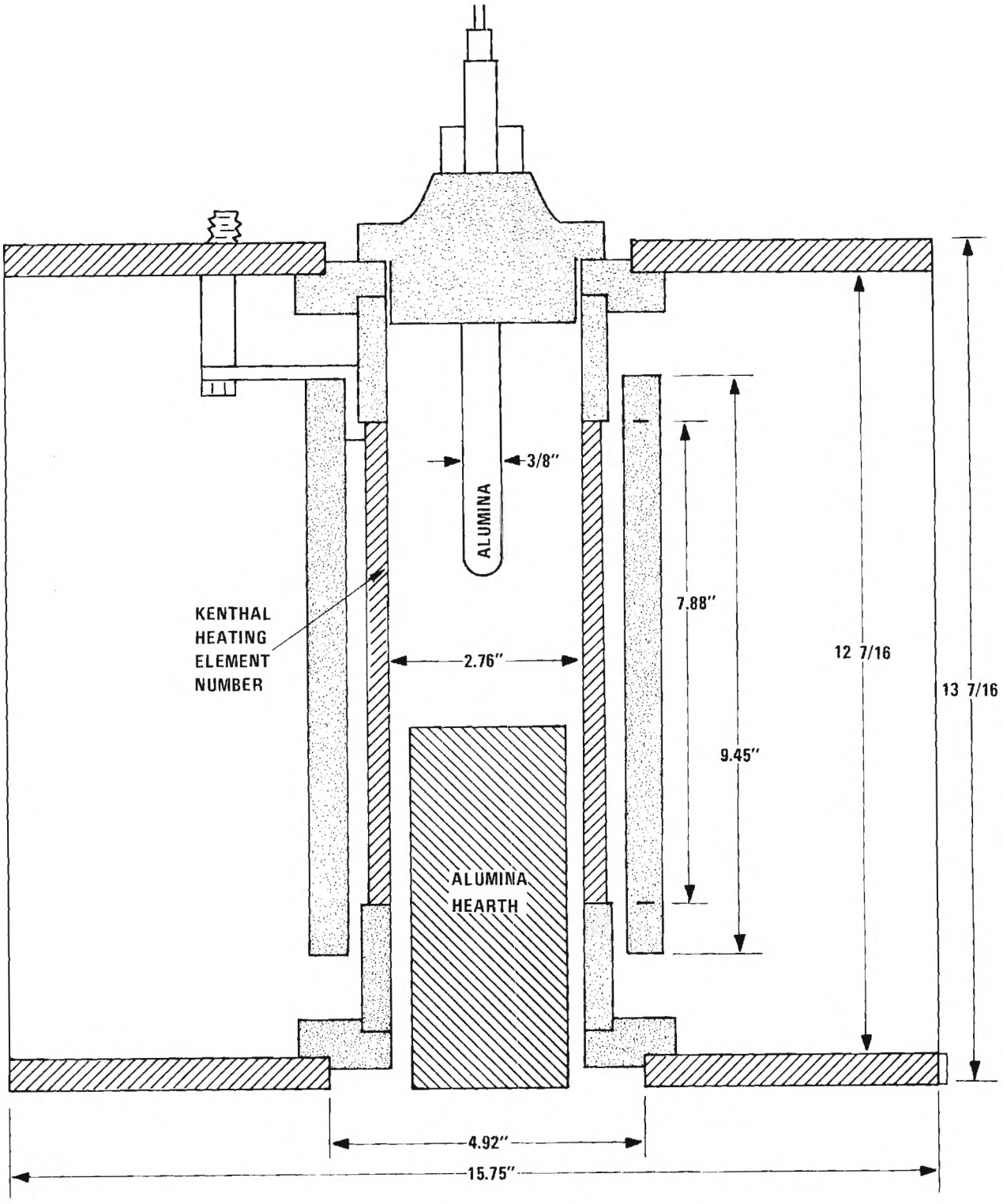

Fig. No. 2.1 Cross Sectional View of Crystal Growing Furnace

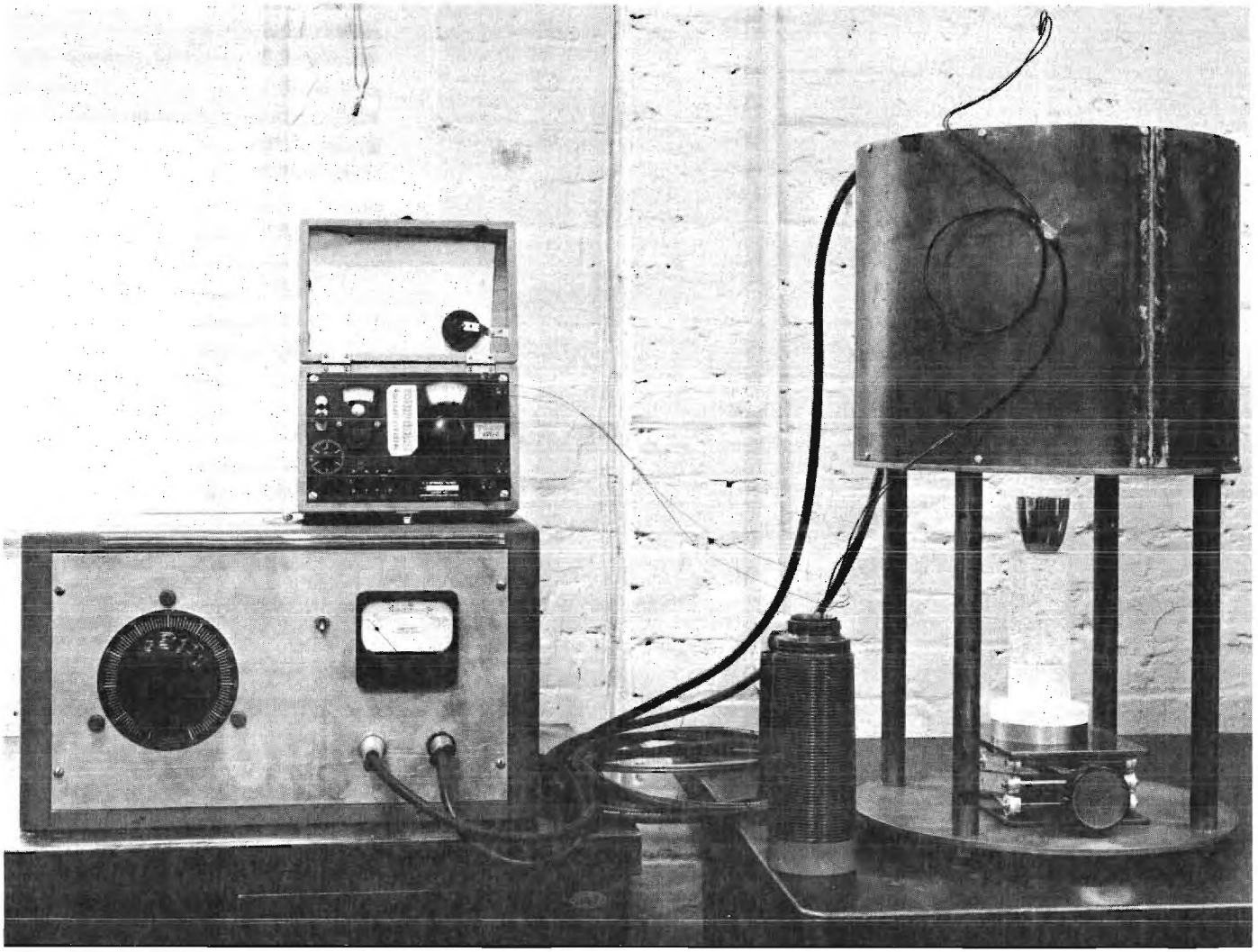

Fig. No. 2.2 Photograph of Complete Furnace and Power Supply

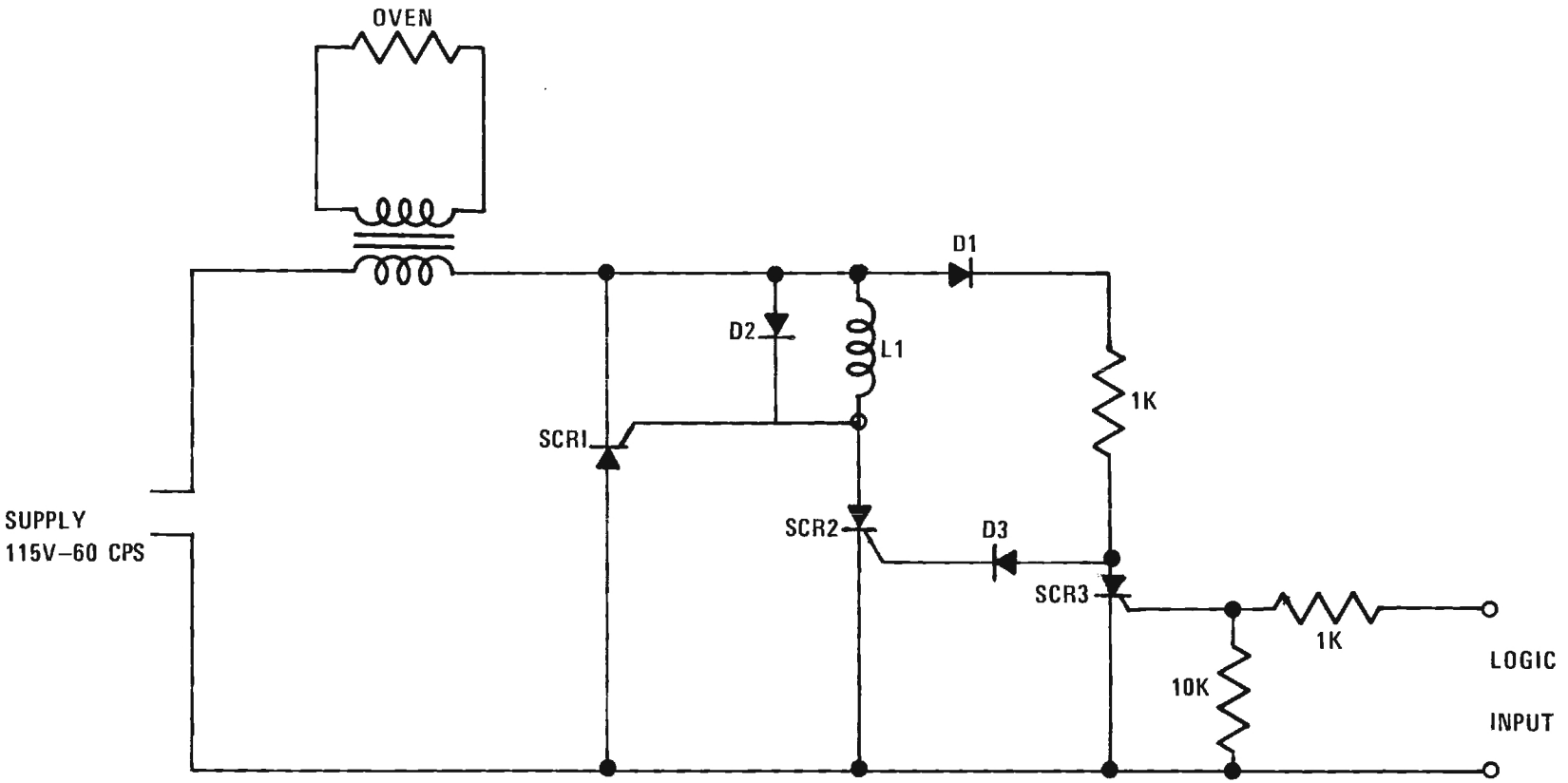

Fig. No. 2.3 Silicon Controlled Rectifier Power Switch

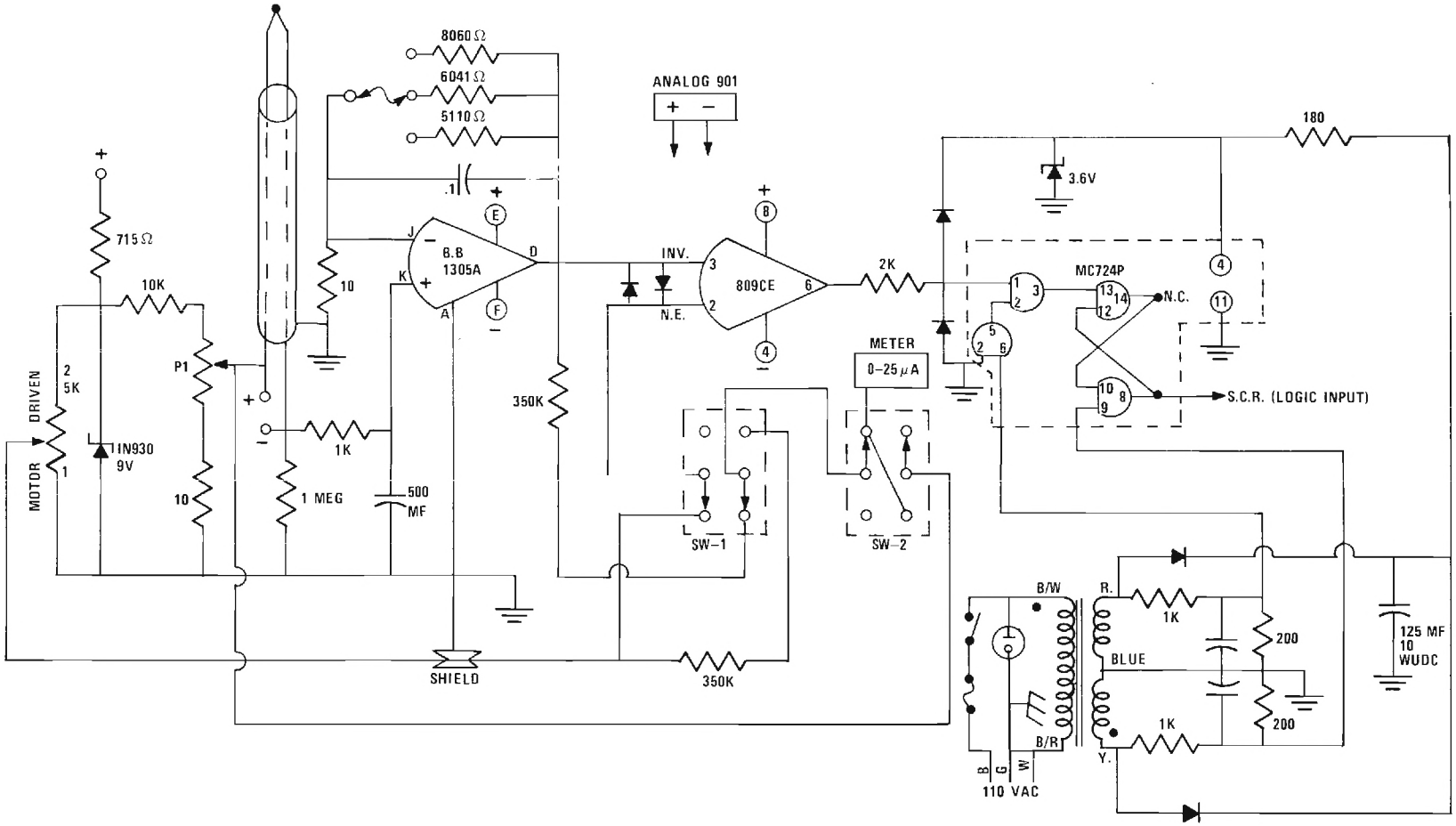

Fig. No. 2.4 Circuit Diagram of Programmed Temperature Controller

Using this approach there is no large dI/dt during turn on and hence a minimum of R.F.I. Large transients can cause serious interference with the logic of the controller and therefore are to be avoided.

The temperature controller and rate generator are designed to provide a uniform temperature rate with respect to time of 0.5° C/hour. The sensitivity of the circuit provides for a temperature swing of no more than $\pm 0.2^{\circ}$ C around the programmed temperature profile. A circuit diagram of the controller is shown in Figure II-4.

C. Reflectivity Measurements

This research has resulted in the first quantitative data of the absorption spectra for single crystal rare earth iron garnets in the 2 to 5 ev range. This was possible because of the application of reflectivity techniques to determine the complex index of refraction. Data have been obtained on GdIG, TbIG and DyIG for both natural faces and mechanically polished surfaces. The results show no significant differences. The raw data has been completely analyzed for GdIG and TbIG; however, the DyIG data has only been carried through the calculation of reflectivity.

The crystals studied were grown from a lead fluoride-lead oxide molten flux and as a result contain a number of impurities, especially lead, which may contribute to some of the observed absorption spectra. We have not analyzed these effects in detail; however Table II-1 indicates the impurities detected as a result of an emission spectrographic run.

Table II-I

Impurities Detected in Rare Earth Iron Garnet Crystals

Impurity	TbIG	GdIG
Lead	> 3%	> 3%
Cadmium	0.002-0.02%	--
Boron	0.01-0.1%	--
Silicon	0.02-0.2%	--
Iron	Strong	Strong
Manganese	0.001-0.01%	--
Magnesium	--	0.0005-0.005%
Bismuth	0.002-0.02%	--
Gadolinium	--	Strong
Copper	--	0.0005-0.005%
Calcium	0.002-0.02%	0.02-0.2%
Aluminum	--	0.0002-0.002%
Terbium	Strong	≈ 0.001%
Erbium	0.1-0.5%	--

A diagram of the reflectivity apparatus is shown in Figure II-5. The light source is a high pressure type B-H6 air-cooled mercury vapor lamp and is focused on the monochrometer entrance slit with a metallic spherical mirror. Slit height is restricted to approximately 0.5 mm to reduce the solid angle subtended by illumination at the crystal surface. The mono-

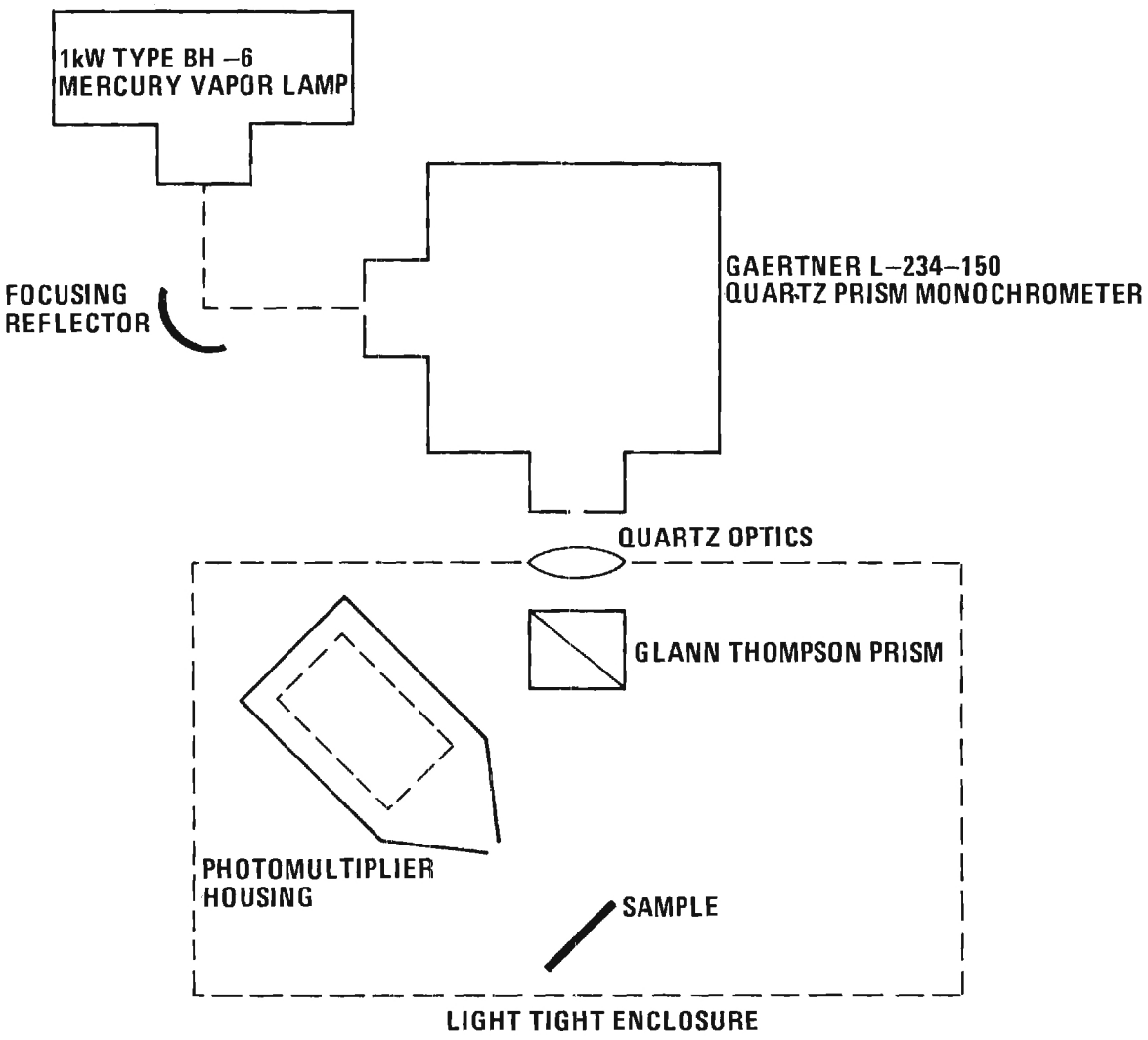

Fig. No. 2.5 Reflectivity Apparatus

chrometer is a standard quartz prism instrument. Exit slit width was maintained at 0.3 mm yielding an effective bandwidth of 0.04 to 0.12 ev over the range of the measurements. A quartz lens images the exit slit on the sample and is aperatured so that the included angle of the light incident on the crystal surface is less than 1°. The angle must be kept small as the analysis of the reflectivity data is sensitive to variations in angle of incidence at the sample. A Glan Thompson prism is used to polarize the light parallel to the plane of incidence. The photomultiplier tube and sample are mounted on concentric vertical shafts which allow independent angular positioning around a common center. A series of accurately machined indexing stops permits reliable angular settings. In addition, the sample may be lowered completely out of the beam for measurement of incident intensity. The EMI 9601B photomultiplier is rotated around its longitudinal axis to a position where its gain is insensitive to variations in the earths magnetic field it experiences as the assembly is rotated in a horizontal plane during the measurement process.

D. Data Reduction

Reflectivity at an air-material interface is a function of the real and imaginary components n and k of the refractive index, the polarization and the angle of incidence and is described analytically by the well-known Fresnel equations. Using light linear polarized in the plane of incidence and measuring reflectivity at two different angles of incidence provides sufficient information to uniquely determine n and k. The transcendental nature of the equations however prevent a closed form solution. To overcome this problem we use a modification of a computer algorithm proposed by Hunter.[5] Given initially assumed values of n and k the computer solves the Fresnel equations, at the two angles of incidence used in the experi-

ment, and computes an error between the calculated and actually measured reflectivities. The error expression used is

$$E = [(R_m(\theta_1) - R_c(\theta_1))/R_m(\theta_1)]^2 + [(R_m(\theta_2) - R_c(\theta_2))/R_m(\theta_2)]^2$$

where $R_m(\theta)$ is the measured reflectivity and $R_c(\theta)$ is the computed reflectivity at the same angle for the assumed n and k. A systematic search over the n-k plane is then carried out to find the point resulting in minimum error E. Our results were obtained with an increment of n and k of 0.002. This technique overcomes many of the problems associated with carrying out a Kramers-Kronig integral analysis. The actual ALGOL program used is reproduced in Appendix II.

From the computed n and k characteristics the details of the light-material interaction can be evaluated by studying the optical conductivity, $\sigma=2nkw$ or the more familiar absorption coefficient, $k=2kw/c$. Information of the absorption fine structure is obtained by approximating the absorption coefficient with a series of Lorentzian shaped lines as:

$$K(E) = K_o + \sum_i \frac{K_i}{(E-E_i)^2 + (\Gamma_i/2)^2} \qquad (2.1)$$

where K_o is a constant absorption level under the fine structure and i is a number to denote different lines. The fit is performed by manually adjusting the parameters K_i, E_i and Γ_i until a satisfactory series approximation is reached. There is of course no guarantee of a unique solution; however from a practical point of view one can place reasonable confidence in the general nature of the results. For each absorption line the oscillator strength is then calculated as

$$f_i = \frac{mn(E_i)c}{N\pi he^2} K(E_i)\Delta E_i = \frac{4mc}{N\pi he^2} \frac{n(E_i)K_i}{\Gamma_i} \qquad (2.2)$$

where $n(E_i)$ is the real part of the refractive index at E_i, N is the number of absorbing atoms per cubic centimeter, $K(E_i) = K_i/(\Gamma_i/2)^2$ is the absorption coefficient of the ith line and $\Delta E_i = \Gamma_i$ is the half width of the ith absorption line.

E. Evaluation of Data and Results

Figure II-6 shows plots of measured reflectivity as a function of energy for samples of GdIG and TbIG. The data were taken on (111) planes, these being perpendicular to the magnetic easy axis in the rare earth iron garnets. It is interesting to note the similarity of the fine structure in the GdIG data above 3 ev with that obtained by Grant[6] for YIG. Our data shows reflectivity peaks at 3.15, 3.35, 3.72, 3.90, 4.10, and 4.35 ev. Grant reports peaks in YIG at 3.14, 3.35, 3.74, 4.04, and 4.35 ev. One would therefore tend to conclude that most of these lines probably are transitions associated with the iron sites since these are common to both YIG and GdIG. Note however that the 3.9 ev line does not correlate with the YIG data and might well be associated with the first excited state transition for gadolinium which occurs at 3.85 ev in gadolinium chloride. The strong peak at 4.35 ev is probably a charge transfer transition, masking the second gadolinium transition which should appear somewhere around 4.32 ev. There is reasonable but not exact correlation with the "charge transfer" lines in the TbIG data. Here the prominent peaks above 3 ev are at 3.02, 3.25, 3.54, 3.70, 3.95, and 4.35 ev. These appear in general to be about 0.1 to 0.15 ev lower in energy than for the GdIG; however, the

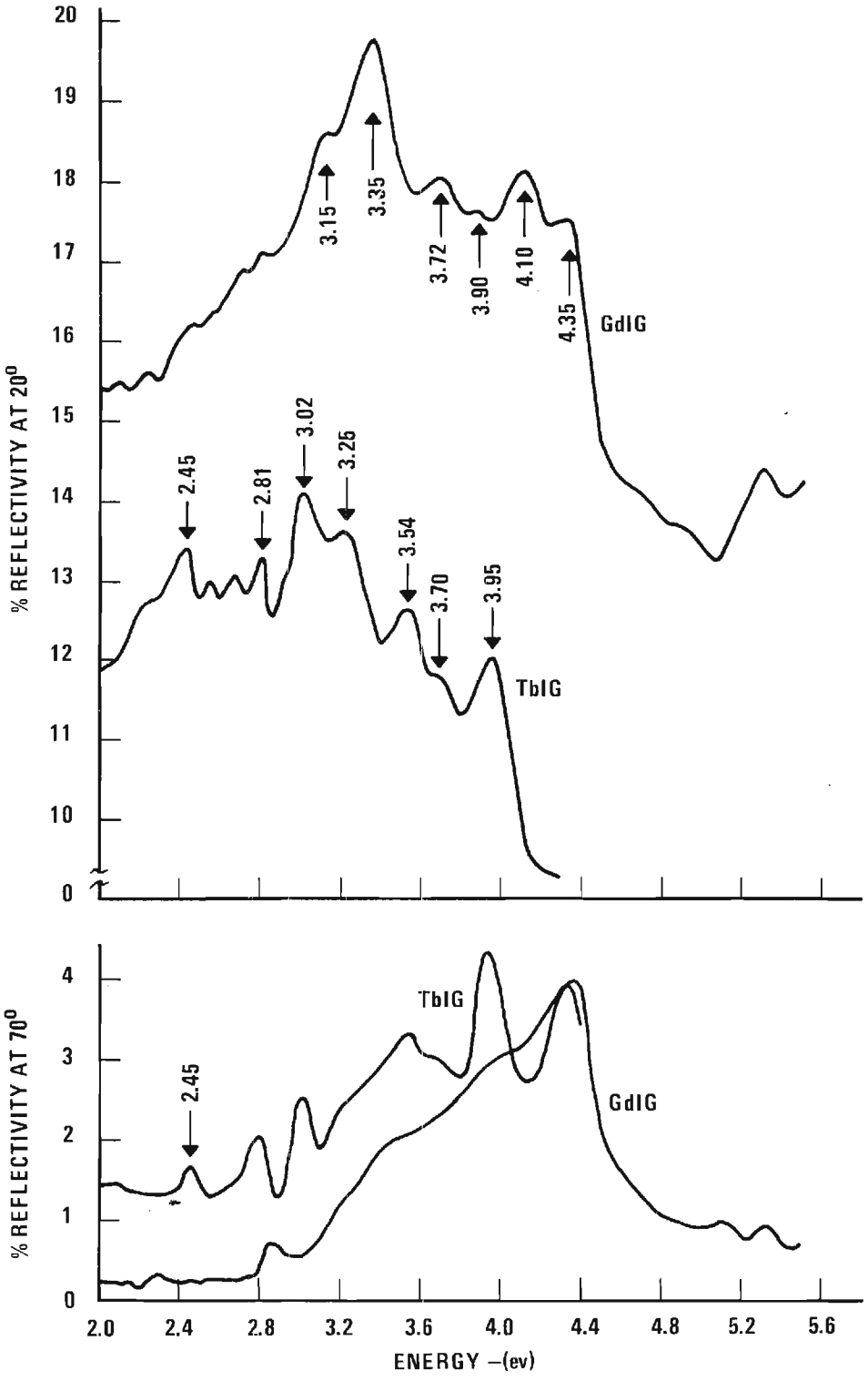

Fig. No. 2.6 Plots of Measured Reflectivity

relative spacing and amplitudes seem to indicate they are probably due to the same transitions.

Note however that below 3 ev the terbium data contains some rather prominent structure which is not duplicated in the GdIG. This extra structure might be anticipated in TbIG if the rare earth electronic transitions are observable for it is known that terbium has a number of excited states in the visible range while Gd does not. Of particular interest is the line at 2.45 ev. It is known from data on hydrated terbium chloride[7] that there is a terbium absorption line at about 20,600 cm^{-1}, i.e., 2.54 ev and Keller and Pettit[8] have observed this transition in fluorescence in terbium doped YGG. The 0.1 ev difference in this sample is consistent with the other data and thus leads to the possibility that the line could be due to terbium absorption.

Figures II-7 and II-8 show plots of the real and imaginary components of the refractive index, n and k, for GdIG and TbIG. In general they reflect the structure apparent in the reflectivity data. It is to be noted however that the imaginary component k appears to demonstrate some effects of the terbium spectra. Comparing k in Figures II-7 and II-8, we see that TbIG exhibits a broader spectrum in the 3.2 ev to 3.6 ev range and much more pronounced lines at 3.9 ev and 4.1 ev. This is consistent with the Tb^{3+} ion spectra reported by Dieke and Hall,[7] which has been included in Figure II-8 for reference.

Figure II-9 shows the absorption coefficient for GdIG computed from the values of k from Figure II-7. The graph shows an apparent base in the absorption constant at about 1×10^5 to 2×10^5 cm^{-1} with some additive fine structure between 3 and 5 ev. MacDonald et al.[9] have measured an absorption coefficient of about 3×10^5 cm^{-1} on 0.1μ thick films, their data also showing a relatively constant absorption in this energy range. The

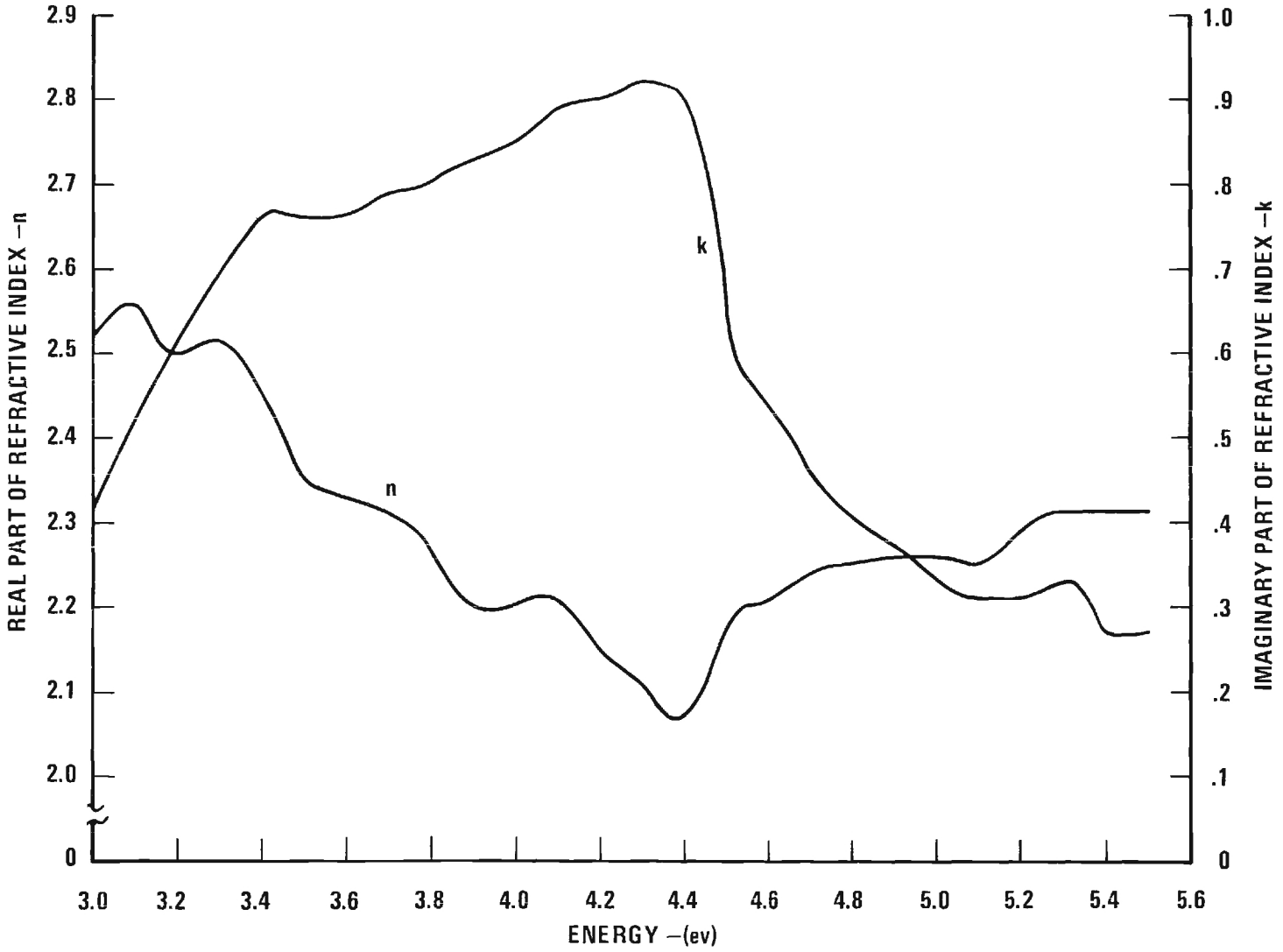

Fig. No. 2.7 Calculated Components of Refractive Index N=n-jk of GdIG

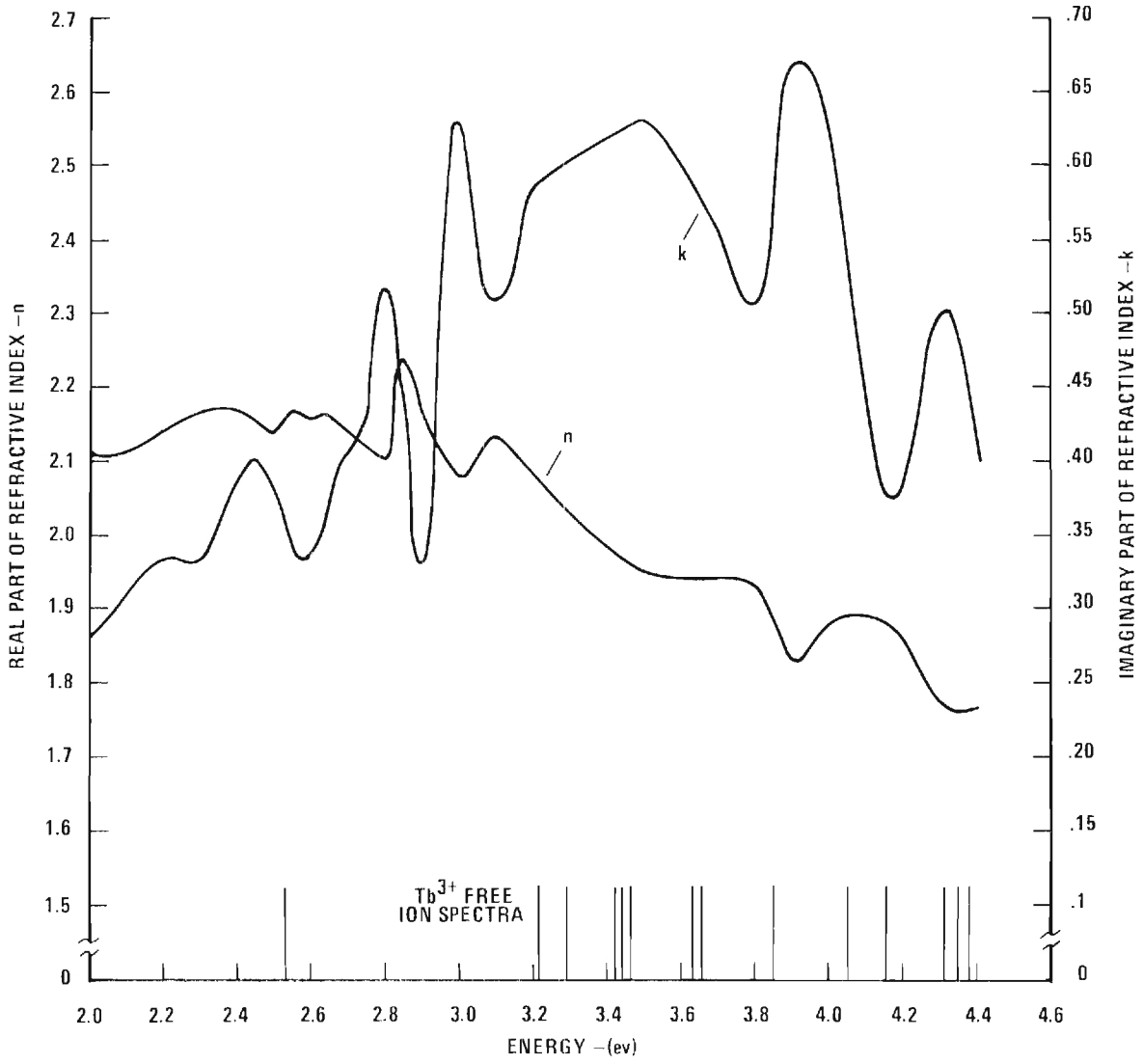

Fig. No. 2.8 Calculated Components of Refractive Index N=n-jk of TbIG

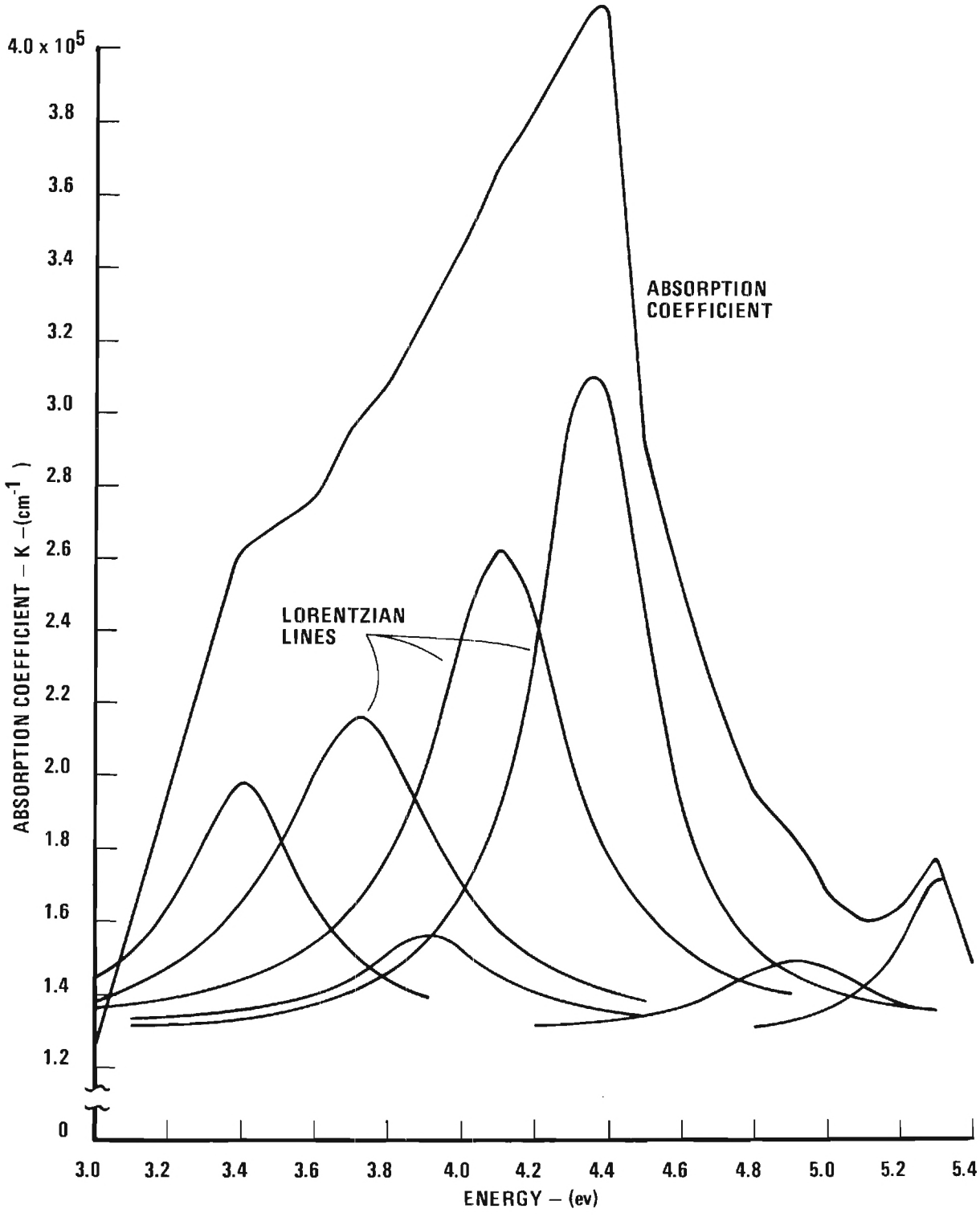

Fig. No. 2.9 Absorption Spectrum for GdIG Single Crystal

agreement is therefore considered to be satisfactory. By assuming a constant absorption of 1.3×10^5 cm^{-1} over the energy range between 3 ev and 5 ev the GdIG fine structure has been approximated with a series of Lorentzian shaped lines. The individual lines are also shown in Figure II-9. Error between the series approximation and actual absorption curve is less than 3% except at the lower energy end.

In general, the half-widths of the individual lines appear to be around 0.4 ev or 0.5 ev. Peak values of K are between 0.2×10^5 cm^{-1} and 3×10^5 cm^{-1}. Table II-2 gives the coefficient for the Lorentzian series according to equation (2.1), and corresponding oscillator strengths by equation (2.2).

Table II-2. Lorentz Series Coefficients for GdIG Absorption

Line Energy (ev)	3.40	3.72	3.90	4.10	4.35	4.90	5.30
$K_i \times 10^3 (cm^{-1} ev^2)$	2.70	6.00	1.50	7.00	5.40	1.00	0.60
Γ_i (ev)	0.40	0.53	0.48	0.46	0.34	0.46	0.24
$f_i \times 10^2$	4.10	6.60	1.60	8.30	8.00	1.20	1.40

Figure II-10 shows similar type data as Figure II-9 except for TbIG. The lines of the Lorentzian series used to fit the absorption coefficient curve are also shown. The large wide line used at 3.5 ev may result from the combined effect of the collection of Tb^{3+} lines in that vicinity, broadened by exchange coupling. Table II-3 lists the appropriate coefficients for the lines of the TbIG fine structure. The TbIG spectra contains lines which appear stronger and narrower than in GdIG. The total absorption coefficient above 3 ev is nearly the same as GdIG; however we have

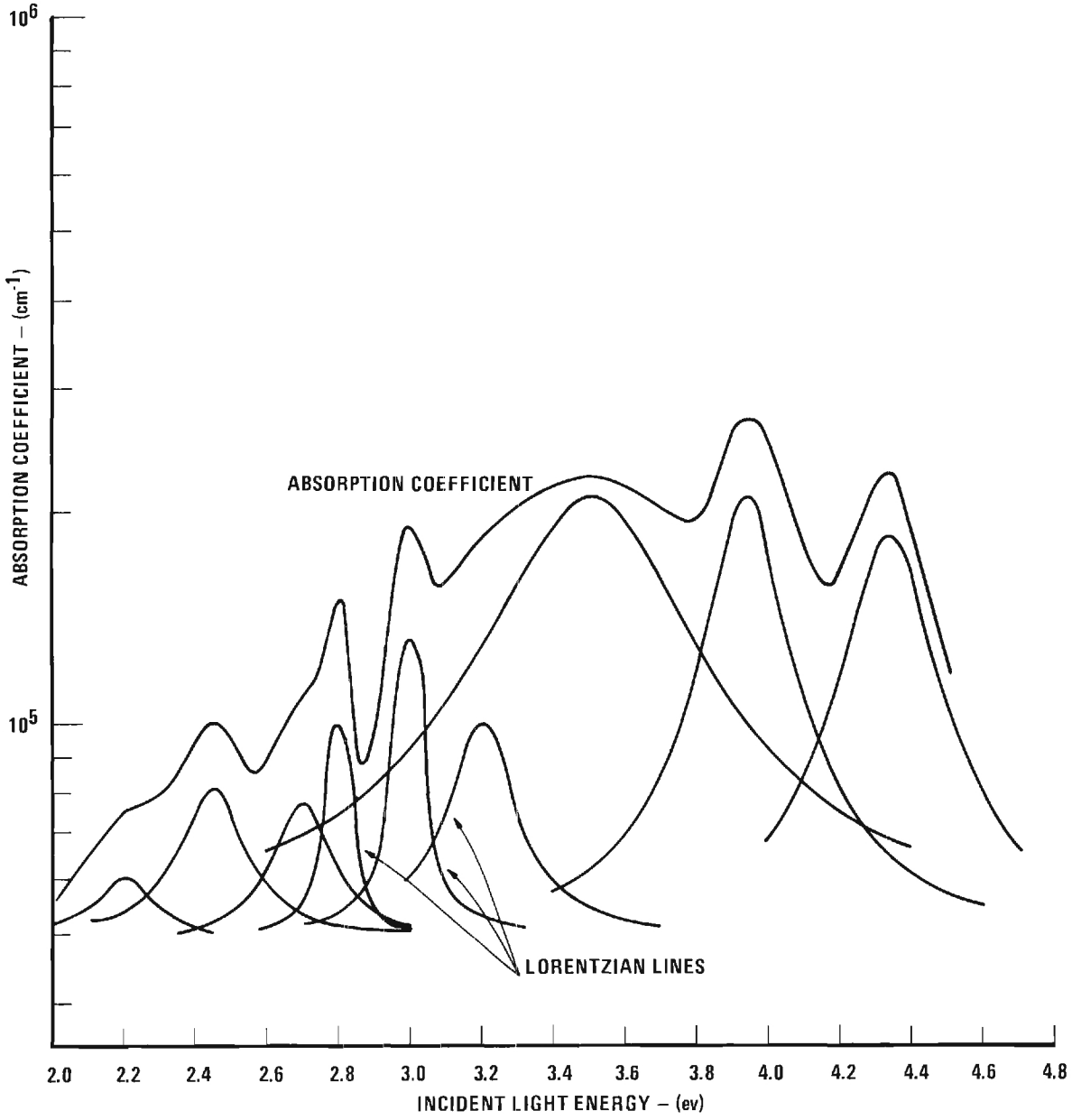

Fig. No. 2.10 Absorption Spectrum for TbIG Single Crystal

chosen a constant base line for the structure somewhat lower than in the GdIG calculations. A base absorption which increases from 0.5×10^5 cm^{-1} at 2 ev to about 1.0×10^5 cm^{-1} at 3 ev and remains constant at that value to higher energies leads to oscillator strengths of the TbIG lines which fall into the same range as the GdIG spectra.

Table II-3. Lorentz Series Coefficients for TbIG Absorption

Line Energy (ev)	2.20	2.45	2.73	2.80	3.02	3.25	3.54	3.95	4.34
$K_i \times 10^3 (cm^{-1} ev^2)$	1.00	3.00	2.20	0.60	1.30	5.00	144	25	25
Γ_i (ev)	0.20	0.20	0.18	0.07	0.08	0.20	0.60	0.25	0.27

An oscillator strength of $f \approx 10^{-2}$ for the TbIG line at 2.45 ev appears large for a terbium ion spin forbidden intraband transition. However, the high spin orbit coupling in rare earth ions relaxes this selection rule considerably. It has also been shown that significantly enhanced transition probabilities result from exchange coupling, and Grant[6] has discussed the enhancement associated with coupling of spin forbidden levels to charge transfer levels through spin-orbit and vibronic coupling. Thus an oscillator strength of this magnitude may not be too unrealistic for a Tb^{3+} transition in TbIG.

The spontaneous lifetime of the excited state for the 2.45 ev terbium line computed from the oscillator strength is $\tau \approx 10^{-6}$ seconds. This is consistent with $\tau \approx 5 \times 10^{-6}$ seconds obtained by extrapolating, to 100% Tb, the results of fluorescent decay measurements[10] in Tb substituted YAG. In the TbAG the concentration of Tb ions is comparable to that in TbIG, but there is no magnetic exchange to reduce τ.

The line width, 0.2 ev, is large for a rare earth transition. In the garnets, however, the rare earth ions exist in a large effective magnetic field as a result of the superexchange coupling to the iron sublattices. The result is a splitting of their levels. A simple effective field theory computation shows the effective field to be $H_{eff} \approx 4 \times 10^5$ Oersteds. If J is a good quantum number then the $^7F_6$ terbium ground state will be split by $\Delta E = 2gJ\mu_B H_{eff} \approx 0.04$ ev, and the excited state, $^5D_4$ will be split $\Delta E \approx 0.03$ ev. Therefore exchange field splitting can account for a line width of approximately 0.07 ev, about 1/3 the value computed from reflectivity data. However, the bandwidth of our monochrometer was about 0.1 ev in this range thus producing an apparent line width somewhat larger than actually exists.

Considering all these factors we feel there is indeed enough evidence to propose the line at 2.45 ev is a terbium ion absorption. This in turn when applied to the equations for the estimated pumping power for memory operation (Equation I-13) gives the previously mentioned estimate of 3.14 milliwatts. We believe these results offer a strong basis for carrying out the complete pumping experiment.

F. Evaluation of Experimental Uncertainties

In order for the previous results to be meaningful it is necessary to be assured that the errors in the data and reduction technique are negligible. To this end we have evaluated in some detail the potential sources of error and estimated their cumulative effect on the observed absorption spectra.

The garnets have cubic symmetry, and cubic crystals are usually regarded as optically isotropic. But this cannot be true for these ferro-

magnetic garnets as they exhibit a detectable Faraday effect. The direction of their magnetization in any domain is a preferred direction. Faraday effect depends upon the magnetic component of the radiation and typically the splitting of the index of refraction for two polarizations is less than our uncertainties in measuring n, the index arising from other sources. The absorption of radiation which we observed was very strong, suggesting a first order (electric dipole type) interaction between the electric vector of the radiation and the electronic structure of the crystal. Such absorption would not be strongly dependent on the orientation of the spins, the magnetization. These several things suggest that we did, indeed, measure index and absorptivity; measurements at known crystal orientations and magnetizations would be required to completely settle the matters, and these measurements we have not made.

The basic measurements, the reflectivities,were subject to especial uncertainties when the reflectivity was low, and it was low (typically 0.01) for all measurements at 70 degree angle of incidence. Imperfections on the crystal surface would scatter the incident radiation and the fraction of this entering the photomultiplier would add to that truly reflected from the extended crystal surface. The scattered light became a smaller fraction of the reflected light at shorter wavelengths where the reflectivity at 70° was higher.

For incidence angle of 20 degrees this scattered radiation added negligibly to the measured reflection.

This scattered radiation should not change rapidly with the direction of observation, and can be estimated from the radiation to the photomultiplier away from specular reflections. This correction was not systematically estimated for every observation as it could have been in principle

but available data indicates this raised the observed reflectivity at 70° by only about 5 parts per hundred for green mercury light on a typical crystal.

The measured reflectivity depended on the quotient of two measured intensities, both measured with the same photomultiplier tube, and associated circuits. The photomultiplier whose axis was horizontal, had to be rotated about a vertical axis to successively measure the direct beam intensity, the reflected beam intensity for 70° incidence and the reflected beam intensity for 20° incidence. The gain of the photomultiplier is sensitive to the direction of the earth's magnetic field through the tube. For the rotation about a vertical axis just described it was found that the gain could vary up to 0.04 of its magnitude. However, this change varied for different orientations of the tube about a horizontal axis, the axis of its cylindrical external envelope; a position was found for which the variation in gain for the several positions at which measurements were made was approximately 0.005, small enough that this systematic error was neglected in comparison to the uncertainties due to fluctuations in the light source and the scattering off surfaces afore mentioned.

The high pressure mercury arc fluctuated in intensity over time intervals of the order of a second. Fluctuations sometimes amounted to 0.1 of the average reading. This was true at all wavelengths through the monochrometer. Direct and reflected beam intensities were measured (relatively) by observing the photomultiplier current with an electrometer (Kiethley 600 A) over several seconds and the average needle position was estimated by the observer. Typically, several readings at the three angles would be made; a particular observation would be repeated only after observation of the other two angles had been measured. This would bring in any

drift of period longer than the fluctuations. Usually there was no drift and a typical fractional variance of several observations had the square root of about 0.01.

The electrometer specifications indicate that the measured current should be within 0.03 of the indicated current. Consistency of readings when the scale was switched suggest that the relative consistency may be better than this, possibly as good as 0.01.

The dark current of the photomultiplier was subtracted from each reading. Usually this correction was a small fraction of the reading itself and should not have contributed to the uncertainty of the reading of relative intensity. At short wavelengths (4 electron volts and more) and for 70 degree reflection the dark current was an appreciable fraction (up to about one third) of the total current. In these cases fluctuations in the dark current and the consequent uncertainty in selecting an average value would have increased the uncertainty of the relative intensity measurement by a small amount.

The "dark current" was observed in such a way that it included current due to light entering the tube by routes other than the optical train. This portion of the dark current was usually negligible except for the direct beam. The measurements were made in a darkened room which reduced light of random direction that entered the apparatus to light from the partially shielded mercury lamp, itself,which might be scattered around the room. Stray light was often of negligible magnitude but it amounted to an increase in the observed "dark current" for the direct beam and the 70° reflection of up to one third on some observations.

These several uncertainties in reflectivity measurements will be summarized before going on to their effect on the computed crystal absorptivity.

Summary of Uncertainties in Reflectivity at a Given Angle

	Source of Uncertainty	Estimated Fractional Magnitude
Systematic	Photomultiplier Orientation	± .005
	Relative Calibration of Electrometer	± .01
	Scattering Off Crystal Imperfections	0 - .05
	Angular Spread of Illuminating Beam	Not Made
Random	Fluctuations of Light Intensity, Direct Beam	± .01
	Fluctuations of Light Intensity, Reflected Beam	± .01*
Resulting uncertainty in intensity of direct beam		± .015
Resulting uncertainty in intensity of reflected beam (not including scattering)		± .015
Resulting uncertainty in reflectivity (not including scattering and effect of angular spread)		± .022
Resulting uncertainty in absorptivity		± .0043
Resulting uncertainty in absorptivity due to scattering		0 - .01
Resulting uncertainty in absorptivity due to beam spread		< .05 (from ( ) Hunter's plots)
Resulting uncertainty in absorptivity due to imperfect polarization		negligible

* Slightly higher when dark current a sizeable fraction of current due to radiation.

The effects of these uncertainties on the absorptivity computed through the Fresnel equations has been estimated from the examination of the equations presented by Hunter[5] and from our own check. The complex index of refraction of our crystals falls in a region where the absorptivity is not extremely sensitive to uncertainities in the observed reflectivities. The region is that around n = 2 (real part of index), k = .25-1.0 (imaginary part of index). Figure 8 of Hunter's paper indicates that the foregoing statement is correct. Our own computer programs gave for the ratios of change in k to the change in reflectivity as

$$\frac{\Delta K}{\Delta R_{20^o}} \sim .07$$

$$\frac{\Delta K}{\Delta R_{70^o}} \sim .18$$

This would indicate that our absorptivities should be correct within one part in a hundred, certainly better than we can believe.

The wavelength at the center of our slit was correct to 10 or 20Å, as close as we could read the scale of the monochrometer. This was indicated by a calibration with a low pressure mercury source.

Our aperture was chosen to keep the beam divergence within one degree each side of the specified direction and one degree each side of the plane of incidence. We have not analyzed the effect of this but Hunter's computations (his Figure 7) indicate the effect is small.

The indensity of our beam was controlled by a pair of Glan -Thompson prisms which were set to deliver plane polarization approximately at 45^o to the slit of the monochrometer. The monochrometer treated the two components

differently but not very strongly so. The beam delivered by the monochrometer at any wavelength was somehow elliptically polarized, but the vertical and horizontal component were of approximately equal amplitude.

Another Glan -Thompson prism selected the horizontal component (the one in the plane of incidence at the crystal). This prism was adjusted to give minimum reflected signal at 70°. This adjustment was very sensitive and it is felt that the setting was certainly within 1/2 degree of the true minimum. One half degree would give about 0.01 for the amplitude of the wrong polarization. This amount of improper polarization would produce no effect on the reflectivity at 70° or any other angle. That two prisms were crossed are capable of reducing the intensity of a beam by 10^{-4}, has been checked, so we may conclude that the uncertainty from improper polarization is negligible.

As a result of the above considerations we feel confident that the experimental errors are insignificant with respect to the accuracy required of the final results.

G. Thermal Considerations of an Optically Pumped Memory

In this section we analyze the thermal effects caused by the pumping radiation. This is an important consideration in the use of garnets since compensation depends on temperature. As discussed in the interim report, however, application of true antiferromagnetic materials, e.g., MnCoO, would not be magnetically affected by temperature change.

Any memory must dissipate the losses associated with reading it or writing into it. The heat balance is particularly important for the garnet memory here under consideration as the local temperature of the storage elements must not deviate appreciably from the compensation temperature.

Intense radiation is to be used to bring about the transition to render a memory element sensitive to an applied magnetic field,that is to "write" into it. After writing and the magnetic field is turned off it is necessary that the temperature not be high enough to uncompensate the garnet bit.

There are several specific questions. First, there is the question of the thermal history of a garnet bit that is at thermal equilibrium with its substrate subsequent to its being addressed by the write beam with just one pulse. More drastic is the situation for a particular bit that is addressed again and again because of some program requirement. The temperature pattern of the garnet for various cycle times is needed. A third question is the temperature response, to both address and cycling, of a bit adjacent to the one addressed.

Any temperature rise of the addressed bit may be tolerable if it cools off fast enough.

The model we have used for these considerations is a layer of gar-

net some 2 microns thick in intimate thermal contact with a substrate of glass or possibly other transparent material. A transparent substrate is envisioned to allow the memory to be read from the opposite side.

Bits on this garnet film are to be located optically; no mechanical groove or other boundary is to separate the bits. One bit is envisioned as a disc 10 microns in diameter and the thickness of the garnet film. The separation of bits is to be two bit diameters or 20 microns, center-to-center.

For uniform illumination of the surface the dissipation will be uniform across the face of the disc and will fall exponentially with distance into the material. The pulses will be short, on the order of a microsecond. In order to have a tractable problem it was necessary to find some temperature distribution at the end of a pulse that would resemble the expected distribution and at the same time lend itself to computation. The choice was a radial gaussian pattern of temperature in the plane of the garnet film about the center of a bit and a half-gaussian distribution extending from the surface on the side of the write beam through the garnet and into the substrate.

$$T = N\eta_1^2\eta_3 \; e^{-r^2\eta_1^2} e^{-z^2\eta_3^2} \tag{2.1}$$

$$\eta_1^2 = \frac{1}{4\alpha(t + \tau_1)} \tag{2.2}$$

$$\eta_3^2 = \frac{1}{4\alpha(t + \tau_2)} \tag{2.3}$$

where r = radius from center of bit,

z = distance into garnet and substrate,

α = diffusivity of substrate and film.

The expression for T satisfies the Fourier equation for heat conduction; τ_1 and τ_2 are chosen to give the desired initial temperature distribution at the end of a write pulse. The multiplier N adjusts the magnitude of the temperature pattern. α for glass and for garnet are not dissimilar quantities and are taken to be the same. In numerical computations, the value chosen was $\alpha = 0.002$ cm^2/sec.

The initial distribution can be chosen so that it is certainly everywhere higher than the temperature expected from absorption of a pulse, or perhaps more close to reality, it can be chosen to represent the same absorption of energy as the expected distribution. The first will certainly give temperature changes that are too large, at all places and times; the latter will give temperature pattern that corresponds to the energy absorbed and has qualitative features that correspond to conduction out of the bit volume during the interval that the write beam is applied.

The back of the substrate is to be kept at constant temperature. No conduction is contemplated off the surface of the garnet toward the write beam. A negative image of the above initial distribution behind the substrate will satisfy the condition that the temperature of the back of the substrate will not change. However, for values of z that correspond to expected substrate thicknesses, one millimeter or more, the temperature change resulting from a pulse or a string of pulses is small enough on the assumption of an infinitely thick substrate that the image has not been used. It could be introduced, however, if thinner substrates or different thermal properties warranted it. In the vicinity of the garnet the contribution of

the image is negligible for the situation contemplated.

For the bit configuration under consideration, the values of τ_1 and τ_3 were chosen to make $\eta_1 r_1$ and $\eta_3 z_1$ equal to one at t = o, the time corresponding to the end of the pulse. τ_1 = 12.5 μsec; τ_3 = 2 μsec are the resulting values.

A single pulse leaves the temperature of the bit and its surrounding volume elevated. The temperature at the origin immediately begins to fall. Away from the origin the temperature typically rises and then falls. Figure II-11shows the behavior at the origin and at the surface of the garnet toward the substrate, r = o, z = 2 microns. T_o is the maximum temperature increase for single pulse, the increase that is to be found at r = 0, z = 0.

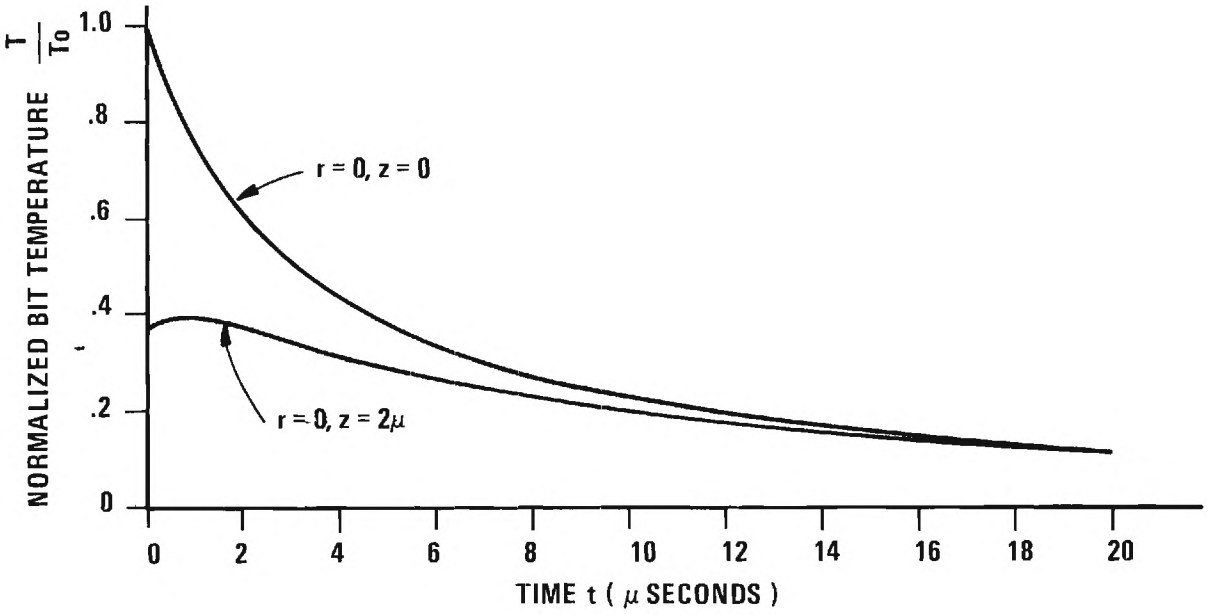

Figure II-11 Time Dependence of Temperature at Excited Bit for 1μsec duration pulse

The temperature rise at the edge of the next bit, that is z = 0, r = 15 microns, is shown on a different scale in Figure 12 . A single pulse will not produce sufficient temperature rise to upset an adjacent bit.

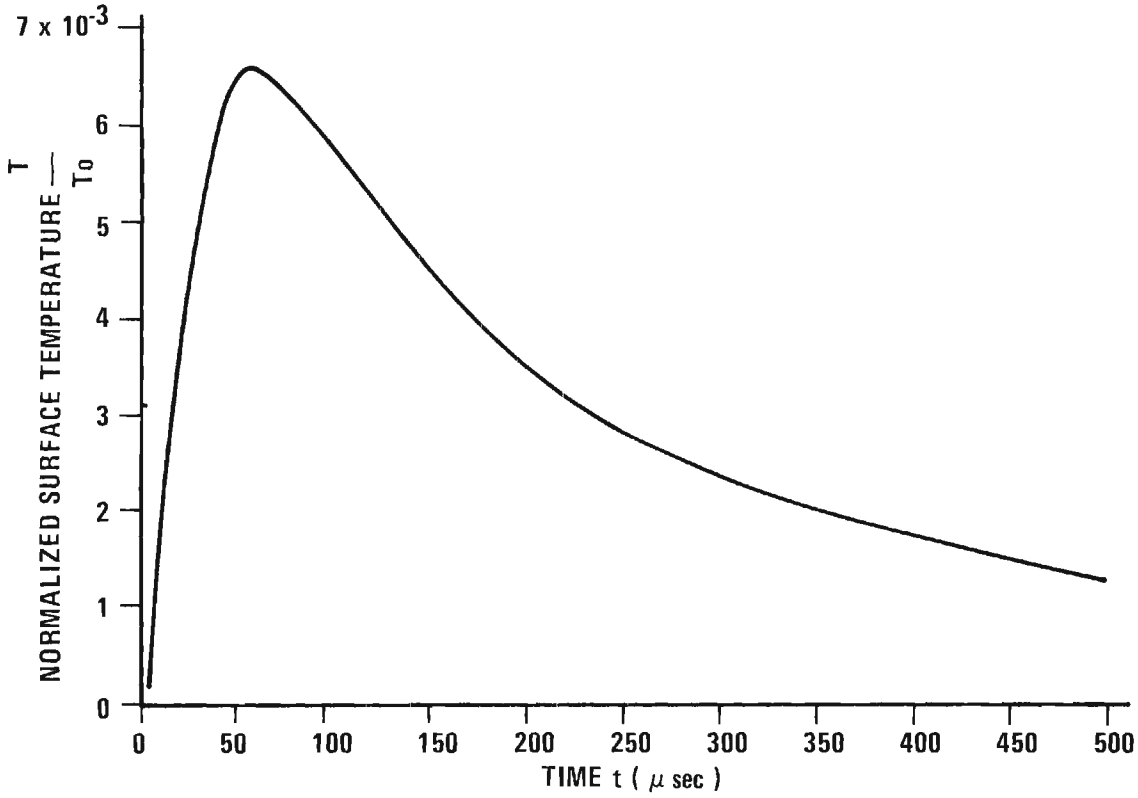

Fig. No. 2.12 Surface Temperature vs Time for a Point 15 Micron From Center of Excited Bit. Note Scale Factor of 10^{-3}

For cyclic address at some specified cycle period, Δt, the maximum temperature at any point can be computed by taking the maximum temperature at that point due to a single pulse and adding to it the temperatures corresponding to intervals of Δt forward to infinite time (corresponding to pulses whose maximum has already past), and backward to zero time. The resulting maximum temperature at the origin and at the edge of an adjacent bit are sketched in Figure II-13 for various cycle times. The expressions for this maximum temperature rise are,

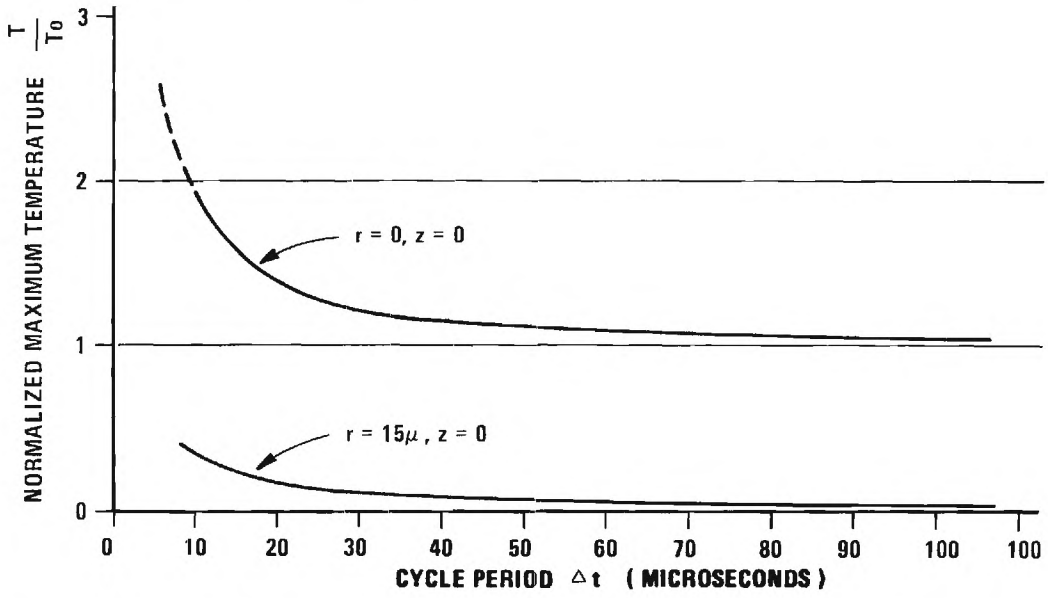

Fig. II.13. Maximum Surface Temperature Excursion as a Function of Cycle Time at the Excited Bit and an Adjacent Bit. T_o is Maximum Surface Temperature at r = 0 for Single Pulse.

$$T_{max} = \sum_{k=0}^{\infty} T(t_{max} + k\Delta t) + \sum_{\ell=1}^{(\ell+1)< \frac{t_{max}}{\Delta t}} T(t_{max} - \ell\Delta t) \qquad (2.4)$$

where t_{max} is the time for maximum temperature due to a single pulse. The first series converges very slowly for small values of Δt. It was evaluated by carrying the series forward on a computer until a limit seemed imminent, at $t = t_2$, say; then an upper and lower bound on the remaining

contribution was computed by

$$I_1 = \frac{1}{\Delta t} \int_{t_2}^{\infty} T(t) \exp \left\{ r_1^2 \eta_1^2(t) + z_1^2 \eta_2^2(t) \right\} dt$$

$$\cong I_2 \exp \left\{ r_1^2 \eta_1^2(t_2) + z_1^2 \eta_2^2(t_2) \right\}$$

$$I_2 = \frac{1}{\Delta t} \int_{t_2}^{\infty} T(t) \exp \left\{ r_1^2 \left[\eta_1^2(t) - \eta_1^2(t_2) \right] + z_1^2 \left[\eta_3^2(t) - \eta_3^2(t_2) \right\} dt$$

$$\cong 2t_2 T(t_2)/\Delta t$$

respectively.

Away from the cyclically addressed bit itself the temperature can be estimated closely by the concept of the average power to the bit (energy per pulse divided by Δt) spreading hemispherically from the origin. Even at the edge of the adjoining bit, just 15 microns from the origin, the temperature computed this way is correct to within the temperature rise that occurs from a single pulse at that point.

For spherical spreading and z = 0.1 cm, r = 0, typical figures for the bottom of the substrate, the computed temperature rise for a 10 μsec pulse period is only 0.0044 T_o (see below) so the neglect of the influence of the image is justified.

For the model here used the relation between the temperature rise at the origin during a pulse and the pulse energy, ε, is

$$T_o = \frac{2\epsilon}{c\rho r_1^2 z_1 \pi^{3/2}}$$

which follows from

$$\epsilon = c\rho \int_0^\infty \int_0^\infty T(r, z, t = 0) 2\pi r dr dz$$

where c = specific heat of garnet and glass,

ρ = density of garnet and glass.

The average power associated with cyclic pulses that each produce temperature rise T_o at the origin is

$$P = \frac{\epsilon}{(\Delta t)} = \frac{c\rho r_1^2 z_1 \pi^{3/2}}{2(\Delta t)} T_o . \qquad (2.8)$$

For hemispherical spreading of this power the temperature (average) at a position

$$R = \sqrt{r^2 + z^2}$$

away from the origin is

$$T(R) = \frac{P}{2\pi k R}$$

$$= \frac{c\rho}{4k} \frac{r_1^2 z_1 \pi^{\frac{1}{2}} T_o}{(\Delta t) R}$$

$$= \frac{r_1^2 z_1 \pi^{\frac{1}{2}}}{4\alpha (\Delta t)} \frac{T_o}{R} \cdot \qquad (2.9)$$

This leads to

$$\frac{T(15\mu)}{T_o} = 0.296 \qquad (2.10)$$

for Δt = 10 μsec, and for glass (α = 0.005 cm^2/sec) with the bit dimensions previously recited. This is substantially the same as given by the series, equation 2.4 and shown in Figure II-13.

Likewise, at the bottom of a substrate one mm thick

$$\frac{T(1\ mm)}{T_o} = 0.0044 \cdot$$

There is the further question of cooling the back side of the substrate. To satisfy the spherical spreading envisioned the heat flux per unit area at the back surface of the substrate of thickness d must be

$$- k \left(\frac{dT}{dz}\right)_{z=d} = - k \left(\frac{dT}{dR}\right) \frac{d}{R} = \frac{c\rho r_1^2 z_1 \pi^{\frac{1}{2}}}{4(\Delta t)} T_o \frac{d}{R^3} \qquad (2.11)$$

$\frac{d}{R}$ is the cosine of the angle the radius vector to the point on the back surface of the substrate makes with the z axis. This has its maximum value at R = d, right on the axis.

The heat transfer to the cooling fluid in contact with the back surface can be represented by hT per unit area where h is the convection or heat transfer coefficient to the cooling fluid. To maintain the spherical spreading

$$hT = - k \left(\frac{dT}{dz}\right)_{z=d}$$

$$h = \frac{- k \left(\frac{dT}{dz}\right)_{z=d}}{T(R)_{z=d}} = \frac{kd}{R^2} \quad .$$

On the axis, where the largest value of h is required, this gives

$$h = \frac{k}{d} \quad .$$

For glass, $k = 0.002 \frac{\text{cal}}{\text{sec cm degK}}$, this requires, for a one mm thick substrate

$$h = \frac{0.002}{0.1} = 0.02 \frac{\text{cal}}{\text{sec cm}^2 \text{ degK}}$$

a value that can be achieved by water or forced air.

If it is possible to pulse a bit volume of the garnet with radiation that will allow it to be switched by an external field without raising

its temperature too much, then it should be possible to cool the whole memory plane; adjacent bits need not be adversely affected so long as a particular bit is not regularly switched more often than every 10μ sec. This is for the configuration envisioned with 250,000 bits/cm^2.

The configuration here studied is not the best for keeping the temperature rise to a minimum, although it is representative of the class of configurations for which the heat transfer is through a solid substrate. Lower, but not markedly lower temperature rises would occur if the "write" pulse entered from the substrate side; an analytical estimate for this case would be more difficult. If a cooling fluid could be located at the surface of the garnet then lower temperature rises would result, but not by an order of magnitude unless the garnet layer could be made thinner.

III. CALCULATIONS OF ENERGY LEVEL STRUCTURE OF GARNET MATERIALS

A. Introduction

We have experimentally observed absorption structure which can tentatively be attributed to the rare earth ion transitions. However, much uncertainty remains because there is presently no detailed knowledge from a theoretical basis to adequately describe the numerous other transitions taking place. This is true not only in the garnets studied here, but in most magnetic materials and represents a significant gap in the information needed to truly characterize the interaction of light with the magnetic lattice.

In order to provide a sound basis on which our experimental work could be built, an effort was extended towards evaluating what techniques appeared feasible in providing a reasonably accurate theoretical evaluation of the atomic nature of the absorptions occurring in the energy range of interest. As a result of this study we have established the basic ground work to complete such calculations but because of funding limitations it has not been possible to carry out the actual calculations.

There are essentially three types of calculations which might be performed to analyze the energy level structure of the materials under study. These are complete band structure calculations, crystal field calculations, and molecular orbital calculations.

B. Band Structure Calculations

There are a variety of approaches which could be taken under this general heading. In each case, however, a meaningful solution is only possible for a relatively simple crystal structure. In the rare earth iron

garnets the crystal structure is extremely complicated. It is possible to identify iron atoms in two different symmetry sites, octahedral and tetrahedral, and the rare earth atom in a dodecahedral site. There are 64 of these basic symmetry groupings in a unit cell of the garnet crystal.[1] A review of the various possible band structure methods indicates that a solution of this type would be hopelessly impractical. In addition for the application being considered, i.e., the interaction of light with the solid, only a knowledge of the energy levels around k = 0 is required and a complete picture of the E vs. k characteristics is not needed.

C. Crystal Field Calculations

Crystal field calculations are the simplest of energy structure computations to carry out, but they also provide the least amount of information. In this approach the ion is viewed as if it were in space as a free ion except that it is in an electrostatic field resulting from the surrounding charged ions on adjacent lattice sites. This electric field is assumed to be small with respect to the internal ionic forces and thus may be considered as a perturbation potential on the free ion. The result is that the free ion energy levels are split and a redistribution of electrons take place at the new energy levels of the perturbed ion.

It is generally found that rigorous calculation of the perturbing field due to adjacent atoms is not possible. A major reason for this is the distributed nature of the charge at the atomic sites. If however the perturbing atoms could be considered as point charges the potential could be calculated with any desired degree of accuracy. For example if the ion in question is surrounded by six perturbing ions located at the corners of a cube then the potential in the vicinity of the first ion would be given by:

$$V = \frac{2e_i}{R}\left[3 + \frac{35}{iR^4}\left(x^4 + y^4 + z^4 - \frac{3}{5}r^4 + \right) \ldots\right]$$

where R = distance from ion to the perturbing point charges,

e_i = magnitude of charge at perturbing sites,

x, y, z, r = coordinates of electron.

While the exact potential cannot be accurately calculated, its symmetry is that of the point charge distribution and in actual calculations the spatial expression in curved brackets is employed with an adjustable coefficient D to control the magnitude. To find the wave functions of the perturbed system it is first assumed they can be expressed as a linear combination of the original unperturbed wave functions. This is valid since a characteristic of a complete orthogonal set of functions is that they may be used in linear combinations to form any other well-behaved function in the same space. Using a truncated approximation, for example four terms, it is then possible to write the perturbed wave functions as:

$$\begin{bmatrix} \Psi_1 \\ \Psi_2 \\ \Psi_3 \\ \Psi_4 \end{bmatrix} = \begin{bmatrix} K_{A1} & K_{B1} & K_{C1} & K_{D1} \\ K_{A2} & K_{B2} & K_{C2} & K_{D2} \\ K_{A3} & K_{B3} & K_{C3} & K_{D3} \\ K_{A4} & K_{B4} & K_{C4} & K_{D4} \end{bmatrix} \begin{bmatrix} \Psi_A \\ \Psi_B \\ \Psi_C \\ \Psi_D \end{bmatrix}$$

where Ψ_1, Ψ_2 --- are the perturbed wave functions

Ψ_A, Ψ_{B1} --- are the original unperturbed functions

and the K's are coefficients which must be determined. These latter are found by the variational method. Applying the variational principle to

these assumed solutions it can be shown that the optimum values of the K's i.e., the ones which lead to an energy minimum are given by the following system of equations:

$$\begin{bmatrix} 0 \\ 0 \\ 0 \\ 0 \end{bmatrix} = \begin{bmatrix} (H_{AA}-E) & H_{AB} & H_{AC} & H_{AD} \\ H_{BA} & (H_{BB}-E) & H_{BC} & H_{BD} \\ H_{CA} & H_{CB} & (H_{CC}-E) & H_{CD} \\ H_{DA} & H_{DB} & H_{DC} & (H_{DD}-E) \end{bmatrix} \begin{bmatrix} K_{A1} \\ K_{B1} \\ K_{C1} \\ K_{D1} \end{bmatrix} \tag{3.1}$$

where the H's represent "matrix elements" given as:

$$H_{AA} = \int_{\text{all volume}} \Psi_A^* (V_{\text{crystal field}}) \Psi_A d\tau$$

$$H_{BA} = \int_{\text{all volume}} \Psi_B^* (V_{\text{crystal field}}) \Psi_A d\tau \text{ etc.}$$

In the above, $d\tau$ is the infinitesimal volume element.

Since the unperturbed wave functions are known the matrix elements can in principle be evaluated, resulting in a number. This is assuming we could actually express the crystal potential completely. For (3.1) to hold for non-zero values of the K's it is necessary that the determinant of the H matrix must be zero. This leads then to the so-called "secular equation":

$$\begin{vmatrix} (H_{AA}-E) & H_{AB} & H_{AC} & H_{AD} \\ H_{BA} & (H_{BB}-E) & H_{BC} & H_{BD} \\ H_{CA} & H_{CB} & (H_{CC}-E) & H_{CD} \\ H_{DA} & H_{DB} & H_{DC} & (H_{DD}-E) \end{vmatrix} = 0$$

Solving this resulting set of equations, assuming the matrix elements are previously determined, results in four values of E. Each value of E, substituted back into (3.1) permits the determination of a set of K coefficients. In this example there are 4 values of E and four sets of coefficients. It is seen that each E gives a different set of K's when substituted back into (3.1). Each set of K's then defines a different wave function of the perturbed ion.

The above sketch covers the basic philosophy of the crystal field theory approach. It provides very useful results when applied to electrons in an inner unfilled shell provided the crystal field potential can be accurately described. Because of the problems previously discussed this is not possible from first principles and the potential must be described in terms of adjustable crystal field parameters which can be manipulated to attempt a fit between experimental data and the calculations. While such parameters have been calculated for many specific materials each new system must be experimentally determined.

The major disadvantage however is that crystal field theory cannot account for electron transitions between anions and cations. This is because the new wave functions calculated contain terms of only one atom. Thus by its very formulation it can only be used to determine transitions within the shells of the ion considered. This limitation can be removed

if the concept is extended to a molecular orbital calculation where the perturbed wave functions are combinations of orbitals from both the cation and anion.

Molecular Orbital Calculations

It is assumed in this model that the solid can be considered as an ordered arrangement of molecular ions. This concept fits the garnets quite well since the crystal is composed of a, c, and d molecular sites. As previously discussed the a site is an octahedrally coordinated Fe ion surrounded by six oxygen anions, the c site is a dodecahedral configuration consisting of the rare earth ion surrounded by eight oxygen ions and the dd site is a tetrahedrally coordinated iron ion.

In a molecular orbital model it is postulated that the wave functions of the molecular group can be described by a combination of atomic orbitals from the constituent ions. It is easy to show that wave functions of this type will indeed provide for a transition between ions. For example consider two molecular orbitals written as

$$\Psi_{M1} = a\Psi_d + b\Psi_L$$

$$\Psi_{M2} = c\Psi_{d'} + d\Psi_{L'}$$

where Ψ_{M1}, Ψ_{M2} = molecular orbitals,

Ψ_d, $\Psi_{d'}$ = atomic orbitals of central metal ion,

Ψ_L, $\Psi_{L'}$ = ligand ion atomic orbitals.

Here the molecular orbitals are made up of a linear combination of atomic orbitals from anion and cation as proposed. The interaction matrix element between these two molecular orbitals is simply

$$M = \int_{\substack{\text{all}\\ \text{space}}} \Psi_{M1}^{*} H \Psi_{M2} d\tau$$

where H is the perturbation Hamiltonian operator inducing the transition. This becomes

$$M = \int (c\Psi_d{}',^{*} + d\Psi_L{}',^{*}) H(a\Psi_d + b\Psi_L) d\tau$$

$$= ca \int (\Psi_d{}',^{*} H \Psi_d) d\tau + db \int (\Psi_L{}',^{*} H \Psi_L) d\tau$$

$$+ cb \int (\Psi_d{}',^{*} H \Psi_L) d\tau + da \int (\Psi_L{}',^{*} H \Psi_d) d\tau \ .$$

Here it is apparent that inter-ion transitions are inherent in a molecular orbital excitation as shown by the last two terms. These terms are transition matrix elements between anion and cation orbitals. The significance of this is the potential capability it provides for explaining the rare earth iron garnet absorption spectra and how this spectra is related to the atomic states of the constituent ions. To date there has been no direct theoretical work which permits the calculation of these so-called "charge transfer" absorption lines in these materials. The following sections detail the theory and mechanics of the molecular orbital approach.

D. General Theory

If we include only the Coulomb interaction, the non-relativistic Hamiltonian for a molecule takes the form

$$H = \sum_i H_i + e^2 \sum_{\substack{i \\ (i<j)}} \sum_j \frac{1}{r_{ij}} \tag{3.2}$$

where H_i is the Hamiltonian for the ith electron moving in the Coulomb field of the nuclei, $r_{ij} = |\vec{r}_i - \vec{r}_j|$, and $\vec{r}_i$ is the position vector of the ith electron relative to some chosen origin of coordinates. This form for the Hamiltonian assumes the Born-Oppenheimer approximation in which the nuclei form a rigid non-rotating framework.

The presence of the electron repulsion term in (3.2) greatly complicates the solution of Schrodinger's equation

$$H\Psi = E\Psi . \tag{3.3}$$

In fact, direct solution has been attempted only for the simplest cases, such as diatomic hydrogen, and even in these simple cases, approximations are necessary.

All practical methods of solution of (3.3) involve the concept of effective field. Each electron in the system is pictured as moving in a Coulomb potential composed of the potential due to the nuclei plus an additional potential due to the average distribution of all the other electrons in the system. With this conceptual picture, it is meaningful to speak of individual electron states Φ, and the solution to equation (3.3) can be approximately written as a product of single electron functions, one factor for each electron in the system (strictly, one incorporates spin, and the solution Ψ is a linear combination of products where the combination is constructed to be antisymmetric in each electron pair). We will call these single electron functions Molecular Orbitals (MO's).

The classic method of solution of (3.3), using the idea of effective field, is the Hartree Forc Self-Consistent Field method (HFSCF). One assumes initial MO's; these are used to determine an average charge distribution which, in turn, determines a potential distribution via Poissons' equation. This potential is used in the one electron equation

$$H_{SCF}\Phi = \epsilon\Phi \tag{3.4}$$

to generate new MO's. The entire procedure is repeated until the "input" solutions agree with the "output" solutions to some prescribed degree of accuracy. In actual application, this method leads to a set of integro-differential equations which are solved numerically, giving solutions in tabular form.

An alternate procedure, developed by Roothaan in 1951, employs the concept of effective field, but does not use this field directly. Roothaan's procedure is to assume that there exists a "best" set of MO's for the system, and that these MO's can be written as a linear combination of atomic orbitals (LCAO), where the atomic orbitals are usually selected to be Slater-type orbitals (STO) of the general form $\chi = cr^{m-s}e^{-ar}$. STO's are discussed in various places in the literature. With this assumption the molecular orbital for the ith electron can be written

$$\Phi_i = \sum_j C_{ji}\chi_j \tag{3.5}$$

where it is assumed

$$\int \chi_p\chi_p dv = 1 . \tag{3.6}$$

We introduce matrices

$$\underline{C}_i = \begin{pmatrix} C_{1i} \\ \cdot \\ \cdot \\ \cdot \\ C_{mi} \end{pmatrix}$$

$$\chi = (\chi_1, \ldots, \chi_m)$$

$$C = \begin{pmatrix} C_{11} & \cdots & C_{1n} \\ \cdot & & \cdot \\ \cdot & & \cdot \\ \cdot & & \cdot \\ C_{m1} & \cdots & C_{mn} \end{pmatrix}$$

$$\Phi = (\Phi_1, \ldots, \Phi_n)$$

and then we can write: (note $m \geq n$ to get n L.I. MO's).

$$\Phi_i = \chi \underline{C}_i \tag{3.7}$$

$$\Phi = \chi C \cdot \tag{3.8}$$

If M is an operator, we define the matrix $\bar{M}$ by

$$\bar{M}_{ij} = \int \bar{\chi}_i \bar{M} \chi_j \cdot \tag{3.9}$$

We then have

$$\int \Phi_i M \Phi_j dv = \underline{C}_i^* \bar{M} \underline{C}_j \tag{3.10}$$

In reference 1 the operator

$$H = \sum_i H_i \tag{3.11}$$

$$J_i : J_i^{\mu} \Phi^{\mu} = e^2 \left(\int \frac{\Phi_i^{\nu} \Phi_i^{\nu} dv^{\nu}}{r_{\mu\nu}} \right) \Phi^{\mu} \tag{3.12}$$

$$K_i : K_i^{\mu} \Phi^{\mu} = e^2 \left(\int \frac{\Phi_i^{\nu} \Phi^{\nu} dv^{\nu}}{r_{\mu\nu}} \right) \Phi_i^{\mu} \tag{3.13}$$

are called, respectively, the Nuclear-Field Hamiltonian, the Coulomb operator, and the exchange operator. The index μ refers to the coordinates of the uth electron. The matrices of these operators in the AO basis are

$$\bar{H}_{pq} = \int \bar{\chi}_p H \chi_q dv \tag{3.14}$$

$$\bar{J}_{i,pq} = \int \bar{\chi}_p J_i \chi_q dv \tag{3.15}$$

$$\bar{K}_{i,pq} = \int \bar{\chi}_p K_i \chi_q dv . \tag{3.16}$$

The Hartree-Fock Hamiltonian operator is defined by

$$F = H + \sum_i (2J_i - K_i) \tag{3.17}$$

or

$$\bar{F} = \bar{H} + \sum_i (2\bar{J}_i - \bar{K}_i) \quad , \tag{3.18}$$

and the overlap matrix is defined by

$$\bar{S}_{pq} = \int \bar{\chi}_p \chi_q dv \quad . \tag{3.19}$$

In terms of these matrices, it is shown that the appropriate eigenvalue equation is

$$\bar{F}\underline{C}_i = \epsilon_i \bar{S}\underline{C}_i \quad . \tag{3.20}$$

The procedure used to solve (3.20) is as follows: an initial set of C_{pq} is assumed, and $\bar{F}$ is calculated, using (3.5), (3.11), (3.12), (3.13), (3.18). This $\bar{F}$ is used in (3.20) which becomes an ordinary eigenvalue problem with prescribed matrices. Of the resulting eigenvalues, the lowest n are assigned to the molecular ground state, and the remaining m-n are regarded as excited-state energies. The eigenvectors $\underline{C}_i$ which result are used to establish new MO's and the cycle is repeated until the input C_{pq} and the output C_{pq} agree. This method obviously gives analytic MO's. The quality of these MO's as compared to those obtained from the classic Hartree-Fock procedure depends on the number of AO's used to form each MO, and is not a completely settled question. In practice, the LCAO-MO's are compared with the HFSCF-MO's, when available, as to detailed overlap, behavior at the origin, and total energy minimization.

It has been found that, in the case of complex structures such as tetrahedral and octahedral metal complexes, even the SCF approximation in

either the classic or Roothaan form is beyond the capability of present computers. Such cases are currently treated by so-called semi-empirical methods.

E. LCAO Treatment of an Octahedral Complex

In this, and following sections, we will apply Roothaan's procedure to a particular system. This section is devoted to further discussion of the LCAO method, the role played by molecular symmetry, and the actual determination of the secular equation for an octahedral complex.

Using the conceptual picture of effective field, we have one-electron solutions to the equation

$$F\Phi = \epsilon\Phi \tag{3.21}$$

In general, if we have a complete set of states $\{\chi_i\}$, the solutions Φ can be expanded in terms of the χ_i to give:

$$F\left(\sum_j a_j\chi_j\right) = \epsilon\left(\sum_j a_j\chi_j\right)$$

or, if we multiply from the left by $\bar{\chi}_i$, and integrate over space:

$$\sum_j a_j \left\{ \int \bar{\chi}_i F\chi_j dv - \epsilon \int \bar{\chi}_i\chi_j dv \right\} = 0$$

or:

$$\sum_j a_j \left\{ \bar{F}_{ij} - \epsilon\bar{S}_{ij} \right\} = 0 \tag{3.22}$$

Equation (3.22) is an infinite-dimensional system of equations if a complete set $\{\chi_j\}$ is used. In practice, this is an untenable situation, and approximations are necessary. The customary approximation is to replace the complete set $\{\chi_j\}$ by a finite set of states which are chosen to be the inner-shell, valence shell, and low-lying excited SCF one-electron atomic states of all the atoms in the molecule. These AO's are usually obtained in analytic form by applying the Roothaan procedure to each atomic system. They may be obtained in the form of linear combinations of STO's containing from 2 to 10, and even more, terms in the literature.

We will describe the application of the semi-empirical method using the octahedral complex FeO_6 as a vehicle. The geometry of the system is as shown in figure III-1.

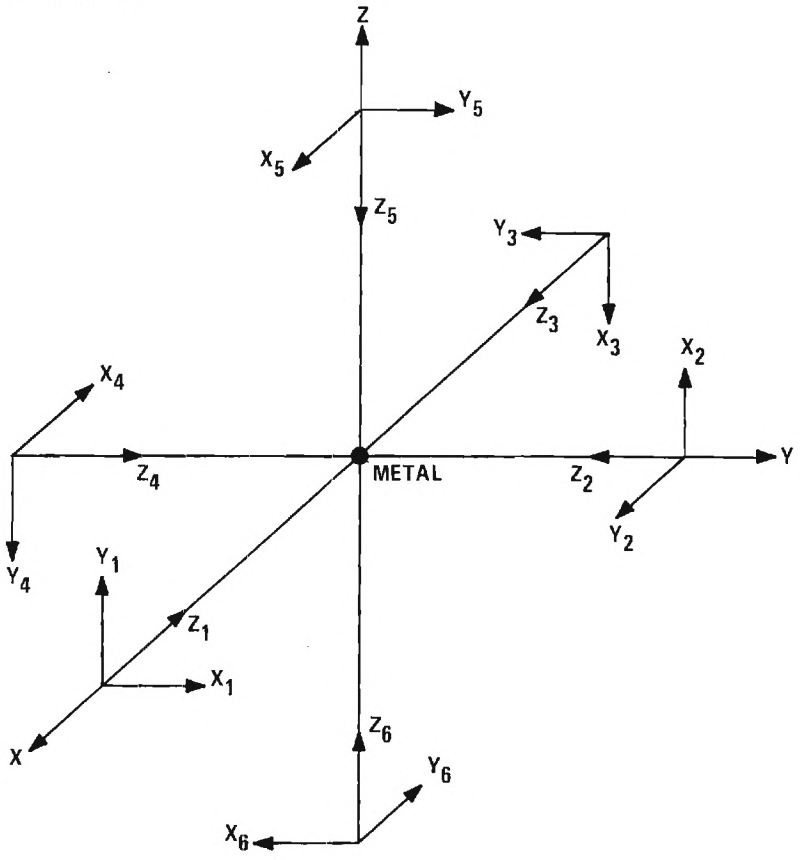

Fig. No. 3.1 Geometry of Coordinate System for Octahedral Site

We will assume that the metal inner shell and excited AO's do not contribute appreciably to the MO's responsible for the observed spectrum of this complex. This seems to be the case in other octahedral complexes that have been treated by the semi-empirical method. Also based on other calculations is the assumption that we need only use 2p orbitals for the ligands. This is the most successful assumption for octahedral complexes; for tetrahedral complexes, it is found that 2s ligand orbitals must be included also, in order to obtain useful results. With these assumptions, our basis set contains 5-3d, 3-4p, and 1-4s orbital from the metal, and 3 x 6 = 18-2p orbitals from the ligands, for a total of 27.

At this point, we introduce into the discussion the role played by the symmetry of the molecule. If we were to construct the matrix representation of the Hartree-Fock Hamiltonian using the present basis set we would have

$$\bar{F} = \left(\int \chi_i F \chi_j dv \right) \quad 1 \leq i, j \leq 27$$

with essentially all entries non-zero. If we knew $\bar{F}$ we could, at this point, proceed to solve (3.22). However, we would not be taking advantage of the symmetry of the system, and our solutions would be difficult to classify. What we should do is take advantage of the concept of reducibility. Due to the symmetry of the molecule, the Hamiltonian has octahedral symmetry. Consequently, the associated MO's should also have octahedral symmetry. That is, if the operations of the octahedral group O_h are performed on a given solution, the resulting solution should describe the same physical situation as the original solution, and hence should correspond to the same energy eigenvalue as the original solution. This is not to say

the two solutions will be identical; in fact, they are linearly independent in general. What it means is, that given a solution, the transformations of the symmetry group can be used to generate a degenerate set of linearly independent solutions which form a closed subset of the basis set. By closed, we mean that the operators associated with the symmetry group operate on any linear combination of the members of the subset to give another linear combination of members of the subset. The closed subset is said to form an invariant subspace.

The basis vectors for the invariant subspaces associated with the various point symmetries are available in the literature. These basis vectors are specific linear combinations of the set of AO's used as a preliminary basis set above, and are generally designated symmetry orbitals. On the following page, we list the symmetry orbitals Ψ_j appropriate to the present problem, and obtained from reference 13. We use σ_i to denote the $2p_z$ orbital of ligand i, and x_i, y_i for the $2p_x$ and $2p_y$ orbitals of ligand i. The significance of the symbols σ_{ijk} will be discussed below.

$$
\begin{aligned}
a_{1g} &\begin{cases} \Psi_1 = \sigma_{111} = 4s \\ \Psi_2 = \sigma_{211} = 1/\sqrt{6}\ (\sigma_1 + \sigma_2 + \sigma_3 + \sigma_4 + \sigma_5 + \sigma_6) \end{cases} \\
e_g &\begin{cases} \Psi_3 = \sigma_{121} = 3d_{x^2y^2} \\ \Psi_4 = \sigma_{122} = 3d_{z^2} \\ \Psi_5 = \sigma_{221} = 1/2(\sigma_1 - \sigma_2 + \sigma_3 - \sigma_4) \\ \Psi_6 = \sigma_{222} = 1/2\sqrt{3}\ (2\sigma_5 + 2\sigma_6 - \sigma_1 - \sigma_2 - \sigma_3 - \sigma_4) \end{cases} \\
t_{1u} &\begin{cases} \Psi_7 = \sigma_{131} = 4p_x \\ \Psi_8 = \sigma_{132} = 4p_y \\ \Psi_9 = \sigma_{133} = 4p_z \\ \Psi_{10} = \sigma_{231} = 1/\sqrt{2}\ (\sigma_1 - \sigma_3) \\ \Psi_{11} = \sigma_{232} = 1/\sqrt{2}\ (\sigma_2 - \sigma_4) \\ \Psi_{12} = \sigma_{233} = 1/\sqrt{2}\ (\sigma_5 - \sigma_6) \\ \Psi_{13} = \sigma_{331} = 1/2(y_2 + x_5 - x_4 - y_6) \\ \Psi_{14} = \sigma_{332} = 1/2(x_1 + y_5 - y_3 - x_6) \\ \Psi_{15} = \sigma_{333} = 1/2(y_1 + x_2 - x_3 - y_4) \end{cases} \\
t_{1g} &\begin{cases} \Psi_{16} = \sigma_{141} = 1/2(y_1 - x_5 + x_3 - y_6) \\ \Psi_{17} = \sigma_{142} = 1/2(x_2 - y_5 + y_4 - x_6) \\ \Psi_{18} = \sigma_{143} = 1/2(x_1 - y_2 + y_3 - x_4) \end{cases} \\
t_{2u} &\begin{cases} \Psi_{19} = \sigma_{151} = 1/2(y_2 - x_5 - x_4 + y_6) \\ \Psi_{20} = \sigma_{152} = 1/2(x_1 - y_5 - y_3 + x_6) \\ \Psi_{21} = \sigma_{153} = 1/2(y_1 - x_2 - x_3 + y_4) \end{cases} \\
t_{2g} &\begin{cases} \Psi_{22} = \sigma_{161} = 3d_{xz} \\ \Psi_{23} = \sigma_{162} = 3d_{yz} \\ \Psi_{24} = \sigma_{163} = 3d_{xy} \\ \Psi_{25} = \sigma_{261} = 1/2(y_1 + x_5 + x_3 + y_6) \\ \Psi_{26} = \sigma_{262} = 1/2(x_2 + y_5 + y_4 + x_6) \\ \Psi_{27} = \sigma_{263} = 1/2(x_1 + y_2 + y_3 + x_4) \end{cases}
\end{aligned}
$$

The combinations of ligand orbitals shown here have been normalized neglecting ligand-ligand overlap. This will be corrected below. The letters listed on the left indicate the type of irreducible representation for which the corresponding basis functions serve as basis vectors. To clarify this statement, a_{1g} indicates a one-dimensional representation of the symmetry operators of the molecular symmetry group. Either Ψ_1 or Ψ_2 may serve as a basis vector for this representation. e_g indicates a two-dimensional representation, and either Ψ_3,Ψ_4 or Ψ_5,Ψ_6 may serve as basis vectors for this representation. t_{1g}, t_{1u}, t_{2g}, t_{2u} indicate four different three-dimensional representations.

To explain the symbol σ_{ijk}, we note that j represents the type of representation a_{1g}, e_g etc. There are 6 in all. Corresponding to each type of representation, there will be several sets of basis vectors which may serve as basis vectors for the representation; e.g., either Ψ_3,Ψ_5 or Ψ_4,Ψ_6 for e_g. The index i labels a particular set within a representation. Finally, the members of a given set are labeled with the index k, k = 1, . . , p where p is the dimension of the representation. We will find that p is the same as the degeneracy of the energy levels which will be associated with the LCAO arising from the basis vectors of a p-dimensional representation.

We quote the following results from Group Theory: If M is any operator which has the symmetry of the system, then

Rule I $$\int \sigma_{\alpha\pi\lambda} \, M \, \sigma_{\beta\rho k} \, dv = 0$$

unless $\pi = \rho \; ; \; \lambda = k$.

Rule II $$\int \sigma_{\alpha\pi\lambda} M \sigma_{\beta\pi\lambda} dv = \int \sigma_{\alpha\pi k} M \sigma_{\beta\pi k} dv .$$

for any k, λ .

As a final illustration, we show the general matrix structure of the matrix representation of a symmetry operator in the symmetry orbital basis shown on the previous page:

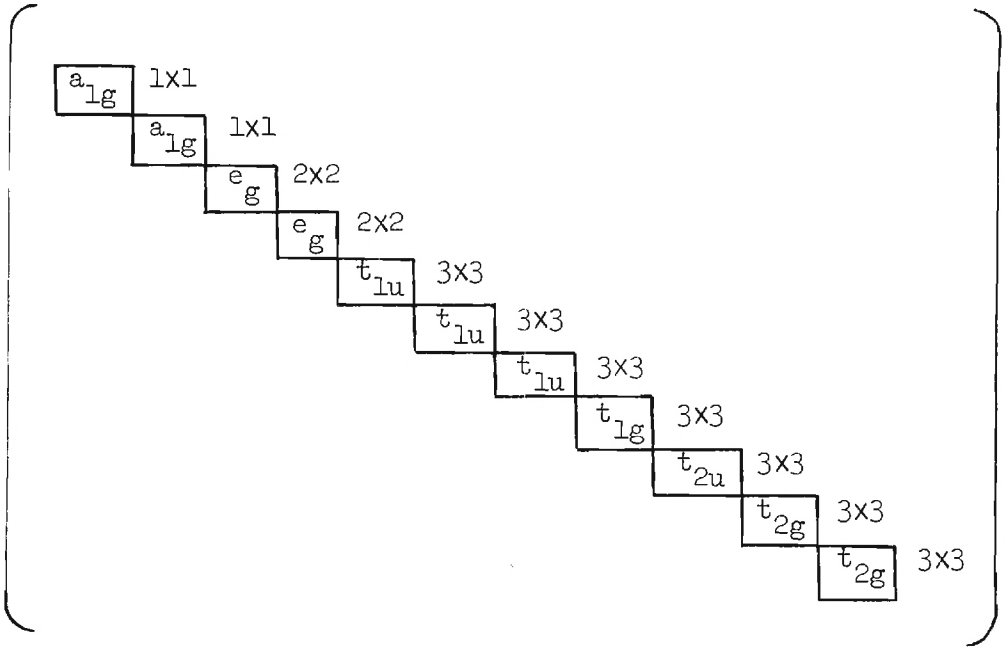

We will see that the number of times a given representation appears along the diagonal determines the dimension of the associated secular equation.

If we now construct the matrix of F-εI in the symmetry orbital basis shown on page 68 , we can use Rule I to show that it takes the form

$$\left(\begin{array}{cccccccccc} 1\ 2\times2 & & & & & & & & & \\ & 2\ 4\times4 & & & & & & & & \\ & & 3\ 9\times9 & & & & & & & \\ & & & 4\ 1\times1 & & & & & & \\ & & & & 5\ 1\times1 & & & & & \\ & & & & & 6\ 1\times1 & & & & \\ & & & & & & 7\ 1\times1 & & & \\ & & & & & & & 8\ 1\times1 & & \\ & & & & & & & & 9\ 1\times1 & \\ & & & & & & & & & 10\ 6\times6 \end{array}\right) = (\bar{F}_{ij} - \epsilon\bar{S}_{ij})$$

Now we note that the condition that equation (3.22) have non-trivial solutions is that:

$$\det\ (\bar{F}_{ij} - \epsilon\bar{S}_{ij}) = 0.$$

With the present form for the matrix, (3.23) can be satisfied if:

$$\det\ (1),\ \text{or}\ \det\ (2),\ \ldots,\ \text{or}\ \det\ (10) = 0.$$

Thus we arrive at a number of secular equations. We will discuss them one at a time.

(1) <u>2 x 2</u>

$$\det\begin{pmatrix} \bar{F}_{11} - \epsilon\bar{S}_{11} & F_{12} - \epsilon\bar{S}_{12} \\ \bar{F}_{21} - \epsilon\bar{S}_{21} & \bar{F}_{22} - \epsilon\bar{S}_{22} \end{pmatrix} = 0$$

We note that $\bar{F}$ and $\bar{S}$ are Hermatian and real, hence $\bar{F}_{12} = \bar{F}_{21}$ and $\bar{S}_{12} = \bar{S}_{21}$. We will use this fact without comment below. We get two, generally distinct, eigenvalues, and solutions:

$$\epsilon_1' : a_1'\Psi_1 + b_1'\Psi_2$$

$$\epsilon_2' : a_2'\Psi_1 + b_2'\Psi_2$$

(2) $\underline{4 \times 4}$

$$\det \begin{pmatrix} \bar{F}_{33} - \epsilon\bar{S}_{33} & 0 & F_{35} - \epsilon S_{35} & 0 \\ 0 & \bar{F}_{44} - \epsilon\bar{S}_{44} & 0 & \bar{F}_{46} - \epsilon\bar{S}_{46} \\ \bar{F}_{35} - \epsilon S_{35} & 0 & \bar{F}_{55} - \epsilon\bar{S}_{55} & 0 \\ 0 & \bar{F}_{46} - \bar{S}_{46} & 0 & \bar{F}_{66} - \epsilon\bar{S}_{66} \end{pmatrix} = 0$$

The vanishing entries are due to Rule I. We can use Rule II to show $\bar{F}_{33} = \bar{F}_{44}$, $\bar{F}_{55} = \bar{F}_{66}$, $F_{35} = F_{46}$, (same for $\bar{S}$). Using this, and the properties of determinants, our equation reduces to

$$\det \begin{pmatrix} \bar{F}_{33} - \epsilon & \bar{F}_{35} - \epsilon\bar{S}_{35} \\ \bar{F}_{35} - \epsilon\bar{S}_{35} & \bar{F}_{55} - \epsilon \end{pmatrix}^2 = 0 ,$$

where we have used $\bar{S}_{ii} = 1$. Thus we get two eigenvalues, each two-fold degenerate. The solutions are:

$$\epsilon_1^2 : \quad a_1^2\Psi_3 + b_1^2\Psi_5 ,$$
$$a_1^2\Psi_4 + b_1^2\Psi_6$$

$$\epsilon_2^{\,2}: \quad a_2^{\,2}\,\Psi_3 + b_2^{\,2}\,\Psi_5\,,$$
$$a_2^{\,2}\,\Psi_4 + b_2^{\,2}\,\Psi_6$$

(3) 9 x 9

Without bothering to write this one out, we use Rule I to get some 0 entries, Rule II to show $\bar{F}_{77} = \bar{F}_{88} = \bar{F}_{99}$; $\bar{F}_{10,10} = \bar{F}_{11,11} = \bar{F}_{12,12}$; $\bar{F}_{13,13} = \bar{F}_{14,14} = \bar{F}_{15,15}$; $\bar{F}_{7,10} = \bar{F}_{8,11} = \bar{F}_{9,12}$; $\bar{F}_{7,13} = \bar{F}_{8,14} = \bar{F}_{9,15}$; $\bar{F}_{10,13} = \bar{F}_{11,14} = \bar{F}_{12,15}$ (Same for $\bar{S}$), and the properties of determinants to arrive at

$$\det \begin{pmatrix} F_{77} - \epsilon & F_{7,10} - \epsilon S_{7,10} & F_{7,13} - \epsilon S_{7,13} \\ F_{7,10} - \epsilon S_{7,10} & F_{10,10} - \epsilon & F_{10,13} - \epsilon S_{10,13} \\ F_{7,13} - \epsilon S_{7,13} & F_{10,13} - \epsilon S_{10,13} & F_{13,13} - \epsilon \end{pmatrix}^3 = 0$$

We get three eigenvalues, each three-fold degenerate. The solutions are:

$$\epsilon_1^{\,3}: \quad a_1^{\,3}\,\Psi_7 + b_1^{\,3}\,\Psi_{10} + c_1^{\,3}\,\Psi_{13}\,,$$
$$a_1^{\,3}\,\Psi_8 + b_1^{\,3}\,\Psi_{11} + c_1^{\,3}\,\Psi_{14}\,,$$
$$a_1^{\,3}\,\Psi_9 + b_1^{\,3}\,\Psi_{12} + c_1^{\,3}\,\Psi_{15}$$

$$\epsilon_2^{\,3}: \quad a_2^{\,3}\,\Psi_7 + b_2^{\,3}\,\Psi_{10} + c_2^{\,3}\,\Psi_{13}\,,$$
$$a_2^{\,3}\,\Psi_8 + b_2^{\,3}\,\Psi_{11} + c_2^{\,3}\,\Psi_{14}\,,$$
$$a_2^{\,3}\,\Psi_9 + b_2^{\,3}\,\Psi_{12} + c_2^{\,3}\,\Psi_{15}$$

$$\epsilon_3^{\,3}: \quad a_3^{\,3}\,\Psi_7 + b_3^{\,3}\,\Psi_{10} + c_3^{\,3}\,\Psi_{13}\,,$$
$$a_3^{\,3}\,\Psi_8 + b_3^{\,3}\,\Psi_{11} + c_3^{\,3}\,\Psi_{14}\,,$$
$$a_3^{\,3}\,\Psi_9 + b_3^{\,3}\,\Psi_{12} + c_3^{\,3}\,\Psi_{15}$$

(4), (5), (6), (7), (8), (9) 1 x 1

These are orbitals which are neither bonding nor anti-bonding with the metal. The energies are just those associated with the atomic levels.

(10) 6 x 6

We use Rule I to get 0 entries, Rule II to show $\bar{F}_{22,22} = \bar{F}_{23,23} = \bar{F}_{24,24}$; $\bar{F}_{25,25} = \bar{F}_{26,26} = \bar{F}_{27,27}$; $\bar{F}_{22,25} = \bar{F}_{23,26} = \bar{F}_{24,27}$ (Same for $\bar{S}$) and use the properties of determinants to obtain:

$$\det \begin{pmatrix} \bar{F}_{22,22} - \epsilon & F_{22,25} - \epsilon S_{22,25} \\ \bar{F}_{22,25} - \epsilon \bar{S}_{22,25} & F_{25,25} - \epsilon \end{pmatrix}^3 = 0$$

Thus we get two eigenvalues, each three-fold degenerate. The solutions are:

$$\epsilon_1^{\,10}: \quad a_1^{\,10}\,\Psi_{22} + b_1^{\,10}\,\Psi_{25}\,,$$
$$a_1^{\,10}\,\Psi_{23} + b_1^{\,10}\,\Psi_{26}\,,$$
$$a_1^{\,10}\,\Psi_{24} + b_1^{\,10}\,\Psi_{27}$$

$$\varepsilon_2^{10}: \quad a_2^{10}\Psi_{22} + b_2^{10}\Psi_{25}\,,$$
$$a_2^{10}\Psi_{23} + b_2^{10}\Psi_{26}\,,$$
$$a_2^{10}\Psi_{24} + b_2^{10}\Psi_{27}$$

F. The Determination of Overlap Integrals

In this section, we will constantly reference the diagram on page 65 and the symmetry orbital list on page 68. We wish to calculate the basic ligand-ligand overlaps; the metal-ligand overlaps $\bar{S}_{12}$, $\bar{S}_{3,5}$, $\bar{S}_{7,10}$, $\bar{S}_{7,13}$ and $\bar{S}_{22,25}$; and the symmetry orbital ligand-ligand overlap $S_{10,13}$, which is just a simple combination of the basic ligand-ligand overlaps.

Ligand-Ligand Overlaps: We will use the shorthand notation

$$\langle\sigma_1|\sigma_2\rangle = \int P_{z_1} P_{z_2}\, dv \quad .$$

By inspection of the figure on page 14, we see:

$$a = \langle\sigma_1|\sigma_2\rangle = \langle\sigma_2|\sigma_3\rangle = \langle\sigma_3|\sigma_4\rangle = \langle\sigma_1|\sigma_4\rangle = \langle\sigma_1|\sigma_5\rangle$$
$$= \langle\sigma_1|\sigma_6\rangle = \langle\sigma_2|\sigma_5\rangle = \langle\sigma_2|\sigma_6\rangle = \langle\sigma_3|\sigma_5\rangle = \langle\sigma_3|\sigma_6\rangle$$
$$= \langle\sigma_4|\sigma_5\rangle = \langle\sigma_4|\sigma_6\rangle$$
$$= \langle\sigma_1|\sigma_3\rangle = \langle\sigma_2|\sigma_4\rangle = \langle\sigma_5|\sigma_6\rangle$$

In order to determine the relations between the x and y ligand-ligand overlaps, it is convenient to use a geometrical device. We assign 3-space vectors to the x and y functions by the following prescription

$$\hat{x}_1 = (3,1,0) \qquad \hat{y}_1 = (3,0,1)$$
$$\hat{x}_2 = (0,3,1) \qquad \hat{y}_2 = (1,3,0)$$
$$\hat{x}_3 = (-3,0,-1) \qquad \hat{y}_3 = (-3,-1,0)$$
$$\hat{x}_4 = (-1,-3,0) \qquad \hat{y}_4 = (0,-3,-1)$$
$$\hat{x}_5 = (1,0,3) \qquad \hat{y}_5 = (0,1,3)$$
$$\hat{x}_6 = (0,-1,-3) \qquad \hat{y}_6 = (-1,0,-3)$$

These vectors have a component of length 3 out the main axis on which the corresponding ligand is located, and a component of length 1 in the direction that the corresponding orbital is oriented. It is obvious that those vector pairs which have the same dot product will correspond to orbitals which have the same overlap. We have:

$\hat{x}_1 \cdot \hat{x}_2 = 3$ $\hat{x}_2 \cdot \hat{x}_3 = -1$ $\hat{x}_3 \cdot \hat{x}_4 = 3$ $\hat{x}_4 \cdot \hat{x}_5 = -1$ $\hat{x}_5 \cdot \hat{x}_6 = -9$
$\hat{x}_1 \cdot \hat{x}_3 = -9$ $\hat{x}_2 \cdot \hat{x}_4 = -9$ $\hat{x}_3 \cdot \hat{x}_5 = -6$ $\hat{x}_4 \cdot \hat{x}_6 = 3$
$\hat{x}_1 \cdot \hat{x}_4 = -6$ $\hat{x}_2 \cdot \hat{x}_5 = 3$ $\hat{x}_3 \cdot \hat{x}_6 = 3$
$\hat{x}_1 \cdot \hat{x}_5 = 3$ $\hat{x}_2 \cdot \hat{x}_6 = -6$
$\hat{x}_1 \cdot \hat{x}_6 = -1$

$\hat{y}_1 \cdot \hat{y}_2 = 3$ $\hat{y}_2 \cdot \hat{y}_3 = -6$ $\hat{y}_3 \cdot \hat{y}_4 = 3$ $\hat{y}_4 \cdot \hat{y}_5 = -6$ $\hat{y}_5 \cdot \hat{y}_6 = -9$
$\hat{y}_1 \cdot \hat{y}_3 = -9$ $\hat{y}_2 \cdot \hat{y}_4 = -9$ $\hat{y}_3 \cdot \hat{y}_5 = -1$ $\hat{y}_4 \cdot \hat{y}_6 = 3$
$\hat{y}_1 \cdot \hat{y}_4 = -1$ $\hat{y}_2 \cdot \hat{y}_5 = 3$ $\hat{y}_3 \cdot \hat{y}_6 = 3$
$\hat{y}_1 \cdot \hat{y}_5 = 3$ $\hat{y}_2 \cdot \hat{y}_6 = -1$
$\hat{y}_1 \cdot \hat{y}_6 = -6$

$\hat{x}_1 \cdot \hat{y}_1 = 0$ $\hat{x}_2 \cdot \hat{y}_1 = 1$ $\hat{x}_3 \cdot \hat{y}_1 = -10$ $\hat{x}_4 \cdot \hat{y}_1 = -3$ $\hat{x}_5 \cdot \hat{y}_1 = 6$ $\hat{x}_6 \cdot \hat{y}_1 = -3$

$\hat{x}_1 \cdot \hat{y}_2 = 6$ $\hat{x}_2 \cdot \hat{y}_2 = 0$ $\hat{x}_3 \cdot \hat{y}_2 = -3$ $\hat{x}_4 \cdot \hat{y}_2 = -10$ $\hat{x}_5 \cdot \hat{y}_2 = 1$ $\hat{x}_6 \cdot \hat{y}_2 = -3$

$\hat{x}_1 \cdot \hat{y}_3 = -10$ $\hat{x}_2 \cdot \hat{y}_3 = -3$ $\hat{x}_3 \cdot \hat{y}_3 = 0$ $\hat{x}_4 \cdot \hat{y}_3 = 6$ $\hat{x}_5 \cdot \hat{y}_3 = -3$ $\hat{x}_6 \cdot \hat{y}_3 = 1$

$\hat{x}_1 \cdot \hat{y}_4 = -3$ $\hat{x}_2 \cdot \hat{y}_4 = -10$ $\hat{x}_3 \cdot \hat{y}_4 = 1$ $\hat{x}_4 \cdot \hat{y}_4 = 0$ $\hat{x}_5 \cdot \hat{y}_4 = -3$ $\hat{x}_6 \cdot \hat{y}_4 = 6$

$\hat{x}_1 \cdot \hat{y}_5 = 1$ $\hat{x}_2 \cdot \hat{y}_5 = 6$ $\hat{x}_3 \cdot \hat{y}_5 = -3$ $\hat{x}_4 \cdot \hat{y}_5 = -3$ $\hat{x}_5 \cdot \hat{y}_5 = 0$ $\hat{x}_6 \cdot \hat{y}_5 = -10$

$\hat{x}_1 \cdot \hat{y}_6 = -3$ $\hat{x}_2 \cdot \hat{y}_6 = -3$ $\hat{x}_3 \cdot \hat{y}_6 = 6$ $\hat{x}_4 \cdot \hat{y}_6 = 1$ $\hat{x}_5 \cdot \hat{y}_6 = -10$ $\hat{x}_6 \cdot \hat{y}_6 = 0$

Thus we obtain:

$$c = \langle x_1|y_5\rangle = \langle x_2|y_1\rangle = \langle x_3|y_4\rangle = \langle x_4|y_6\rangle = \langle x_5|y_2\rangle = \langle x_6|y_3\rangle$$

$$d = \langle x_1|x_6\rangle = \langle x_2|x_3\rangle = \langle x_4|x_5\rangle = \langle y_1|y_4\rangle = \langle y_2|y_6\rangle = \langle y_3|y_5\rangle$$

$$e = \langle x_1|x_2\rangle = \langle x_1|x_5\rangle = \langle x_2|x_5\rangle = \langle x_3|x_4\rangle = \langle x_3|x_6\rangle = \langle x_4|x_6\rangle$$
$$= \langle y_1|y_2\rangle = \langle y_1|y_5\rangle = \langle y_2|y_5\rangle = \langle y_3|y_4\rangle = \langle y_3|y_6\rangle = \langle y_4|y_6\rangle$$

$$f = \langle x_1|y_4\rangle = \langle x_1|y_6\rangle = \langle x_2|y_3\rangle = \langle x_2|y_6\rangle = \langle x_3|y_2\rangle = \langle x_3|y_5\rangle$$
$$= \langle x_4|y_1\rangle = \langle x_4|y_5\rangle = \langle x_5|y_3\rangle = \langle x_5|y_4\rangle = \langle x_6|y_1\rangle = \langle x_6|y_2\rangle$$

$$g = \langle x_1|y_2\rangle = \langle x_2|y_5\rangle = \langle x_3|y_6\rangle = \langle x_4|y_3\rangle = \langle x_5|y_1\rangle = \langle x_6|y_4\rangle$$

$$h = \langle x_1|x_4\rangle = \langle x_2|x_6\rangle = \langle x_3|x_5\rangle = \langle y_1|y_6\rangle = \langle y_2|y_3\rangle = \langle y_4|y_5\rangle$$

$$k = \langle x_1|x_3\rangle = \langle x_2|x_4\rangle = \langle x_5|x_6\rangle = \langle y_1|y_3\rangle = \langle y_2|y_4\rangle = \langle y_5|y_6\rangle$$

$$\ell = \langle x_1|y_3\rangle = \langle x_2|y_4\rangle = \langle x_3|y_1\rangle = \langle x_4|y_2\rangle = \langle x_5|y_6\rangle = \langle x_6|y_5\rangle$$

Next, we will re-express these integrals in terms of the basic two-atom overlaps:

$$S\ (\alpha_{\beta\gamma},\ \alpha'_{\beta'\gamma'},\ r)$$

where $\alpha, \alpha' \sim$ S, p or d

$\beta, \beta' \sim \sigma$ or π type of overlap

$\gamma, \gamma' \sim$ M(Metal) or L(ligand)

$r \sim$ Separation between centers.

We will perform the explicit transformation for one case, and list the results for the other cases.

$$a = \langle \sigma_1 | \sigma_2 \rangle = \int P_{z_1} P_{z_2} \, dv$$

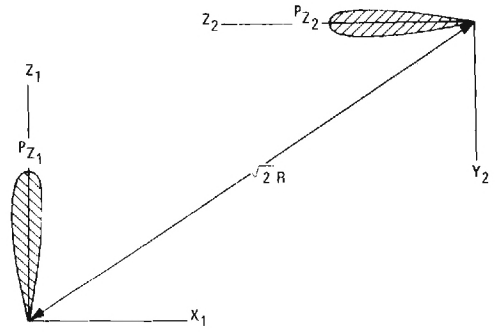

Fig. No. 3.2 Diagram of Two $2p_z$ Ligand Orbitals in Original Coordinate System

We perform a rotation of both coordinate systems such that the new z_1 and z_2 axes point to each other (45° rotation)

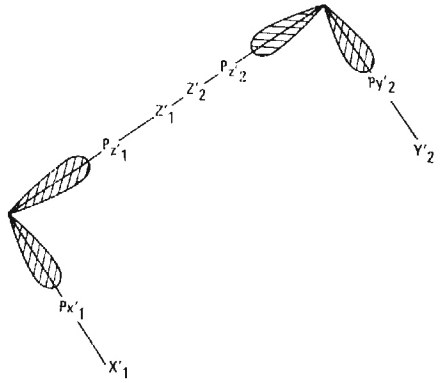

Fig. No. 3.3 $2p_z$ Ligand Orbitals Transformed in p_σ & p_π Components

We obtain:

$$P_{z_1} = \frac{f(r_1)}{r_1} z_1 \rightarrow \frac{f(r_1)}{r_1} \left[z_1' \cos 45° - x_1' \sin 45° \right]$$

$$P_{z_2} = \frac{f(r_2)}{r_2} z_2 \rightarrow \frac{f(r_2)}{r_2}\left[z_2'\cos 45^\circ - y_2'\sin 45^\circ\right]$$

and

$$\int P_{z_1} P_{z_2} dv \rightarrow \tfrac{1}{2}\int P_{z_1}' P_{z_2}' dv - \tfrac{1}{2}\int P_{z_1}' P_{y_2}' dv \quad (0 \text{ by Symmetry})$$

$$- \tfrac{1}{2}\int P_{z_2}' P_{x_1}' dv + \tfrac{1}{2}\int P_{x_1}' P_{y_2}' dv \quad (0 \text{ by Symmetry})$$

or:

$$a = \tfrac{1}{2} S(P_{\sigma L}, P_{\sigma L}, \sqrt{2}\, R) + \tfrac{1}{2} S(P_{\pi L}, P_{\pi L}, \sqrt{2}\, R)$$

In similar fashion:

$$b = S(P_{\sigma L}, P_{\sigma L}, 2R)$$

$$c = S(P_{\pi L}, P_{\pi L}, \sqrt{2}\, R)$$

$$d = - S(P_{\pi L}, P_{\pi L}, \sqrt{2}\, R)$$

e, f, k will not enter the final calculation

$$g = \tfrac{1}{2} S(P_{\sigma L}, P_{\sigma L}, \sqrt{2}\, R) + \tfrac{1}{2} S(P_{\pi L}, P_{\pi L}, \sqrt{2}\, R)$$

$$h = \tfrac{1}{2} S(P_{\sigma L}, P_{\sigma L}, \sqrt{2}\, R) + \tfrac{1}{2} S(P_{\pi L}, P_{\pi L}, \sqrt{2}\, R)$$

$$\ell = - S(P_{\pi L}, P_{\pi L}, 2R)$$

We define $\alpha = S(P_{\sigma L}, P_{\sigma L}, \sqrt{2}\, R)$

$\beta = S(P_{\pi L}, P_{\pi L}, \sqrt{2}\, R)$

$\gamma = S(P_{\sigma L}, P_{\sigma L}, 2R)$

$S = S(P_{\pi L}, P_{\pi L}, 2R)$

Then: $a = (\alpha + \beta)/2$

$b = \gamma$

$c = \beta$

$d = -\beta$

$g = (\alpha + \beta)/2$

$h = (\alpha + \beta)/2$

$\ell = - S$

Ligand Symmetry Orbital Normalization: At this point, it is convenient to determine the correct normalization factors for the ligand symmetry orbitals. We will consider one case explicitly, and list the results for the others.

$$\Psi_2 : \quad N_2^2 \int \Psi_2'^2 dv = 1$$

$$\Psi_2' = \sigma_1 + \sigma_2 + \sigma_3 + \sigma_4 + \sigma_5 + \sigma_6$$

$$\int \Psi_2'^2 \, dv = 6 + 2\langle\sigma_1|\sigma_2\rangle + 2\langle\sigma_1|\sigma_3\rangle + 2\langle\sigma_1|\sigma_4\rangle + 2\langle\sigma_1|\sigma_5\rangle + 2\langle\sigma_1|\sigma_6\rangle$$

$$+ 2\langle\sigma_2|\sigma_3\rangle + 2\langle\sigma_2|\sigma_4\rangle + 2\langle\sigma_2|\sigma_5\rangle + 2\langle\sigma_2|\sigma_6\rangle$$

$$+ 2\langle\sigma_3|\sigma_4\rangle + 2\langle\sigma_3|\sigma_5\rangle + 2\langle\sigma_3|\sigma_6\rangle$$

$$+ 2\langle\sigma_4|\sigma_5\rangle + 2\langle\sigma_4|\sigma_6\rangle$$

$$+ 2\langle\sigma_5|\sigma_6\rangle$$

$$= 6 + 6b + 24a$$

$$= 6 + 6\gamma + 24\left[\tfrac{1}{2}(\alpha + \beta)\right]$$

$$= 6(1 + 2\alpha + 2\beta + \gamma)$$

and

$$N_2 = [6(1 + 2\alpha + 2\beta + \gamma)]^{-\frac{1}{2}}$$

Similarly

$$N_5 = [4(1 - \alpha - \beta + \gamma)]^{-\frac{1}{2}}$$

$$N_6 = [12(1 - \alpha - \beta + \gamma)]^{-\frac{1}{2}}$$

$$N_{10} = N_{11} = N_{12} = [2\ (1 - \gamma)]^{-\frac{1}{2}}$$

$$N_{13} = N_{14} = N_{15} = [4\ (1 + 2\beta + S)]^{-\frac{1}{2}}$$

$$N_{25} = N_{26} = N_{27} = [4\ (1 + \alpha + \beta - S)]^{-\frac{1}{2}}$$

All other pertinent normalizations are unity.

$\underline{\bar{S}_{10,13}}$ $\qquad S_{10,13} = 4N_{10}N_{13}(\alpha-\beta)$

Metal-Ligand Overlaps: We will write these out explicitly, using diagrams to show the type of overlap in each case.

$$\bar{S}_{12} = N_2 \int (4S)\ (\sigma_1 + \sigma_2 + \sigma_3 + \sigma_4 + \sigma_5 + \sigma_6)dv$$

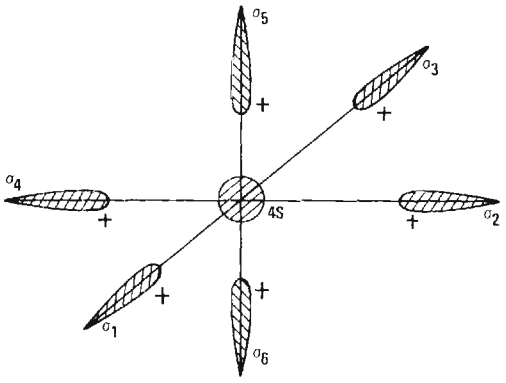

Fig. No. 3.4 Diagram of Orbital Geometry for a_{1g} Symmetry

$$= 6N_2 \int (4S)\ \sigma_1 dv$$

$$\bar{S}_{35} = N_5 \int (3d_{x^2-y^2})\ (\sigma_1 - \sigma_2 + \sigma_3 - \sigma_4)dv$$

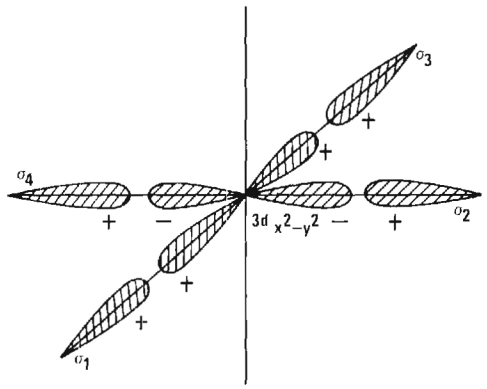

Fig. No. 3.5 Diagram of Orbital Geometry for e_g Symmetry

$$= 4N_5 \int (3d_{x^2-y^2})\sigma_1 dv$$

$$\bar{S}_{7,10} = N_{10} \int (4P_x)\ (\sigma_1 - \sigma_3)dv$$

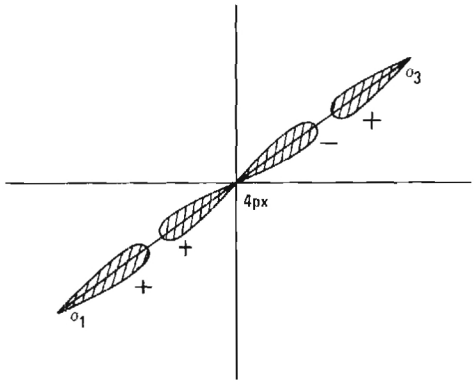

Fig. No. 3.6 Diagram of Orbital Geometry for $t_{1\mu}$ Symmetry

$$= 2N_{10} \int (4P_x)\ \sigma_1 dv$$

$$\bar{S}_{7,13} = N_{13} \int (4P_x)\ (y_2 + x_5 - x_4 - y_6)dv$$

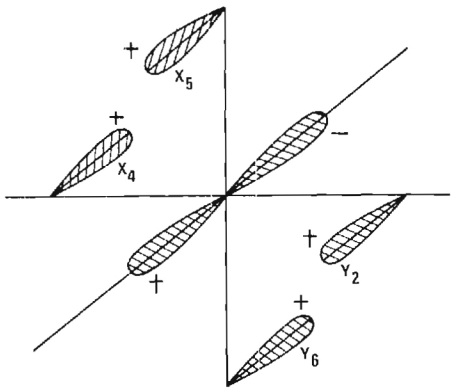

Fig. No. 3.7 Diagram of Orbital Geometry for t_{2u} Symmetry

$$= 4N_{13} \int (4P_x)\ y_2 dv$$

$$\bar{S}_{22,25} = N_{25} \int (3d_{xz})\ (y_1 + x_5 + x_3 + y_6)dv$$

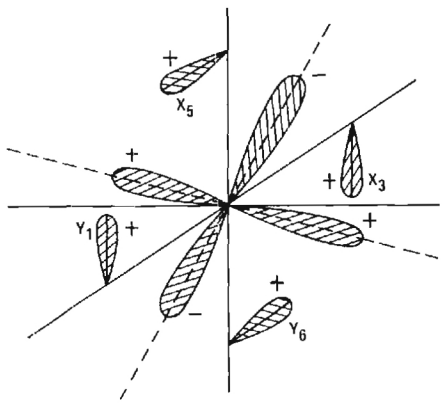

Fig. No. 3.8 Diagram of Orbital Geometry for t_{2g} Symmetry

$$= 4N_{25} \int (3d_{xz}) y_1 dv$$

G. Hamiltonian Matrix Elements

The diagonal Hamiltonian matrix elements will be estimated in terms of effective atomic ionization energies. The atomic valence state ionization energies (VSIE) for various starting configurations and net atomic charges are known. We assume that within the molecule, the atoms may be treated as fractionally charged with VSIE given by

$$VSIE = Aq^2 + Bq + C$$

where q is the net atomic charge. If we have VSIE for a given starting configuration for q = 0, +1, +2; we can fix A, B and C. If we only have information about one or two charge states, we assume values for some of the coefficients equal to those for a similar starting configuration where the VSIE are known.

For the metal orbitals, we have the following table:

VSIE	Starting Configuration	A	B	C
3d	d^m	13.8	86.2	41.9
3d	$d^{m-1}s$	13.8	101.5	70.0
3d	$d^{m-1}p$	13.8	101.9	81.2
4s	$d^{m-1}s$	7.4	63.8	57.3
4s	$d^{m-2}s^2$	7.4	73.0	68.3
4s	$d^{m-2}sp$	7.4	67.3	81.4
4p	$d^{m-1}p$	7.3	50.8	29.9
4p	$d^{m-1}p^2$	7.3	57.8	39.7
4p	$d^{m-1}sp$	7.3	57.8	40.3

Here, the VSIE are in units of 1000 cm^{-1}, and q is in units of the electronic charge.

In the model we are using, the atomic orbitals chosen are those appropriate to the neutral atoms. What we will do for the Hamiltonian matrix elements between metal orbitals is the following: We assign the metal atom-in-molecule an effective configuration $(3d)^d\ (4s)^s\ (4p)^p$ with an effective charge $q = 8 - (d + s + p)$. We assume initial values for d, s and p, and for the corresponding q we evaluate the various VSIE using the table on the previous page. We then assume that the metal orbital Hamiltonian matrix elements can be represented by a linear combination of atomic VSIE, for ionization from the corresponding atomic level, for several different starting configurations. We select the coefficients in the expansion as the simplest functions of s, p and d which will reduce the expression to the known VSIE for integral charge states:

$$- H_{3d,3d} = (1\text{-}s\text{-}p)\ [dVSIE{:}d^m]_q + s[dVSIE{:}d^{m-1}s]_q + p[dVSIE{:}d^{m-1}p]_q$$

$$- H_{4s,4s} = (2\text{-}s\text{-}p)[sVSIE{:}d^{m-1}s]_q + (s\text{-}1)[sVSIE{:}d^{m-2}s^2]_q + p[sVSIE{:}d^{m-2}sp]_q$$

$$- H_{4p,4p} = (2\text{-}2\text{-}p)[pVSIE{:}d^{m-1}p]_q + (p\text{-}1)[pVSIE{:}d^{m-2}p^2]_q + s[pVSIE{:}d^{m-2}sp]_q$$

With a particular starting set d,s,p we solve the eigenvalue problem for the system, and obtain the eigenvectors. We use the eigenvectors to calculate the effective charge in each of the metal orbitals, and thus the net metal charge. Having done this, we recalculate the effective VSIE by the preceding prescription, and solve the eigenvalue problem again, repeating the cycle. We continue in this way until the assumed configuration agrees with the calculated configuration.

To handle the ligand Hamiltonian matrix elements, we assume $H_{2p\pi,2p\pi} = H_{2p\sigma,2p\sigma} + 10{,}000\ cm^{-1}$ (see Ballhausen and Gray, p. 130).[13] For $H_{2p\sigma,2p\sigma}$ we use (VSIE:2p)/(1 + q/6), that is, the atomic VSIE for oxygen modified by a factor which accounts for the excess negative charge on the ligands.

Symmetry Orbital Matrix Elements

In the above, we have been discussing the atomic orbital matrix elements of the molecular Hamiltonian. To handle the symmetry orbital matrix elements we must first consider the symmetry orbital normalization. The symmetry orbitals listed on page 68have been normalized neglecting ligand-ligand overlap. This was explicitly compensated for in later calculation of the overlap integrals. We will now compensate for overlap in the Hamiltonian matrix elements.

The symmetry orbitals may be expressed in terms of atomic orbitals via

$$\Psi_i = \sum_k a_{ik} \Phi_{ik} \quad ; \quad i = 1, \ldots, 27$$

with

$$\sum_k a_{ik}^2 = 1$$

If we incorporate ligand-ligand overlap, we have:

$$\int \Psi_i^2 dv = \frac{1}{N_i^2} = \sum_{k,m} a_{ik} a_{in} S(ik,in)$$

where S(ik,in) is the atomic overlap

$$\int \Phi_{ik}\Phi_{in}dv$$

Using the fact that the atomic orbitals are normalized, we can write

$$\frac{1}{N_i^2} = \sum_k a_{ik}^2 + 2\sum_{k<n} a_{ik}a_{in}S(ik,in)$$

$$= 1 + 2\sum_{k<n} a_{ik}a_{in}S(ik,in)$$

$$= 1 + X_i$$

or

$$X_i = \frac{1 - N_i^2}{N_i^2}$$

(We have already obtained expressions for the N_i on page 81 and X_i will appear in other expressions below).

Now, the diagonal Hamiltonian matrix elements between symmetry orbitals are:

$$H_{ii} = N_i^2 \int \Psi_i H \Psi_i dv$$

$$= N_i^2 \sum_{k,n} a_{ik}a_{in}H_{ik,in}$$

where

$$H_{ik,in} = \int \Phi_{ik} H \Phi_{in} dv$$

is the matrix element of the molecular Hamiltonian between atomic orbitals. We can write this as:

$$H_{ii} = N_i^2 \sum_k a_{ik}^2 H_{ik,ik} + 2N_i^2 \sum_{k<n} a_{ik} a_{in} H_{ik,in} .$$

To proceed further, we need some prescription for obtaining the off-diagonal matrix elements $H_{ik,in}$. First of all we note that:

1. If the atoms in the molecule are widely separated, the overlap between orbitals on different atoms vanishes.

2. If the atoms in the molecule are widely separated, the molecular Hamiltonian operating on an orbital of a given atom is essentially the Hamiltonian of that atom operating on the orbital, and since the orbital is an eigenstate of the atomic Hamiltonian, the orbital is just reproduced. Thus for this case

$$\int \Phi_{ik} H \Phi_{in} dv \cong E_{in} \int \Phi_{ik} \Phi_{in} dv = 0$$

Thus, we see that the off-diagonal matrix elements of the molecular Hamiltonian between atomic orbitals vanish when the overlap integral vanishes. As a first approximation then, $H_{ik,in}$ is taken to be proportional to the overlap integral S(ik,in), and the proportionality constant is taken to be $-2\sqrt{H_{ik,ik} H_{in,in}}$. The factor of 2 is based on empirical fitting. Thus

$$H_{ik,in} = -2\sqrt{H_{ik,ik}\,H_{in,in}}\;S(ik,in)$$

Next we note that for a given i, the Φ_{ik} all have the same geometrical relation to the remainder of the molecule, and $H_{ik,ik}$ should be independent of k, for fixed i. (This is just Rule II on page 70). So, finally:

$$H_{ik,ik} = H_{ii}' \text{ (determined from VSIE)}$$

$$H_{ik,in} = 2H_{ii}'\,S(ik,in) \quad (H_{ii} \text{ is negative})$$

$$= N_i^2\,H_{ii}'\,(1 + 2X_i)$$

or

$$H_{ii} = (2 - N_i^2)\,H_{ii}'$$

For the off-diagonal symmetry orbital matrix elements:

$$H_{ij} = N_iN_j\int \Psi_i H \Psi_j = N_iN_j \sum_{k,n} a_{ik}a_{jn}H_{ik,jn}$$

$$= N_iN_j \sum_{k,n} a_{ik}a_{jn}\left(-2\sqrt{H_{ik,ik}H_{jn,jn}}\right) S(ik,jn)$$

$$= -2\,N_iN_j \sum_{kn} a_{ik}a_{jn}\sqrt{H_{ii}'\,H_{jj}'}\;S(ik,jn)$$

$$= -2\sqrt{H_{ii}' H_{jj}'} \sum_{k,n} a_{ik}a_{jn} S(ik,jn)$$

or

$$H_{ij} = -2\sqrt{H_{ii}' H_{jj}'} \bar{S}_{ij}$$

Population Analysis to Determine Effective Charges

The H_{ii}' are calculated from VSIE, and the overlap integrals $\bar{S}_{ij}$ are calculated directly. The H_{ij} are determined by the preceding analysis (using assumed s, p and d for the first run). The eigenvalue equations are solved, and the eigenvectors are obtained. The molecular orbitals will then appear in the form of linear combinations of symmetry orbitals

$$\Psi = A\Psi_m + B\Psi_L^{\sigma} + C\Psi_L^{\pi}$$

We will apply the condition that the molecular orbitals and the symmetry orbitals be normalized. Thus

$$A^2 + B^2 + C^2 = 1$$

and

$$\Psi \text{ (normalized)} = \frac{A\Psi_n + B\Psi_L^{\sigma} + C\Psi_L^{\pi}}{\sqrt{1 + 2AB\bar{S}_{ML}^{\sigma} + 2AC\bar{S}_{ML}^{\pi} + 2BC\bar{S}_{L}^{\sigma}{}_{L}^{\pi}}}$$

By assigning half the overlap population to the metal, the effective charge

is:

$$q_e = \frac{A^2 + AB\bar{S}_{ML^\sigma} + AC\bar{S}_{ML^\pi}}{1 + 2AB\bar{S}_{ML^\sigma} + 2AC\bar{S}_{ML^\pi} + 2BC\bar{S}_{L^\sigma L^\pi}}$$

This quantity is determined for each metal orbital, using all the individual molecular orbitals in turn, and the sum of all these quantities for a given type of metal orbital (3d, 4s, or 4p) determine the value of s, p or d to be used for that orbital. Once these numbers are found, the value of q can be determined, and the cycle repeated.

H. Actual Results

During a no cost extension to the project, we carried out the molecular orbital calculations outlined in this chapter. The programs were written in an extended ALGOL language called GTL (Georgia Tech Language) and contain constructs and library subroutines not generally available outside Georgia Tech. For this reason the actual programs used will not be copied into this report. They are, however, available to any interested persons simply by writing to the authors.

The overlap integrals are computed by a numerical integration process rather than employing the tabular method previously used by other investigators. This permits us to use complete self consistant field atomic functions. It is believed that we therefore have obtained more accurate overlaps than in any previous calculations.

Computation of the actual eigenstates and eigenfunctions is carried out with programs written to solve n^{th} order secular equations and compute the charge population of each orbital. In our solutions, we have achieved self consistant solutions with a manual approach. The programs are run from a remote terminal so the investigator is in direct communication with the running program. An assumed charge distribution is entered manually via the keyboard. The program solves the appropriate secular equations, determines the occupation of each orbital and then calculates and prints the resulting charge distribution. The operator compares this to what he originally inserted, modifies his estimate and inserts a new trial distribution. The process is repeated until the error between initial and final values is equal to or less than .02 electrons per orbital.

Figure III-9 shows the calculated energy level distribution and observable transition energies for the octahedral iron site in the garnets. Figure III-10 shows the same type of data for the tetrahedral site. The nomenclature of the various type orbitals is consistant with that usually found in the literature. Specifically, we have followed Ballhausen and Gray [13] in all our work.

It should be pointed out that in addition to the energy level structure illustrated in figure III-9 and III-10 we also have complete molecular orbital wave functions from which Faraday rotation can be computed. Faraday rotation calculations have not been carried out because of time limitations and our prime interest being the transition energy assignment. However, carrying out the Faraday rotation calculations would be another very important contribution to the magneto-optic memory technology. This is a result of our present inability to a priori select materials with a high ratio of Faraday rotation to absorption. Using the programs and resulting wave functions of the type developed during this program, a theoretical evaluation of this key parameter could easily be carried out. Much time consuming and expensive experimental work could thus be eliminated and efforts could then be directed to the materials indicating the greatest theoretical potential.

For the purpose of this research contract, however, we are primarily interested in determining the location of rare earth ion transitions in the complex optical spectra. To do this the measured spectra is compared with the octahedral and tetrahedral iron ion site transitions. In this

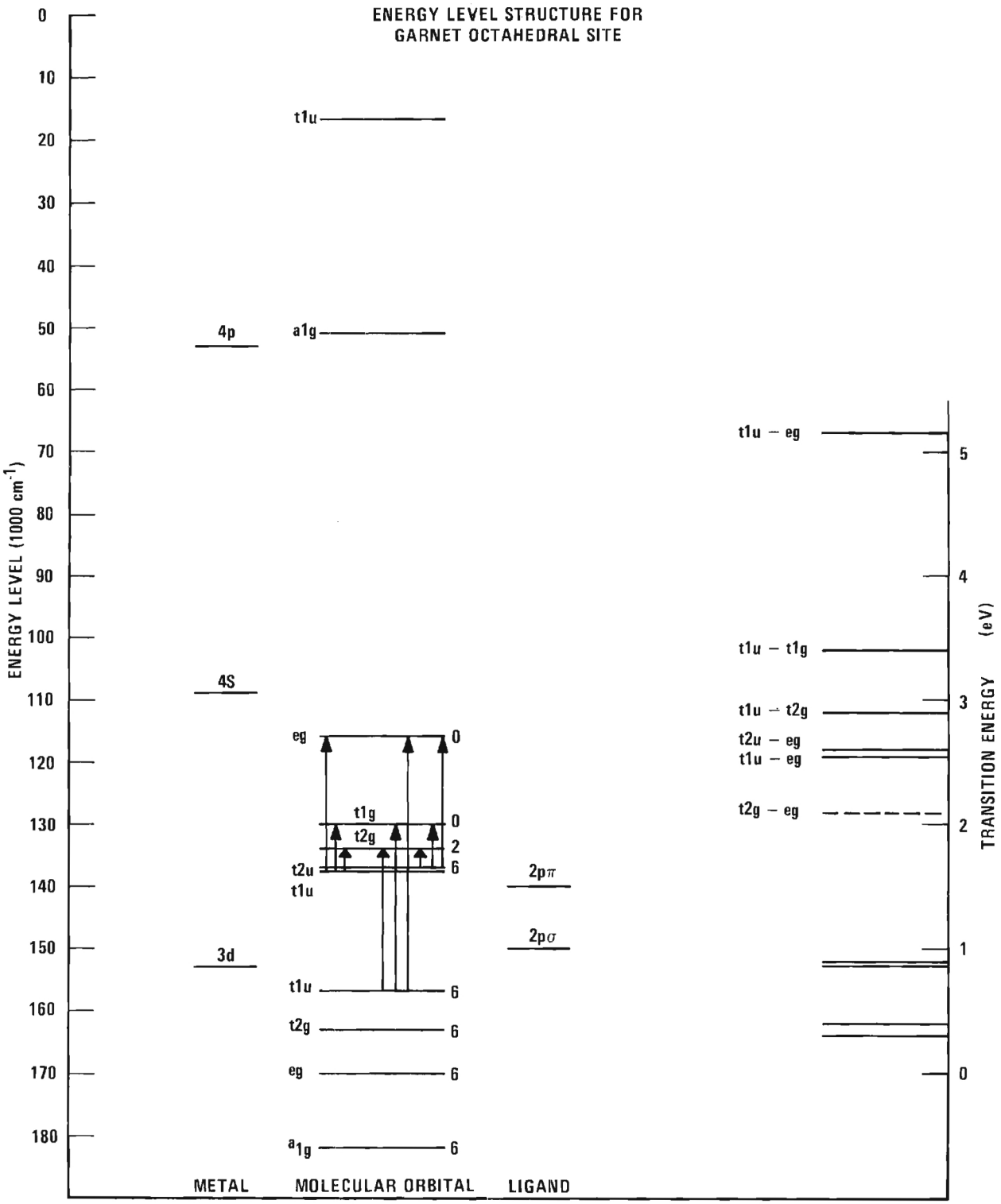

Fig. No. 3.9 Energy Levels of Octahedral Fe Site

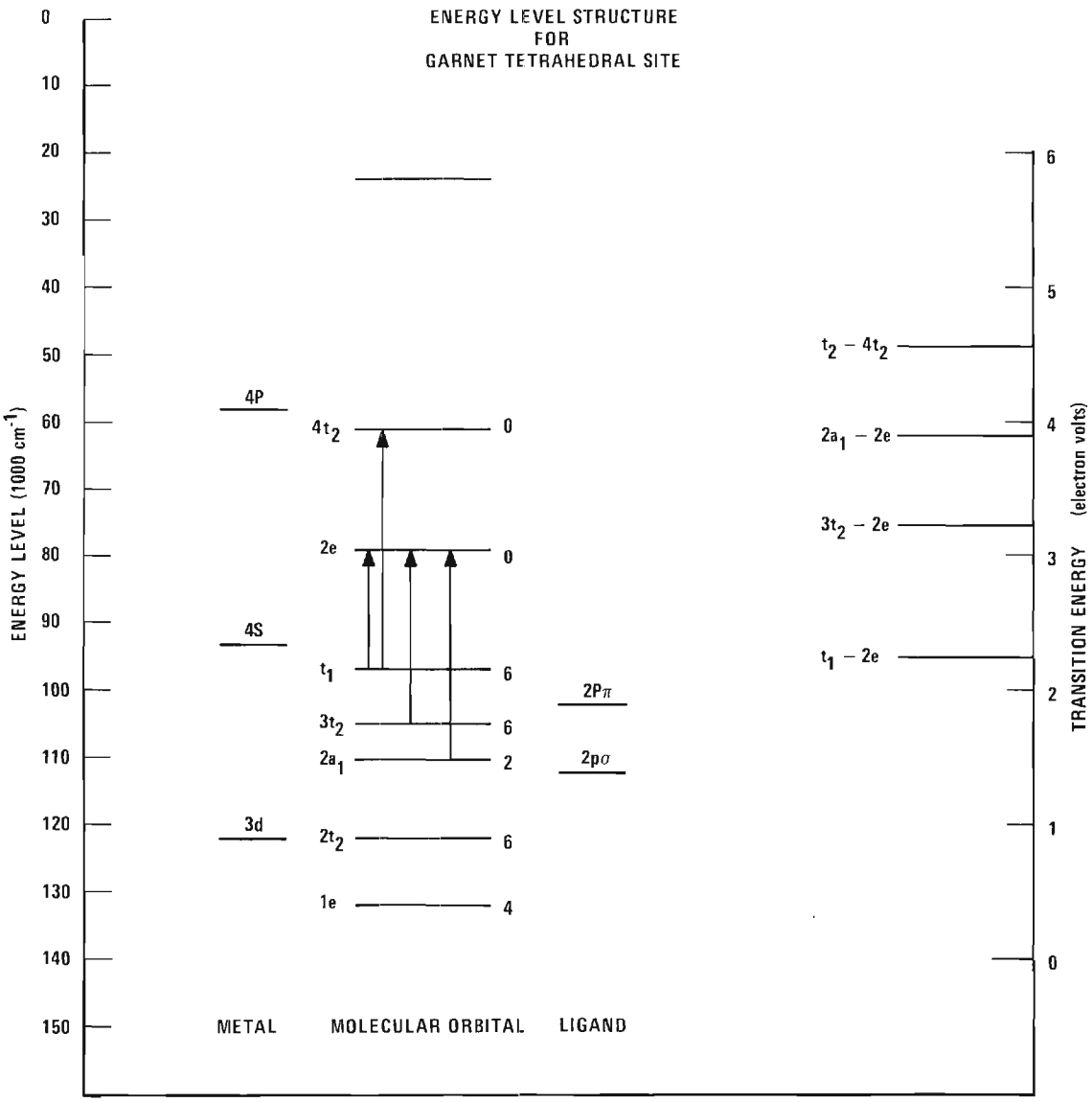

Fig. No. 3.10 Energy Levels of Tetrahedral Fe Site

way we can identify and hence eliminate the iron transitions and hopefully locate the rare earth ion transitions. We believe in fact that this has been achieved and that both a terbium and gadolinium transition have been found. The results of this comparison are shown in figure III-11.

Figure III-11 shows the experimentally observed transition spectra for gadolinium and terbium iron garnet. Peak heights are not to exact scale but transition energy is correct. As discussed in section II, we believe the TbIG lines at 3.25, 3.54, 3.95 and 4.34 ev are the same transitions as those at 3.40, 3.72, 4.1 and 4.35 ev in GdIG. This is based on their relative amplitudes and inter-line energies. The spectra do not overlap over the entire energy range because we were interested in the possibility of observing rare earth transitions. For gadolinium these appear between 3 and 5 ev and in terbium between 2 and 4 ev.

The absolute location of the molecular orbital energy levels is somewhat arbitrary since the calculations involve two adjustable constants. However we have used constants which gave a best fit approximation to the optical spectra of gadolinium orthoferrite for the octahedral case and MnO_4^- for the tetrahedral case. The final results are the transition energy levels indicated in figure III-11. The observed transitions have been assigned to the theoretical lines as indicated by the dotted inter-connections.

The fit seems amazingly good when considering the rather large approximations made in the theory. The relatively consistant fit leads us to believe the assignments are essentially correct. The result is that for the first time we have a valid means of predicting the source of the transitions at high energies in these materials and are able to show explicitedly that the oxygen atoms contribute significantly.

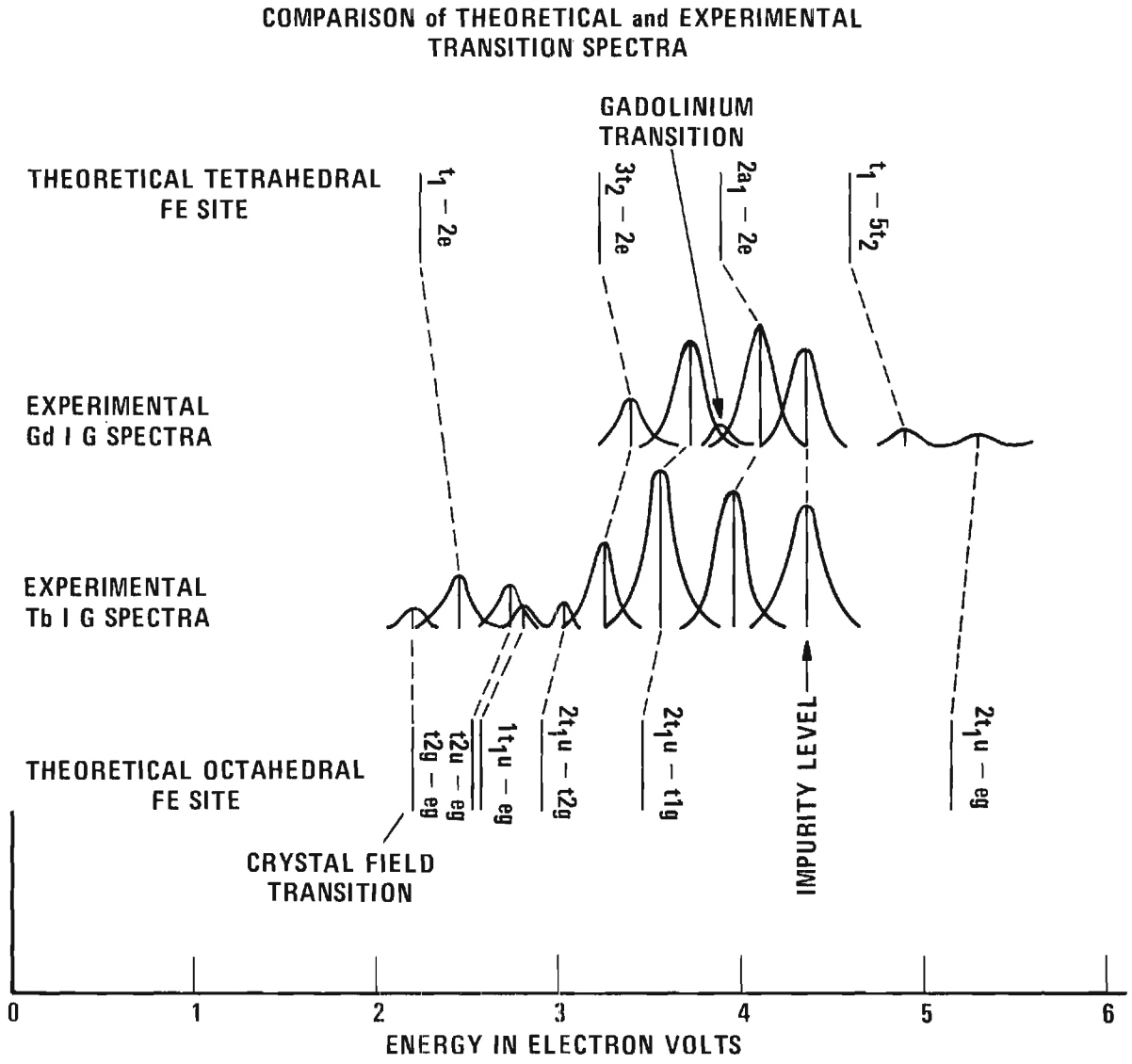

Fig. No. 3.11 Comparison of Experimental and Theoretical Optical Transition Energies

Consider, for example, the $t_{1\mu}$ orbital of the octahedral site. The eigenfunction as determined by the calculations is given as

$$\psi(1t_{1\mu}) = 0.16\psi_{4p} + .71\Sigma\psi_{2p}(\sigma) + .56\Sigma\psi_{2p}(\pi)$$

where the symbol ψ_{4p} simply represents the complete function for an iron atom 4p wave function and the symbols $\Sigma\psi_{2p}(\sigma)$ and $\Sigma\psi_{2p}(\pi)$ stand for normalized combinations of oxygen $2p(\sigma)$ and $2p(\pi)$ orbitals belonging to the same irreducible representation of the octahedral point group. Note that $(0.16)^2 + (.71)^2 + (.56)^2 \neq 1$. This is because the individual components are not orthogonal to each other and correct normalization must include the overlap terms. This has been carried out in the solution presented and the total wave function $\psi(t_{1\mu})$ is in fact normalized. Now consider the transition $1t_{1\mu}$ - eg. The wave function for Eg is

$$\psi(eg) = .69\ \psi_{3d} - .83\ \Sigma\psi_{2p}\ (\sigma)$$

ie it contains a significant fraction of iron 3d atomic characteristic. Such a transition has often been referred to as charge transfer since $\psi(t_{1\mu})$ is predominantly oxygen in nature and $\psi(eg)$ is significantly metal in nature. The same is true for the transition $t_{2\mu}$ - eg.

Another type of transition characterized explicitly by this analysis is of the inter-oxygen orbital transition. This is illustrated by the transition $2t_{1\mu} - t_{1g}$. The $t_{1\mu}$ orbital is predominantly oxygen in nature as shown before. The t_{1g} orbital is completely made up of

oxygen atomic function. This is called a non-bonding level since it cannot mix with the metal wave functions. The t_{1g} orbital is given as

$$\psi(t_{1g}) = \Sigma\psi_{2p}\pi.$$

The transition t_{1u} - t_{1g} is therefore predominantly an oxygen-oxygen transition or more accurately stated it is a transition between molecular orbitals of predominantly oxygen atomic characteristics.

This is the first verification, to our knowledge, of a complete analysis of this type being carried through. The results provide the basic wave functions necessary to explain the reversal of Faraday rotation associated with the charge transfer type transitions.

The line at 4.45 ev can not be accounted for by the molecular orbital energy levels. We believe that this line results from an impurity level possibly associated with lead flouride included in the samples. This line is not shifted, as the rest seem to be, and might therefore be explained on the basis of a non lattice dependent inclusion where the iron site transitions would be consistantly shifted from slightly different lattice spacings.

The line at 3.9 ev for the gadolinium iron garnet shows no apparent correlation with the molecular orbital transition spectra and is therefore believed in fact to be a gadolinium transition. This is one line which therefore should be evaluated with a direct pumping experiment to evaluate the potential of the pumping concept. It has, however, the disadvantage

of being relatively high in energy and inconvenient to reach with conventional lasers. Recently, ultra violent lasers have been introduced onto the market and the problem is not nearly so difficult to instrument today as it would have been a year ago.

The resulting assignments have accounted for nearly all the observed lines. Disconcertingly we have been able to associate the 2.45 ev line with a tetrahedral iron site transition of the type t_1 - 2e. We had previously hoped this was the terbium 2.54 ev line shifted by a lattice distortion. It is still possible that the terbium transition makes up part of this observed transition. If this is the case, then it is possible that it can be more easily pumped than originally believed by borrowing energy from the overlapping allowed molecular orbital transitions. This needs further investigation.

In an effort to answer the question of the presence of the terbium transition, we have taken additional reflectivity data in the vicinity of the 2.45 ev line. This subsequent data however was taken in a swept mode rather than point by point as previously. Figure III-12 shows the measured reflectivity of 70° angle of incidence. The large structure at 494 microns, ie, 2.5 ev is the line previously located at 2.45 ev. Note, however, the small but very definite reflectivity peak at 480 microns. This corresponds to an energy of 2.58 ev which is very close to the free terbium ion transition energy of 2.54 ev. This structure though relatively small is consistantly repeatable. The same structure does not show up in the 20° reflectivity however. This could be due to the result of a change in relative angle between the incident light and axis of quantization of the material; however, we have not had time to pursue the matter to resolve the uncertainty. There is a good possibility this is

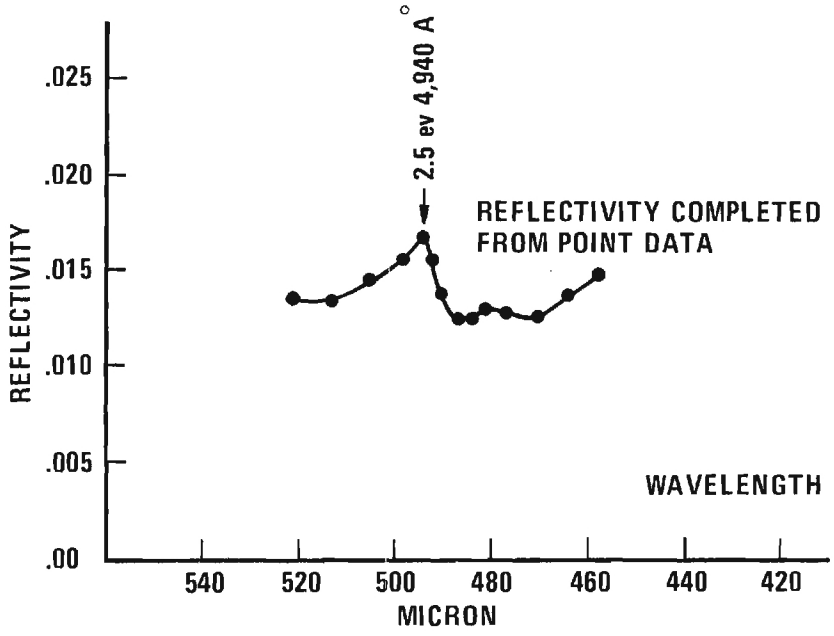

Fig. No. 3.12 TbIG Reflectivity Around 2.5 eV

the absorption line corresponding to the terbium ion transition. More data is required to establish the absorption coefficient.

The results of these calculations have permitted us for the first time to explain the significant fine structure associated with the optical absorption spectrum of the garnets. By identifying those lines associated with the iron site transitions we have been able to locate the location of lines which are potentially useful for the proposed optical pumping mode of memory operation.

VI. Conclusions

This program has undertaken the task of evaluating the feasibility of optical pumping for modifying the local state of an antiferromagnetic film. We have theoretically analyzed the pumping process itself and associated thermal considerations. It is concluded that from a theoretical point of view, optical pumping is very attractive, offering potentially high access and cycle rates and low light power.

We have grown gadolinium, terbium and dysprosium garnets and have published the first absorption spectra data for these type of bulk single crystals over the 2 ev to 5 ev energy range. This data was not previously in the literature and was needed to experimentally evaluate the transition probabilities for the pumping process. This work was presented at the 1969 Intermag Conference in Amsterdam.

Finally, in order to understand the complex absorption spectra a theoretical molecular orbital calculation was carried out. The purpose of this work was to attempt to locate those transitions due to iron ion sites and hence from the remaining spectra locate potential rare earth transitions. This was the first attempt to carry out such an analysis for the materials and it has been very successful. The results of this phase of the work have been submitted for presentation at the 1969 Magnetism Conference to be held in Philadelphia. As a result of the molecular orbital calculations we have tentatively identified a gadolinium transition at 3.9 ev in GdIG and a terbium transition in the vicinity of 2.5 to 2.58 ev in TbIG.

These results pave the way for the final step required to completely evaluate the optical pumping process. Time and money restrictions kept us

from instrumenting this final step in the overall feasibility study. It is believed that enough positive information has been obtained, however, to provide increased motivation to carry out this work. In addition to the garnets, we have proposed that certain antiferromagnetic materials such as MnCrO might be more ideally suited for the proposed pumping scheme. The techniques used to evaluate the optical properties of oxides developed during this contract could be applied directly to these materials. The potential for fast access high density magnetic memories achieved by optical pumping appears significantly great to warrant additional research in this area.

REFERENCES

1. J. T. Chang, J. F. Dillon, Jr., and U. F. Gianola, "Magneto-Optical Variable Memory Based Upon the Properties of a Transparent Ferrimagnetic Garnet and Its Compensation Temperature," Journal of Applied Physics, 36, No. 3, March 1965 (1110)

2. F. Fortani, N. Minnaja, "A Proposal for a Magneto-Optical Variable Memory," IEEE Proceedings, April 1966 (711)

3. S. Geller et al, "Magnetic Study of the Heavier Rare Earth Iron Garnets," Phys. Rev. 137, No. 3A, February 1, 1965 (A1034)

4. A. Sano and A. Serra, "Static and Dynamic Properties of a Gadolinium Garnet," IEEE Trans. on Magnetics, Mag. 4, No. 4, December 1968 (646)

5. W. Hunter, "Errors in Using the Reflective vs. Angle of Incidence Method for Measuring Optical Constants," J. Opt. Soc. Am. 55, No. 10, Part 1, October 1965 (1197)

6. P. Grant, "Reflectivity of YIG and YGG: Observation of Charge Transfer and Crystal Field Transitions," Applied Physics Letters, 11, No. 5, September 1, 1967 (166)

7. G. H. Dieke and L. A. Hall, "Flourescent Lifetimes of Rare Earth Salts and Ruby," J. Chem. Phys., 27, No. 2, August 1957 (465)

8. S. Keller and G. Pettit, "Visible Luminescence of Rare Earth Yttrium Gallium Garnets," Phys. Rev. 121, No. 6, March 15, 1961 (1639)

9. R. MacDonald, OiVoegeli, and C. D. Mee, "Magneto-Optical Properties of Garnet Films," Journal of Applied Physics, 38 (10) 4100-02 September 1967

10. W. Holloway, Jr., and M. Kestigian, "Concentration Quenching of the Tb^{3+} Ion Flourescence in $Y_3Al_5O_{12}$ Crystals[9]," Phys. Letters, 21, No. 4, June 1, 1966 (364)

11. S. Geller and M. Gilleo, "The Crystal Structure and Ferrimagnetism of Yttrium - Iron Garnet," J. Phys. Chem. Solids, Vol. 3, 1957 (307)

12. C. J. J. Roothaan, "New Developments in Molecular Orbital Theory", Reviews of Modern Physics, Vol. 23, No. 2, Pg. 69, 1951

13. C. J. Ballhausen, H. B. Gray, "Molecular Orbital Theory", W. A. Benjamin, Inc., New York, 1965.

APPENDIX I

DERIVATION OF PUMPING TRANSITION PROBABILITY

The transition probability for the transfer of an atom to an energy state above ground level is calculated by first order perturbation theory. We assume the radiation interaction is small and that the Hamiltonian of the atom can be expressed as

$$H = H_o + H_I \quad \text{where}$$

$$H_o\Phi_n = E_n\Phi_n, \quad \Phi_n \text{ being eigenfunctions of stable states of the atom}$$

In general the perturbation is time varient, i.e., the radiation is not only periodic but is applied at t = 0, and hence the solution for the perturbed states must satisfy the time varient Schroedinger equation, i. e.,

$$H\psi = j\hbar \frac{d\psi}{dt}$$

We know the general solution for ψ is separable into the product of spacially dependent and time dependent parts, or

$$\psi(\bar{r},t) = \mu(\bar{r})e^{\frac{-jEt}{\hbar}}.$$

Since the unperturbed wave functions

$$\Phi_n = \mu_n(\bar{r})e^{\frac{-jE_nt}{\hbar}}$$

form a complete orthonormal set, the perturbed wave functions can be written as an expansion in them so we get

$$\psi(\bar{r},t) = \Sigma_n c_n \mu_n(\bar{r}) e^{\frac{-jE_n t}{\hbar}}.$$

Now

$$\frac{d\psi}{dt} = \sum_{n-1}^{n} - \frac{jE_n t}{\hbar} C_n \mu_n(\bar{r}) e^{\frac{-jE_n t}{\hbar}} + \mu_n(\bar{r}) e^{\frac{-jE_n t}{\hbar}} \cdot C_n$$

so Schroedinger's equation becomes

$$H \Sigma C_n \mu_r(\bar{r}) e^{\frac{-jE_n t}{\hbar}} = \Sigma \left[E_n C_n \mu_n(\bar{r}) e^{\frac{-jE_n t}{\hbar}} + j\hbar C_n U_n(\bar{r}) e^{\frac{-jE_n t}{\hbar}} \right]$$

or

$$\Sigma C_n (H_o + H_I)(U_n(r) e^{\frac{-jE_n t}{\hbar}}) = \Sigma \left[C_n E_n \mu_n(r) e^{\frac{-jE_n t}{\hbar}} + \Sigma j \dot{C}_n \hbar U_n(r) e^{\frac{-jE_n t}{\hbar}} \right]$$

Since $H_o \mu_n = E_n \mu_n$ we can write,

$$\Sigma C_n E_n \mu_n e^{\frac{-jE_n t}{\hbar}} + \Sigma C_n H_I \mu_n e^{\frac{-jE_n t}{\hbar}} = \Sigma C_n E_n \mu_n e^{\frac{-jE_n t}{\hbar}} + \Sigma j \dot{C}_n \hbar \mu_n e^{\frac{-jE_n t}{\hbar}}$$

The technique of solving for the C's is to multiply through both sides by μ_k and integrate over all space, thus

$$\Sigma C \bar{\mu}_k H_I \mu_n e^{\frac{-jE_n t}{\hbar}} = \Sigma j \dot{C}_n \bar{\mu}_k \mu_n e^{\frac{-jE_n t}{\hbar}},$$

and integrating over all space, recalling that $\int \bar{\mu}_k \mu d\tau = \delta_{kw}$

we obtain

$$\sum_{o}^{\infty} C_n \left[\int \mu_k H_I \mu_n d\tau\right] e^{\frac{-jE_n t}{\hbar}} = j\dot{C}_k \hbar e^{\frac{-jE_k t}{\hbar}}$$

or

$$(j\hbar)^{-1} \sum_{n=o}^{\infty} C_n \left[\int \bar{\mu}_k H_I \mu_n d\tau\right] e^{\frac{-j(E_n - E_k)t}{\hbar}} = \dot{C}_k.$$

The various approximations associated with first second -- etc. order of perturbation are found by describing H_I as $H_I(o) + \lambda H_I$ and expanding the C's as a power series in λ. Thus

$$(j\hbar)^{-1} \sum_{n=o}^{\infty} (C_n^{(o)} + \lambda C_n^{(1)} + \lambda^2 C_n^{(2)}) \lambda H_I e^{+jw_{kn}t} = \dot{C}_k^{(o)} + \lambda \dot{C}_k^{(1)} + \lambda^2 \dot{C}_k^{(2)}$$

$$\text{where } \lambda H_I = \lambda \int \bar{\mu}_k H_I \mu_n d\tau$$

and the approximation has been carried to the second order. Equating like coefficients of λ we get

$$0 = \dot{C}_k^{(o)}$$

$$(j\hbar)^{-1} \Sigma\, C_n^{(o)} H_I e^{jw_{kn}t} = \dot{C}_k^{(1)}$$

$$(j\hbar)^{-1} \Sigma\, C_n^{(1)} H_I e^{jw_{kn}t} = \dot{C}_k^{(2)}$$

We are thus able to derive the first order perturbation coefficients from the zeroth order coefficients which we know are independent of time by the first equation. Since the system is assumed to be in the ground state at t = 0 then the unperturbed C's must all be zero except $C_m^{(o)}$ which is to be 1, i. e., m is ground state. Therefore we have,

$$(j\hbar)^{-1} H_I e^{jw_{km}t} = \dot{C}_k^{(1)}$$

and integrating both sides with respect to time gives

$$C_k^{(1)} = (j\hbar)^{-1} \int H_I e^{jw_{km}t} \, dt.$$

If the interaction is independent of time then

$$C_k^{(1)} = - \frac{H_I}{\hbar} \quad \frac{e^{jw_{km}t} - 1}{w_{km}}$$

$$\text{where } H_I = \int \bar{\mu}_k H_I \mu_m \, d\tau.$$

The probability of finding the system in state k at time t after the perturbation was turned on is

$$C_k \bar{C}_k = \frac{4|H_I|^2}{\hbar} \quad \frac{\sin^2 \frac{1}{2} w_{km} t}{w_{km}^2}$$

Now assume H_I, the interaction Hamiltonian operator, is given as

$$H_I = o \qquad ; \qquad t<o$$

$$H_I = H_I(o) \sin wt \quad ; \quad t \geq 0 .$$

Then for t>o

$$C_k^{(1)} = (j\hbar)^{-1} H_I(o) \int \sin wt e^{jw_{km}} \, dt$$

or carrying out the integration

$$C_k^{(1)} = (j\hbar)^{-1} H_I(o) \left[\frac{e^{j(w_{km} + w) t} - 1}{w_{km} + w} - \frac{e^{j(w_{km} - w) t} - 1}{w_{km} - w} \right]$$

and the probability of finding the system in state, i.e., $C_k \bar{C}_k$ is

$$C_k \bar{C}_k = \frac{|H_I(o)|^2}{\hbar^2} \quad \frac{1 - 2 \cos (w_{km} - w) t}{(w_{km} - w)^2}$$

or

$$C_k \bar{C}_k = \frac{4|H_I(o)|^2}{\hbar^2} \quad \frac{\sin^2 \frac{1}{2} (w_{km} - w) t}{(w_{km} - w)^2}$$

where only the transition to the higher level state has been considered.

If state k is represented as an energy level in a continuous density of states of an excited band then describing the band by

$$N(w) \quad \frac{\text{states}}{\text{cm}^3 \text{erg}}$$

the probability of finding the system in any state between E_k and E_k + dE is

$$\bar{C}_k C_k = \frac{4|H_I^o|^2}{\hbar^2} \frac{\sin^2 \frac{1}{2}(w_{km} - w)\, t}{(w_{km} - w)^2} \, n(w)\, dw.$$

The interaction Hamiltonian for radiation of vector potential A is

$$H_I = \frac{je\hbar}{mc} \int \bar{\mu}_k (e^{jk.r}) A_o \cdot \nabla \mu_m d\tau$$

$$\text{so } |H_I^o|^2 = \frac{e^2 \hbar^2 A_o^2}{m^2 c^2} \left| \int \bar{\mu}_k e^{jk.r} \nabla \mu_m d\tau \right|^2$$

The Poynting Vector $\frac{c}{4\pi}$ E x H can be calculated from A since

$$E = -\frac{1}{c}\frac{dA}{dt} \qquad \text{and } H = \nabla \times A$$

The result is $P_D = \frac{w^2}{2\pi C} |A_o|^2 \frac{\text{erg}}{\text{sec cm}^2}$ = I (Intensity of Radiation)

Making this substitution into $|H_I^o|^2$ and noting that if $\lambda >>$ (dimensions of atom), $e^{jk.r} \approx 1$,

$$|H_I^o|^2 = \frac{e^2 \hbar^2}{m^2 c^2} \frac{2\pi I}{w^2} \left| \int \mu_k \nabla \mu_n d\tau \right|^2$$

and

$$\bar{C}_k C_k = \frac{8\pi I n(w) e^2}{m^2 c w^2} \left| \int \mu_k \nabla \mu_n d\tau \right|^2 \frac{\sin^2 \frac{1}{2}(w_{kn} - w)\, t}{(w_{kn} - w)^2} \, dw$$

The integral $\int \mu_k \nabla \mu_n d\tau = \frac{m}{\hbar^3} w_{km} \int \bar{\mu}_k r_A \mu_m d\tau$ i.e. the expected interaction displacement so

$$C_k \bar{C}_k = \frac{8\pi I n(w)}{m^2 c w^2} \quad \frac{m^2 w_{km}^2}{3\hbar^2} \quad |M|^2 \quad \frac{\sin^2 \frac{1}{2}(w_{km} - w)\, t}{(w_{km} - w)^2} \, dw.$$

Integrating over w in order to find the probability of finding the system in the upper band - making the usual approximation

$$\int \frac{\sin^2 \frac{1}{2}(w_{km} - w)\, t \; dw}{w_{km} - w^2} = \tfrac{1}{2}\pi t$$

so $$p = \frac{4\pi^2 I}{3c\hbar^2} \; n(w)|M|^2 t \; .$$

The transition rate then to the upper level is

$$w = \frac{4\pi^2}{3c\hbar^2} \; I \; n(w)|M|^2 \qquad \frac{\text{transition}}{\text{sec cm}^3} \; .$$

APPENDIX II

Computer Program for Computing n & k From Reflectivity Data

```
BEGIN←
  ALPHA FILE IN F1 14(1,5);←
  ALPHA FILE OUT F2 14 (1,5);←
  STRING STR1(200), STR2(72);←
  ARRAY PHI[0:2],RP[0:2],  E[0:2,0:2];←

  REAL  DELTA,N,NO,K,KO,SIPHI,CSPHI,AA,AB,A,B,←
  RSA,RSB,RPA,RPB,R20,R45,R70,ALFA,LAMDA;←
  INTEGER  X,Y,I,XMIN,YMIN;←
  LABEL  AGN,ABSP;←
  REAL PROCEDURE READATA;←
  BEGIN REAL R;  LABEL RD;←
  RD:   R:=READCON(FALSE);←
  IF R=2 THEN READATA:=INREAL ELSE BEGIN←
  PRINT #$#;  GO TO RD;  END;←
  END READATA;←
  INPUT(F1,STR1);  OUTPUT(F2,STR2);←
  PRINT #NO=#;←
  NO:=READATA;←
  PRINT #KO=#;←
  KO:=READATA←

  PRINT #LAMDA=#;←
  LAMDA:=READATA;←
  PRINT #VALUES FOR R20  R45  R70  ARE#;←
  R20:=READATA;  R45:=READATA;  R70:=READATA;←
  PHI[0]:=0.34907;PHI[1]:=0.78540;PHI[2]:=1.22173;←
  DELTA:=0.01;←
  AGN:  FOR X:=0 STEP 1 UNTIL 2 DO BEGIN←
  N:=NO+(X-1)×DELTA;←
  FOR Y:=0 STEP 1 UNTIL 2 DO BEGIN←
  K:=KO+(Y-1)×DELTA;←
  FOR L:=0 STEP 1 UNTIL 2 DO BEGIN←
  SIPHI:=SIN(PHI[1]); CSPHI:=COS(PHI[1]);←
  AA:=SQRT((N*2-(K*2)-(SIPHI*2))*2 + 4 (N*2) (K*2));←
  AB:=N*2-K*2-SIPHI*2;←
  A:=SQRT(0.5 (AA+AB));←
  B:=SQRT(0.5 (AA-AB));←
  RSA:=(A-CSPHI)*2 + B*2;←
  RSB:=(A+CSPHI)*2 + B*2;←
  RPA:=(A-(SIPHI*2/CSPHI))*2 + B*2;←
  RPB:=(A+(SIPHI*2/CSPHI))*@ + B*2;←
  RP[1]:=((RSA/RSB)×(RPA))/RPB; END;←
  E[X,Y]:=(R20-RP[0]*2 + (R45-RP[1])*2;←
  +(R70-RP[2])*2;←
  END;  END;←
  XMIN:=0; YMIN:=0;←
  FOR X:=0 STEP 1 UNTIL 2 DO←
  FOR Y:=0 STEP 1 UNTIL 2 DO←
```

```
IF E[XMIN,YMIN] GTR E[X,Y] THEN←
BEGIN  XMIN:=X;  YMIN:=Y;  END;←
IF XMIN=1 AND YMIN=1 THEN GO TO ABSP;←
NO:=NO+(XMIN-1)↘DELTA; KO:=KO+(YMIN-1)↘DELTA;←
GO TO AGN;←
ABSP:   ALFA:=(12.566↘NO KO 1@-07)↘LAMDA;←
PRINT #ALPHA # ALFA;←
PRINT #NO=#NO #KO=#KO;←
END.←
```

Appendix III - Radial Functions

Radial functions for Fe

4s and 4p:

$$R_{4\ell} = \sum_{k=\ell+1}^{4} \chi_{k\ell} C_{k\ell,4}$$

$$\chi_{k\ell} = \frac{(2\zeta_{k\ell})^{k+\frac{1}{2}}}{\sqrt{(2k)!}} r^{k-1} \underline{C}^{-\zeta_{k\ell} r}$$

$C_{1s,4}$	- 0.02078	ζ_{1s}	25.38
$C_{2s,4}$	0.07052	ζ_{2s}	9.75
$C_{3s,4}$	- 0.1744	ζ_{3s}	4.48
$C_{4s,4}$	1.0125	ζ_{4s}	1.40
$C_{2p,4}$	0.02750	ζ_{2p}	10.60
$C_{3p,4}$	- 0.09561	ζ_{3p}	4.17
$C_{4p,4}$	1.00414	ζ_{4p}	1.08

(The radial function for 4p is that appropriate to $(3d)^6(4p)^2$).

3d:

$$R_{3d} = C_1 \chi_{3d}(\zeta_1) + C_2 \chi_{3d}(\zeta_2)$$

C_1	0.5366	ζ_1	5.35
C_2	0.6678	ζ_2	1.80

(The radial function for 3d is that appropriate to the neutral $(3d)^6(4s)^2$ configuration).

Radial functions for oxygen

2s:

$$R_{2s} = \sum_{p=1}^{6} \frac{(2\zeta_{po})^{m_{po}+\frac{1}{2}}}{\sqrt{(2m_{po})!}} r^{m_{po}-1} e^{-\zeta_{po} r} C_{po,2s}$$

P	M_{po}	ζ_{po}	$C_{po,2s}$
1	1	7.616	- 0.21979
2	1	13.3243	- 0.00573
3	2	1.7582	0.42123
4	2	2.5627	0.54368
5	2	4.2832	0.23061
6	2	5.9445	0.17856

2p:

$$R_{2p} = \sum_{p=1}^{4} \frac{(2\zeta_{pl})^{m_{pl}+\frac{1}{2}}}{\sqrt{(2m_{pl})!}} r^{m_{pl}-1} e^{-\zeta_{pl} r} C_{pl,2p}$$

P	m_{pl}	ζ_{pl}	$C_{pl,2p}$
1	2	1.1536	0.16371
2	2	1.7960	0.57600
3	2	3.4379	0.33392
4	2	7.9070	0.01495

Numerical coefficients for the radial functions

2s:

$$R_{2s} = \sum_{p=1}^{6} A_p \, e^{-\zeta_p r} \, r^{m_p^A - 1}$$

A_1	=	ζ_1^A	= 7.616	M_1^A	= 1
A_2	=	ζ_2^A	= 13.3243	M_2^A	= 1
A_3	=	ζ_3^A	= 1.7582	M_3^A	= 2
A_4	=	ζ_4^A	= 2.5627	M_4^A	= 2
A_5	=	ζ_5^A	= 4.2832	M_5^A	= 2
A_6	=	ζ_6^A	= 5.9445	M_5^A	= 2

2p:

$$R_{2p} = \sum_{p=1}^{4} B_p \, e^{-\zeta_p r} \, r^{m_p^B - 1}$$

B_1	= 0.2701984	ζ_1^B	= 1.1536	M_1^B	= 2
B_2	= 2.8751313	ζ_2^B	= 1.7960	M_2^B	= 2
B_3	= 8.4497702	ζ_3^B	= 3.4379	M_3^B	= 2
B_4	= 3.0348687	ζ_4^B	= 7.9070	M_4^B	= 2

3d:

$$R_{3d} = \sum_{p=1}^{2} C_p \, e^{-\zeta_p r} \, r^{m_p^C - 1}$$

C_1	= 80.1359965	ζ_1^C	= 5.35	M_1^C	= 3
C_2	= 2.2031239	ζ_2^C	= 1.80	M_2^C	= 3

4s:

$$R_{4s} = \sum_{p=1}^{4} D_p \, r^{m_p^D - 1} e^{-\zeta_p r}$$

D_1	= - 5.313895	ζ_1^D	= 25.38	M_1^D	= 1
D_2	= 24.1709217	ζ_2^D	= 9.75	M_2^D	= 2
D_3	= - 13.9945283	ζ_3^D	= 4.48	M_3^D	= 3
D_4	= 0.5186160	ζ_4^D	= 1.40	M_4^D	= 4

4p:

$$R_{4p} = \sum_{p=1}^{3} E_p \, r^{m_p^E - 1} e^{-\zeta_p r}$$

E_1	= 11.6162707	ζ_1^E	= 10.60	M_1^E	= 2
E_2	= -5.9692291	ζ_2^E	= 4.17	M_2^E	= 3
E_3	= 0.1599838	ζ_3^E	= 1.08	M_3^E	= 4

Appendix IV - Explicit Forms of Atomic Functions for Overlap Integrals

$$(2s) = \sqrt{\frac{1}{4\pi}}\ R_{2s}(r)$$

$$(2p_i) = \sqrt{\frac{3}{4\pi}}\ R_{2p}(r)\ \frac{X_i}{r} \qquad (i = 1, 2, 3)$$

$$(3d_{ij}) = \sqrt{\frac{15}{4\pi}}\ R_{3d}(r)\ \frac{X_i X_j}{r^2} \qquad (i \neq j;\ i,j = 1,2,3)$$

$$(3d_{z^2}) = \sqrt{\frac{5}{16\pi}}\ R_{3d}(r)\ \frac{(3z^2 - r^2)}{r^2}$$

$$(3d_{x^2-y^2}) = \sqrt{\frac{15}{16\pi}}\ R_{3d}(r)\ \frac{(x^2 - y^2)}{r^2}$$